National Library of Canada
Bibliothèque nationale du Canada

Acquisitions and Bibliographic Services Branch
Direction des acquisitions et des services bibliographiques

395 Wellington Street
Ottawa, Ontario
K1A 0N4

395, rue Wellington
Ottawa (Ontario)
K1A 0N4

Your file Votre référence

Our file Notre référence

NOTICE

The quality of this microform is heavily dependent upon the quality of the original thesis submitted for microfilming. Every effort has been made to ensure the highest quality of reproduction possible.

If pages are missing, contact the university which granted the degree.

Some pages may have indistinct print especially if the original pages were typed with a poor typewriter ribbon or if the university sent us an inferior photocopy.

Reproduction in full or in part of this microform is governed by the Canadian Copyright Act, R.S.C. 1970, c. C-30, and subsequent amendments.

AVIS

La qualité de cette microforme dépend grandement de la qualité de la thèse soumise au microfilmage. Nous avons tout fait pour assurer une qualité supérieure de reproduction.

S'il manque des pages, veuillez communiquer avec l'université qui a conféré le grade.

La qualité d'impression de certaines pages peut laisser à désirer, surtout si les pages originales ont été dactylographiées à l'aide d'un ruban usé ou si l'université nous a fait parvenir une photocopie de qualité inférieure.

La reproduction, même partielle, de cette microforme est soumise à la Loi canadienne sur le droit d'auteur, SRC 1970, c. C-30, et ses amendements subséquents.

Canada

DYNAMICS AND CONTROL OF MULTI-BODY TETHERED SATELLITE SYSTEMS

by

MEHDI KESHMIRI

Department of Mechanical Engineering
McGill University, Montreal
January 1995

A thesis submitted to the Faculty of Graduate Studies and Research
in partial fulfillment of the requirement of the degree of
Doctor of Philosophy

© Mehdi Keshmiri, 1995

National Library of Canada
Bibliothèque nationale du Canada

Acquisitions and Bibliographic Services Branch
Direction des acquisitions et des services bibliographiques

395 Wellington Street
Ottawa, Ontario
K1A 0N4

395, rue Wellington
Ottawa (Ontario)
K1A 0N4

Your file Votre référence

Our file Notre référence

THE AUTHOR HAS GRANTED AN IRREVOCABLE NON-EXCLUSIVE LICENCE ALLOWING THE NATIONAL LIBRARY OF CANADA TO REPRODUCE, LOAN, DISTRIBUTE OR SELL COPIES OF HIS/HER THESIS BY ANY MEANS AND IN ANY FORM OR FORMAT, MAKING THIS THESIS AVAILABLE TO INTERESTED PERSONS.

L'AUTEUR A ACCORDE UNE LICENCE IRREVOCABLE ET NON EXCLUSIVE PERMETTANT A LA BIBLIOTHEQUE NATIONALE DU CANADA DE REPRODUIRE, PRETER, DISTRIBUER OU VENDRE DES COPIES DE SA THESE DE QUELQUE MANIERE ET SOUS QUELQUE FORME QUE CE SOIT POUR METTRE DES EXEMPLAIRES DE CETTE THESE A LA DISPOSITION DES PERSONNE INTERESSEES.

THE AUTHOR RETAINS OWNERSHIP OF THE COPYRIGHT IN HIS/HER THESIS. NEITHER THE THESIS NOR SUBSTANTIAL EXTRACTS FROM IT MAY BE PRINTED OR OTHERWISE REPRODUCED WITHOUT HIS/HER PERMISSION.

L'AUTEUR CONSERVE LA PROPRIETE DU DROIT D'AUTEUR QUI PROTEGE SA THESE. NI LA THESE NI DES EXTRAITS SUBSTANTIELS DE CELLE-CI NE DOIVENT ETRE IMPRIMES OU AUTREMENT REPRODUITS SANS SON AUTORISATION.

ISBN 0-612-05731-3

Canada

IN THE NAME OF GOD

Dedication

to

my late mother

Abstract

In this thesis, dynamics and control of multi-body tethered satellite systems are investigated. First a dynamical model is developed that takes into account the three dimensional librational motion of the system as well as the nonlinear vibrations of the tethers, both in longitudinal and transverse directions. The assumed modes method is used to discretize the continuous tethers. Using Lagrange's equations, splitting the vector of generalized coordinates to a set of subvectors, where each subvector corresponds to a specific tether, a set of nonlinear ordinary differential equations governing the motion of the system is obtained in the explicit analytical form. A fourth order strain energy expression is used in the formulation to allow the possibility of moderately large deformation of the tethers. The equations are applicable whether the length of the tethers are constant (station-keeping phase) or changing with time (deployment and retrieval phases). They are transformed into vector form for simulation purposes.

Among the external forces, the aerodynamic forces and their effects on the dynamics and stability of the system are given more attention. The free molecular flow model is used to calculate the aerodynamic forces on the end-bodies as well as on the tethers. In addition, internal damping forces resulting from the material damping of the tethers are considered in this investigation. These forces, which are very difficult to model accurately, are modelled using a viscous damping model.

Equilibrium configurations of the system, as special solutions of the equations of

motion, in the absence or presence of the aerodynamic forces, are studied in more detail. A closed form solution to the static equilibrium equations is obtained when there is no external force acting on the system other than the gravitational force. The set of nonlinear equations of motion is then linearized analytically about a particular equilibrium configuration for stability and eigenvalue analysis. The natural frequencies of some single-tether as well as multi-tether systems are calculated using these linearized equations.

Stability of a single-tether system in low orbit missions is investigated, ignoring the aerodynamic forces on the main-satellite as well as on the tether. Assuming a particular geometrical configuration for the subsatellite and using the linearized equations, the effect of the aerodynamic forces, particularly aerodynamic lift, on the stability of the system as well as the equilibrium configuration of the system is examined through the eigenvalue analysis. This analysis is then extended to multi-body systems.

Finally the problem of controlling the nonlinear system through the application of Lyapunov's stability theory is examined for multi-body tethered systems, ignoring the transverse oscillations of the tethers. Initially, based on the Hamiltonian of the system, a Lyapunov function is introduced for a system with massless and rigid tethers. It leads to a *linear* tension control law. When the mass of the tethers is taken into account the Lyapunov function is modified and a new tension control law is developed which is no longer linear. With the assumption that the longitudinal oscillations of the tethers are small compared to the length of the tethers, a Lyapunov function is constructed for systems with elastic tethers. At the end, a hybrid control law is examined to improve the performance of the controlled system.

Résumé

Cette thèse a pour objet l'étude de la dynamique et de la commande de systèmes satellisés composés de plusieurs éléments reliés par des fils. Un modèle dynamique est tout d'abord établi: ce modéle tient compte du mouvement de rotation tridimensionel du système ainsi que des vibrations non-linéaires des fils, dans les sens transversal et longitudinal. La méthode des modes imposés est utilisée pour discrétiser les fils continus. En utilisant les équations de Lagrange, et en séparant le vecteur de coordonnées généralisées en un ensemble de sous-vecteurs, où chaque sous-vecteur correspond à un fil spécifique, un ensemble d'équations différentielles ordinaires non-linéaires dictant le mouvement du système est alors obtenu sous une forme analytique explicite. Une expression du quatrième ordre de l'énergie de déformation est utilisée dans la formulation pour que les grandes déformations des fils soient possibles. Ces équations sont applicables si la longueur des fils est constante (phase de maintien en position) ou variable dans le temps (phase de déploiement et de repliement). Elles sont transformées sous forme vectorielle pour les besoins des simulations.

Parmi les forces externes, les forces aérodynamiques et leurs effets sur la dynamique et la stabilité du système sont très importants. Le modèle d'écoulement moléculaire libre est utilisé pour calculer les forces aérodynamiques sur les extiémites des éléments ainsi que sur les fils. De plus, les forces d'amortissement internes résultant du matériau composant les fils sont prises en compte dans cette étude. Ces forces, qui sont très difficiles à représenter précisément, sont modélisées en utilisant un modèle d'amortissement visqueux.

Les configurations d'équilibre du système, solutions spéciales des équations du mouvement, sont étudiées plus en détail en l'absence ou la présence des forces

aérodynamiques. Une solution exacte des équations d'équilibre statique est obtenue en l'absence de forces externes agissant sur le système à l'exception de la gravité. L'ensemble des équations non-linéaires du mouvement est alors linéarisé analytiquement autour d'une position d'équilibre particulière pour l'analyse de la stabilité et des valeurs propres. Les fréquences naturelles d'un seul fil ainsi que celles des systèmes composés de plusieurs fils sont calculées en utilisant ces équations linéarisées.

La stabilité d'un système ne comprenant qu' un seul fil est étudiée lors de missions à basse orbite, en négligeant les forces aérodynamiques sur le satellite principal ainsi que sur le fil. En supposant une configuration géométrique particulière pour le sous-satellite et en utilisant les équations linéarisées, l'effet des forces aérodynamiques, en particulier la portance aérodynamique, sur la stabilité du système ainsi que la position d'équilibre du système sont étudiés par une analyse des valeurs propres. Cette analyse est alors étendue aux systèmes à plusieurs éléments.

Finalement, le problème de commande du système non-linéaire est étudié en appliquant la théorie de stabilité de Lyapunov pour les systèmes composés de plusieurs éléments reliés, en ignorant les oscillations transversales des fils. Initialement une fonction de Lyapunov, basée sur l' Hamiltonien du système est introduite pour un système utilisant des fils sans masse et rigides. Ceci conduit à une loi de commande linéaire de la tension. En tenant compte de la masse des fils, la fonction de Lyapunov est modifiée pour obtenir une nouvelle loi de commande de la tension qui n'est plus linéaire. Une fonction de Lyapunov est élaborée pour des systèmes avec des fils élastiques en supposant que les oscillations longitudinales des fils sont petites par rapport à leurs longueurs. Enfin, une loi hybride de commande est étudiée pour améliorer la performance du système asservi.

Acknowledgment

I wish to express my sincere gratitude to Prof. A.K. Misra for his continuous guidance, encouragement, kindness and caring throughout the course of this research. His precise and critical reviews, sincerity, patience during the period of this research are gratefully appreciated.

I gratefully express my best regards to the Ministry of Higher Education of the Islamic Republic of Iran who provided me a scholarship and made my presence here possible. I also sincerely acknowledge the support given to this research by Natural Sciences and Engineering Research Council of Canada. Besides I express my gratitude to the McGill University for awarding me the David Stewart and Hydro Quebec Major Fellowships in 1992-1995.

Sincere thanks are also due to the department of Mechanical Engineering for making my stay at McGill a pleasant one. Among them I would like to extend special thanks to Prof. M.P. Paidoussis and Ms. Barbara Whiston for their kindness. Among the friends and colleagues whose friendship is a real honor for me, special thanks to Mr. Jafar Sadigh for his valuable advice and academic discussions.

I would like to extend my deepest appreciation to my family, specially my wife, Mrs. Zahra Mirza Jafar, my children, Mohammad, Mahdieh, and Hamid for their constant support, encouragement, patience, and sacrifices they made during my studies.

Contents

Nomenclature

General Conventions

$a(0)$	magnitude of variable a at initial time, $t = 0$
$\vec{\boldsymbol{a}}$	a boldface character with an arrow represents a physical vector
$\hat{\boldsymbol{a}}$	a boldface character with a hat represents a unit vector
$\dot{\vec{\boldsymbol{a}}}, \ddot{\vec{\boldsymbol{a}}}$	first and second time derivatives of $\vec{\boldsymbol{a}}$ in the inertial frame
$\overset{\circ}{\vec{\boldsymbol{a}}}_k$	time derivative of $\vec{\boldsymbol{a}}_k$ in the k-th tether frame
$\mathbf{A}$	column vector or matrix $\mathbf{A}$ with scalar elements
$\mathbf{A}^T$	transpose of $\mathbf{A}$
$\boldsymbol{\mathcal{A}}$	column vector or matrix $\boldsymbol{\mathcal{A}}$ with vectorial elements
$\boldsymbol{\mathcal{A}}^T$	transpose of $\boldsymbol{\mathcal{A}}$
$(\bar{\ })$	definition of a parameter in the bead model
$(\ )^e, (\ )_e$	magnitude of ( ) at an equilibrium point $\mathbf{q}^e$
$(\ )^*$	magnitude of ( ) at the nominal solution $\mathbf{q}^*$
$\delta(\ )$	small deviation from the nominal or equilibrium value of ( )

Specific Symbols

$\{0\}$	column vector with appropriate number of 0 elements
$[0]$	matrix with appropriate number of 0 elements
$\vec{\mathbf{0}}$	zero vector
$\{\vec{\mathbf{0}}\}$	column vector with appropriate number of $\vec{\mathbf{0}}$ elements
$[\vec{\mathbf{0}}]$	matrix with appropriate number of $\vec{\mathbf{0}}$ elements

$\vec{a}$	microgravity acceleration
A_b	base surface area of a cylinder; $A_b = \pi R_c^2$
A_c	projection surface area of a cylinder; $A_c = 2R_c H_c$
A_{jk}	a nondimensional mass coefficient, Eq. (2.14)
A_p	surface area of a plate
A_s	projected surface area of a sphere; $A_s = \pi R_s^2$
$\mathbf{A}$	generalized mass matrix in Eq. (4.44)
b_k	magnitude of $\vec{\mathbf{b}}_k$
$\vec{\mathbf{b}}_k$	defined in Eq. (2.7)
B_k	a nondimensional mass coefficients, Eq. (2.14)
$\mathbf{B}$	defined in Eq. (4.44)
C_k	an arbitrary positive constant; Eq. (7.38)
C_k'	an arbitrary positive constant in Lyapunov's approach
$\mathbf{C}$	damping matrix resulted from material damping
dx_k	undeformed length of an element of the k-th tether
ds_k	deformed length of an element of the k-th tether
$\vec{\mathbf{d}}_{B_k}$	defined in Eq. (4.7)
$\vec{\mathbf{d}}_{\mathbf{b}_k}, \vec{\mathbf{d}}_{\mathbf{r}_k}, \vec{\mathbf{d}}_{\mathbf{t}_k}$	defined in Eq. (4.5)
$\mathbf{D}$	damping matrix
D_{jk}	a nondimensional mass coefficient, Eq. (7.43)
e	eccentricity of the orbit
$\mathbf{e}_k$	defined in Eq. (4.2)
EA_k	modulus of elasticity of the k-th tether
$\mathbf{f}$	vector of generalized forces
$\vec{f}$	aerodynamic force on a body
$\vec{f}^{(D)}, \vec{f}^{(S)}$	aerodynamic forces resulting from diffuse and specular reflections
$\vec{f}_n, \vec{f}_t$	normal and tangential components of the aerodynamic force
F_{jk}	a nondimensional mass coefficient, Eq. (2.32)

$\bar{\boldsymbol{F}}_O$	external forces other than aerodynamic and gravitational forces
G	universal gravitational coefficient
G_{jk}	a nondimensional mass coefficient, Eq. (7.51)
$\mathbf{G}_{jk}$	a participating term in the equations of motion, Eq. (2.71)
h	altitude of an object from the Earth's surface
h_0	reference altitude
h_k	altitude of body k
h_{t_k}	altitude of an arbitrary point of tether k
$\mathbf{h}_k$	defined in Eq. (4.10)
H	Heaviside function; also Hamiltonian of the system
H_0	scale height
H_{cyl}	height of cylinder
$\mathbf{H}_{jk}$	a participating term in the equations of motion, Eq. (2.71)
i	inclination angle; also $\sqrt{-1}$
$\hat{\mathbf{i}}_c, \hat{\mathbf{j}}_c, \hat{\mathbf{k}}_c$	unit vectors along the orbital frame
$\hat{\mathbf{i}}_k, \hat{\mathbf{j}}_k, \hat{\mathbf{k}}_k$	unit vectors along the k-th tether frame
$\hat{\mathbf{I}}, \hat{\mathbf{J}}, \hat{\mathbf{K}}$	unit vectors along the inertial frame
$\bar{K}_k$	stiffness of the k-th segment in the bead model
$K_{\ell_k}, K_{\theta_k}, K_{\phi_k}$	arbitrary positive constants in Lyapunov's approach corresponding to the k-th tether
$\mathbf{K}$	stiffness matrix
ℓ_0	reference length
ℓ_*	equivalent length in a single-tether system; $\ell_* = \dfrac{m_1 L}{m_1 + m_2}$
ℓ_{c_k}	command length corresponding to the k-th tether
ℓ_{f_k}	final length corresponding to the k-th tether
ℓ_k	nominal length of the k-th tether
L	nominal length of the tether in a single-tether system; also Lagrangian of the system

$\mathbf{L}_k$	an N_{q_k} dimensional column vector defined by Eq. (2.85)
m	total mass of the system
m_*	equivalent mass in a single tether system; $m_* = \dfrac{m_1 m_2}{m_1 + m_2}$
m_k	instantaneous mass of the k-th body
$\bar{m}_k$	instantaneous mass of the k-th tether; $\bar{m}_k = \rho_k \ell_k$
$\vec{m}$	aerodynamic torque on a body
M	mass of the Earth
$\mathbf{M}$	mass matrix
$\mathbf{M}_{kj}$	$N_{q_k} \times N_{q_j}$ submatrix of mass matrix
$\hat{n}_A$	unit inward normal to the surface dA
N	number of bodies
$\bar{N}_k$	number of segments associated with tether k in the bead model
N_q	total number of generalized coordinates
N_{q_e}	total number of elastic degrees of freedom
N_{q_k}	number of generalized coordinates corresponding to tether k
$\mathbf{p}_k$	defined in Eq. (4.3)
$\mathbf{P}_{jk}$	a participating term in the equations of motion, Eq. (2.71)
$\mathbf{q}$	vector of generalized coordinates
$\mathbf{q}_k$	subvector of generalized coordinates corresponding to the k-th tether
$\mathbf{Q}$	vector of generalized forces
$\mathbf{Q}_k$	subvector of generalized forces corresponding to $\mathbf{q}_k$
$\mathbf{Q}_A, \mathbf{Q}_D, \mathbf{Q}_E, \mathbf{Q}_O$	vectors of the generalized forces corresponding to the aerodynamic forces, material damping of the tethers, elasticity of the tethers, and other external forces, respectively
r_k	magnitude of $\vec{\mathbf{r}}_k$
r_{t_k}	magnitude of $\vec{\mathbf{r}}_{t_k}$
$\vec{\mathbf{r}}_k$	position vector of body $k+1$ measured from body k

$\vec{\mathbf{r}}_{t_k}$	position vector of an element of tether k measured from body k
R_c	orbit radius
R_{cyl}	radius of cylinder
$\vec{\mathbf{R}}_c$	position vector of the centre of mass measured from the centre of the Earth
R_E	radius of the Earth
$\vec{\mathbf{R}}_k$	position vector of body k measured from the centre of mass
$\vec{\mathbf{R}}_{t_k}$	position vector of an arbitrary point of tether k measured from the centre of mass
s_k	nondimensional distance along tether k; $s_k = x_k/\ell_k$
S	compensating term in Lyapunov approach; Eq. (7.26)
$\bar{S}_k$	total number of segments prior to tether k in the bead model
$\mathbf{S}_k$	a participating term in the equations of motion, Eq. (2.71)
t	time
$\hat{\boldsymbol{t}}_A$	unit tangential vector in the plane of $\vec{\boldsymbol{V}}_R$ and $\hat{\boldsymbol{n}}_A$
T	total kinetic energy of the system
T_0, T_1, T_2	zero order, first order, and quadratic terms in $\dot{\mathbf{q}}$ in the kinetic energy expression
T_k	tension in the k-th tether
T_{orb}	orbital kinetic energy of the system
T_{att}	kinetic energy of the system associated with attitude motion
$\vec{\boldsymbol{T}}$	thruster force
u	component of $\vec{\boldsymbol{V}}$, along x-axis (Chapter 7)
u_{ℓ_k}	longitudinal elongation of the k-th tether
u_k	elastic displacement of an element of the k-th tether along x_k
U	total potential energy of the system
U_E	elastic potential energy of the system
U_{E_k}	elastic potential energy corresponding to the k-th tether

U_G	gravitational potential energy of the system
U_{G_0}, U_{G_1}	defined in Eq. (7.16)
P_0, P_1	defined in Eq. (7.19)
$U_{G_{orb}}$	orbital gravitational potential energy of the system
$U_{G_{att}}$	gravitational potential energy of the system associated with attitude motion
$\mathbf{U}_k$	real part of eigenvector $\mathbf{W}_k$
v	component of $\vec{V}$, along y-axis (Chapter 7)
v_k	elastic displacement of an element of the k-th tether along y_k
$\hat{v}_R$	unit vector along $\vec{V}_R$
V_R	magnitude of $\vec{V}_R$
V_t	tangential component of $\vec{V}$
$\vec{V}$	relative velocity of subsatellite (Chapter 7)
$\mathbf{V}_k$	imaginary part of eigenvector $\mathbf{W}_k$
$\vec{V}_k$	relative velocity of air with respect to body k
$\vec{V}_R$	relative velocity of air with respect to an object
$\vec{V}_{t_k}$	relative velocity of air with respect to an arbitrary point of tether k
w	component of $\vec{V}$, along z-axis (Chapter 7)
w_k	elastic displacement of an element of the k-th tether along z_k
$\mathbf{W}_k$	eigenvector corresponding to λ_k
$\bar{\mathbf{W}}$	complex conjugate of $\mathbf{W}$
x_k, y_k, z_k	tether coordinate system corresponding to tether k
X_e, Y_e, Z_e	orbital coordinate system
X_I, Y_I, Z_I	inertial coordinate system
$\mathbf{X}_k$	vector of admissible functions associated with longitudinal elastic displacement u_k
$\mathbf{X}_{t_k}$	defined in Eq. (D.1)

$\mathbf{X}_{*k}$	integral of $\mathbf{X}_k$ with respect to s_k; Eq. (D.1)
$\mathbf{X}'_k, \mathbf{X}''_k$	first and second derivatives of $\mathbf{X}_k$ with respect to s_k; Eq. (D.1)
$\mathbf{Y}_k$	vector of admissible functions associated with transverse elastic displacement v_k
$\mathbf{Y}_{*k}$	integral of $\mathbf{Y}_k$ with respect to s_k; Eq. (D.1)
$\mathbf{Y}'_k, \mathbf{Y}''_k$	first and second derivatives of $\mathbf{Y}_k$ with respect to s_k; Eq. (D.1)
$Z_1, \ldots, Z_{15}$	intermediate parameters
$\mathbf{Z}_k$	vector of admissible functions associated with transverse elastic displacement w_k
$\mathbf{Z}_{*k}$	integral of $\mathbf{Z}_k$ with respect to s_k; Eq. (D.1)
$\mathbf{Z}'_k, \mathbf{Z}''_k$	first and second derivatives of $\mathbf{Z}_k$ with respect to s_k; Eq. (D.1)

Greek Letters

α	local angle of attack
α_0	a gravitational coefficient; $\sqrt{GM/R_c^3}$
α_k	reeling rate of the k-th tether from body k
$\vec{\alpha}_k$	defined in Eq. (D.3)
β_k	reeling rate of the k-th tether to body $k+1$
$\vec{\beta}_k$	defined in Eq. (D.3)
γ	structural damping coefficient
$\vec{\gamma}_k$	defined in Eq. (D.3)
δ_{jk}	Kronecker delta corresponding to indices j and k,
ϵ_k	strain in an element of the k-th tether
ζ	damping ratio
$\vec{\zeta}_k$	defined in Eq. (D.2)
$\vec{\zeta}_{*k}$	defined in Eq. (D.2)
η_k	real part of eigenvalue λ_k
$\boldsymbol{\eta}_k$	vector of generalized coordinates associated with transverse

	elastic displacement v_k
θ_0	argument of perigee
θ_c	true anomaly
θ_k	pitch angle of the k-th tether with respect to orbital frame
θ_s	$\theta_s = \theta_0 + \theta_c$
$\vec{\boldsymbol{\vartheta}}_k$	defined in Eq. (D.2)
$\vec{\boldsymbol{\vartheta}}_{*k}$	defined in Eq. (D.2)
κ	an arbitrary coefficient in Eq. (3.32)
$\vec{\boldsymbol{\kappa}}_k$	defined in Eq. (D.2)
λ_k	k-th eigenvalue of the system
$\bar{\lambda}_k$	complex conjugate of λ_k
μ_k	a dimensionless mass coefficient associated with tether and body k; $\mu_k = (m_k + \bar{m}_k)/m$
$\bar{\mu}_k$	a non-dimensional reference mass coefficient associated with tether k; $\bar{\mu}_k = (\rho_k \ell_0)/m$
$\boldsymbol{\nu}_k$	vector of generalized coordinates associated with transverse elastic displacement w_k
$\bar{\xi}_k$	extension of the k-th segment in the bead model
$\boldsymbol{\xi}_k$	vector of generalized coordinates associated with longitudinal elastic displacement u_k
ρ	density of the local atmosphere
ρ_0	reference density
ρ_k	mass of the k-th tether per unit length
$\hat{\rho}_k$	nondimensional mass of unit length of k-th tether; $\hat{\rho}_k = \dfrac{\rho_k}{m}$
$\vec{\boldsymbol{\varrho}}_k$	defined in Eq. (D.2)
σ_n, σ_t	accommodation coefficients for normal and tangential momentum exchange
$\vec{\boldsymbol{\sigma}}_k$	defined in Eq. (D.3)

$\vec{\varsigma}_k$	defined in Eq. (D.2)
ϕ_k	roll angle of the k-th tether with respect to the orbital frame
ψ	angle between the lifting panel and the normal to the tether; also angle between the cylinder and the tether (Chapter 7)
$\bar{\omega}$	mean orbital rate
ω_k	k-th natural frequency; also imaginary part of eigenvalue λ_k
ω_I, ω_O	in-plane and out-of-plane natural frequencies of the system
$\boldsymbol{\Gamma}_1, \boldsymbol{\Gamma}_2, \boldsymbol{\Gamma}_3$	terms corresponding to the kinetic, gravitational potential, and strain potential energy, respectively, appearing in the equations of motion
Λ	magnitude of $\vec{\boldsymbol{\Lambda}}$
$\vec{\boldsymbol{\Lambda}}$	angular velocity of atmosphere
$\vec{\boldsymbol{\Lambda}}_k$	defined in Eq. (D.3)
$\boldsymbol{\Omega}$	diagonal matrix of the natural frequencies
$\vec{\boldsymbol{\Omega}}_k$	absolute angular velocity of the k-th tether frame

Calligraphic Letters

$\mathcal{D}_{B_k}$	N_{q_k} dimensional column vector defined in Eq. (4.4)
$\mathcal{D}_{\mathbf{r}_k}, \mathcal{D}_{\mathbf{b}_k}, \mathcal{D}_{\mathbf{t}_k}$	N_{q_k} dimensional column vectors defined in Eq. (2.61)
$\mathcal{E}_k$	strain energy per unit length of the k-th tether
$\mathcal{J}_{\mathbf{r}_k}, \mathcal{J}_{\mathbf{b}_k}, \mathcal{J}_{\mathbf{t}_k}$	N_{q_k} order Jacobian matrices defined in Eq. (4.33)
$\mathcal{L}$	Lyapunov function
$\mathcal{P}_{\mathbf{r}_k}, \mathcal{P}_{\mathbf{b}_k}, \mathcal{P}_{\mathbf{t}_k}$	N_{q_k} dimensional column vectors defined in Eq. (4.33)
$\mathcal{R}_{\mathbf{r}_k}, \mathcal{R}_{\mathbf{b}_k}, \mathcal{R}_{\mathbf{t}_k}$	N_{q_k} dimensional column vectors defined in Eq. (4.36)

List of Figures

List of Tables

Chapter 1

INTRODUCTION

1.1 Introductory Remarks

The idea of using tethers goes back to the last century. Connecting large masses by a long thin string in space was suggested by Tsiolkovsky [1] in 1895 to harness weak gravity gradient forces for stabilization purposes. Sixty five years later in 1960, a Russian engineer Artsutanov [2] proposed the idea of anchoring a geostationary satellite to the Earth's surface by a long cable (tether). However, as far as the actual application is concerned, it was initially associated with the retrieval of stranded astronauts [3, 4]. The problems related with such a retrieval were clearly demonstrated in the study by Starly and Adlhoch [3]. Successful experiments during Gemini XI, XII in September and November of 1966, respectively, established the feasibility of using tethered systems [5].

The era of tethers in space really came into being when Colombo et al. [6] put forward the proposal of a Shuttle-borne Skyhook for low-orbital altitude research. In fact, Bekey [7] considers Colombo to be the father of space tethers. Since then, scores of applications of tethers in space have been proposed and analyzed. These include applications in conjunction with the Shuttle or the proposed Space Station as well as independent tethered missions.

Because of the wide range of potential applications, there has been a lot of interest in tethered satellite systems (TSS) in recent years and one can find a fairly rich literature on their dynamics and control. Since the proposed applications involved only two bodies, until recent years, the interest of the investigators was focused on two-body tethered systems. A large number of research works concerning the dynamics and control of two-body tethered satellite systems have been reviewed by Misra and Modi [8] and Beletsky and Levin [9]. There have been several proposals recently to use tethered systems that involve more than two bodies connected together by tethers, generally called multi-tethered or N-body tethered satellite systems; the available literature on these is comparatively scarce.

The literature review in this thesis starts with a brief review of the dynamics and control of two-body tethered systems. It is not exhaustive; only those investigations directly related to the goal of this thesis are discussed. The literature review is based on the nature of scientific development rather than the historical sequence. Thus one can conveniently follow where the spots of difficulties lie and consequently what issues should be addressed in a study like this. The review of related investigations are lumped into four different groups; dynamical modelling, aerodynamic effects, control strategies, and multi-body systems. Since our main objective is to contribute to the study of the dynamics and control of *multi-body* tethered satellite systems, in a separate section the available literature on their dynamics and control is reviewed.

Prior to the literature review, a few applications related to multi-tethered systems are described in the next section. The interested readers can find a fairly good number of applications of tethered satellite systems in general in [7, 10].

1.2 Some Proposed Applications of Multi-Body Tethered Satellite Systems

1.2.1 Upper Atmospheric Measurements

Limitation of the value of experimental data using sounding rockets and potential of tethered satellite systems for simultaneous measurement at several locations have led to several proposals involving multi-tethered satellite systems for upper atmospheric measurements. A one dimensional constellation of probes can be lowered by the Shuttle or any other free-flying satellite into the atmosphere in order to provide simultaneous data collection at different altitudes. The first probe can be tethered to the Shuttle while the others can be connected together by tethers (Ref. [11]).

1.2.2 Gravity Related Applications

Microgravity Laboratory

A laboratory facility on board the Space-Station can be situated vertically in the proximity of the center of gravity of the Space-Station. Two opposing tethers with end masses can be deployed vertically from the Space-Station, one upward and one downward [11]. The length of the tethers can be varied to control the position of the center of gravity of the system, placing it on the microgravity modules to minimize their gravity gradient acceleration and set it at the microgravity level (10^{-4} g and less). Among the various microgravity laboratories proposed recently, one can name the Materials Technology Lab (MTL) and the Biological Laboratory. MTL is projected to be a common module, equipped as a lab, to perform a variety of experiments related to the materials technology. Some biological processes that could be studied would be animal and plant growth, and human performance in microgravity.

Variable Low-Gravity Laboratory

In contrast to the previous application, a laboratory facility can be attached by a crawler to a tether deployed vertically from the Space Station and can be positioned at different points along this tether [11]. The gravity gradient between the system center of gravity and the laboratory can be varied by changing the distance of the crawler and the laboratory from the system's center of gravity. Usually, the gravity level inside the laboratory varies with time even if it is located at a constant distance relative to the Space-Station, because the system's gravity characteristics change with the orbital motion. A constant gravity level could be maintained by adjusting the lab position to compensate for orbital variations. This lab could be used to examine the effects of low gravity on physical and biological processes such as crystal growth, fluid mechanics, plant and animal growth, etc. It has been calculated that the laboratory could attain g-levels of 10^{-6}, 10^{-4}, 10^{-2}, and 10^{-1} at a distance above the center of gravity of approximately 2.25 m, 225 m, 22.5 km, and 225 km, respectively, with a 500 kg subsatellite tethered to a Shuttle or Space-Station orbiting at an altitude of 375 km.

1.2.3 Tether Communication Antenna

An insulated conducting tether, with plasma contactors at both ends, may be connected to a spacecraft located in the middle. Variations in the tether current can be used to generate ULF, ELF,or VLF waves for communication. Waves would be emitted by a loop antenna composed of the tether, magnetic field lines, and the ionosphere [11]. These waves may provide instantaneous worldwide communication by spreading over most of the Earth via the process of ducting. With a 20 to 100 km tether and a wire current of the order of 10 A, it appears possible to inject into the Earth-ionosphere line power levels of the order of 1 W by night and 0.1 W by day.

There are many other possible applications of multi-body TSS which will not be described here for the sake of brevity.

1.3 Literature Review on Dynamical Modelling

Before reviewing the literature on dynamical modelling, it may be useful to make a few comments on the dynamics of tether satellites. A tethered satellite system used for a particular mission undergoes three phases: (i) deployment, (ii) station-keeping, and (iii) retrieval. A reel mechanism is needed to perform the deployment and retrieval operations. After placing the main satellite on the desired orbit, the subsatellites can be deployed to the planned altitudes. Once they are positioned appropriately, tasks such as atmospheric experiments could be carried out during the station-keeping phase. After completion of the mission, the reel mechanism reels the subsatellites back to the main satellite; this is the retrieval phase.

Dynamics of a tethered system involves orbital dynamics as well as attitude dynamics. The motion of the center of mass of the system around the earth is called orbital dynamics, while the motion of the system relative to its center of mass is referred to as attitude dynamics. Orbital dynamics is negligibly affected by the attitude dynamics [12], as the energy associated with the former is much larger than that of the latter. On the other hand, the orbital motion does affect the attitude dynamics significantly.

Since many parameters play major roles in governing the system behaviour, the general dynamics of tethered systems is rather complicated. The center of mass moves around the Earth in a Keplerian orbit; the system swings around its center of mass; the tethers oscillate longitudinally as well as in transverse directions; the subsatellites move away from or towards the main satellite during deployment or retrieval phases, respectively, making the system non-autonomous; tension in the tethers ranges from less than 0.1N (very weak) to more than 100N, when the length of a tether changes from say, 20 m (quite short) to 100 km (very long). The fact that the air density varies by several orders of magnitude along the tether and that the atmosphere rotates with the Earth complicates the motion further. A good model of the system is thus necessary to provide a basis for the analysis and control of its dynamics.

It is well-known that the librational motion of the system is inherently unstable when it undergoes the retrieval phase [13]. The system can become unstable even during the deployment phase if the deployment rate is larger than a certain amount [14]. Thus a control strategy is required to control the system; however it is much easier to control the system during deployment compared with retrieval. During the station-keeping phase, when the unstretched lengths of the tethers are constant, the dynamics of the system is much simpler compared to the other two phases. However, it has been shown [15] that for a particular combination of system parameters the librational motion and consequently vibrational motion of a two-body tethered system becomes unstable even in the station-keeping phase if the atmospheric effects are taken into account.

The first study on the control of tethered systems was conducted by Rupp [13]. Although he made a key development in this area, his dynamical model was a drastic simplification of the actual system. The tether was assumed to be massless and rigid, and the librational motion of the system was confined to the orbital plane. He concluded that the deployment phase is basically stable and the retrieval phase is inherently unstable. He proposed a tension control law in order to control the motion of the system.

In some applications, the mass of the tether is expected to be of the same order of magnitude as that of the subsatellite when the tether is long enough, and hence cannot be ignored. Another important parameter is the elasticity of the tethers, because the proposed tethers are very thin (sometimes less than 1 mm in diameter) and long (up to 100 km), and hence flexible. Therefore the tethers vibrate axially as well as transversely during the deployment, station-keeping or retrieval phases.

Many studies have been carried out after the preliminary work by Rupp to include mass and flexibility of the tether, which play important roles in the vibrational and consequently librational dynamics of the system. Some of the pioneering works in this regards are cited in the following. Baker et al. [14], Kalaghan et al. [16], and Bainum and Kumar [17] considered mass of the tether and added the out-of-plane libration as well as longitudinal oscillation of the tether to the dynamical model. Initially the researchers modelled the longitudinal oscillation of the tether by a single displacement similar to that of a spring mass system. However, as the mass is distributed along the tether, a more accurate representation involves combination of axial modes similar to those of an elastic bar. Neglecting the longitudinal oscillation of the tether, Kulla [18] and Buckens [19] considered the transverse oscillations of the tether. Kalaghan et al. [16] also considered the transverse motion of the tether; but it was mixed up with the librational motion of the tether because of the way the coordinate system was selected. Longitudinal as well as transverse oscillations of the tether were modelled in the works by Kohler et al. [20], Modi and Misra [21], Xu [22], Modi and Misra [23], and Glaese and Pastrick [24]. It is found that the amplitude of the transverse oscillations grew significantly during the uncontrolled retrieval. Assuming that the energy and the mode of the vibratory motion remain constant, von Flotow [25] comcluded that this amplitude remains more or less unchanged.

1.3.1 Formulation

Different approaches have been used to derive the governing equations of motion. In general, these equations are obtained using an analytical approach based on the balance of work and energy or a vectorial approach based on the balance of forces and moments. Since a tethered satellite system has both rigid body and elastic motions, the equations of motion are in reality a set of hybrid partial-ordinary differential equations. However, because of the difficulties associated with the solution of these hybrid equations, they are eventually transformed to a set of ordinary differential equations by discretization.

There are a few studies in which the equations of motion are given in the hybrid form. Xu [22] derived the set of hybrid equations for a single-tether system using extended Hamilton's principle; the partial differential equations were then converted to the ordinary form using Galerkin's method. Pasca et al. [26] and Pasca and Lorenzini [27] started from Lagrangian density and came up with the hybrid equations for the station-keeping phase. The nonlinear hybrid equations were used to study the linearized motion, and to obtain the eigenfrequencies and equilibrium configurations of the system. Other researchers such as Beletsky and Levin [28], Matteis and Luciano [29], and Kim and Vadali [30] obtained hybrid equations using the Newtonian method to study the dynamics or steady state configurations of the system. Using Galerkin's method Kim and Vadali [30] transformed the hybrid differential equations to the ordinary form.

In most of the investigations, starting from discretization of the system, researchers derived the ordinary differential equations of motion without getting involved in hybrid equations. Having discretized the system, some researchers used an energy based method, such as Lagrange's equations or Kane's method, to derive the equations of motion, while others used a vectorial approach such as the Newtonian one . Misra and Modi [31], Banerjee and Kane [32], Xu, et al. [33], and Tyc et al. [34] can be cited among many researchers who used an energy based approach, while researchers such as No and Cochran [35, 36] and Quadrelli and Lorenzini [37] can be named among those who implemented a method of balance of forces and moments to derive the equations of motion.

In general, there are two different approaches to discretize a flexible body; mathematical discretization and physical discretization. Mathematical discretization, in contrast to the physical one which must be done at the beginning of modelling, can be done either before or after the derivation of the equations of motion. The former directly results in the ordinary differential equations of motion, while the latter implies conversion of the governing hybrid partial-ordinary differential equations to a set of ordinary differential equations. Finite difference procedure and Galerkin-type methods, including Rayleigh-Ritz and the assumed modes methods, belong to the mathematical approach. Discretization using lumped masses, rod elements, and finite elements are the well known physical discretization approach.

Finite difference and Galerkin-type methods are fairly standard procedures and need no elaboration. Finite difference has been used to analyze elastic oscillations of tethered satellites by Kulla [18], Kohler et al. [20] and Berry [38]. Galerkin-type methods, particularly the assumed modes method, have been used extensively in tether dynamics studies. Some examples are Banerjee and Kane [39], Modi and Misra [23], Bainum et al. [40], Pasca et al. [26], Kim and Vadali [30], and Tyc et al. [34].

Among the above-mentioned physical discretization schemes, the lumped mass scheme is the most common one. The other two have been rarely used. However they are reviewed here for the sake of completeness. Lumped mass or bead model was initially used by Kalaghan et al. [16] at Smithsonian Astrophysical Observatory (SAO) to study the dynamics of TSS. Elasticity and material damping of the tether were taken into account through massless tether segments which were assumed to be longitudinal spring-dashpot systems. A weakness of this approach is the large number of beads required for simulation. However unlike linear continuum models, large lateral deformation could be easily handled. Lang [41] has used a bead model to develop GTOSS, a general software for tethered systems. The software has the capability of handling several tethers and end-bodies. Netzer and Kane [42] used a bead model to study the librational dynamics. They did not, however, consider tether elasticity in their study.

Recently Kim and Vadali [30] studied the tether dynamics using a bead model and compared the results with those obtained from a linear and a nonlinear continuum models. Unlike the Kalaghan et al. [16] model, which measured the position vectors from the centre of the Earth, they measured the position of a bead relative to the centre of mass of the orbiting system. They considered revolute joints between the masses and springs and used spherical coordinate systems to represent the position vector between any two adjacent masses. The equations of motion were obtained using the Newtonian approach. There have been other investigations of tether satellite systems that have used bead models. Some examples are the studies by Quadrelli and Lorenzini [37], No and Cochran [35, 36]. It may be pointed out that all the bead models cited above were for systems in which the tether had no rotation about its nominal axis; however, except Netzer and Kane [42], all considered variable length.

Discretizing the tether into a series of rod elements, Puig-Suari and Longuski [43] modelled the lateral motion of the tether. The mass density of the rods was assumed to be uniform and Lagrange's equations were used to derive the equations of motion. Although the discretization allowed for any configuration of the tether, the elastic behaviour of the tether was not captured because the strain energy was not included in the formulation. Banerjee [44] discretized the tether into a series of beam elements connected by rotational springs to study deployment of tethers. The model could account for large bending and rotation, but no axial extension. Finite element method, which is usually used for two or three dimensional structures with irregular geometry, was used by Kohler et al. [20] to discretize the tether. For uniaxial structures with uniform geometry such as tethers, the advantage of this method is debatable.

1.4 Literature Review on Effects of Aerodynamic Forces

The major external forces on any TSS are the gravitational force, solar radiation pressure, aerodynamic forces and electrodynamic forces; depending on the position of the system one of them may have a dominant effect. A subsatellite may be deployed into the upper atmosphere from the Shuttle using a very long tether. At this altitude the aerodynamic forces are significantly large compared to the other external forces, even gravity gradient, and affects the overall dynamics and control of the system substantially.

Normally the station-keeping phase is stable (at least, marginally stable) and the effects of the aerodynamic forces had been presumed to provide damping and hence enhance the stability. However, Beletsky and Levin [28] contended that in-plane swinging motion can become unstable due to the combined effects of air drag gradient, attitude motion, and elasticity of the tether; but they gave no details. Onada and Watanabe [15] studied the effect of atmospheric density gradient on the stability and control of tethered subsatellite systems analytically, using a fairly simple model for dynamics and aerodynamics of the subsatellite. They have shown that the uncontrolled motion of a spherical subsatellite deployed into a region where the effect of the atmosphere is significant, can be unstable due to the combined effects of the tether stiffness and atmospheric density gradient. Matteis et al. [29] considered the material damping in the tether and carried out a parametric study of the equilibrium configuration and stability of a tethered subsatellite system.

In the works described above, a very simple model was used in which only the aerodynamic drag on the subsatellite was taken into account. Thus there was no examination of the effects of the aerodynamic force on the tether as well as of the aerodynamic lift on the subsatellite. The latter was ignored because the subsatellite usually was assumed to be a sphere on which the aerodynamic lift is zero. Pasca and Lorenzini [27] studied the equilibrium configuration of the system in the presence of atmospheric forces. They considered the aerodynamic force on the tether as well as the aerodynamic drag on both the subsatellite and the main-satellite, but not the aerodynamic lift on the end-bodies. No and Cochran [35, 36] used a more complete model for aerodynamics and dynamics of the system, which can handle non-spherical bodies, to study the dynamics and stability of an orbiter-tether-maneuverable subsatellite system. They used this model to control the system in the station-keeping phase using an aerodynamic control. However they did not specifically examine in their study the role played by the different components of the aerodynamic force (lift and drag) in the uncontrolled motion. In the existing literature, study of the effects of the subsatellite aerodynamic lift on the equilibrium configuration and stability of the uncontrolled system is missing.

There are other researchers (Bainum et al. [40], Kalaghan et al. [16], and Xu [22], Kim and Vadali [45]) who considered aerodynamic forces in their study, but they made no systematic analysis of the effects of these forces on the stability of the system. Even in the numerical simulation of the dynamics of the system, they used a rather simple aerodynamical model for the subsatellite.

1.5 Literature Review on Control Schemes

Because of the complicated dynamics of tethered satellite systems, their control is a challenging problem, especially during deployment and retrieval phases. Control of the system in the retrieval phase is much more difficult, since the system is inherently unstable in this phase. Various control schemes have been proposed by the researchers from the very beginning of the tethered satellite application proposals, i.e. , since 1970's. Based on the nature of the control schemes implemented, they can be basically categorized into five types:

(i) Tension control laws

(ii) Length or reel rate control laws

(ii) Thruster augmented control laws

(iv) Offset control laws

(v) Aerodynamic control laws

These are reviewed briefly. The control schemes can also be categorized based on other criteria, such as the design methodology like linear or nonlinear control synthesis.

1.5.1 Tension Control Laws

In tension control laws, the tension in the tether is modulated using an appropriate feedback of the generalized coordinates and/or their derivatives. This method was the first to be proposed to control tethered satellite systems; therefore a fairly rich literature can be found on this control law, among which is the pioneering work of Rupp [13]. In Rupp's control law the tension in the tether is modulated as a function of the command length ℓ_c, actual length ℓ and its time derivative $\dot{\ell}$:

$$T = k_1\ell + k_2\dot{\ell} + k_3\ell_c \ .$$

He applied this control scheme to the in-plane motion of a two-body tethered system. Baker et al. [14] modified the above law to improve the performance. Instead of an arbitrary command length, they used a function of actual length as command length, i.e.:

$$\ell_c = a_1\ell + a_2 \ .$$

Bainum and Kumar [17] applied linear optimal control theory to devise a tension law based on the feedback of the tether length, length rate, in-plane pitch angle and its rate. The control strategy was very effective during deployment, but was not so successful during retrieval. Modi et al. [46] showed that out-of-plane librational motion can grow up to 45°, while using the above control scheme. They thus proposed a modified control law that includes the additional nonlinear feedback of the out-of-plane tether angular rate. The pitch motion was damped out while the roll was bounded to a limit cycle of about 10° amplitude through this control.

During retrieval, not only rotations but also vibrations increase gradually. If the dynamical model consists of rotational motion and longitudinal oscillations only, the system is controllable using the above mentioned feedback. However, if transverse vibrations are also modeled, the system is no longer stable. To control vibrations, Xu [22] extended the work of Modi et al. [46] by feeding back a linear combination of in-plane coordinates and nonlinear combination of out-of-plane coordinates (including librational and vibrational motions).

The above mentioned tension control law require a feed-forward length command that must be chosen carefully for proper operation of the control system. The design methodology was not based on stability consideration of the nonlinear system, therefore the final state may be critically affected by the initial conditions. The tension control law can also be obtained based on the Lyapunov approach (or related mission function approach). It was first implemented for the design of deployment/retrieval control law by Fujii and Ishijima [47]. Using a similar model and similar approach Vadali and Kim [48] introduced a different tension control law. Later they applied the Lyapunov approach to a more realistic model of the system which included mass of the tether. These works are reviewed in more detail in Chapter 7.

1.5.2 Length or Reel Rate Control Laws

An alternative to the tension control laws is the length or reel rate control laws. As opposed to the tension control laws, in the reel rate control laws the nominal length of the unstretched tether or its time derivatives are modulated using feedback of the state variables. This is equivalent to specifying the rotational speed of the drum or reel mechanism.

Kohler et al. [20] originally proposed this concept. Misra and Modi [49] proposed the general form of this control law to study the planar motion of two-body tethered satellite systems in the presence of longitudinal and transverse oscillations. It was shown that the rotations during retrieval could be bounded, while both transverse and longitudinal vibrations grew, when the length rate involved only linear feedback pitch rate. This suggests that feedback of vibrations is necessary for successful retrieval. Xu [22] applied this idea and compared the results with those obtained using tension control laws. He concluded that reel rate control laws have basically similar performance as tension control laws.

Similar to the tension control laws, the Lyapunov approach was used by Vadali and Kim [48] and Monshi et al. [50] to obtain various reel rate laws for two-body tethered systems.

1.5.3 Thruster Control Laws

Tension control laws or length rate control laws are unreliable during the terminal stage of retrieval when the equilibrium tension becomes very small because of small length of the tether. The tension might even become zero (slack tether) due to longitudinal oscillations. To alleviate this difficulty, Banerjee and Kane [32] proposed to use a set of thrusters (in addition to a torque control law) to control the retrieval dynamics. In addition to the tether-aligned thrusters to augment the natural tension, they also proposed the use of transverse thrusters to stabilize the attitude motion and speed up the retrieval process. In this scheme the in-line thrusters fired when the tension was below 2 N and an appropriate transverse thruster was fired when pitch and roll angles grew beyond certain limit.

Xu et al. [33] considered control of both rotations and vibrations during retrieval using a set of three thrusters. They used linear feedback of rotational and vibrational rates to modulate the thrusters. Because of the unavailability of attitude motion information in the first TSS mission, Lorenzini et al. [51] proposed a simpler thruster control scheme.

Thruster control laws have been used by other researchers, like Kim and Vadali [45] and Fleurisson et al. [52], in conjunction with the other control schemes to obtain a better performance during the transition period, when the length of the tether is small.

1.5.4 Offset Control Laws

When the tether is short and the subsatellite is in the vicinity of the Space-Station or the mother spacecraft, thruster firings are not allowed due to safety reasons. On the other hand, tension control laws or reel rate control laws are ineffective during this terminal stage. Because of these difficulties offset control laws have been proposed recently as an alternative to the thruster controller by Lakshmanan et al. [53]. This control law functions generally by changing the offset of the point of attachment of the tether to the main-satellite, which must not be treated as a point mass any more. In their dynamical model, Lakshmanan et al. [53] considered the attitude motion of the main-satellite, which was modelled as a platform, as well as the tether. Although they considered mass of the tether, their model did not account for the flexibility of the tether. Controllability of the linearized equations was established and a comparative study of three different control strategies, tension control law, thruster control law, and offset control law, was conducted. They found that the offset controller requires more time to reach a steady state position compared to the other control laws. However, it is likely to improve as the tether length diminishes. Later on, Modi et al. [54, 55] validated the mathematical model aimed at studying the offset control law by a ground based experimental facility.

Pradhan et al. [56] included the flexibility of the tether in the modelling and studied the dynamics and control of tethered satellite systems in the presence of offsets. The system consisted of a rigid platform from which a point mass subsatellite could be deployed or retrieved by a flexible tether, and was undergoing planar motion in a Keplerian orbit. They observed that the control of only the rigid degrees of freedom is not sufficient as the flexible dynamics of the tether becomes unstable during retrieval. The offset control strategy was found to be effective if a passive damper was added to reduce the tether oscillations.

Basically the offset control technique is similar to the act of balancing a rod on the palm of one's hand. As can be expected, for a given angular disturbance the motion of the tether would grow proportional to the length of the tether. Hence this control procedure is most effective when the length of the tether is small.

1.5.5 Aerodynamic Control Laws

In a recent study of the effect of atmosphere on the dynamics of a tethered satellite system, No and Cochran [35] proposed using an aerodynamic control law to damp out the librational motion and longitudinal oscillations of the tether. They developed the control law using the numerically linearized equations of motion and the LQR method. They compared the performance of this control law with a thruster control law for a system in the station-keeping phase. They concluded that the aerodynamic control yields results comparable to those obtained by using reaction thrusters and torquers.

1.6 Literature Review on Dynamics and Control of Multi-Tether Systems

Study of multi-body tethered satellite systems started with the work of Liu [57] in 1985. He formulated the dynamics of three-body tethered systems. The tethers were assumed to be straight and massless. Even though he considered only the in-plane motion of a cargo transportation system, the equations of motion were very complicated. This was because of his selection of coordinates which happened to be subjected to constraints. Pointing out this complexity, he did not present any numerical results for his set of combined algebraic and differential equations.

Lorenzini [58] analyzed the dynamics of a proposed system for performing micro-gravity experiments in which the g-laboratory was tethered to the Space-Station. In 1987, the same author discussed the control strategies for deployment of the system and for damping out the oscillations in the station-keeping phase [59]. The system considered was a three-body tethered system consisting of the Space-Station, the micro-g/variable-g laboratory and another scientific platform. The g-laboratory was in between the other two bodies and crawled along a 10-km-long, 2-mm-diameter kevlar tether. The analysis was concentrated on the in-plane motion. The tethers were assumed to be massless, but their longitudinal vibrations were considered. Two mathematical models were used, one using the Lagrangian approach and the other Newtonian.

In 1987, Misra, Amier and Modi [60] used the Lagrangian approach to analyze the in-plane motion of three-body systems for fixed-length as well as variable-length tethers. The coordinates used were different from those of Lorenzini. The tethers were assumed to have negligible mass. In the case of fixed length tethers, they found three equilibrium configurations, but the equilibrium along the local vertical was found to be the only stable one. Frequencies of librational motion about the stable equilibrium configuration were calculated. The variable-length case included deployment of a constellation as well as cargo transportation. Among the results, the most significant one was the observation that large librations could occur in the cargo transportation case when the length of one of the tethers became small.

The four-mass tethered system of the Space-Station-based Elevator/Crawler micro- and variable gravity facility, consisting of two platforms, the Space-Station, and an elevator, was studied by Lorenzini et al. [61] and by Cosmo et al. [62]. The former study mainly calculated the accelerations and the g-levels of the Space-Station and the Elevator. The latter analysis considered the dynamics and control of two-dimensional motion of the system. The degrees of freedom included lengths of the tethers, longitudinal elastic oscillations and in-plane lateral deflections (these are the lateral deflections of the point masses not the lateral *elastic* vibrations of the tethers). They formulated the problem with the Lagrangian approach and found the eigenvalues and eigenvectors of the system. It was noticed that the longitudinal oscillations are strongly coupled to the in-plane librational and lateral motions.

All the bodies connected by the tethers were modelled as point masses in all of the above-mentioned studies. On the other hand, Bachmann et al. [63] included the rigid body rotational motion of the Space-Station in a three body Space-Station-based Tethered Elevator system; they also considered the offset of the tether attachment point from the Station center of mass. The equations of motion were derived using the Lagrangian approach. Tethers were assumed massless and longitudinally elastic in the formulation stage, but rigid in numerical computations.

None of the above studies on multi-tethered systems considered transverse oscillations of the tethers. Kumar et al. [64] conducted a fairly basic study of the in-plane transverse oscillations of a three-body, two-tethered system in a circular orbit. They did not, however, include the longitudinal oscillations of the tethers in their model.

From the Lagrangian of the system, they obtained the linearized equations of motion. The resulting equations were used to analyze the librational as well as transverse elastic motions of the tethers in the vicinity of the stable equilibrium configuration. They obtained no nonlinear equations of the system and their study was restricted to the station-keeping phase.

Misra and Modi [65] formulated the general three-dimensional dynamics of N-body tethered systems using a multiple-pendulum model. The tethers were again assumed to be massless and rigid. The equations obtained were valid for large motion as well as for variable-length tethers and for any arbitrary orbit. A study on the librational frequencies was carried out by considering small motion in the neighborhood of the local vertical equilibrium configuration for the special case of a circular orbit.

It is clear that in the available literature there has been no dynamical modelling of multi-body tethered satellite systems that considers the transverse as well as the longitudinal elastic oscillations; this is true even for a three-body tethered system.

1.7 Purpose and Scope of the Thesis

Although one can find a rich body of literature on the dynamics and control of tethered satellite systems, it is clear from the literature review above that dynamics and control of *multi-tethered* systems is in an early development stage. Most of the investigations dealt with the librational motion of multi-body systems. Only two or three studies considered the longitudinal or transverse oscillations of the tethers for three or four-body systems, but none considered both oscillations simultaneously.

Hence, the goal of this thesis is aimed at developing a general formulation of the dynamics and control of N-body tethered satellite systems that considers librations as well as three dimensional elastic oscillations. From the control point of view, there are very few investigations dealing with control of a multi-tethered system and none of these was based on stability consideration of nonlinear systems such as Lyapunov's approach. The thesis attempts to fill this gap.

In the existing studies on the effects of the atmosphere on the stability and dynamics of a tethered satellite system, usually simple aerodynamic models which consider only the aerodynamic drag on the subsatellite, and occasionally the drag on the tether, have been used so far. No study has been conducted to analyze the effect of aerodynamic lift on the stability of the system. This is done systematically in the thesis.

1.8 Outline of the Thesis

This thesis may be divided into two parts. The first part presents a general dynamical model of N-body tethered satellite systems and develops the nonlinear as well as the linearized equations governing the motion of the system, while the second part deals with the study of the effect of aerodynamic forces on the dynamics and stability of the system as well as development of a tension control law based on the Lyapunov approach.

In Chapter 2, the dynamical model is developed taking into account:

(i) three dimensional librations;

(ii) mass of the tethers;

(iii) longitudinal vibrations including variation of the longitudinal strain along the tethers;

(iv) three dimensional transverse vibrations;

(v) aerodynamic forces in a rotating atmosphere considering the oblateness of the Earth;

(vi) geometric nonlinearity, i.e., nonlinear relation between strain and displacement, which becomes important for short tethers.

The continuous tethers are discretized using the assumed modes method and then equations governing the motion of the system are derived using Lagrange's equations. The set of ordinary differential equations is given in explicit form.

The generalized forces resulting from the aerodynamic forces acting on the end-bodies and the tethers as well as those due to the material damping in the tethers are discussed in Chapter 3. Free molecular flow model is used to calculate the aerodynamic forces in the upper atmosphere. After examining various approaches to model the material damping of the tethers, a viscous damping model is chosen to evaluate the effect of material damping on the dynamics and stability of multi-body tethered satellite systems.

In Chapter 4, the nonlinear equations of motion are initially transformed into vector form. Possible equilibrium configurations of the system are then determined. Static equilibrium equations of the system in the absence of external forces are solved in a closed form. Equations of motion are linearized analytically about any equilibrium configuration of the system. The linearized equations are given at the end.

Natural frequencies of vibrational as well as librational motion of different multi-body systems are presented in Chapter 5. The idea of a segmented-tether model is presented to obtain the higher frequencies of the system. Then the dynamics of a Tether Elevator/Crawler System (TECS) is studied for various scenarios, and simulation results are presented.

In Chapter 6, stability of low orbit systems, which is affected by aerodynamic forces is studied. A qualitative study of the effect of aerodynamic forces, particularly of the aerodynamic lift, is conducted through eigenvalue analysis of the linearized equations of motion of a single-tether system. Stabilization of the system using aerodynamic panels is analyzed by considering a specific geometrical configuration for the subsatellite; a sphere with attached panels. The analysis is then extended to the case of multi-tether systems.

Control of the nonlinear dynamics of multi-body systems using Lyapunov's stability theory is considered in Chapter 7. Because of the complexity of the system and difficulties associated with applying Lyapunov's direct method, the transverse oscillations of the tethers are ignored and only the longitudinal oscillations are modelled.

Some closing comments and suggestions for further work are given in Chapter 8.

Chapter 2

EQUATIONS OF MOTION

2.1 Introductory Remarks

In reality all dynamical systems are distributed-parameter systems, i.e. the parameters describing the system properties are distributed spatially. However, in the modelling process some of them are modeled as discrete systems in the very first step, while the others are modeled as distributed-parameter systems. Dynamics of a discrete model is described by ordinary differential equations, in contrast to a distributed-parameter model which is governed by partial or hybrid partial-ordinary differential equations.

There are different approaches to derive the governing equations (ordinary or partial differential equations). They can be divided into two major categories: vectorial and analytical approaches. In a vectorial approach, individual components of the system are considered; thus the calculation of internal forces resulting from kinematical constraints is necessary. In fact, this is the main drawback of this approach as far as the dynamical formulation is concerned. However, it has some advantage in the design stage. Newton's approach is a well known example of the vectorial approach. Analytical approach, on the other hand, considers the system as a whole and formulates the problems of mechanics in terms of the kinetic energy, the potential energy, and the virtual work associated with nonconservative forces. In contrast to vectorial mechanics, this approach formulates the problem using generalized coordinates and forces, which are not necessarily physical coordinates and forces. One may name the extended Hamilton's principle, and Lagrange's method belonging to this class of approach.

All of the methods mentioned above can be used to derive the equations of motion of a discrete system. To derive the partial differential equations governing the dynamics of a distributed system, one must use either Newton's equations or the extended Hamilton's principle. There is some ambiguity regarding using analytical methods for a system of variable mass (Ref. [66]). It is addressed in more detail in Appendix F.

Since, except for some simple classical examples, there is no closed-form solution for distributed parameter systems, one has to obtain an approximate solution by means of spatial discretization. Discretization essentially transforms a problem described by partial or partial-ordinary differential equations into a problem expressed by a set of ordinary differential equations. Discretization methods are divided into two major classes; the first represents the solution as a finite series consisting of space-dependent functions multiplied by time dependent generalized coordinates, while the second divides the continuous element, say a tether, into a number of segments. The first method is more analytical in nature while the second is more intuitive in character.

Among the discretization methods based on series expansions, *assumed modes method* and *Galerkin's method* [67] are very well known and most often used methods. The former is an energy based method, while the latter minimizes a weighted residual based on the hybrid partial differential equations of motion. In the assumed modes method, discretization starts once the energy expressions of the system are derived. Hence, in this method a set of admissible functions, which are differentiable half as many times as the order of the system and satisfy only the geometric boundary conditions of the problem, is used to discretize the continuous elements of the system. In Galerkin's method discretization process follows derivation of the equations of motion and boundary conditions. Thus, instead of admissible functions one has to use a set of comparison functions, which are differentiable as many times as the order of the system and satisfy all boundary conditions of the problem, for discretization purpose. In fact this is a drawback of the second method to discretize a complex system . Moreover, generally, it is difficult to obtain a set of comparison functions for a rather complex system.

There are other issues such as geometry, computational objective, etc. which must be considered in selecting a certain approach to derive the equations of motion and an appropriate approach to discretize the continuous system. Their discussion is beyond the scope of this thesis. The interested reader is referred to [67].

In this Chapter, kinematics of the system is considered first; this is followed by the derivation of energy expressions of the system. The assumed modes method is used to discretize the continuous tethers. Ordinary differential equations describing the dynamical behaviour of the system are derived next using Lagrange's equations applicable for discrete systems.

2.2 System Description

The system under consideration is shown in Figs. 2.1 and 2.2 . Figure 2.1 shows the geometry associated with the orbital motion. The centre of mass of the system, C, can be located with respect to the centre of the Earth E , by the radial distance R_c, the inclination angle i of the orbital plane to the equatorial plane, the argument of the perigee θ_0, and the true anomaly θ_c. Figure 2.2 shows the overall system in some detail. It consists of N bodies connected by $N-1$ tethers. The former, i.e. the end-bodies, have masses $m_i, i = 1, 2, \ldots, N$, while the tethers have masses $\rho_i, i = 1, 2, \ldots, N-1$, per unit length. Note that m_i is the mass of body i including the unreeled tether located on it. The mass of tether i is given by $\bar{m}_i = \rho_i \ell_i$. The i-th tether, with undeformed length, ℓ_i, connects bodies i and $i+1$, and the tethers make an open chain configuration. To have a more general model and include systems with crawlers, it is assumed that every tether is reeled partially by the corresponding end-bodies. Tether i is reeled out at a rate of $\rho_i \alpha_i \dot{\ell}_i$ from body i and reeled in at a rate of $\rho_i \beta_i \dot{\ell}_i$ to body $i+1$. It follows that the rate of change of mass of body i is given by

$$\dot{m}_i = \rho_{i-1}\beta_{i-1}\dot{\ell}_{i-1} - \rho_i \alpha_i \dot{\ell}_i \quad , \tag{2.1}$$

while

$$\alpha_i - \beta_i = 1 \quad . \tag{2.2}$$

Dimensionless coefficients α_i and β_i can be either positive or negative and in general, they are functions of time.

Coordinate systems, X_I, Y_I, Z_I , X_c, Y_c, Z_c and x_i, y_i, z_i are introduced to describe the motion. The last two coordinate systems are rotating coordinate systems, while the first is an inertial system having its origin at the centre of the Earth. The set of coordinates axes X_c, Y_c, and Z_c, the *orbital frame*, has its origin at the centre of mass C of the system and is so oriented that X_c-axis coincides with the local vertical, directed radially outwards from the centre of the Earth to the centre of mass, Z_c-axis is along the orbit normal, and Y_c-axis completes the triad. The unit vectors $\hat{\mathbf{i}}_c, \hat{\mathbf{j}}_c$, and $\hat{\mathbf{k}}_c$ are along the X_c, Y_c, and Z_c axes, respectively. The set of coordinate axes x_i, y_i, and z_i which is called the *tether frame* corresponding to the i-th tether, is located at the i-th body such that x_i is along the nominal tetherline of the i-th tether directed from body i to body $i+1$. The orientation of these axes with respect to the orbital coordinate system can be defined by only two rotations θ_i and ϕ_i, implying an assumption that the rotation about the axis of the tether is negligible. At first, the rotation θ_i is given about the Z_c-axis resulting in x_i', y_i', z_i' axes and then the rotation ϕ_i is applied about the negative y_i'-axis yielding axes x_i, y_i, and z_i. θ_i is called the pitch angle, while ϕ_i is the roll angle corresponding to the i-th tether. Hence, the transformation relating the unit vectors along X_c, Y_c, Z_c and x_i, y_i, z_i axes can be expressed as

$$\begin{Bmatrix} \hat{\mathbf{i}}_i \\ \hat{\mathbf{j}}_i \\ \hat{\mathbf{k}}_i \end{Bmatrix} = \begin{bmatrix} \cos\phi_i & 0 & \sin\phi_i \\ 0 & 1 & 0 \\ -\sin\phi_i & 0 & \cos\phi_i \end{bmatrix} \begin{bmatrix} \cos\theta_i & \sin\theta_i & 0 \\ -\sin\theta_i & \cos\theta_i & 0 \\ 0 & 0 & 1 \end{bmatrix} \begin{Bmatrix} \hat{\mathbf{i}}_c \\ \hat{\mathbf{j}}_c \\ \hat{\mathbf{k}}_c \end{Bmatrix}$$

$$= \begin{bmatrix} \cos\theta_i\cos\phi_i & \sin\theta_i\cos\phi_i & \sin\phi_i \\ -\sin\theta_i & \cos\theta_i & 0 \\ -\cos\theta_i\sin\phi_i & -\sin\theta_i\sin\phi_i & \cos\phi_i \end{bmatrix} \begin{Bmatrix} \hat{\mathbf{i}}_c \\ \hat{\mathbf{j}}_c \\ \hat{\mathbf{k}}_c \end{Bmatrix} . \tag{2.3}$$

The unit vectors $\hat{\mathbf{i}}_i, \hat{\mathbf{j}}_i$, and $\hat{\mathbf{k}}_i$ are along x_i, y_i, and z_i axes, respectively.

Since the tethers are very long and thin, their flexibility is taken into account. They have longitudinal as well as transverse displacements excited by the gravity gradient, atmospheric forces, Coriolis forces during deployment or retrieval, and other external forces. The transverse vibrational displacements along y_i and z_i (in and perpendicular to the tether plane, formed by the X_c and x_i axes, respectively) are denoted by v_i and w_i, while the longitudinal vibrational displacement is represented by u_i. These displacements are functions of both time as well as the spatial coordinate x_i and together with the rigid displacement form the position vector $\vec{\mathbf{r}}_{\mathbf{t}_i}$, which will be described later.

One must distinguish between the undeformed and deformed tether length. Here ℓ_i (associated with the "material coordinate") denotes the length of the undeformed tether, while ℓ_i^* is the length of the deformed tether, connecting the i-th body to body $i+1$, measured along the curved tetherline. Obviously, if there is no transverse vibration in the tether, ℓ_i^* will be measured along a straight line, called the ***nominal tetherline***, but it is still not equal to ℓ_i, since there is a longitudinal strain in the tether.

For given θ_i and ϕ_i, the line connecting the two ends of tether i, the tetherline, can be defined uniquely with respect to the orbital frame X_c, Y_c, Z_c: with u_i, v_i, and w_i the position of an element of the tether can be determined uniquely with respect to this line. Since u_i, v_i, and w_i are measured from the already rotated tetherline, the small elastic displacement assumption would be reasonable, although the formulation presented here is valid for moderately large elastic deformation as well.

The motion of the system can be divided into three components:

1. The entire system rotates around the Earth (orbital dynamics);
2. The system rotates around the centre of mass of the system (librational dynamics);
3. The tethers vibrate longitudinally and transversely (structural dynamics).

These three types of motion are coupled to each other. The last two motions affect the first (orbital motion) only slightly [12]. Hence it is assumed that the orbit could be calculated separately without any significant loss of accuracy. The orbit is assumed here to be Keplerian. Obviously the librational and vibrational motions are affected by the orbital motion and are more complicated.

2.3 Basic Assumptions

To introduce the dynamical model, some reasonable assumptions based on the physical insight to the problem are necessary. Without such assumptions the mathematical model becomes very complicated. However, if the assumptions are not quite correct or they are too simplifying the mathematical model will not represent the real situation. For example, in the very early stage of research on this subject, some investigators neglected the out-of-plane rotation of the system and vibrations of the tether. Corresponding mathematical models of the system are oversimplified and do not describe the dynamics of the real system very well. The most important thing is to grasp the significant factors and eliminate the trivial ones.

The following assumptions are made in this thesis to obtain a reasonable model of the system:

(i) The centre of mass, C, is assumed to be moving in an Keplerian orbit around the Earth.

(ii) Orbital motion is assumed to be unaffected by the librational motions and vibrations of the tethers. This allows separate analysis of the orbital motion.

(iii) Since the sizes of the bodies are much smaller than the lengths of the tethers, they are regarded as point masses so that their attitude motion can be neglected. When the tethers are very short during the terminal phase of retrieval or initial phase of deployment, the assumption is not valid; however, it holds good for the major part of the mission. The finite size of the bodies, of course, is taken into account in calculating the aerodynamic forces.

(iv) It is assumed that most of the unreeled part of the tethers have negligible relative velocity with respect to the bodies in which they are located. The velocity change takes place smoothly in a small portion of the tethers such that no energy is dissipated in this process. It is also assumed that the reel inertia is negligible and the role played by reel dynamics is insignificant.

(v) It is assumed that the atmosphere rotates with the Earth, and the air density varies exponentially with altitude.

(vi) The tethers are assumed to be linearly elastic and have no bending resistance.

(vii) Vibrations of the tethers are small in amplitude compared to their instantaneous length. In spite of this assumption, the nonlinearity in the strain displacement relation is taken into account; the reason will be given later.

(viii) It is assumed that the system is in the gravity field of the Earth. The gravitational perturbing forces due to the attraction of the Sun and the Moon are ignored. The effect of asphericity of the Earth on its gravity field is ignored as well.

2.4 Kinematics of the System

2.4.1 Displacements

Let us denote the position vector of the centre of mass of body i by $\vec{\mathbf{R}}_i, i = 1,2,\ldots,N$, and that of an arbitrary point on the i-th tether by $\vec{\mathbf{R}}_{t_i}, i = 1,2,\ldots,N-1$, with respect to the centre of mass of the entire system, C (Fig. 2.3). These position vectors can be expressed in terms of the rotations θ_i, ϕ_i, lengths ℓ_i and vibrational displacements u_i, v_i, and $w_i, i = 1,2,\ldots,N-1$, of the tethers. Since C is the centre of mass of the system, we can write

$$\sum_{i=1}^{N} m_i\vec{\mathbf{R}}_i + \sum_{i=1}^{N-1} \rho_i \int_0^{\ell_i} \vec{\mathbf{R}}_{t_i}\, dx_i \;= \vec{\mathbf{0}} \;. \tag{2.4}$$

Now let us define $\vec{\mathbf{r}}_i$ and $\vec{\mathbf{r}}_{t_i}$ as the position vector of the center of mass of body $i+1$ and that of any arbitrary point on the i-th tether, with respect to body i (Fig. 2.3). From the geometry of the system we have

$$\begin{aligned}
\vec{\mathbf{R}}_i &= \vec{\mathbf{R}}_{i-1} + \vec{\mathbf{r}}_{i-1} = \vec{\mathbf{R}}_1 + \sum_{j=1}^{i-1}\vec{\mathbf{r}}_j \;, \\
\vec{\mathbf{R}}_{t_i} &= \vec{\mathbf{R}}_i + \vec{\mathbf{r}}_{t_i} = \vec{\mathbf{R}}_1 + \sum_{j=1}^{i-1}\vec{\mathbf{r}}_j + \vec{\mathbf{r}}_{t_i} \;.
\end{aligned} \tag{2.5}$$

Substituting Eq. (2.5) into Eq. (2.4) and solving for $\vec{\mathbf{R}}_1$ we obtain

$$\vec{\mathbf{R}}_1 = -\sum_{i=1}^{N}\frac{m_i}{m}\left(\sum_{j=1}^{i-1}\vec{\mathbf{r}}_j\right) - \sum_{i=1}^{N-1}\frac{\bar{m}_i}{m}\left(\sum_{j=1}^{i-1}\vec{\mathbf{r}}_j\right) - \sum_{i=1}^{N-1}\frac{\rho_i}{m}\int_0^{\ell_i}\vec{\mathbf{r}}_{t_i}\, dx_i \;, \tag{2.6}$$

where $\bar{m}_i$ and m denote mass of the i-th tether and total mass of the system, respectively. Defining $\mu_i = \dfrac{m_i + \bar{m}_i}{m}$, $\bar{\mu}_i = \dfrac{\rho_i \ell_0}{m}$, and

$$\vec{\mathbf{b}}_i = \frac{1}{\ell_0}\int_0^{\ell_i}\vec{\mathbf{r}}_{t_i} dx_i \;, \tag{2.7}$$

where ℓ_0 is a reference length, we can simplify Eq. (2.6) to

$$\vec{\mathbf{R}}_1 = -\sum_{i=1}^{N} \mu_i \left(\sum_{j=1}^{i-1} \vec{\mathbf{r}}_j \right) - \sum_{i=1}^{N-1} \bar{\mu}_i \vec{\mathbf{b}}_i \quad , \tag{2.8}$$

with the understanding that $\bar{m}_N = 0$ (there is no N-th tether). Using the Heaviside function

$$H(a-b) = \begin{cases} 0 & \text{if} \quad b > a \; , \\ 1 & \text{if} \quad b \leq a \; , \end{cases} \tag{2.9}$$

one can rewrite $\vec{\mathbf{R}}_1$ as

$$\vec{\mathbf{R}}_1 = -\sum_{i=1}^{N} \mu_i \left(\sum_{j=1}^{N-1} H(i-j-1) \vec{\mathbf{r}}_j \right) - \sum_{i=1}^{N-1} \bar{\mu}_i \vec{\mathbf{b}}_i \quad . \tag{2.10}$$

If we interchange the sequence of summation over i and j in the first term and change the index i to j in the second term , we will have

$$\vec{\mathbf{R}}_1 = \sum_{j=1}^{N-1} \left[- \left(\sum_{i=1}^{N} \mu_i H(i-j-1) \right) \vec{\mathbf{r}}_j - \bar{\mu}_j \vec{\mathbf{b}}_j \right] \quad . \tag{2.11}$$

Back substituting Eq. (2.11) in Eq. (2.5) leads to

$$\begin{aligned} \vec{\mathbf{R}}_k &= \sum_{j=1}^{N-1} \left[- \left(\sum_{i=1}^{N} \mu_i H(i-j-1) \right) \vec{\mathbf{r}}_j - \bar{\mu}_j \vec{\mathbf{b}}_j \right] + \sum_{j=1}^{k-1} \vec{\mathbf{r}}_j \\ &= \sum_{j=1}^{N-1} \left[- \left(\sum_{i=1}^{N} \mu_i H(i-j-1) \right) \vec{\mathbf{r}}_j - \bar{\mu}_j \vec{\mathbf{b}}_j + H(k-j-1) \vec{\mathbf{r}}_j \right] \\ &= \sum_{j=1}^{N-1} \left[\left(H(k-j-1) - \sum_{i=1}^{N} \mu_i H(i-j-1) \right) \vec{\mathbf{r}}_j - \bar{\mu}_j \vec{\mathbf{b}}_j \right] \quad . \end{aligned} \tag{2.12}$$

Since $H(k-j-1) = 1 - H(j-k)$ and $\sum_{i=1}^{N} \mu_i = 1$ then

$$\begin{aligned} \vec{\mathbf{R}}_k &= \sum_{j=1}^{N-1} \left[\left\{ \left(\sum_{i=1}^{N} [1 - H(i-j-1)] \mu_i \right) - H(j-k) \right\} \vec{\mathbf{r}}_j - \bar{\mu}_j \vec{\mathbf{b}}_j \right] \\ &= \sum_{j=1}^{N-1} \left[\left\{ \left(\sum_{i=1}^{j} \mu_i \right) - H(j-k) \right\} \vec{\mathbf{r}}_j - \bar{\mu}_j \vec{\mathbf{b}}_j \right] \quad . \end{aligned} \tag{2.13}$$

Defining nondimensional mass coefficients

$$B_j = \sum_{i=1}^{j} \mu_i \quad , \qquad A_{kj} = B_j - H(j-k) \quad , \tag{2.14}$$

we obtain the important kinematic relation between the orbital frame position vectors $\vec{\mathbf{R}}_k, k = 1, 2, \ldots, N$, and the local position vectors $\vec{\mathbf{r}}_j$, $\vec{\mathbf{r}}_{t_j}$, $, j = 1, 2, \ldots, N-1$,

$$\vec{\mathbf{R}}_k = \sum_{j=1}^{N-1} \left(A_{kj}\vec{\mathbf{r}}_j - \bar{\mu}_j \vec{\mathbf{b}}_j \right) \quad , \tag{2.15}$$

where $\vec{\mathbf{b}}_j$ is as defined in Eq. (2.7). One may note that the mass coefficients B_j and A_{kj} are generally time dependent.

2.4.2 Velocities and Accelerations

Using Eq. (2.15) and the fact that $\dot{A}_{ij} = \dot{B}_j$ while $\bar{\mu}_j$ is a constant, the velocity and acceleration of the centre of mass of the i-th body with respect to the centre of mass of the system, C, can be shown to be

$$\begin{aligned} \dot{\vec{\mathbf{R}}}_i &= \sum_{j=1}^{N-1} \left(\dot{B}_j \vec{\mathbf{r}}_j + A_{ij}\dot{\vec{\mathbf{r}}}_j - \bar{\mu}_j \dot{\vec{\mathbf{b}}}_j \right) \quad , \\ \ddot{\vec{\mathbf{R}}}_i &= \sum_{j=1}^{N-1} \left(\ddot{B}_j \vec{\mathbf{r}}_j + 2\dot{B}_j \dot{\vec{\mathbf{r}}}_j + A_{ij}\ddot{\vec{\mathbf{r}}}_j - \bar{\mu}_j \ddot{\vec{\mathbf{b}}}_j \right) \quad , \end{aligned} \tag{2.16}$$

where

$$\dot{\vec{\mathbf{r}}}_j = \mathring{\vec{\mathbf{r}}}_j + \vec{\boldsymbol{\Omega}}_j \times \vec{\mathbf{r}}_j \quad , \qquad \dot{\vec{\mathbf{b}}}_j = \mathring{\vec{\mathbf{b}}}_j + \vec{\boldsymbol{\Omega}}_j \times \vec{\mathbf{b}}_j \quad , \tag{2.17}$$

and similar relations hold good for $\ddot{\vec{\mathbf{r}}}_j$ and $\ddot{\vec{\mathbf{b}}}_j$. Here $\mathring{(\ )}_j$ represents the time derivative of the vector $(\ )_j$ with respect to the j-th tether coordinate frame and $\vec{\boldsymbol{\Omega}}_j$ is the angular velocity of that frame with respect to the inertial frame. The components of $\vec{\boldsymbol{\Omega}}_j$ along x_j, y_j, z_j directions can be written in matrix form as follows:

$$\begin{aligned} \begin{Bmatrix} \Omega_{x_j} \\ \Omega_{y_j} \\ \Omega_{z_j} \end{Bmatrix} &= \begin{bmatrix} \cos\phi_j & 0 & \sin\phi_j \\ 0 & 1 & 0 \\ -\sin\phi_j & 0 & \cos\phi_j \end{bmatrix} \begin{bmatrix} \cos\theta_j & \sin\theta_j & 0 \\ -\sin\theta_j & \cos\theta_j & 0 \\ 0 & 0 & 1 \end{bmatrix} \begin{Bmatrix} 0 \\ 0 \\ \dot{\theta}_c + \dot{\theta}_j \end{Bmatrix} \\ &+ \begin{bmatrix} \cos\phi_j & 0 & \sin\phi_j \\ 0 & 1 & 0 \\ -\sin\phi_j & 0 & \cos\phi_j \end{bmatrix} \begin{Bmatrix} 0 \\ -\dot{\phi}_j \\ 0 \end{Bmatrix} = \begin{Bmatrix} (\dot{\theta}_c + \dot{\theta}_j)\sin\phi_j \\ -\dot{\phi}_j \\ (\dot{\theta}_c + \dot{\theta}_j)\cos\phi_j \end{Bmatrix} , \end{aligned} \tag{2.18}$$

where $\dot{\theta}_c$ is the orbital angular velocity of the centre of mass. In the vectorial form the angular velocity $\vec{\boldsymbol{\Omega}}_j$ can be written as

$$\vec{\boldsymbol{\Omega}}_j = \left(\dot{\theta}_c + \dot{\theta}_j\right)\sin\phi_j \hat{\mathbf{i}}_j - \dot{\phi}_j \hat{\mathbf{j}}_j + \left(\dot{\theta}_c + \dot{\theta}_j\right)\cos\phi_j \hat{\mathbf{k}}_j \quad . \tag{2.19}$$

Subsequently the velocity and acceleration of any arbitrary point of the i-th tether with respect to C are given by

$$\dot{\vec{\mathbf{R}}}_{t_i} = \dot{\vec{\mathbf{R}}}_i + \dot{\vec{\mathbf{r}}}_{t_i} \ , \qquad \ddot{\vec{\mathbf{R}}}_{t_i} = \ddot{\vec{\mathbf{R}}}_i + \ddot{\vec{\mathbf{r}}}_{t_i} \ , \tag{2.20}$$

where $\dot{\vec{\mathbf{r}}}_{t_i}$ is defined similar to $\dot{\vec{\mathbf{r}}}_i$ in Eq. (2.17)

2.5 Energy Expressions

2.5.1 Kinetic Energy of the System

The total kinetic energy of the system T consists of two parts, the kinetic energy of the bodies and that of the tethers. Each tether has two parts, the reeled and unreeled parts. Assuming zero velocity for the unreeled part with respect to the corresponding body and including its mass to the mass of the body, the kinetic energy of the system is expressed by

$$T = \sum_{i=1}^{N} \frac{1}{2} m_i \left(\dot{\vec{\mathbf{R}}}_c + \dot{\vec{\mathbf{R}}}_i\right) \cdot \left(\dot{\vec{\mathbf{R}}}_c + \dot{\vec{\mathbf{R}}}_i\right) + \sum_{i=1}^{N-1} \frac{1}{2} \rho_i \int_0^{\ell_i} \left(\dot{\vec{\mathbf{R}}}_c + \dot{\vec{\mathbf{R}}}_{t_i}\right) \cdot \left(\dot{\vec{\mathbf{R}}}_c + \dot{\vec{\mathbf{R}}}_{t_i}\right) dx_i \ , \tag{2.21}$$

where $\dot{\vec{\mathbf{R}}}_c$ is the velocity of the centre of mass of the system with respect to the centre of the Earth. Expanding the dot products and performing some algebra we obtain

$$\begin{aligned} T &= \frac{1}{2} m \dot{\vec{\mathbf{R}}}_c \cdot \dot{\vec{\mathbf{R}}}_c + \left[\sum_{i=1}^{N} m_i \dot{\vec{\mathbf{R}}}_i + \sum_{i=1}^{N-1} \rho_i \int_0^{\ell_i} \dot{\vec{\mathbf{R}}}_{t_i} dx_i\right] \cdot \dot{\vec{\mathbf{R}}}_c \\ &+ \sum_{i=1}^{N} \frac{1}{2} m_i \dot{\vec{\mathbf{R}}}_i \cdot \dot{\vec{\mathbf{R}}}_i + \sum_{i=1}^{N-1} \frac{1}{2} \rho_i \int_0^{\ell_i} \dot{\vec{\mathbf{R}}}_{t_i} \cdot \dot{\vec{\mathbf{R}}}_{t_i} dx_i \ . \end{aligned} \tag{2.22}$$

It is shown in Appendix C that the term inside the square brackets is equal to zero[1], i.e. ,

$$\sum_{i=1}^{N} m_i \dot{\vec{\mathbf{R}}}_i + \sum_{i=1}^{N-1} \rho_i \int_0^{\ell_i} \dot{\vec{\mathbf{R}}}_{t_i} dx_i = 0 \ . \tag{2.23}$$

Hence, the kinetic energy can be rewritten as

$$T = T_{orb} + T_{att} \ , \tag{2.24}$$

[1]Derivation of this result is not trivial since masses $m_i, i = 1, 2, \ldots, N$, as well as the integral limits are generally time dependent.

where

$$T_{orb} = \frac{1}{2} m \dot{\vec{\mathbf{R}}}_c \cdot \dot{\vec{\mathbf{R}}}_c \quad , \tag{2.25}$$

and

$$T_{att} = \sum_{i=1}^{N} \frac{1}{2} m_i \dot{\vec{\mathbf{R}}}_i \cdot \dot{\vec{\mathbf{R}}}_i \; + \; \sum_{i=1}^{N-1} \frac{1}{2} \rho_i \int_0^{\ell_i} \dot{\vec{\mathbf{R}}}_{\mathbf{t}_i} \cdot \dot{\vec{\mathbf{R}}}_{\mathbf{t}_i} \, dx_i \quad . \tag{2.26}$$

Here, T_{orb} is the orbital kinetic energy while T_{att} is the remaining part of the kinetic energy associated with attitude motion of the system and vibrations of the tethers. Usually T_{att} is much smaller than T_{orb} and does not affect the orbital motion. Hence the orbital motion may be calculated separately. T_{att} can be developed further. Substitution of $\dot{\vec{\mathbf{R}}}_{\mathbf{t}_i}$ from Eq. (2.20) into Eq. (2.26) results in

$$\begin{aligned} T_{att} &= \sum_{i=1}^{N} \frac{1}{2} m_i \dot{\vec{\mathbf{R}}}_i \cdot \dot{\vec{\mathbf{R}}}_i + \sum_{i=1}^{N-1} \frac{1}{2} \rho_i \int_0^{\ell_i} \left(\dot{\vec{\mathbf{R}}}_i + \dot{\vec{\mathbf{r}}}_{\mathbf{t}_i} \right) \cdot \left(\dot{\vec{\mathbf{R}}}_i + \dot{\vec{\mathbf{r}}}_{\mathbf{t}_i} \right) dx_i \\ &= \sum_{i=1}^{N} \frac{1}{2} (m_i + \bar{m}_i) \dot{\vec{\mathbf{R}}}_i \cdot \dot{\vec{\mathbf{R}}}_i + \sum_{i=1}^{N-1} \rho_i \dot{\vec{\mathbf{R}}}_i \cdot \int_0^{\ell_i} \dot{\vec{\mathbf{r}}}_{\mathbf{t}_i} dx_i + \sum_{i=1}^{N-1} \frac{1}{2} \rho_i \int_0^{\ell_i} \dot{\vec{\mathbf{r}}}_{\mathbf{t}_i} \cdot \dot{\vec{\mathbf{r}}}_{\mathbf{t}_i} dx_i \; , \end{aligned} \tag{2.27}$$

where as defined earlier, $\bar{m}_N = 0$.

Differentiating Eq. (2.7) with respect to time and using the result given in Appendix A, we have

$$\begin{aligned} \dot{\vec{\mathbf{b}}}_i = \frac{d}{dt} \left(\frac{1}{\ell_0} \int_0^{\ell_i} \vec{\mathbf{r}}_{\mathbf{t}_i} dx_i \right) &= \frac{1}{\ell_0} \left[\int_0^{\ell_i} \dot{\vec{\mathbf{r}}}_{\mathbf{t}_i} dx_i \; - \beta_i \dot{\ell}_i \vec{\mathbf{r}}_{\mathbf{t}_i}(\ell_i, t) + \alpha_i \dot{\ell}_i \vec{\mathbf{r}}_{\mathbf{t}_i}(0, t) \right] \\ &= \frac{1}{\ell_0} \left[\int_0^{\ell_i} \dot{\vec{\mathbf{r}}}_{\mathbf{t}_i} dx_i \; - \beta_i \dot{\ell}_i \vec{\mathbf{r}}_i \right] \quad , \end{aligned} \tag{2.28}$$

since $\vec{\mathbf{r}}_{\mathbf{t}_i}(\ell_i, t) = \vec{\mathbf{r}}_i$ and $\vec{\mathbf{r}}_{\mathbf{t}_i}(0, t) = \vec{\mathbf{0}}$. Note that $\dot{\vec{\mathbf{r}}}_{\mathbf{t}_i} = (\frac{\partial}{\partial t} + \dot{x}_i \frac{\partial}{\partial x_i}) \vec{\mathbf{r}}_{\mathbf{t}_i}$ taking into account the fact that the tether may be moving axially and therefore introducing a convective derivative term. Here $\frac{\partial}{\partial t}$ represents the partial derivative with respect to time in the inertial frame. Equation (2.28) implies that

$$\int_0^{\ell_i} \dot{\vec{\mathbf{r}}}_{\mathbf{t}_i} dx_i = \ell_0 \dot{\vec{\mathbf{b}}}_i + \beta_i \dot{\ell}_i \vec{\mathbf{r}}_i \quad . \tag{2.29}$$

Using Eq. (2.29) and substituting for $\dot{\vec{\mathbf{R}}}_i$ and $\hat{\rho}_i\beta_i\dot{\ell}_i$ from Eqs. (2.16) and (B.16) into Eq. (2.27) one obtains

$$
\begin{aligned}
T_{att} = m \Bigg\{ & \sum_{i=1}^{N} \frac{1}{2}\mu_i \left(\sum_{j=1}^{N-1} \dot{B}_j \vec{\mathbf{r}}_j + A_{ij}\dot{\vec{\mathbf{r}}}_j - \bar{\mu}_j \dot{\vec{\mathbf{b}}}_j \right) \cdot \left(\sum_{k=1}^{N-1} \dot{B}_k \vec{\mathbf{r}}_k + A_{ik}\dot{\vec{\mathbf{r}}}_k - \bar{\mu}_k \dot{\vec{\mathbf{b}}}_k \right) \\
& + \sum_{i=1}^{N-1} \bar{\mu}_i \dot{\vec{\mathbf{b}}}_i \cdot \left(\sum_{k=1}^{N-1} \dot{B}_k \vec{\mathbf{r}}_k + A_{ik}\dot{\vec{\mathbf{r}}}_k - \bar{\mu}_k \dot{\vec{\mathbf{b}}}_k \right) - \sum_{i=1}^{N-1} \dot{B}_i \vec{\mathbf{r}}_i \cdot \left(\sum_{k=1}^{N-1} \dot{B}_k \vec{\mathbf{r}}_k \right. \\
& \left. + A_{ik}\dot{\vec{\mathbf{r}}}_k - \bar{\mu}_k \dot{\vec{\mathbf{b}}}_k \right) + \sum_{i=1}^{N-1} \frac{1}{2}\hat{\rho}_i \int_0^{\ell_i} \dot{\vec{\mathbf{r}}}_{\mathbf{t}_i} \cdot \dot{\vec{\mathbf{r}}}_{\mathbf{t}_i} \, dx_i \Bigg\} \quad , \qquad (2.30)
\end{aligned}
$$

where $\hat{\rho}_i = \dfrac{\rho_i}{m}$. After expanding the dot product over the brackets and carrying out some algebra, one obtains

$$
\begin{aligned}
T_{att} = m \Bigg\{ & \sum_{j=1}^{N-1}\sum_{k=1}^{N-1} \Bigg[\frac{1}{2}\left(\sum_{i=1}^{N}\mu_i\right) \dot{B}_j \dot{B}_k \vec{\mathbf{r}}_j \cdot \vec{\mathbf{r}}_k + \left(\sum_{i=1}^{N}\mu_i A_{ij}\right) \dot{B}_k \dot{\vec{\mathbf{r}}}_j \cdot \vec{\mathbf{r}}_k \\
& - \left(\sum_{i=1}^{N}\mu_i\right) \bar{\mu}_j \dot{B}_k \dot{\vec{\mathbf{b}}}_j \cdot \vec{\mathbf{r}}_k + \frac{1}{2}\left(\sum_{i=1}^{N}\mu_i A_{ij} A_{ik}\right) \dot{\vec{\mathbf{r}}}_j \cdot \dot{\vec{\mathbf{r}}}_k - \left(\sum_{i=1}^{N}\mu_i A_{ij}\right) \bar{\mu}_k \dot{\vec{\mathbf{r}}}_j \cdot \dot{\vec{\mathbf{b}}}_k \\
& + \frac{1}{2}\left(\sum_{i=1}^{N}\mu_i\right) \bar{\mu}_k \bar{\mu}_j \dot{\vec{\mathbf{b}}}_j \cdot \dot{\vec{\mathbf{b}}}_k + \bar{\mu}_j \dot{B}_k \dot{\vec{\mathbf{b}}}_j \cdot \vec{\mathbf{r}}_k + \bar{\mu}_j A_{jk} \dot{\vec{\mathbf{r}}}_k \cdot \dot{\vec{\mathbf{b}}}_j - \bar{\mu}_j \bar{\mu}_k \dot{\vec{\mathbf{b}}}_j \cdot \dot{\vec{\mathbf{b}}}_k \\
& - \dot{B}_j \dot{B}_k \vec{\mathbf{r}}_j \cdot \vec{\mathbf{r}}_k - A_{jk} \dot{B}_j \vec{\mathbf{r}}_j \cdot \dot{\vec{\mathbf{r}}}_k + \bar{\mu}_j \dot{B}_k \dot{\vec{\mathbf{b}}}_j \cdot \vec{\mathbf{r}}_k \Bigg] \\
& + \sum_{j=1}^{N-1} \frac{1}{2}\hat{\rho}_j \int_0^{\ell_j} \dot{\vec{\mathbf{r}}}_{\mathbf{t}_j} \cdot \dot{\vec{\mathbf{r}}}_{\mathbf{t}_j} \, dx_j \Bigg\} \quad . \qquad (2.31)
\end{aligned}
$$

Defining

$$
F_{jk} = \sum_{i=1}^{N} \mu_i A_{ij} A_{ik} \quad , \qquad (2.32)
$$

factoring out similar terms, and implementing the results of Appendix B lead to

$$
\begin{aligned}
T_{att} = m \Bigg\{ & \sum_{j=1}^{N-1}\sum_{k=1}^{N-1} \Bigg[-\frac{1}{2} \dot{B}_j \dot{B}_k \vec{\mathbf{r}}_j \cdot \vec{\mathbf{r}}_k + \frac{1}{2} F_{jk} \dot{\vec{\mathbf{r}}}_j \cdot \dot{\vec{\mathbf{r}}}_k - \frac{1}{2} \bar{\mu}_j \bar{\mu}_k \dot{\vec{\mathbf{b}}}_j \cdot \dot{\vec{\mathbf{b}}}_k \\
& + \bar{\mu}_j A_{jk} \dot{\vec{\mathbf{r}}}_k \cdot \dot{\vec{\mathbf{b}}}_j - A_{jk} \dot{B}_j \vec{\mathbf{r}}_j \cdot \dot{\vec{\mathbf{r}}}_k + \bar{\mu}_j \dot{B}_k \dot{\vec{\mathbf{b}}}_j \cdot \vec{\mathbf{r}}_k \Bigg] \\
& + \sum_{j=1}^{N-1} \frac{1}{2}\hat{\rho}_j \int_0^{\ell_j} \dot{\vec{\mathbf{r}}}_{\mathbf{t}_j} \cdot \dot{\vec{\mathbf{r}}}_{\mathbf{t}_j} \, dx_j \Bigg\} \quad . \qquad (2.33)
\end{aligned}
$$

2.5.2 Gravitational Potential Energy of the System

Similar to the kinetic energy of the system the total gravitational potential energy of the system consists of two major parts; that due to the end-bodies and the tethers, respectively, i.e.,

$$U_G = -\sum_{i=1}^{N} \frac{GMm_i}{|\vec{\mathbf{R}}_c + \vec{\mathbf{R}}_i|} - \sum_{i=1}^{N-1} \rho_i \int_0^{\ell_i} \frac{GM}{|\vec{\mathbf{R}}_c + \vec{\mathbf{R}}_{t_i}|} dx_i \ , \tag{2.34}$$

where G is the universal gravitational constant, M is the mass of the Earth and $\vec{\mathbf{R}}_c$ is the position vector of the centre of mass measured from the centre of the Earth. Here the end bodies are again assumed to be point masses and the Earth is assumed to be spherical.

Using binomial expansion and retaining terms up to the third order one obtains

$$\begin{aligned} \frac{GM}{|\vec{\mathbf{R}}_c + \vec{\mathbf{R}}|} = \frac{GM}{\left[\left(\vec{\mathbf{R}}_c + \vec{\mathbf{R}}\right)\cdot\left(\vec{\mathbf{R}}_c + \vec{\mathbf{R}}\right)\right]^{\frac{1}{2}}} &= GM\left(\vec{\mathbf{R}}_c\cdot\vec{\mathbf{R}}_c + 2\vec{\mathbf{R}}_c\cdot\vec{\mathbf{R}} + \vec{\mathbf{R}}\cdot\vec{\mathbf{R}}\right)^{-\frac{1}{2}} \\ &= \frac{GM}{R_c}\left[1 - \frac{\vec{\mathbf{R}}_c\cdot\vec{\mathbf{R}}}{R_c^2} - \frac{\vec{\mathbf{R}}\cdot\vec{\mathbf{R}}}{2R_c^2} + \frac{3}{8}\left(\frac{2\vec{\mathbf{R}}_c\cdot\vec{\mathbf{R}}}{R_c^2}\right)^2\right] \ , \end{aligned} \tag{2.35}$$

where $R_c = |\vec{\mathbf{R}}_c|$. From Eq. (2.34) now we get

$$\begin{aligned} U_G = \frac{-GM}{R_c} m &+ \frac{GM}{R_c^3}\vec{\mathbf{R}}_c\cdot\left(\sum_{i=1}^{N} m_i\vec{\mathbf{R}}_i + \sum_{i=1}^{N-1}\rho_i\int_0^{\ell_i}\vec{\mathbf{R}}_{t_i}dx_i\right) \\ &+ \frac{GM}{2R_c^3}\left[\sum_{i=1}^{N} m_i\left(\vec{\mathbf{R}}_i - \frac{3}{R_c^2}\left(\vec{\mathbf{R}}_c\cdot\vec{\mathbf{R}}_i\right)\vec{\mathbf{R}}_c\right)\cdot\vec{\mathbf{R}}_i\right. \\ &\left. + \sum_{i=1}^{N-1}\rho_i\int_0^{\ell_i}\left(\vec{\mathbf{R}}_{t_i} - \frac{3}{R_c^2}\left(\vec{\mathbf{R}}_c\cdot\vec{\mathbf{R}}_{t_i}\right)\vec{\mathbf{R}}_c\right)\cdot\vec{\mathbf{R}}_{t_i}dx_i\right] \ . \end{aligned} \tag{2.36}$$

Since by definition of the centre of mass the first bracket is equal to zero, the gravitational potential energy can be written as

$$U_G = U_{G_{orb}} + U_{G_{att}} \ , \tag{2.37}$$

where

$$U_{G_{orb}} = -\frac{GM}{R_c} m \ , \tag{2.38}$$

and is relevant to the orbital motion of the system. On the other hand,

$$U_{G_{att}} = \frac{GM}{2R_c^3}\left[\sum_{i=1}^{N} m_i \left(\vec{\mathbf{R}}_i - 3(\hat{\mathbf{i}}_c\cdot\vec{\mathbf{R}}_i)\hat{\mathbf{i}}_c\right)\cdot\vec{\mathbf{R}}_i \right.$$
$$\left. + \sum_{i=1}^{N-1}\rho_i\int_0^{\ell_i}\left(\vec{\mathbf{R}}_{t_i} - 3(\hat{\mathbf{i}}_c\cdot\vec{\mathbf{R}}_{t_i})\hat{\mathbf{i}}_c\right)\cdot\vec{\mathbf{R}}_{t_i}dx_i\right] \quad , \tag{2.39}$$

where $\hat{\mathbf{i}}_c$ is the unit vector along X_c-axis, i.e, $\vec{\mathbf{R}}_c = R_c\hat{\mathbf{i}}_c$.

Substituting for $\vec{\mathbf{R}}_{t_i}$ and $\vec{\mathbf{R}}_i$ from Eq. (2.5) and performing similar algebra as that performed for the kinetic energy, we come up with the following expression for $U_{G_{att}}$ as a function of local position vectors $\vec{\mathbf{r}}_j$ and $\vec{\mathbf{r}}_{t_j}, j = 1, 2, \ldots, N-1$;

$$U_{G_{att}} = m\alpha_0^2\left\{\sum_{j=1}^{N-1}\sum_{k=1}^{N-1}\left[\frac{1}{2}F_{jk}\left\{\vec{\mathbf{r}}_j - 3(\hat{\mathbf{i}}_c\cdot\vec{\mathbf{r}}_j)\hat{\mathbf{i}}_c\right\}\cdot\vec{\mathbf{r}}_k + \bar{\mu}_j A_{jk}\left\{\vec{\mathbf{r}}_k\right.\right.\right.$$
$$\left. -3(\hat{\mathbf{i}}_c\cdot\vec{\mathbf{r}}_k)\hat{\mathbf{i}}_c\right\}\cdot\vec{\mathbf{b}}_j - \frac{1}{2}\bar{\mu}_j\bar{\mu}_k\left\{\vec{\mathbf{b}}_j - 3(\hat{\mathbf{i}}_c\cdot\vec{\mathbf{b}}_j)\hat{\mathbf{i}}_c\right\}\cdot\vec{\mathbf{b}}_k\right]$$
$$\left. + \sum_{j=1}^{N-1}\frac{1}{2}\hat{\rho}_j\int_0^{\ell_i}\left\{\vec{\mathbf{r}}_{t_j} - 3(\hat{\mathbf{i}}_c\cdot\vec{\mathbf{r}}_{t_j})\hat{\mathbf{i}}_c\right\}\cdot\vec{\mathbf{r}}_{t_j}dx_j\right\} \quad . \tag{2.40}$$

where $\alpha_0 = \sqrt{\frac{GM}{R_c^3}}$ and is not a constant in general.

2.5.3 Strain Energy of the System

The tethers are very long and thin thus flexible. When they deform, some strain energy is stored in the tethers. In the linear theory of strings, it is assumed that the initial tension in the string is large enough so that transverse displacements cause negligible change in this tension. But in the case of tethered satellite systems, the tension in the tethers, which are caused more or less by gravity gradient and centrifugal forces, varies as the lengths change. When the tethers become shorter and shorter during retrieval, these forces weaken, since they are proportional to length ℓ_i, in general. Therefore one can not neglect the effect of transverse displacements on the tension. This implies that the longitudinal vibration is strongly coupled with transverse vibrations in this case.

Considering an infinitesimal element AB of the i-th tether having an undeformed length dx_i (Fig. 2.4), one can express the strain energy stored in this element as

$$dU_{E_i} = \frac{EA_i}{2}\epsilon_i^2 dx_i \quad , \tag{2.41}$$

where

$$\epsilon_i = \frac{ds_i - dx_i}{dx_i} \quad , \tag{2.42}$$

and ds_i is the deformed length of the element. Geometry of the deformed element yields

$$\epsilon_i = \frac{1}{dx_i}\left\{\left[(dx_i + du_i)^2 + dv_i^2 + dw_i^2\right]^{\frac{1}{2}} - dx_i\right\} = \left[\left((1 + \frac{\partial u_i}{\partial x_i}\right)^2 + \left(\frac{\partial v_i}{\partial x_i}\right)^2 + \left(\frac{\partial w_i}{\partial x_i}\right)^2\right]^{\frac{1}{2}} - 1 \quad . \tag{2.43}$$

Since $\frac{\partial u_i}{\partial x_i}, \frac{\partial v_i}{\partial x_i}$, and $\frac{\partial w_i}{\partial x_i}$ are small compared to one, the above expression for ϵ_i can be expanded using the binomial theorem. Retaining te:ms upto the third order we have

$$\epsilon_i = \frac{\partial u_i}{\partial x_i} + \frac{1}{2}\left[\left(\frac{\partial v_i}{\partial x_i}\right)^2 + \left(\frac{\partial w_i}{\partial x_i}\right)^2\right] - \frac{1}{2}\left(\frac{\partial u_i}{\partial x_i}\right)\left[\left(\frac{\partial v_i}{\partial x_i}\right)^2 + \left(\frac{\partial w_i}{\partial x_i}\right)^2\right] \quad . \tag{2.44}$$

The first term in the right hand side is the strain caused by longitudinal displacement u_i and the remaining terms are the strain caused by transverse displacements v_i and w_i. The third order terms have much smaller effect than the second order terms and in most calculations can be neglected. However they are retained here to have a consistent energy expression upto the fourth order.

Substituting Eq. (2.44) into Eq. (2.41), retaining terms upto the fourth order, integrating the result over ℓ_i, and adding up the strain energy of all the tethers, one obtains

$$U_E = \sum_{i=1}^{N-1} EA_i \int_0^{\ell_i} \mathcal{E}_i dx_i \quad , \tag{2.45}$$

where

$$\mathcal{E}_i = \frac{1}{2}\left\{\frac{\partial u_i}{\partial x_i} + \frac{1}{2}\left[\left(\frac{\partial v_i}{\partial x_i}\right)^2 + \left(\frac{\partial w_i}{\partial x_i}\right)^2\right]\right\}^2 - \frac{1}{2}\left(\frac{\partial u_i}{\partial x_i}\right)^2\left[\left(\frac{\partial v_i}{\partial x_i}\right)^2 + \left(\frac{\partial w_i}{\partial x_i}\right)^2\right] \quad . \tag{2.46}$$

2.6 Orbital Motion

Although the kinetic energy and potential energy of the orbital motion, T_{orb} and $U_{G_{orb}}$, have no direct contributions in the attitude motion of the system, the orbital motion of the system has a great effect on the dynamics of the system through the orbital rate, $\dot{\theta}_c$. Energies associated with the attitude motion of the system are negligible compared to the energies associated with the orbital motion. Hence, the orbital motion can be calculated separately. Effects of small perturbations due to the attitude motion and other disturbances can be compensated with a control system such that the entire system moves in a Keplerian orbit.

A Keplerian orbit is a planar orbit resulting from central force motion. This motion is characterized by

$$\dot{\theta}_c = \frac{h}{R_c} \quad ,$$
$$R_c = \frac{h^2}{GM(1 + e\cos\theta_c)} \quad , \tag{2.47}$$

where h is a constant, representing the angular momentum per unit mass of the system and e is the eccentricity of the orbit. R_c, θ_c are as defined earlier. Angular momentum per unit mass, and orbital energy of the system are related through

$$h = \sqrt{\frac{(GM)^2(e^2 - 1)}{2(T_{orb} + U_{G_{orb}})/m}} \quad . \tag{2.48}$$

Equation (2.47) represents an ellipse, parabola, or hyperbola depending on whether $e < 1, e = 1$, or $e > 1$, respectively. When e is zero the orbit is circular. We will be concerned with either a circular or an elliptic orbit, which is a closed trajectory around the centre of the Earth.

The mean orbital rate of the motion is given by

$$\bar{\omega} = \left(\frac{GM}{a^3}\right)^{\frac{1}{2}} \quad , \tag{2.49}$$

where a is the semi-major axis of the orbit, given by

$$a = \frac{h}{GM(1-e^2)} \quad . \tag{2.50}$$

Solving Eqs. (2.47)-(2.50) for $\dot{\theta}$ and R_c, one obtains

$$\begin{aligned} \dot{\theta}_c &= \bar{\omega}(1-e^2)^{-\frac{3}{2}}(1+e\cos\theta_c)^2 \quad , \\ R_c &= \left(\frac{GM}{\bar{\omega}^2}\right)^{\frac{1}{3}} \frac{1-e^2}{1+e\cos\theta_c} \quad . \end{aligned} \tag{2.51}$$

In the case of a circular orbit, $e = 0$, $\dot{\theta}_c$ and R_c are constants and are simply related by

$$\dot{\theta}_c = \left(\frac{GM}{R_c^3}\right)^{\frac{1}{2}} \quad , \tag{2.52}$$

where R_c is the orbit radius. However when e is nonzero the instantaneous orbital rotational velocity, $\dot{\theta}_c$, and the orbit radius, R_c, vary with θ_c, i.e. they vary with time. $\dot{\theta}_c$ oscillates around $\bar{\omega}$.

The above relations show that one can establish the orbital motion knowing $T_{orb} + U_{G_{orb}}$ and e of the system, or equivalently angular momentum per unit mass h and semi-major axis a of the system.

2.7 Discretization of the Continuous Tethers

As was mentioned in Section 2.1, a continuous tether can be discretized using either an analytical approach or a bead model. Here in this thesis, we discretize the system following the former approach, using the assumed modes method, and construct a set of generalized coordinates based on that. Then we derive the governing ordinary differential equations of motion in the next Section.

The elastic displacements of an element of the i-th tether at a distance x_i, measured from the mass m_i along the undeformed tether, are denoted by u_i, v_i, and w_i, along x_i, y_i, and z_i axes, respectively. The first one is the longitudinal displacement, while the last two are the transverse displacements of the element. Therefore the displacement vectors $\vec{\mathbf{r}}_i$ and $\vec{\mathbf{r}}_{t_i}$ can be written as

$$\vec{\mathbf{r}}_i = (\ell_i + u_{\ell_i})\hat{\mathbf{i}}_i \ , \qquad \vec{\mathbf{r}}_{t_i} = (x_i + u_i)\hat{\mathbf{i}}_i + v_i\hat{\mathbf{j}}_i + w_i\hat{\mathbf{k}}_i \ . \tag{2.53}$$

where u_{ℓ_i} is the longitudinal displacement at $x_i = \ell_i$.

In the assumed modes method the elastic displacements, which are functions of both x_i and time t, can be expanded in terms of a set of admissible functions as follows:

$$\begin{aligned} &u_i(x_i, t) = \mathbf{X}_i^T(s_i)\boldsymbol{\xi}_i(t) \ , \quad v_i(x_i, t) = \mathbf{Y}_i^T(s_i)\boldsymbol{\eta}_i(t) \ , \\ &w_i(x_i, t) = \mathbf{Z}_i^T(s_i)\boldsymbol{\nu}_i(t) \ , \end{aligned} \tag{2.54}$$

where $s_i = x_i/\ell_i$ is a non-dimensional distance, and $\mathbf{X}_i, \mathbf{Y}_i, \mathbf{Z}_i$ are column vectors containing longitudinal and transverse admissible functions corresponding to the i-th tether. The admissible functions are arbitrary, but they must satisfy at least the geometric boundary conditions in an energy formulation.

Considering the system configuration and definition of the longitudinal and transverse elastic displacements, one can realize that the geometric boundary conditions of tether i can be expressed as

$$\begin{aligned} u_i(0, t) = 0 \ , &\qquad u_i(\ell_i, t) = u_{\ell_i} \neq 0 \ , \\ v_i(0, t) = v_i(\ell_i, t) = 0 \ , &\qquad w_i(0, t) = w_i(\ell_i, t) = 0 \ . \end{aligned} \tag{2.55}$$

There are infinite sets of functions that satisfy the above boundary conditions. Among them the following functions are chosen as admissible functions in this formulation:

$$X_{ik}(s_i) = s_i^{2k-1} \quad , \qquad Y_{ik}(s_i) = Z_{ik}(s_i) = \sqrt{2}\sin(k\pi s_i) \quad . \tag{2.56}$$

In three-dimensional motion, N point masses can have a maximum of $3N$ degrees of freedom. Confining the centre of mass to a specified trajectory reduces this number to $3N-3$. Since the system under consideration consists of N point masses connected by $N-1$ elastic tethers in a chain configuration, the motion of the system can be described by $3N-3$ rigid degrees of freedom, corresponding to the rigid body motion of the tethers, and N_e elastic degrees of freedom for all tethers.

The generalized coordinates of the system, which make an N_q dimensional column vector $\mathbf{q}$, are chosen here as

$$\mathbf{q} = \left\{\mathbf{q}_1, \mathbf{q}_2^T, \ldots, \mathbf{q}_{N-1}\right\}^T \tag{2.57}$$

where the N_{q_i} dimensional subvector $\mathbf{q}_i$ is the contribution of the i-th tether to the generalized coordinates vector and consists of

$$\mathbf{q}_i = \left\{\theta_i, \phi_i, \ell_i, \xi_i^T, \eta_i^T, \nu_i^T\right\}^T . \tag{2.58}$$

θ_i, ϕ_i, ℓ_i describe the rigid body motion of the i-th tether while ξ_i, η_i, ν_i describe its elastic motion. It is clear that the total number of generalized coordinates, N_q, is the summation of generalized coordinates corresponding to the all tethers, N_{q_i}, $i = 1, 2, \ldots, N-1$, i.e.

$$N_q = \sum_{i=1}^{N-1} N_{q_i} \quad . \tag{2.59}$$

Such a definition of the generalized coordinates leads to a very interesting characteristic of the system which helps us to reduce the effort involved in deriving the equations of motion analytically, which can be considerable otherwise. Considering the expressions for $\vec{\mathbf{r}}_i, \vec{\mathbf{r}}_{\mathbf{t}_i}$, and $\vec{\mathbf{b}}_i$ in Eqs. (2.53) and (2.7) and the fact that they are only function of the i-th subset of generalized coordinate, $\mathbf{q}_i$, we can write their partial derivatives with respect to $\mathbf{q}_n$ as

$$\frac{\partial \vec{\mathbf{r}}_i}{\partial \mathbf{q}_n} = \begin{cases} \{0\} \\ \mathcal{D}_{\mathbf{r}_n} \end{cases} , \quad \frac{\partial \vec{\mathbf{b}}_i}{\partial \mathbf{q}_n} = \begin{cases} \{0\} \\ \mathcal{D}_{\mathbf{b}_n} \end{cases} , \quad \frac{\partial \vec{\mathbf{r}}_{\mathbf{t}_i}}{\partial \mathbf{q}_n} = \begin{cases} \{0\} & \text{if} \quad i \neq n \\ \mathcal{D}_{\mathbf{t}_n} & \text{if} \quad i = n \end{cases} , \tag{2.60}$$

where $\mathcal{D}_{\mathbf{r}_n}$, $\mathcal{D}_{\mathbf{b}_n}$, $\mathcal{D}_{\mathbf{t}_n}$ are N_{q_n} dimensional column vectors with vectorial elements defined by

$$\mathcal{D}_{\mathbf{r}_n} = \frac{\partial \vec{\mathbf{r}}_n}{\partial \mathbf{q}_n} , \qquad \mathcal{D}_{\mathbf{b}_n} = \frac{\partial \vec{\mathbf{b}}_n}{\partial \mathbf{q}_n} , \qquad \mathcal{D}_{\mathbf{t}_n} = \frac{\partial \vec{\mathbf{r}}_{\mathbf{t}_n}}{\partial \mathbf{q}_n} . \tag{2.61}$$

Expressions for these are given in Appendix D. Note that $\dfrac{\partial(\,)}{\partial \mathbf{q}_n}$ is N_{q_n} dimensional vector in which its elements are the partial derivatives of ( ) with respect to the elements of $\mathbf{q}_n$. Advantage of Eq. (2.60) is taken in this formulation extensively.

2.8 Equations of Motion

For the model used and the way that generalized coordinates are defined here, the best approach seems to be the *Lagrangian approach*. In the rather general case, N_q, the number of generalized coordinates, is greater than the number of degrees of freedom and the generalized coordinates are related through the following nonholonomic constraints:

$$\sum_{r=1}^{N_q} (a_{ir}\, dq_r) + a_{i0} dt = 0 \quad , \qquad i = 1, 2, \ldots, N_c \quad , \tag{2.62}$$

where a_{ir} and a_{i0} are functions of $\mathbf{q}$ and t. Equation of motion corresponding to the generalized coordinate q_r is given by

$$\frac{d}{dt}\left(\frac{\partial T}{\partial \dot{q}_r}\right) - \frac{\partial T}{\partial q_r} + \frac{\partial U}{\partial q_r} = Q_r + \sum_{i=1}^{N_c} a_{ir}\Lambda_i \quad , \tag{2.63}$$

where T and U are the kinetic energy and potential energy of the system, respectively. Q_r represents the generalized force corresponding to q_r due to nonconservative external forces, while $\Lambda_i, i = 1, 2, \ldots, N_c$, are unknown coefficients called *Lagrange's multipliers*.

In the absence of constraints, where N_q is equal to the number of degrees of freedom, Eq. (2.63) is simplified as

$$\frac{d}{dt}\left(\frac{\partial T}{\partial \dot{q}_r}\right) - \frac{\partial T}{\partial q_r} + \frac{\partial U}{\partial q_r} = Q_r \quad . \tag{2.64}$$

For a simple system with a constant mass, in which $\vec{\mathbf{r}} = \vec{\mathbf{r}}(\mathbf{q}, t)$ and the kinetic energy expression is given by $T = m\dot{\vec{\mathbf{r}}}\cdot\dot{\vec{\mathbf{r}}}/2$, one can easily show that

$$\frac{d}{dt}\left(\frac{\partial T}{\partial \dot{\mathbf{q}}}\right) - \frac{\partial T}{\partial \mathbf{q}} = m\ddot{\vec{\mathbf{r}}}\cdot\frac{\partial \vec{\mathbf{r}}}{\partial \mathbf{q}} \quad , \tag{2.65}$$

where $\dfrac{\partial(\ )}{\partial \mathbf{q}}$ and $\dfrac{\partial(\ )}{\partial \dot{\mathbf{q}}}$ are N_q dimensional vectors whose elements are partial derivatives of ( ) with respect to the elements of $\mathbf{q}$ and $\dot{\mathbf{q}}$, respectively.

In a general case where m is a function of time or generalized coordinates, as in our problem where the mass of the bodies and the tethers change during deployment and retrieval, the above relation does not hold . There are some other terms appearing in the right hand side of Eq. (2.65) due to the derivatives of mass coefficients with respect to time, generalized coordinates, and generalized speeds. In this case one should exercise more care in the differentiation procedure.

Having done so for the derivatives of the kinetic energy of the system under consideration and performing some algebra, we obtain

$$\begin{aligned}
\varGamma_1 &= \frac{d}{dt}\left(\frac{\partial T_{att}}{\partial \dot{\mathbf{q}}}\right) - \frac{\partial T_{att}}{\partial \mathbf{q}} \\
&= m\left\{\sum_{j=1}^{N-1}\sum_{k=1}^{N-1}\left[\bar{\mu}_j\frac{\partial B_k}{\partial \mathbf{q}}\ddot{\vec{\mathbf{b}}}_j\cdot\vec{\mathbf{r}}_k + A_{jk}\frac{\partial B_j}{\partial \mathbf{q}}\vec{\mathbf{r}}_j\ddot{\vec{\mathbf{r}}}_k - 2\dot{B}_j\frac{\partial B_k}{\partial \mathbf{q}}\dot{\vec{\mathbf{r}}}_j\cdot\vec{\mathbf{r}}_k - \left(\frac{1}{2}\frac{\partial F_{jk}}{\partial \mathbf{q}}\right.\right.\right. \\
&\quad \left. + A_{jk}\frac{\partial B_j}{\partial \mathbf{q}}\right)\dot{\vec{\mathbf{r}}}_j\cdot\dot{\vec{\mathbf{r}}}_k - \ddot{B}_j\frac{\partial B_k}{\partial \mathbf{q}}\vec{\mathbf{r}}_j\cdot\vec{\mathbf{r}}_k\bigg] + \bigg[\left(\dot{F}_{jk} + A_{kj}\dot{B}_k - A_{jk}\dot{B}_j\right)\dot{\vec{\mathbf{r}}}_j\cdot\frac{\partial \vec{\mathbf{r}}_k}{\partial \mathbf{q}} \\
&\quad + 2\bar{\mu}_k\dot{B}_j\dot{\vec{\mathbf{r}}}_j\cdot\frac{\partial \vec{\mathbf{b}}_k}{\partial \mathbf{q}} - A_{jk}\ddot{B}_j\vec{\mathbf{r}}_j\cdot\frac{\partial \vec{\mathbf{r}}_k}{\partial \mathbf{q}} + \bar{\mu}_j\ddot{B}_k\frac{\partial \vec{\mathbf{b}}_j}{\partial \mathbf{q}}\cdot\vec{\mathbf{r}}_k\bigg] + \bigg[\bigg(F_{jk}\frac{\partial \vec{\mathbf{r}}_k}{\partial \mathbf{q}} \\
&\quad \left. + \bar{\mu}_k A_{kj}\frac{\partial \vec{\mathbf{b}}_k}{\partial \mathbf{q}}\right)\cdot\ddot{\vec{\mathbf{r}}}_j + \left(\bar{\mu}_j A_{jk}\frac{\partial \vec{\mathbf{r}}_k}{\partial \mathbf{q}} - \bar{\mu}_j\bar{\mu}_k\frac{\partial \vec{\mathbf{b}}_k}{\partial \mathbf{q}}\right)\cdot\ddot{\vec{\mathbf{b}}}_j\bigg] + \sum_{j=1}^{N-1}\hat{\rho}_j\left(\frac{d}{dt}\frac{\partial}{\partial \dot{\mathbf{q}}}\right. \\
&\quad \left.\left. - \frac{\partial}{\partial \mathbf{q}}\right)\left(\int_0^{\ell_j}\frac{1}{2}\dot{\vec{\mathbf{r}}}_{t_j}\cdot\dot{\vec{\mathbf{r}}}_{t_j}dx_j\right)\right\} \quad .
\end{aligned} \tag{2.66}$$

Further simplification can be made by using Eqs. (B.12) and (B.13) and interchanging indices k and j in some terms to obtain

$$\begin{aligned}\boldsymbol{\Gamma}_1 = m \Bigg\{ \sum_{j=1}^{N-1}\sum_{k=1}^{N-1} & \Bigg[\bar{\mu}_j \frac{\partial B_k}{\partial \mathbf{q}} \ddot{\vec{\mathbf{b}}}_j \cdot \vec{\mathbf{r}}_k + A_{jk} \frac{\partial B_j}{\partial \mathbf{q}} \vec{\mathbf{r}}_j \ddot{\vec{\mathbf{r}}}_k - 2\dot{B}_j \frac{\partial B_k}{\partial \mathbf{q}} \dot{\vec{\mathbf{r}}}_j \cdot \vec{\mathbf{r}}_k + \frac{1}{2}\delta_{jk} \frac{\partial B_j}{\partial \mathbf{q}} \dot{\vec{\mathbf{r}}}_j \cdot \dot{\vec{\mathbf{r}}}_k \\ & - \ddot{B}_j \frac{\partial B_k}{\partial \mathbf{q}} \vec{\mathbf{r}}_j \cdot \vec{\mathbf{r}}_k \Bigg] + \Bigg[2\bar{\mu}_k \dot{B}_j \dot{\vec{\mathbf{r}}}_j \cdot \frac{\partial \dot{\vec{\mathbf{b}}}_k}{\partial \mathbf{q}} - A_{jk} \ddot{B}_j \vec{\mathbf{r}}_j \cdot \frac{\partial \vec{\mathbf{r}}_k}{\partial \mathbf{q}} + \bar{\mu}_j \ddot{B}_k \frac{\partial \vec{\mathbf{b}}_j}{\partial \mathbf{q}} \cdot \vec{\mathbf{r}}_k \\ & - \dot{B}_j \left(2A_{jk} + \delta_{jk}\right) \dot{\vec{\mathbf{r}}}_j \cdot \frac{\partial \dot{\vec{\mathbf{r}}}_k}{\partial \mathbf{q}} \Bigg] + \Bigg[\left(F_{jk} \frac{\partial \vec{\mathbf{r}}_k}{\partial \mathbf{q}} + \bar{\mu}_k A_{kj} \frac{\partial \vec{\mathbf{b}}_k}{\partial \mathbf{q}} \right) \cdot \ddot{\vec{\mathbf{r}}}_j + \left(\bar{\mu}_j A_{jk} \frac{\partial \vec{\mathbf{r}}_k}{\partial \mathbf{q}} \right. \\ & \left. - \bar{\mu}_j \bar{\mu}_k \frac{\partial \vec{\mathbf{b}}_k}{\partial \mathbf{q}} \right) \cdot \ddot{\vec{\mathbf{b}}}_j \Bigg] + \sum_{j=1}^{N-1} \hat{\rho}_j \left(\frac{d}{dt}\frac{\partial}{\partial \dot{\mathbf{q}}} - \frac{\partial}{\partial \mathbf{q}} \right) \left(\int_0^{\ell_j} \frac{1}{2} \dot{\vec{\mathbf{r}}}_{t_j} \cdot \dot{\vec{\mathbf{r}}}_{t_j} dx_j \right) \Bigg\} \quad . \qquad (2.67)\end{aligned}$$

Contribution of the gravitational potential energy in the equations of motion corresponding to $\mathbf{q}$ is $\dfrac{\partial U_{G_{att}}}{\partial \mathbf{q}}$. After some algebraic manipulation they can be written as

$$\begin{aligned}\boldsymbol{\Gamma}_2 = & \frac{\partial}{\partial \mathbf{q}} U_{G_{att}} \\ = & m\alpha_0^2 \Bigg\{ \sum_{j=1}^{N-1}\sum_{k=1}^{N-1} \Bigg[\bar{\mu}_j \frac{\partial B_k}{\partial \mathbf{q}} \left(\vec{\mathbf{b}}_j - 3(\hat{\mathbf{i}}_c \cdot \vec{\mathbf{b}}_j)\hat{\mathbf{i}}_c \right) \cdot \vec{\mathbf{r}}_k + \frac{1}{2}\frac{\partial F_{jk}}{\partial \mathbf{q}} \left(\vec{\mathbf{r}}_j - 3(\hat{\mathbf{i}}_c \cdot \vec{\mathbf{r}}_j)\hat{\mathbf{i}}_c \right) \cdot \vec{\mathbf{r}}_k \Bigg] \\ & + \Bigg[\left(F_{jk} \frac{\partial \vec{\mathbf{r}}_k}{\partial \mathbf{q}} + \bar{\mu}_k A_{kj} \frac{\partial \vec{\mathbf{b}}_k}{\partial \mathbf{q}} \right) \cdot \left\{ \vec{\mathbf{r}}_j - 3(\hat{\mathbf{i}}_c \cdot \vec{\mathbf{r}}_j)\hat{\mathbf{i}}_c \right\} + \left(\bar{\mu}_j A_{jk} \frac{\partial \vec{\mathbf{r}}_k}{\partial \mathbf{q}} \right. \\ & \left. - \bar{\mu}_j \bar{\mu}_k \frac{\partial \vec{\mathbf{b}}_k}{\partial \mathbf{q}} \right) \cdot \left\{ \vec{\mathbf{b}}_j - 3(\hat{\mathbf{i}}_c \cdot \vec{\mathbf{b}}_j)\hat{\mathbf{i}}_c \right\} \Bigg] \\ & + \sum_{j=1}^{N-1} \Bigg[\hat{\rho}_j \frac{\partial}{\partial \mathbf{q}} \left(\int_0^{\ell_j} \frac{1}{2} \left\{ \vec{\mathbf{r}}_{t_j} - 3(\hat{\mathbf{i}}_c \cdot \vec{\mathbf{r}}_{t_j})\hat{\mathbf{i}}_c \right\} \cdot \vec{\mathbf{r}}_{t_j} dx_j \right) \Bigg] \Bigg\} \quad . \qquad (2.68)\end{aligned}$$

Strain energy contributes the following term to the equations of motion of $\mathbf{q}$:

$$\boldsymbol{\Gamma}_3 = \frac{\partial U_E}{\partial \mathbf{q}} = \sum_{j=1}^{N-1} EA_j \frac{\partial}{\partial \mathbf{q}} \left(\int_0^{\ell_j} \mathcal{E}_j dx_j \right) \quad . \qquad (2.69)$$

Substituting $\boldsymbol{\Gamma}_1, \boldsymbol{\Gamma}_2$, and $\boldsymbol{\Gamma}_3$ into Eq. (2.64) and rearranging some terms, we get

$$\frac{\mathbf{Q}}{m} = \sum_{j=1}^{N-1}\sum_{k=1}^{N-1} \left\{ \bar{\mu}_j \frac{\partial B_k}{\partial \mathbf{q}} \left[\ddot{\vec{\mathbf{b}}}_j + \alpha_0^2 \left\{ \vec{\mathbf{b}}_j - 3(\hat{\mathbf{i}}_c \cdot \vec{\mathbf{b}}_j)\hat{\mathbf{i}}_c \right\} \right] \cdot \vec{\mathbf{r}}_k - \frac{\partial B_k}{\partial \mathbf{q}} \left(2\dot{B}_j \dot{\vec{\mathbf{r}}}_j \right.\right.$$
$$\left. + \ddot{B}_j \vec{\mathbf{r}}_j \right) \cdot \vec{\mathbf{r}}_k - A_{kj} \frac{\partial B_k}{\partial \mathbf{q}} \left[\ddot{\vec{\mathbf{r}}}_j + \alpha_0^2 \left\{ \vec{\mathbf{r}}_j - 3(\hat{\mathbf{i}}_c \cdot \vec{\mathbf{r}}_j)\hat{\mathbf{i}}_c \right\} \right] \cdot \vec{\mathbf{r}}_k$$
$$\left. + \frac{1}{2}\delta_{kj} \frac{\partial B_k}{\partial \mathbf{q}} \left[\dot{\vec{\mathbf{r}}}_j \cdot \dot{\vec{\mathbf{r}}}_k + \alpha_0^2 \left\{ \vec{\mathbf{r}}_j - 3(\hat{\mathbf{i}}_c \cdot \vec{\mathbf{r}}_j)\hat{\mathbf{i}}_c \right\} \cdot \vec{\mathbf{r}}_k \right] \right\}$$
$$+ \sum_{j=1}^{N-1}\sum_{k=1}^{N-1} \left[-\dot{B}_j \left(2A_{jk} + \delta_{jk} \right) \dot{\vec{\mathbf{r}}}_j \cdot \frac{\partial \vec{\mathbf{r}}_k}{\partial \mathbf{q}} + 2\bar{\mu}_j \dot{B}_k \dot{\vec{\mathbf{b}}}_j \cdot \frac{\partial \vec{\mathbf{r}}_k}{\partial \mathbf{q}} - A_{jk} \ddot{B}_j \vec{\mathbf{r}}_j \cdot \frac{\partial \vec{\mathbf{r}}_k}{\partial \mathbf{q}} \right]$$
$$+ \sum_{j=1}^{N-1}\sum_{k=1}^{N-1} \left\{ \left(F_{jk} \frac{\partial \vec{\mathbf{r}}_k}{\partial \mathbf{q}} + \bar{\mu}_k A_{kj} \frac{\partial \vec{\mathbf{b}}_k}{\partial \mathbf{q}} \right) \cdot \left[\ddot{\vec{\mathbf{r}}}_j + \alpha_0^2 \left\{ \vec{\mathbf{r}}_j - 3(\hat{\mathbf{i}}_c \cdot \vec{\mathbf{r}}_j)\hat{\mathbf{i}}_c \right\} \right] \right.$$
$$\left. + \left(\bar{\mu}_j A_{jk} \frac{\partial \vec{\mathbf{r}}_k}{\partial \mathbf{q}} - \bar{\mu}_j \bar{\mu}_k \frac{\partial \vec{\mathbf{b}}_k}{\partial \mathbf{q}} \right) \cdot \left[\ddot{\vec{\mathbf{b}}}_j + \alpha_0^2 \left\{ \vec{\mathbf{b}}_j - 3(\hat{\mathbf{i}}_c \cdot \vec{\mathbf{b}}_j)\hat{\mathbf{i}}_c \right\} \right] \right\}$$
$$+ \sum_{j=1}^{N-1} \left\{ \hat{\rho}_j \alpha_0^2 \frac{\partial}{\partial \mathbf{q}} \left(\int_0^{\ell_j} \frac{1}{2} \left\{ \vec{\mathbf{r}}_{t_j} - 3(\hat{\mathbf{i}}_c \cdot \vec{\mathbf{r}}_{t_j})\hat{\mathbf{i}}_c \right\} \cdot \vec{\mathbf{r}}_{t_j} dx_j \right) + \hat{\rho}_j \left(\frac{d}{dt}\frac{\partial}{\partial \dot{\mathbf{q}}} \right.\right.$$
$$\left.\left. - \frac{\partial}{\partial \mathbf{q}} \right) \left(\int_0^{\ell_j} \frac{1}{2} \dot{\vec{\mathbf{r}}}_{t_j} \cdot \dot{\vec{\mathbf{r}}}_{t_j} dx_j \right) + \frac{EA_j}{m} \frac{\partial}{\partial \mathbf{q}} \left(\int_0^{\ell_j} \mathcal{E}_j dx_j \right) \right\} \quad . \tag{2.70}$$

In fact $\mathbf{q}$ consists of the subsets $\mathbf{q}_n, n = 1, 2, \ldots, N-1$, defined in Eq. (2.58). Since $\vec{\mathbf{r}}_k, \vec{\mathbf{b}}_k, \vec{\mathbf{r}}_{t_k}$, and $\mathcal{E}_k$ have no partial derivatives with respect to $\mathbf{q}_n$ except when $k = n$, the above equations can be further simplified. Having done so, one obtains the equation of motion corresponding to $\mathbf{q}_n$ in the following form

$$\sum_{j=1}^{N-1} \mathbf{G}_{nj} + \sum_{j=1}^{N-1} \mathbf{H}_{nj} + \sum_{j=1}^{N-1} \mathbf{P}_{nj} + \mathbf{S}_n = \frac{1}{m}\mathbf{Q}_n \quad , \tag{2.71}$$

where

$$\mathbf{G}_{nj} = \frac{\partial B_n}{\partial \mathbf{q}_n} \left\{ \left[\bar{\mu}_j \left(\ddot{\vec{\mathbf{b}}}_j + \alpha_0^2 \left\{ \vec{\mathbf{b}}_j - 3(\hat{\mathbf{i}}_c \cdot \vec{\mathbf{b}}_j)\hat{\mathbf{i}}_c \right\} \right) - \left(2\dot{B}_j \dot{\vec{\mathbf{r}}}_j + \ddot{B}_j \vec{\mathbf{r}}_j \right) \right.\right.$$
$$\left.\left. - A_{nj} \ddot{\vec{\mathbf{r}}}_j - \frac{\alpha_0^2}{2} \left(2A_{nj} - \delta_{nj} \right) \left\{ \vec{\mathbf{r}}_j - 3(\hat{\mathbf{i}}_c \cdot \vec{\mathbf{r}}_j)\hat{\mathbf{i}}_c \right\} \right] \cdot \vec{\mathbf{r}}_n + \frac{1}{2}\delta_{nj} \dot{\vec{\mathbf{r}}}_j \cdot \dot{\vec{\mathbf{r}}}_n \right\} \ , \tag{2.72}$$

$$\mathbf{H}_{nj} = \left[-\dot{B}_j \left(2A_{jn} + \delta_{jn} \right) \dot{\vec{\mathbf{r}}}_j + 2\bar{\mu}_j \dot{B}_n \dot{\vec{\mathbf{b}}}_j - A_{jn} \ddot{B}_j \vec{\mathbf{r}}_j \right] \cdot \mathcal{D}_{\mathbf{r}_n} \quad , \tag{2.73}$$

$$\mathbf{P}_{nj} = (F_{jn}\mathcal{D}_{\mathbf{r}_n} + \bar{\mu}_n A_{nj}\mathcal{D}_{\mathbf{b}_n})\cdot\left[\ddot{\vec{\mathbf{r}}}_j + \alpha_0^2\left\{\vec{\mathbf{r}}_j - 3(\hat{\mathbf{i}}_c\cdot\vec{\mathbf{r}}_j)\hat{\mathbf{i}}_c\right\}\right]$$
$$+ (\bar{\mu}_j A_{jn}\mathcal{D}_{\mathbf{r}_n} - \bar{\mu}_j\bar{\mu}_n\mathcal{D}_{\mathbf{b}_n})\cdot\left[\ddot{\vec{\mathbf{b}}}_j + \alpha_0^2\left\{\vec{\mathbf{b}}_j - 3(\hat{\mathbf{i}}_c\cdot\vec{\mathbf{b}}_j)\hat{\mathbf{i}}_c\right\}\right] \quad , \qquad (2.74)$$

$$\mathbf{S}_n = \hat{\rho}_n\alpha_0^2\frac{\partial}{\partial\mathbf{q}_n}\left(\int_0^{\ell_n}\frac{1}{2}\left\{\vec{\mathbf{r}}_{\mathbf{t}_n} - 3(\hat{\mathbf{i}}_c\cdot\vec{\mathbf{r}}_{\mathbf{t}_n})\hat{\mathbf{i}}_c\right\}\cdot\vec{\mathbf{r}}_{\mathbf{t}_n}dx_n\right) + \hat{\rho}_n\left(\frac{d}{dt}\frac{\partial}{\partial\dot{\mathbf{q}}_n}\right.$$
$$\left.-\frac{\partial}{\partial\mathbf{q}_n}\right)\left(\int_0^{\ell_n}\frac{1}{2}\dot{\vec{\mathbf{r}}}_{\mathbf{t}_n}\cdot\dot{\vec{\mathbf{r}}}_{\mathbf{t}_n}dx_n\right) + \frac{EA_n}{m}\frac{\partial}{\partial\mathbf{q}_n}\left(\int_0^{\ell_n}\mathcal{E}_n dx_n\right) \quad , \qquad (2.75)$$

where $\mathcal{D}_{\mathbf{r}_n}, \mathcal{D}_{\mathbf{b}_n}$, and $\mathcal{D}_{\mathbf{t}_n}$ are as defined earlier.

2.8.1 Librational Motion

Equations of motion corresponding to the libration motion of the n-th tether is obtained if $\mathbf{q}_n$ is substituted by ψ_n, where ψ_n is either in-plane libration, θ_n, or out-of-plane libration, ϕ_n. Since the mass coefficients B_j have no partial derivatives with respect to θ_n or ϕ_n, the first summation in Eq. (2.71), vanishes. The component of $\mathbf{S}_n$ corresponding to the libration degrees of freedom can be also simplified by noting that

$$\hat{\rho}_n\left(\frac{d}{dt}\frac{\partial}{\partial\dot{\psi}_n} - \frac{\partial}{\partial\psi_n}\right)\left(\int_0^{\ell_n}\frac{1}{2}\dot{\vec{\mathbf{r}}}_{\mathbf{t}_n}\cdot\dot{\vec{\mathbf{r}}}_{\mathbf{t}_n}dx_n\right) = \hat{\rho}_n\left(\frac{d}{dt}\int_0^{\ell_n}\dot{\vec{\mathbf{r}}}_{\mathbf{t}_n}\cdot\frac{\partial\vec{\mathbf{r}}_{\mathbf{t}_n}}{\partial\psi_n}dx_n\right.$$
$$\left.-\int_0^{\ell_n}\dot{\vec{\mathbf{r}}}_{\mathbf{t}_n}\cdot\frac{\partial\dot{\vec{\mathbf{r}}}_{\mathbf{t}_n}}{\partial\psi_n}dx_n\right) = \hat{\rho}_n\int_0^{\ell_n}\ddot{\vec{\mathbf{r}}}_{\mathbf{t}_n}\cdot\frac{\partial\vec{\mathbf{r}}_{\mathbf{t}_n}}{\partial\psi_n}dx_n - \beta_n\hat{\rho}_n\dot{\ell}_n\left(\dot{\vec{\mathbf{r}}}_{\mathbf{t}_n}\cdot\frac{\partial\vec{\mathbf{r}}_{\mathbf{t}_n}}{\partial\psi_n}\right)_{x_n=\ell_n}$$
$$-\alpha_n\hat{\rho}_n\dot{\ell}_n\left(\dot{\vec{\mathbf{r}}}_{\mathbf{t}_n}\cdot\frac{\partial\vec{\mathbf{r}}_{\mathbf{t}_n}}{\partial\psi_n}\right)_{x_n=0} \quad , \qquad (2.76)$$

where the last term is zero because components of $\mathcal{D}_{\mathbf{t}_n}$ vanish at $x = 0$ in the case of librational degrees of freedom. Using the results of Appendix D one can note that

$$\left(\dot{\vec{\mathbf{r}}}_{\mathbf{t}_n}\right)_{x_n=\ell_n} = \dot{\vec{\mathbf{r}}}_n \quad , \quad \left(\frac{\partial\vec{\mathbf{r}}_{\mathbf{t}_n}}{\partial\psi_n}\right)_{x_n=\ell_n} = \frac{\partial\vec{\mathbf{r}}_n}{\partial\psi_n} \quad . \qquad (2.77)$$

After some manipulation, S_{ψ_n} can be expressed as

$$S_{\psi_n} = \hat{\rho}_n \int_0^{\ell_n} \left(\ddot{\vec{\mathbf{r}}}_{t_n} + \alpha_0^2 \left[\vec{\mathbf{r}}_{t_n} - 3(\hat{\mathbf{i}}_c \cdot \vec{\mathbf{r}}_{t_n})\hat{\mathbf{i}}_c\right]\right) \cdot \frac{\partial \vec{\mathbf{r}}_{t_n}}{\partial \psi_n} dx_n + \dot{B}_n \dot{\vec{\mathbf{r}}}_n \cdot \frac{\partial \vec{\mathbf{r}}_n}{\partial \psi_n} \quad . \tag{2.78}$$

Hence the equation of motion governing the libration of the n-th tether is given by

$$\sum_{j=1}^{N-1} H_{\psi_{nj}} + \sum_{j=1}^{N-1} P_{\psi_{nj}} + S_{\psi_n} = \frac{Q_{\psi_n}}{m} \quad , \tag{2.79}$$

where $H_{\psi_{nj}}$ and $P_{\psi_{nj}}$ are the components of $\mathbf{H}_{nj}$ and $\mathbf{P}_{nj}$, defined in Eqs. (2.73) and (2.74) respectively, corresponding to the libration degrees of freedom, and S_{ψ_n} is as defined in Eq. (2.78). Note that since $\mathcal{E}_n$ is a function of the spatial coordinate x_n and elastic generalized coordinates only, the elastic potential energy has no contribution in the librational equations of motion directly.

2.8.2 Vibrational Motion

Similar to the librational motion the first summation in Eq. (2.71), vanishes again and same equation as Eq. (2.79) holds for the vibrational motion

$$\sum_{j=1}^{N-1} H_{\epsilon_{nj}} + \sum_{j=1}^{N-1} P_{\epsilon_{nj}} + S_{\epsilon_n} = \frac{Q_{\epsilon_n}}{m} \quad , \tag{2.80}$$

provided that S_{ϵ_n} is re-defined as follows:

$$\begin{aligned} S_{\epsilon_n} = \hat{\rho}_n \int_0^{\ell_n} \left(\ddot{\vec{\mathbf{r}}}_{t_n} + \alpha_0^2 \left\{\vec{\mathbf{r}}_{t_n} - 3(\hat{\mathbf{i}}_c \cdot \vec{\mathbf{r}}_{t_n})\hat{\mathbf{i}}_c\right\}\right) \cdot \frac{\partial \vec{\mathbf{r}}_{t_n}}{\partial \epsilon_n} dx_n + \dot{B}_n \dot{\vec{\mathbf{r}}}_n \cdot \frac{\partial \vec{\mathbf{r}}_n}{\partial \epsilon_n} \\ + \frac{EA_n}{m} \int_0^{\ell_n} \frac{\partial \mathcal{E}_n}{\partial \epsilon_n} dx_n \quad . \end{aligned} \tag{2.81}$$

Here ϵ_n is one of the elastic generalized coordinates ξ_n, η_n, ν_n which describe longitudinal and transverse oscillations of the n-th tether, respectively.

2.8.3 Longitudinal Rigid-Body Motion, ℓ_n

Indeed this is the most challenging part of derivation of the equations of motion, because of two reasons: firstly, component of $\mathbf{G}_{nj}$ corresponding to ℓ_n in Eq. (2.71) does not vanish since the mass coefficients are length-dependent and secondly, the upper limit of the integrals appearing in the expression for $\mathbf{S}_n$ is our generalized coordinate, ℓ_n, under consideration. Partial differentiation of these integrals with respect to ℓ_n is carried out in Appendix E. The equation of motion corresponding to ℓ_n is then given by

$$\sum_{j=1}^{N-1} G_{\ell_{nj}} + \sum_{j=1}^{N-1} H_{\ell_{nj}} + \sum_{j=1}^{N-1} P_{\ell_{nj}} + S_{\ell_n} = \frac{Q_{\ell_n}}{m} \quad , \tag{2.82}$$

where $G_{\ell_{nj}}$, $H_{\ell_{nj}}$, $P_{\ell_{nj}}$ are the corresponding component of $\mathbf{G}_{nj}$, $\mathbf{H}_{nj}$, $\mathbf{H}_{nj}$ defined in Eqs. (2.72)-(2.74), respectively, while S_{ℓ_n} is given by

$$\begin{aligned} S_{\ell_n} = \hat{\rho}_n \int_0^{\ell_n} \left[\ddot{\vec{\mathbf{r}}}_{\mathbf{t}_n} + \alpha_0^2 \left\{\vec{\mathbf{r}}_{\mathbf{t}_n} - 3(\hat{\mathbf{i}}_c \cdot \vec{\mathbf{r}}_{\mathbf{t}_n})\hat{\mathbf{i}}_c\right\}\right] \cdot \left(\frac{\partial \vec{\mathbf{r}}_{\mathbf{t}_n}}{\partial x_n} + \frac{\partial \vec{\mathbf{r}}_{\mathbf{t}_n}}{\partial \ell_n}\right) dx_n + \dot{B}_n \dot{\vec{\mathbf{r}}}_n \cdot \hat{\mathbf{i}}_n \\ + \frac{EA_n}{m} \int_0^{\ell_n} \frac{\partial \mathcal{E}_n}{\partial \ell_n} dx_n + \frac{EA_n}{m} \left(\mathcal{E}_n\right)_{x_n=\ell_n} + \hat{\rho}_n \left(\alpha_n - \frac{1}{2}\right) \left[\dot{\vec{\mathbf{r}}}_{\mathbf{t}_n} \cdot \dot{\vec{\mathbf{r}}}_{\mathbf{t}_n}\right]_{x_n=0} \end{aligned} \tag{2.83}$$

Combining Eqs. (2.78), (2.81), and (2.83) and using the definition of $\boldsymbol{\mathcal{D}}_{\mathbf{r}_n}$ and $\boldsymbol{\mathcal{D}}_{\mathbf{t}_n}$ in Appendix D, one can replace $\mathbf{S}_n$ defined by Eq. (2.75) by the following equation

$$\begin{aligned} \mathbf{S}_n = \hat{\rho}_n \int_0^{\ell_n} \left(\ddot{\vec{\mathbf{r}}}_{\mathbf{t}_n} + \alpha_0^2 \left\{\vec{\mathbf{r}}_{\mathbf{t}_n} - 3(\hat{\mathbf{i}}_c \cdot \vec{\mathbf{r}}_{\mathbf{t}_n})\hat{\mathbf{i}}_c\right\}\right) \cdot \boldsymbol{\mathcal{D}}_{\mathbf{t}_n} dx_n + \dot{B}_n \dot{\vec{\mathbf{r}}}_n \cdot \boldsymbol{\mathcal{D}}_{\mathbf{r}_n} \\ + \frac{EA_n}{m} \int_0^{\ell_n} \frac{\partial \mathcal{E}_n}{\partial \mathbf{q}_n} dx_n + \mathbf{L}_n \quad . \end{aligned} \tag{2.84}$$

where $\mathbf{L}_n$ is an N_{q_n} dimensional vector in which all the elements are zero except the one that corresponds to the generalized coordinate ℓ_n. It is given by

$$L_{\ell_n} = \frac{EA_n}{m} \left(\mathcal{E}_n\right)_{x_n=\ell_n} + \hat{\rho}_n \left(\alpha_n - \frac{1}{2}\right) \left[\dot{\vec{\mathbf{r}}}_{\mathbf{t}_n} \cdot \dot{\vec{\mathbf{r}}}_{\mathbf{t}_n}\right]_{x_n=0} \quad . \tag{2.85}$$

2.8.4 Some Special Cases

Case 1: $\dot{B}_j = 0$

In fact $\dot{B}_j = 0, j = 1, 2, \ldots, N-1$ represent the case that each body, except the body 1, are reeled in/out only from the previous body, i.e. body $j+1$ is deployed or retrieved only from body j. Since $\dot{B}_j = 0$, consequently $\dfrac{\partial Bj}{\partial \mathbf{q}} = \{0\}$. Hence $\mathbf{G}_{nj}$ and $\mathbf{H}_{nj}$ vanish in Eq. (2.71), and the equations of motion are given by

$$\sum_{j=1}^{N-1} \mathbf{P}_{nj} + \mathbf{S}_n = \frac{1}{m}\mathbf{Q}_n \quad , \tag{2.86}$$

where $\mathbf{P}_{nj}, \mathbf{S}_n$ and $\mathbf{Q}_n$ are as defined earlier.

Case 2: Massless Tethers

In the absence of tether masses $\mathbf{G}_{nj}, \mathbf{H}_{nj}$ and $\mathbf{S}_n$ become zero and the equations of motion are simply given by

$$F_{jn}\mathcal{D}_{\mathbf{r}_n}\cdot\left[\ddot{\vec{\mathbf{r}}}_j + \alpha_0^2\left\{\vec{\mathbf{r}}_j - 3(\hat{\mathbf{i}}_c\cdot\vec{\mathbf{r}}_j)\hat{\mathbf{i}}_c\right\}\right] + \frac{EA_n}{m}\frac{\partial}{\partial \mathbf{q}_n}\left(\int_0^{\ell_n}\mathcal{E}_n dx_n\right) = \frac{1}{m}\mathbf{Q}_n \quad . \tag{2.87}$$

These equations match those obtained by Misra and Modi [65], if $\vec{\mathbf{r}}_j$ is defined by

$$\vec{\mathbf{r}}_j = \ell_j\hat{\mathbf{i}}_j \quad , \tag{2.88}$$

and elasticity of the tethers is ignored. Note that even in the case of massless tethers, the tethers can be modelled as massless springs. Hence generally the position vectors $\vec{\mathbf{r}}_j$ are expressed by

$$\vec{\mathbf{r}}_j = (\ell_j + \xi_j)\hat{\mathbf{i}}_j \quad , \tag{2.89}$$

where ξ_j denotes the longitudinal stretch of the j-th tether.

Equation (2.71) together with Eqs. (2.72), (2.73), (2.74), and (2.84) describe the general dynamics of an N-body tethered system. They are used extensively in this thesis for further analysis.

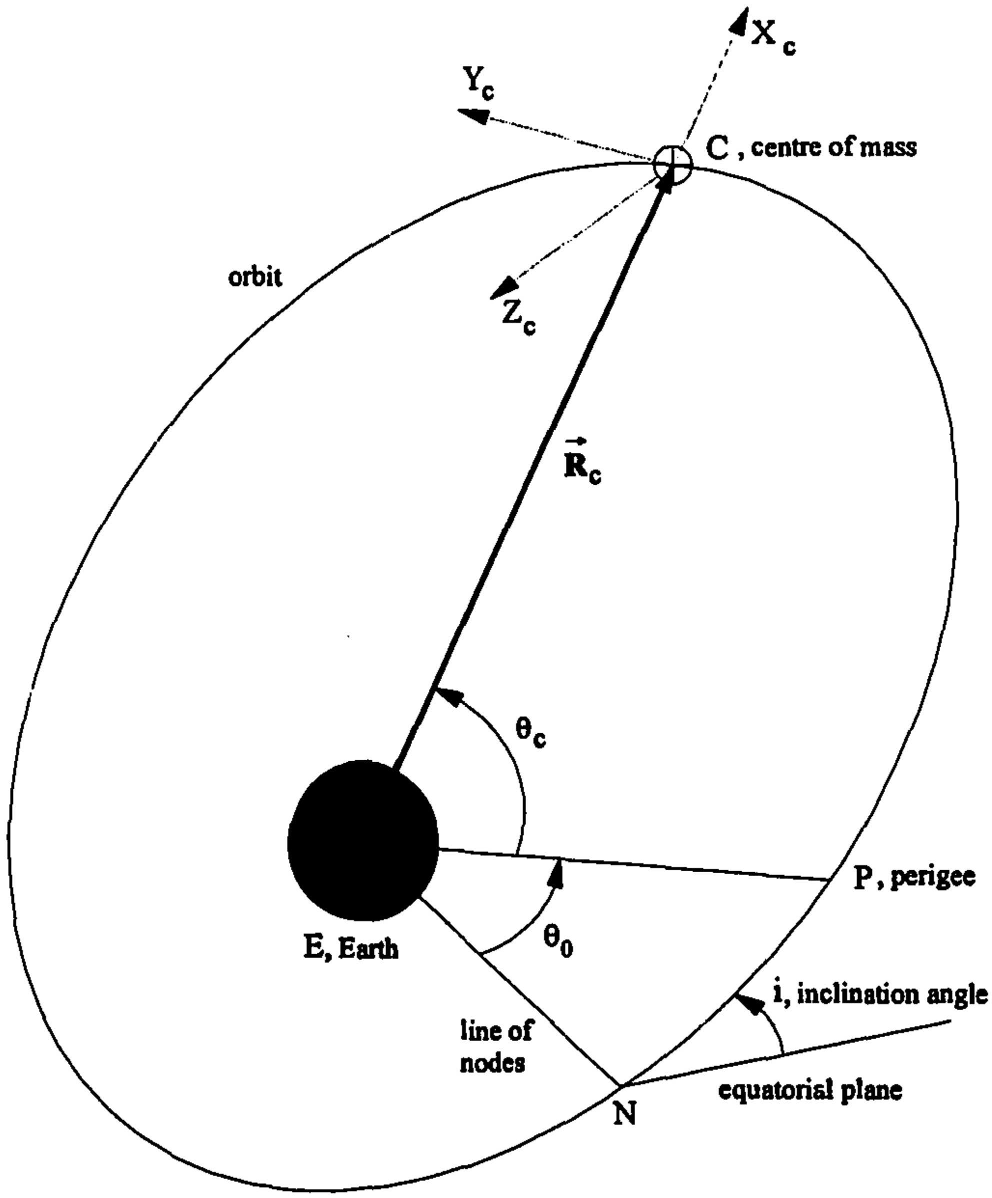

Figure 2.1: Geometry of orbital motion

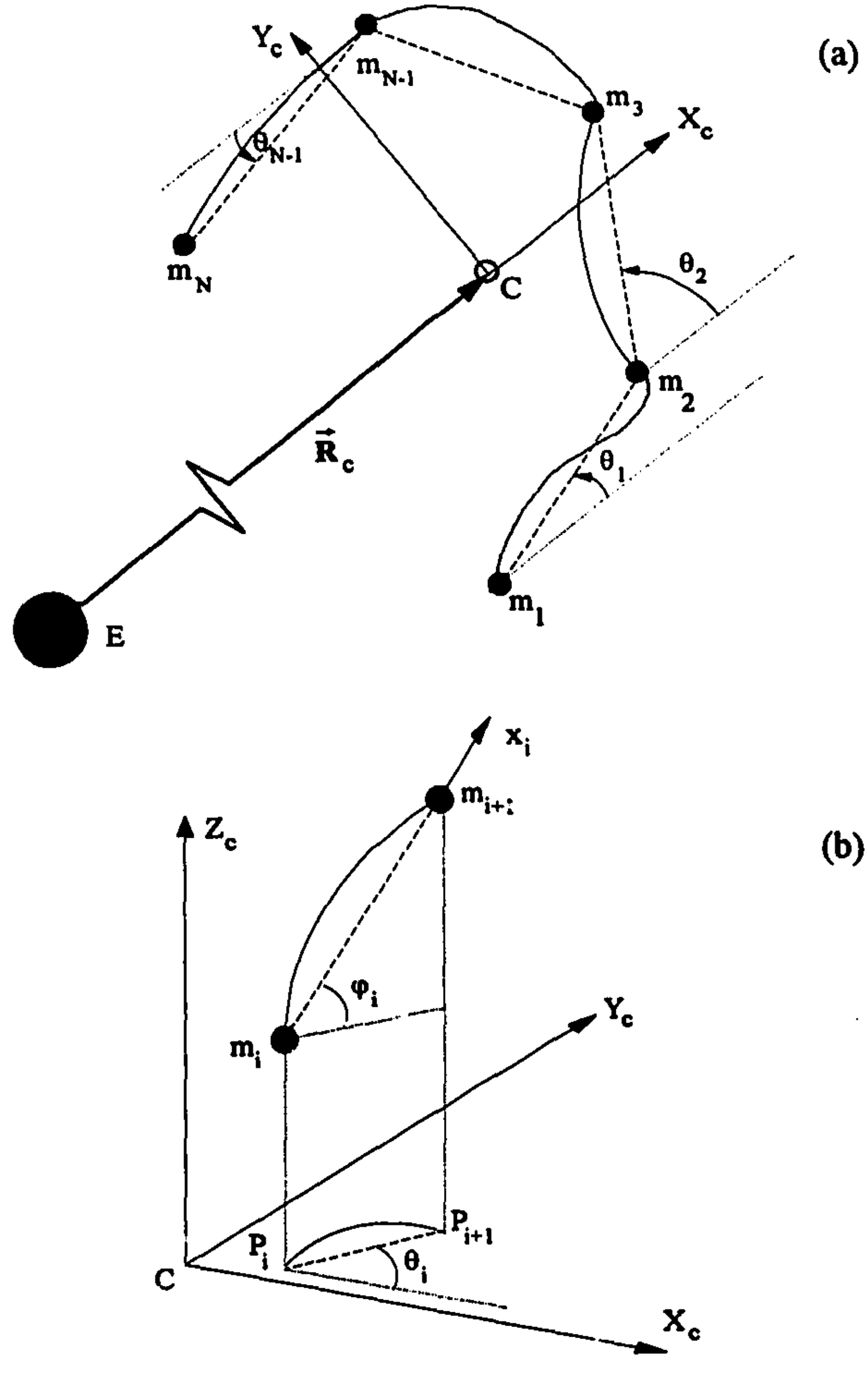

Figure 2.2: Geometry of the system: (a) projection of the N-body system in the orbital plane; (b) Definition of angles θ_i and ϕ_i.

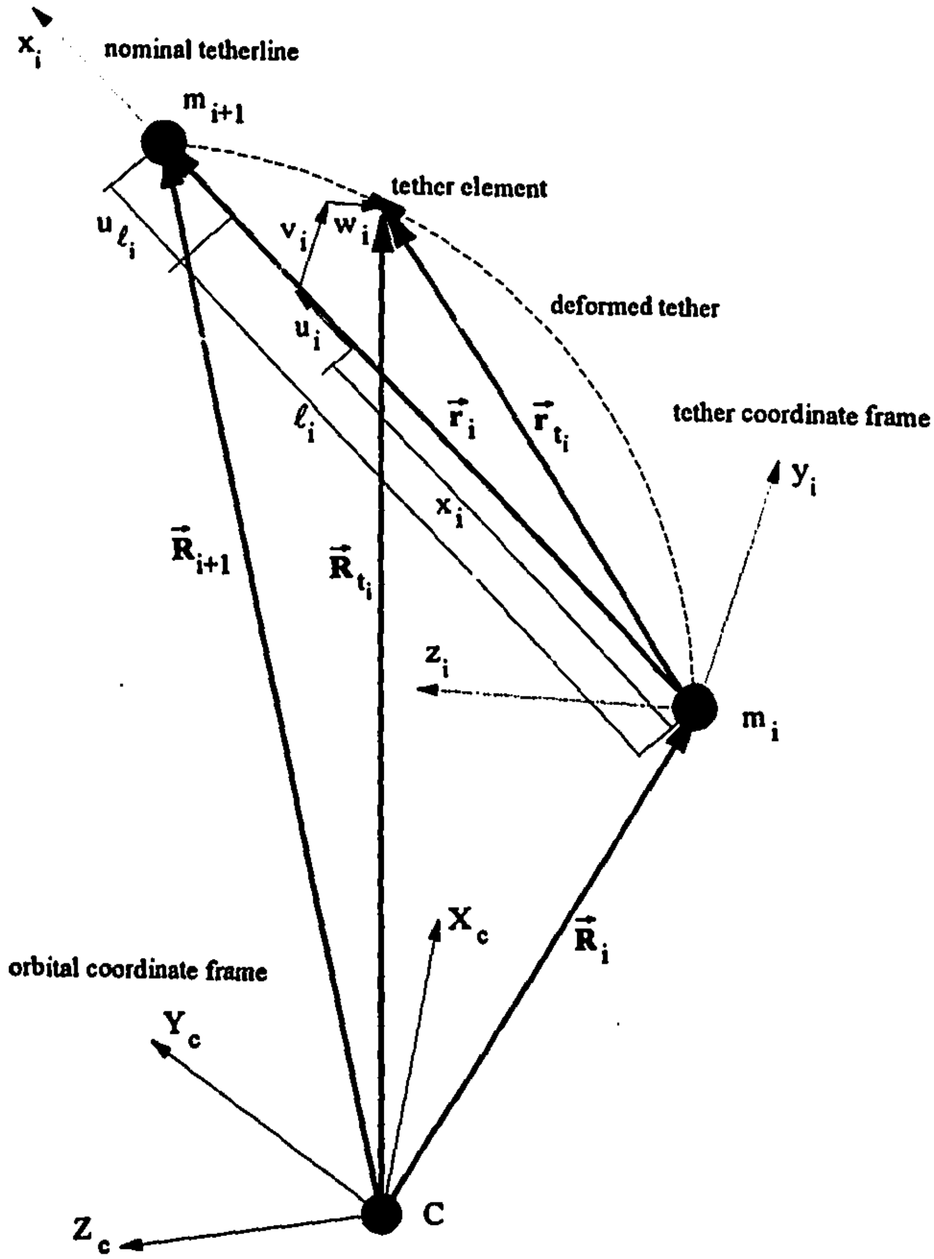

Figure 2.3: Definitions of position vectors in orbital and local tether coordinate frames

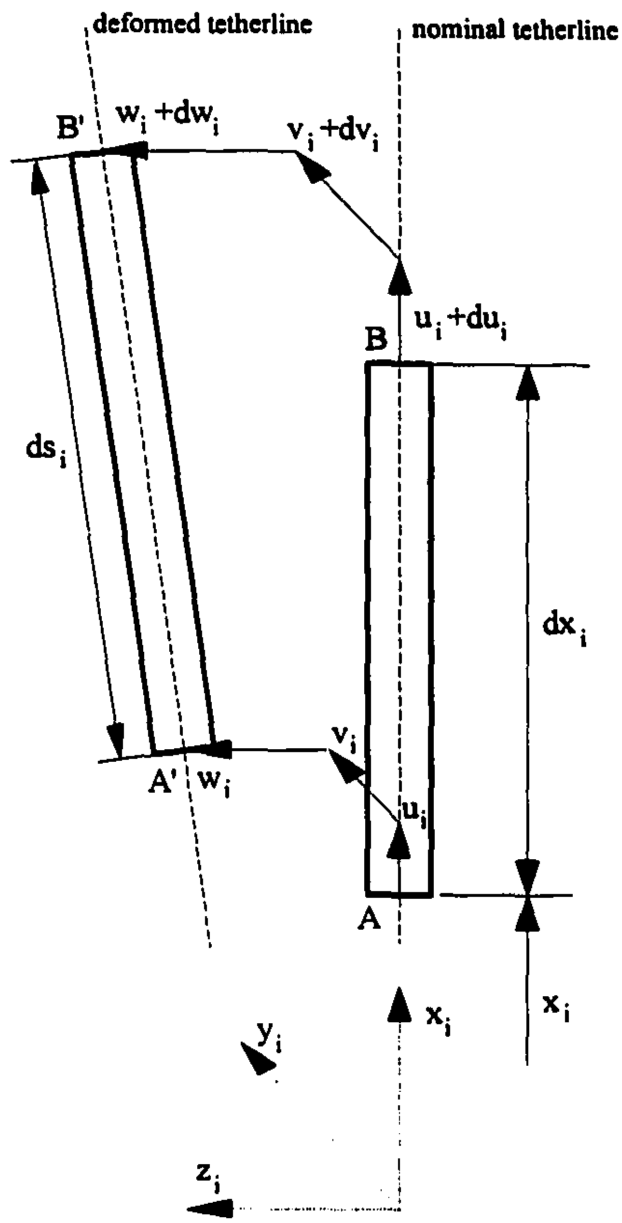

Figure 2.4: Deformation of the tether.

Chapter 3

DERIVATION OF THE GENERALIZED FORCES

3.1 Introductory Remarks

Although there are various environmental forces affecting the system dynamics such as solar radiation pressure, the Earth's magnetic field, luni-solar perturbations, aerodynamic forces, etc., we would consider the aerodynamic forces as the only significant environmental forces here, because of their larger magnitude in the case of low altitude orbits. In most of the research works in which atmospheric effects were considered, only the aerodynamic drag on the subsatellite was taken into account, while the aerodynamic lift acting on it as well as the aerodynamic forces on the tether were ignored. There are some studies in which the atmospheric drag on the tether was also included, however it was assumed that the relative velocity of air remained constant along the tether.

To obtain a more general aerodynamical model, in this formulation, some of the above shortcomings are eliminated. The aerodynamic forces on all the bodies as well as on the tethers are calculated assuming free molecular flow regime, which is described briefly in the next section. Moreover the aerodynamic forces are determined assuming that:

- the atmosphere is rotating with the Earth;

- the air density varies exponentially with the altitude;

- the bodies at the end of the tethers have no attitude motion relative to the tethers, i.e. the angles of attack required in aerodynamic calculations are simply related to the librational motion of the tethers.

In many of the investigations related to tether satellite systems, the effects of material damping on the elastic vibrations of the tethers have been neglected and the vibrating tethers have been modelled as conservative continuum systems. This is because the inclusion of material damping increases the complexity of the model. However, it must be included in a general model because:

- it has a significant effect on the stability of the system;

- it has a positive effect on the computational effort required.

The generalized forces resulting from material damping are considered in this formulation assuming viscous damping.

In addition to these two kinds of forces, there might be other external forces such as those from the thrusters that contribute to the generalized forces. They are discussed in a general manner at the end of this chapter. Splitting the generalized forces into these three categories we can then write

$$\mathbf{Q} = \mathbf{Q}_A + \mathbf{Q}_D + \mathbf{Q}_O \quad . \tag{3.1}$$

where $\mathbf{Q}_A, \mathbf{Q}_D$, and $\mathbf{Q}_O$ represent generalized forces corresponding to the aerodynamic, material damping, and other external forces, respectively.

3.2 Aerodynamic Forces

At high altitude, say 90 km or so, the atmospheric composition is significantly different from that at the sea level, and it can no longer be treated as a continuum.

Tsien [68] as well as other researchers such as Siegel [69], and Hayes and Probstein [70] have proposed a division of fluid mechanics into various regimes according to the degree of rarefaction as measured by the value of the Knudsen number. This basic parameter is defined as the ratio of the mean free path λ, the average distance travelled by a molecule before collision with another molecule, to a characteristic length L, e.g. typical dimension of a subsatellite. In general, the atmosphere can be categorized as: (i) ordinary continuum, where the density is sufficiently high so that intermolecular collisions dominate over collisions with the boundaries ($\lambda/L \ll 1$, say 10^{-2}); and (ii) free molecular flow, where the gas is sufficiently rarefied so that collisions with the boundaries dominate over collisions between molecules ($\lambda/L \gg 1$, say 10^{2}). Between these two limiting regimes there is of course a wide class of flows of varying character, which form the transient regime. In terms of altitude, that up to 90 km, from 90 km to 140 km, and beyond 140 km, correspond approximately to continuum, transient, and free molecule regimes, respectively.

In practice, a subsatellite will be located in either the transient or free molecule regime, where the aerodynamic effects must be calculated differently from that in the case of the continuum model. Because of the simplicity of the free molecular flow model on one hand and the purpose of this thesis, which is aimed at a conceptual study of the atmospheric effects, on the other hand, we calculate the aerodynamic forces using only the free molecular flow model in this formulation.

3.2.1 Free Molecular Flow Model

The free molecular flow model [1], relies on the kinetic theory of gases. For aerodynamic calculations, one is interested in the transfer of momentum from atmospheric molecules to the satellite or the tether. There are two canonical limiting cases in this model that bound the molecular-momentum transfer at the object surface: spec-

[1] For more details the interested reader is referred to Ref [71]

ular reflection and diffuse reflection, where the former is essentially a deterministic concept while the latter is a probabilistic one. The real case lies between these two limiting cases and the transferred momentum depends on various characteristics of the system.

Introducing two factors, σ_n and σ_t, called accommodation coefficients for normal and tangential momentum exchange, or for brevity normal and tangential accommodation coefficients, we can express the aerodynamic force acting on an element of surface dA by

$$d\vec{f} = d\vec{f}_n + d\vec{f}_t \quad , \tag{3.2}$$

where

$$\begin{aligned} d\vec{f}_n &= \sigma_n d\vec{f}_n^{(D)} + (1-\sigma_n) d\vec{f}_n^{(S)} \quad , \\ d\vec{f}_t &= \sigma_t d\vec{f}_t^{(D)} + (1-\sigma_t) d\vec{f}_t^{(S)} \quad . \end{aligned} \tag{3.3}$$

Subscripts t and n are used to specify the tangential and normal components, while superscripts D and S denote specular and diffuse reflections, respectively. $d\vec{f}_n^{(D)}$, $d\vec{f}_t^{(D)}$, $d\vec{f}_n^{(S)}$, and $d\vec{f}_t^{(S)}$ for an element dA, Fig. 3.1-a, are given by [71]

$$\begin{aligned} d\vec{f}_n^{(D)} &= H(\cos\alpha)\rho V_R \cos\alpha [V_R \cos\alpha + V_b]\, \hat{\boldsymbol{n}}_A dA \quad , \\ d\vec{f}_t^{(D)} &= H(\cos\alpha)\rho V_R^2 \sin\alpha\cos\alpha\, \hat{\boldsymbol{t}}_A dA \quad , \\ d\vec{f}_n^{(S)} &= 2H(\cos\alpha)\rho V_R^2 \cos^2\alpha\, \hat{\boldsymbol{n}}_A dA \quad , \\ d\vec{f}_t^{(S)} &= \vec{0} \quad , \end{aligned} \tag{3.4}$$

where H is the Heaviside function ($H(x) = 0$ if $x < 0$, and $H(x) = 1$ if $x \geq 0$), ρ is the density of local atmosphere, $\vec{V}_R$ with magnitude V_R is the relative velocity of air with respect to the element, $\hat{\boldsymbol{n}}_A$ is the unit inward normal to the surface dA, α is the local angle of attack, $\hat{\boldsymbol{t}}_A$ is the unit tangential vector in the plane of $\vec{V}_R$ and $\hat{\boldsymbol{n}}_A$, and V_b is the mean velocity of the gas molecules which is related to the surface temperature. At the altitude of interest, V_b is typically about 5% of V_R, and hence is ignored in this formulation. From Fig. 3.1 one can write

$$\cos\alpha = \frac{\vec{V}_R \cdot \hat{n}_A}{V_R} \quad ,$$
$$\hat{t}_A = \frac{\hat{n}_A \times (\vec{V}_R \times \hat{n}_A)}{||\hat{n}_A \times (\vec{V}_R \times \hat{n}_A)||} \quad , \tag{3.5}$$

where $\hat{t}_A$ is clearly not defined if $\vec{V}_R \times \hat{n}_A = \vec{0}$.

Substituting Eqs. (3.3)-(3.5) into Eq. (3.2), ignoring V_b, and recognizing that

$$\hat{t}_A \sin\alpha = \hat{v}_R - \hat{n}_A \cos\alpha \quad , \tag{3.6}$$

we arrive at

$$d\vec{f} = H(\cos\alpha)\rho V_R^2 \cos\alpha \left[(2 - \sigma_n - \sigma_t)\cos\alpha \ \hat{n}_A + \sigma_t \hat{v}_R\right] dA \quad , \tag{3.7}$$

where $\hat{v}_R$ is the unit vector along $\vec{V}_R$. The aerodynamic force and torque acting on the body can now be found by integrating Eq. (3.7) over the body surface. They are given by

$$\vec{f} = \rho V_R^2 \left[\sigma_t S_P \hat{v}_R + (2 - \sigma_n - \sigma_t)\vec{S}_{PP}\right] \quad ,$$
$$\vec{m} = \rho V_R^2 \left[\sigma_t S_P \vec{c}_P \times \hat{v}_R + (2 - \sigma_n - \sigma_t)\vec{G}_{PP}\right] \quad , \tag{3.8}$$

where

$$S_P = \oint H(\cos\alpha)\cos\alpha \ dA \quad , \qquad \vec{c}_P = \frac{1}{S_P}\oint H(\cos\alpha)\cos\alpha \ \vec{r} dA \quad ,$$
$$\vec{S}_{PP} = \oint H(\cos\alpha)\cos^2\alpha \ d\vec{A} \quad , \qquad \vec{G}_{PP} = \frac{1}{S_P}\oint H(\cos\alpha)\cos^2\alpha \ \vec{r} \times d\vec{A} \quad , \tag{3.9}$$

provided the small effects of rotations of the body are neglected.

The accommodation coefficients usually have average values in the range of $0.8 < \sigma_n, \sigma_t < 0.9$. The limiting cases, specular and diffuse reflections, are resulted by setting $\sigma_n = \sigma_t = 0$ and $\sigma_n = \sigma_t = 1$, respectively.

Using the above results and the geometrical configuration of a particular body one can find the aerodynamic forces acting on that particular body. The aerodynamic forces are presented here for the following cases:

- For a sphere with projection surface area $A_s = \pi R_s^2$,

$$\vec{\boldsymbol{f}}_s = \frac{1}{2}\rho A_s V_R (2 - \sigma_n + \sigma_t)\vec{\boldsymbol{V}}_R \ . \tag{3.10}$$

- For a plate with normal unit vector $\hat{\boldsymbol{n}}$ and surface area A_p,

$$\vec{\boldsymbol{f}}_p = \rho A_P \ |\vec{\boldsymbol{V}}_R \cdot \hat{\boldsymbol{n}}| \left[\sigma_t \vec{\boldsymbol{V}}_R + (2 - \sigma_n - \sigma_t)(\vec{\boldsymbol{V}}_R \cdot \hat{\boldsymbol{n}})\hat{\boldsymbol{n}}\right] \ . \tag{3.11}$$

- For a cylinder along unit vector $\hat{\boldsymbol{n}}$, with base surface area $A_b = \pi R_{cyl}^2$ and projection surface area $A_c = 2R_{cyl}H_{cyl}$,

$$\begin{aligned}\vec{\boldsymbol{f}}_c = {} & \rho\sigma_t \left(A_b \ |\vec{\boldsymbol{V}}_R \cdot \hat{\boldsymbol{n}}| + A_c \ |\vec{\boldsymbol{V}}_R \cdot \hat{\boldsymbol{t}}|\right) \vec{\boldsymbol{V}}_R + \rho(2 - \sigma_n - \sigma_t) \\ & \times \left[A_b \ |\vec{\boldsymbol{V}}_R \cdot \hat{\boldsymbol{n}}|(\vec{\boldsymbol{V}}_R \cdot \hat{\boldsymbol{n}})\hat{\boldsymbol{n}} - \frac{2}{3}A_c \ |\vec{\boldsymbol{V}}_R \cdot \hat{\boldsymbol{t}}|(\vec{\boldsymbol{V}}_R \times \hat{\boldsymbol{n}}) \times \hat{\boldsymbol{n}}\right] \ .\end{aligned} \tag{3.12}$$

- For an element dx of the tether with diameter d_t along unit vector $\hat{\boldsymbol{n}}$,

$$d\vec{\boldsymbol{f}}_t = \rho d_t \ |\vec{\boldsymbol{V}}_R \cdot \hat{\boldsymbol{t}}| \left[\sigma_t \vec{\boldsymbol{V}}_R - \frac{2}{3}(2 - \sigma_n - \sigma_t)(\vec{\boldsymbol{V}}_R \times \hat{\boldsymbol{n}}) \times \hat{\boldsymbol{n}}\right] dx \ . \tag{3.13}$$

Note that for the above configurations, because of symmetry, the aerodynamic torque $\vec{\boldsymbol{m}}$ on the body is equal to zero.

3.2.2 Relative Velocity of Air

The relative velocity, $\vec{\boldsymbol{V}}_R$ of a particular point of the system with respect to air depends on the orbital velocity of the centre of mass of the system, the velocity of the atmosphere due to its rotation about the Earth's axis and the velocity of the point relative to the centre of mass of the system due to the rotations and vibrations of the tethers. The last one is so small compared to the other two parts that it has been neglected in many investigations. However, it is included in this formulation.

A simple model for the speed of the atmosphere is that the latter rotates at the same angular velocity as the Earth. This makes calculation of the relative velocity of the air, relatively simple. In fact this is the model used in this formulation. However, in reality the atmospheric speed is greater at lower latitudes.

Hence the relative velocity of body i and of a specific point on the i-th tether of the system under consideration are given by

$$\begin{aligned} \vec{V}_i &= -\left[\dot{\vec{\mathbf{R}}}_c + \dot{\vec{\mathbf{R}}}_i - \vec{A} \times \left(\vec{\mathbf{R}}_c + \vec{\mathbf{R}}_i\right)\right] \quad , \\ \vec{V}_{t_i} &= -\left[\dot{\vec{\mathbf{R}}}_c + \dot{\vec{\mathbf{R}}}_{t_i} - \vec{A} \times \left(\vec{\mathbf{R}}_c + \vec{\mathbf{R}}_{t_i}\right)\right] \quad , \end{aligned} \tag{3.14}$$

where $\vec{A} = \Lambda\hat{\mathbf{K}}$ is the angular velocity of the atmosphere, $\vec{\mathbf{R}}_i, \dot{\vec{\mathbf{R}}}_i, \vec{\mathbf{R}}_{t_i}$, and $\dot{\vec{\mathbf{R}}}_{t_i}$ are as defined in section 2.4, while the orbital velocity $\dot{\vec{\mathbf{R}}}_c$ is given by

$$\dot{\vec{\mathbf{R}}}_c = \dot{R}_c\,\hat{\mathbf{i}}_c + R_c\,\dot{\theta}_c\,\hat{\mathbf{j}}_c \quad . \tag{3.15}$$

Let us define the Earth-centered inertial axes, X_I, Y_I, Z_I, such that Z_I-axis is from south to north direction, X_I-axis is in the equatorial plane along the line of nodes (assumed fixed) and Y_I-axis completes the triad. Let $\hat{\mathbf{I}}, \hat{\mathbf{J}}, \hat{\mathbf{K}}$ be the unit vectors along the X_I, Y_I, Z_I axes, respectively. The orientation of the orbital coordinate axes with respect to the inertial coordinates is specified by the orbit inclination angle i and angle $\theta_s = \theta_0 + \theta_c$, where θ_0 is the argument of the perigee while θ_c is the true anomaly. At first, the rotation i is given about X_I axis resulting in X_c', Y_c', Z_c' axes and then rotation θ_s is applied about Z_c' axis yielding X_c, Y_c, Z_c axes. Hence the unit vectors associated with the orbital and inertial coordinate systems are related by

$$\begin{Bmatrix} \hat{\mathbf{I}} \\ \hat{\mathbf{J}} \\ \hat{\mathbf{K}} \end{Bmatrix} = \begin{bmatrix} 1 & 0 & 0 \\ 0 & \cos i & -\sin i \\ 0 & \sin i & \cos i \end{bmatrix} \begin{bmatrix} \cos\theta_s & -\sin\theta_s & 0 \\ \sin\theta_s & \cos\theta_s & 0 \\ 0 & 0 & 1 \end{bmatrix} \begin{Bmatrix} \hat{\mathbf{i}}_c \\ \hat{\mathbf{j}}_c \\ \hat{\mathbf{k}}_c \end{Bmatrix} \quad . \tag{3.16}$$

where i, the inclination angle should not be mixed up with index i. Performing the matrix multiplications in Eq. (3.16), we obtain

$$\vec{A} = \Lambda\hat{\mathbf{K}} = \Lambda\left(\sin\theta_s \ \sin i \ \hat{\mathbf{i}}_c + \cos\theta_s \ \sin i \ \hat{\mathbf{j}}_c + \cos i \ \hat{\mathbf{k}}_c\right) \quad . \tag{3.17}$$

It can be shown that for orbits inclined to the equatorial plane, the out-of-orbit component of the relative velocity is larger in the neighbourhood of the equatorial nodes. This leads in turn to periodic attitude excitation. Hence for aerodynamic stabilization schemes one must guard against the destabilizing possibilities that accompany *parametric* excitation, in the case of inclined orbits.

3.2.3 Density of the Atmosphere

The atmosphere density ρ is very difficult do model accurately. The rarefied fringe of the upper atmosphere is an exceedingly complex physical system. Many gaseous species interact continuously, influenced by outside energy sources including the Earth's rotation, the Earth's magnetic field, sunlight, and the Sun's unsteady electrically charged effluent. Even more important, one must be aware of large fluctuations in density even at a fixed altitude. The two dominant causes of these fluctuations are the Earth's day-night (diurnal) cycle and solar activity fluctuations. For precise calculations, the chemical composition and species temperatures must also be available. A good reference for the Earth's atmosphere is Ref [72].

Once again, since our purpose here is to analyze the effects of the atmosphere from phenomena point of view rather than quantitatively, a simple exponential model is used to express the atmospheric density variation. In other words, the air density, ρ, is represented approximately by

$$\rho = \rho_0 \exp\left(-\frac{h - h_0}{H_0}\right) \quad , \tag{3.18}$$

where ρ_0 is the reference density at the reference altitude h_0 and H_0 is the scale height. The altitudes h_i and h_{t_i} of body i and of any particular point on the i-th tether are simply given by

$$h_i = R_c - R_E + \vec{\mathbf{R}}_i \cdot \hat{\mathbf{i}}_c \ ,$$

$$h_{t_i} = R_c - R_E + \vec{\mathbf{R}}_{t_i} \cdot \hat{\mathbf{i}}_c \ , \tag{3.19}$$

where R_E is the radius of the Earth.

Measurements have shown that the radius of the Earth is slightly shorter along the N-S direction than that along the W-E direction. Hence, strictly speaking, the Earth cannot be assumed to be spherical. It is more like an ellipsoid. The semi-major axis a_0 of the Earth is 6378.16 km while the semi-minor axis b_0 is 6356.78 km [73] and the equatorial plane is essentially a circle. Supposing that the air density is the same everywhere on the Earth's surface, one can see easily from Eqs. (3.18) and (3.19) that this 20 km oblateness would affect the air density significantly even for a circular orbit. This is because the air density varies with altitude exponentially. The system will have a lower altitude in the equatorial region compared to that over the north and south poles. Thus it experiences larger aerodynamic forces in the equatorial plane. In this thesis the same model as in Xu [22] has been used for the oblateness of the Earth, i.e.,

$$R_E = \frac{a_0 b_0}{\left[b_0^2(1 - \sin^2 i \ \sin^2 \theta_s) + a_0^2 \sin^2 i \ \sin^2 \theta_s\right]^{\frac{1}{2}}} \ . \tag{3.20}$$

Another important parameter that affects the air density is the orbital eccentricity, e. R_c does not remain constant when $e \neq 0$. Thus the system is sometimes far above the Earth and therefore is influenced by less aerodynamic forces, while at some other time it is closer to the Earth. Obviously the difference depends on how large e is.

3.2.4 Generalized Aerodynamic Forces

Once $\vec{f}_i$ and $d\vec{f}_{t_i}$, aerodynamic forces on the i-th body and an element of the i-th tether, are known, the generalized aerodynamic forces can be calculated from

$$\mathbf{Q}_A = \sum_{i=1}^{N} \vec{f}_i \cdot \frac{\partial \vec{\mathbf{R}}_i}{\partial \mathbf{q}} + \sum_{i=1}^{N-1} \int_0^{\ell_i} d\vec{f}_{t_i} \cdot \frac{\partial \vec{\mathbf{R}}_{t_i}}{\partial \mathbf{q}} \quad , \tag{3.21}$$

where the first summation is the contribution of the aerodynamic forces on the end-bodies, while the second one is due to that on the tethers. Once again substituting from Eqs. (2.5) and (2.15) for $\vec{\mathbf{R}}_i$ and $\vec{\mathbf{R}}_{t_i}$ and considering Eq. (2.60), Eq. (3.21) can be transformed to

$$\mathbf{Q}_{A_n} = \int_0^{\ell_n} \mathcal{D}_{t_n} \cdot d\vec{f}_{t_n} + \sum_{i=1}^{N} (A_{in} \mathcal{D}_{r_n} + \bar{\mu}_n \mathcal{D}_{b_n}) \cdot \vec{F}_{A_i} \quad , \tag{3.22}$$

where $\vec{F}_{A_i}$ is defined as

$$\vec{F}_{A_i} = \begin{cases} \vec{f}_i + \int_0^{\ell_i} d\vec{f}_{t_i} \ , & i = 1, 2, \ldots, N-1 \ , \\ \vec{f}_N \ , & i = N \end{cases} \tag{3.23}$$

3.3 Generalized Structural Damping Forces

As the tethers oscillate, some energy is dissipated in the deforming process, which one can account for through material damping. The damping mechanism is quite complex and may be described adequately only by considering the microscopic phenomenon inside the material. To state it simply, there is some hysteresis phenomenon when the material is subject to vibration. The area enclosed by the hysteresis curve indicates the energy dissipation which turns to heat.

There are two commonly used models to describe material damping, i.e. ,structural damping and viscous damping. For a better understanding, let us consider a bar or a string undergoing longitudinal oscillation where the governing equation of motion is given by

$$\rho \frac{\partial^2 u}{\partial t^2} = EA \frac{\partial^2 u}{\partial x^2} + Q_D \quad , \tag{3.24}$$

where the generalized damping force, Q_D, for both viscous and structural damping cases can be written as

$$Q_D = c\, EA \frac{\partial}{\partial t}\left(\frac{\partial^2 u}{\partial x^2}\right) \quad . \tag{3.25}$$

In the case of viscous damping, c is a constant damping coefficient and in the case of structural damping, $c = (\gamma/\omega)$ depends on the driving frequency ω, where γ is a constant called structural damping coefficient.

Using the assumed modes method, $u(x,t) = \sum_{n=1}^{N} \chi_n(x) q_n(t)$, the equations of motion of the discretized system are given by the following matrix form

$$\mathbf{M}\ddot{\mathbf{q}} + \mathbf{D}\dot{\mathbf{q}} + \mathbf{K}\mathbf{q} = \{0\} \quad , \tag{3.26}$$

provided that there is no external force on the system. $\mathbf{M}, \mathbf{D}$, and $\mathbf{K}$ will be diagonal matrices if χ_n's are chosen as the eigenfuctions of the undamped system (in the string or bar problem). In the case of viscous damping, matrix $\mathbf{D}$ is simply given by

$$\mathbf{D} = c\,\mathbf{K} \quad , \tag{3.27}$$

where as was mentioned earlier c is a constant. However in the case of structural damping $\mathbf{D}$ has the following form

$$\mathbf{D} = \gamma \mathbf{\Omega}^{-1}\mathbf{K} \quad , \tag{3.28}$$

where $\mathbf{\Omega}$ is a diagonal matrix consisting of the natural frequencies of the undamped system.

By analogy with a mass-dashpot-spring system, one can see that viscous damping produces a damping ratio proportional to the natural frequency of each mode

$$\zeta_n = \frac{c}{2}\omega_n \quad , \tag{3.29}$$

while in the case of structural damping all dynamical modes have the same damping ratio

$$\zeta_n = \frac{\gamma}{2} \quad . \tag{3.30}$$

When some other functions rather than the eigenfuctions of the undamped system are chosen as the admissible functions, matrices $\mathbf{M}, \mathbf{D}, \mathbf{K}$ are no longer diagonal. In this case Eq. (3.27) is still valid for viscous damping while Eq. (3.28) does not hold any more. In order to have a diagonal damping matrix after decomposition process $\mathbf{D}$ must satisfy the following matrix equation;

$$\mathbf{D}\mathbf{M}^{-1}\mathbf{K} = \mathbf{K}\mathbf{M}^{-1}\mathbf{D} \quad . \tag{3.31}$$

It has been shown that the Cauchy series

$$\mathbf{D} = \mathbf{M} \sum_{i=-\infty}^{\infty} \kappa_i \left(\mathbf{M}^{-1}\mathbf{K}\right)^i \quad , \tag{3.32}$$

where the coefficients κ_i are a set of arbitrary variables, is a solution of Eq. (3.31). These coefficients can be set to obtain the desired damping ratio for the interested frequencies. To have a constant damping ratio for all the modes of the discretized system, $\zeta_n = \dfrac{\gamma}{2}$, $n = 1, 2, \ldots, N_q$, Eq. (3.32) is substituted by

$$\mathbf{D} = \mathbf{M} \sum_{i=0}^{N_q-1} \kappa_i \left(\mathbf{M}^{-1}\mathbf{K}\right)^i \quad , \tag{3.33}$$

where κ_i's are obtained from the following set of linear algebraic equations

$$\sum_{i=0}^{N_q} \kappa_i \omega_n^{2i-1} = \gamma \quad , \qquad n = 1, 2, \ldots, N_q \quad , \tag{3.34}$$

and ω_n is the n-th natural frequency of the system.

In practice instead of the above technique, Rayleigh's approach, which is in fact a specific case of Cauchy series, is used. In this approach, the damping matrix, $\mathbf{D}$, is assumed to be a linear combination of the mass matrix, $\mathbf{M}$, and the stiffness matrix, $\mathbf{K}$, i.e. ,

$$\mathbf{D} = \kappa_0 \mathbf{M} + \kappa_1 \mathbf{K} \tag{3.35}$$

where again the coefficients κ_0 and κ_1 can be calculated based on the desired damping ratio for any two modes of interest. To obtain an equal damping ratio for modes k

and n, $\zeta_k = \zeta_n = \frac{\gamma}{2}$, those coefficients must satisfy the following equations

$$\begin{cases} \dfrac{1}{\omega_k}\kappa_0 + \omega_k\kappa_1 = \gamma \ , \\ \\ \dfrac{1}{\omega_n}\kappa_0 + \omega_n\kappa_1 = \gamma \ . \end{cases} \tag{3.36}$$

For a nonlinear system, introduction of damping forces becomes more complicated, because the stiffness forces cannot be represented simply as multiplication of a stiffness matrix and the generalized coordinate vector. The problem becomes even more complicated in the case of a system consisting of rigid and flexible parts, because of the presence of coupling terms in the mass matrix. However we can extend the above discussion to these cases by an extension of the definition of the stiffness matrix. For a linear system, like a simple bar or string, the stiffness matrix $\mathbf{K}$ is simply given by

$$\mathbf{K} = \frac{\partial \mathbf{Q}_E}{\partial \mathbf{q}} \ , \tag{3.37}$$

where $\mathbf{Q}_E$ is the array of generalized forces corresponding to the internal elastic forces, given by

$$\mathbf{Q}_E = \frac{\partial U_E}{\partial \mathbf{q}} \ . \tag{3.38}$$

Therefore, once the elastic potential energy of the system is known, one can construct the stiffness matrix using Eqs. (3.37) and (3.38), and then introduce the appropriate damping matrix using the viscous damping approach, Rayleigh's approach, or Cauchy series.

In this thesis, to avoid this complexity, viscous damping is used to represent the effects of material damping on the system dynamics, i.e. Eq. (3.27) in conjunction with Eq. (3.37) is used to introduce generalized forces due to material damping, i.e.

$$\mathbf{Q}_D = c\,\frac{\partial \mathbf{Q}_E}{\partial \mathbf{q}}\dot{\mathbf{q}} = c\,\frac{\partial}{\partial \mathbf{q}}\left(\frac{\partial U_E}{\partial \mathbf{q}}\right)\dot{\mathbf{q}} \ . \tag{3.39}$$

3.4 Other External Forces

The generalized forces corresponding to other external forces, if there are any, other than those mentioned above are simply obtained from

$$\mathbf{Q}_O = \sum_{i=1}^{N_f} \vec{F}_{O_i} \cdot \frac{\partial \vec{R}_{F_i}}{\partial \mathbf{q}} \quad , \tag{3.40}$$

where N_f is the number of the external forces, $\vec{F}_{O_i}$ is the pnysical external force vector, and $\vec{R}_{F_i}$ is the position vector of the point of application of $\vec{F}_{O_i}$ with respect to the centre of mass of the system.

Normally, non-elastic internal forces have no contribution to the generalized external forces, because of the cancellation of the work done by opposite forces. However for the system under consideration the work done by the tension in the tethers, which are in fact internal forces, must be taken into account in the case of retrieval and deployment. Using the above equation and the fact that the tension forces act along the tethers, one can show that these forces contribute only to the generalized forces corresponding to the rigid body longitudinal motion of the tethers, ℓ_i.

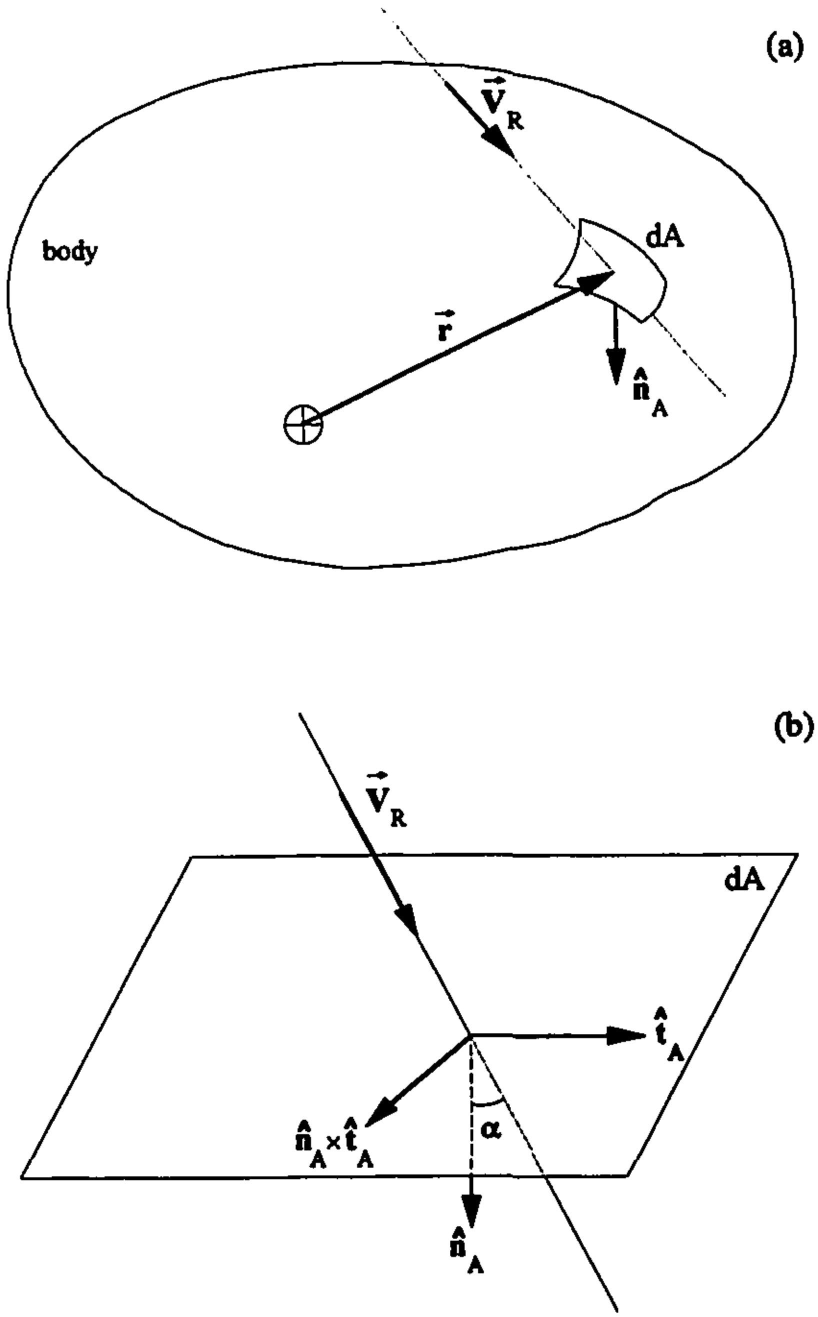

Figure 3.1: Geometry of an object: (a) molecules incident on an element of the body surface; (b) Orthogonal triad of surface-oriented unit vectors.

Chapter 4

LINEARIZATION AND EIGENVALUE ANALYSIS

4.1 Introductory Remarks

The equations of motion given by Eq. (2.71), derived in Chapter 2, must be transformed to the vector form

$$\mathbf{M}\ddot{\mathbf{q}} = \mathbf{f} \quad , \tag{4.1}$$

for any further operation such as dynamical simulation, eigenvalue analysis, or control synthesis. In Eq. (4.1) $\mathbf{M}$ is the $N_q \times N_q$ dimensional mass matrix and is a function of generalized coordinates, $\mathbf{q}$ and time t, $\mathbf{f}$ is the N_q dimensional array of generalized forces and is a function of generalized speeds, $\dot{\mathbf{q}}$, as well as generalized coordinates and time.

4.2 Vector Form of the Equations of Motion

Only those terms in Eq. (2.71) involving second order derivatives with respect to time contribute to the mass matrix. Hence it is more appropriate to rewrite this equation in the following form

$$\mathbf{p}_n + \mathbf{e}_n = \frac{1}{m}\mathbf{Q}_n \; , \qquad n = 1, 2, \ldots, N-1 \quad , \tag{4.2}$$

where $\mathbf{p}_n$ is given by

$$\mathbf{p}_n = \hat{\rho}_n \int_0^{\ell_n} \boldsymbol{\mathcal{D}}_{\mathbf{t}_n} \cdot \ddot{\vec{\mathbf{r}}}_{\mathbf{t}_n} dx_n + \sum_{j=1}^{N-1} \Big[-A_{jn} \boldsymbol{\mathcal{D}}_{\mathbf{r}_n} \cdot \ddot{B}_j \vec{\mathbf{r}}_j + (F_{jn} \boldsymbol{\mathcal{D}}_{\mathbf{r}_n} + \bar{\mu}_n A_{nj} \boldsymbol{\mathcal{D}}_{\mathbf{b}_n}$$
$$- A_{nj} \boldsymbol{\mathcal{D}}_{B_n}) \cdot \ddot{\vec{\mathbf{r}}}_j + (\bar{\mu}_j A_{jn} \boldsymbol{\mathcal{D}}_{\mathbf{r}_n} - \bar{\mu}_j \bar{\mu}_n \boldsymbol{\mathcal{D}}_{\mathbf{b}_n} + \bar{\mu}_j \boldsymbol{\mathcal{D}}_{B_n}) \cdot \ddot{\vec{\mathbf{b}}}_j \Big] \quad , \tag{4.3}$$

while $\mathbf{e}_n$ consists of the remaining terms in the left hand side of Eq. (2.71). In the above equation $\boldsymbol{\mathcal{D}}_{B_n}$ is

$$\boldsymbol{\mathcal{D}}_{B_n} = \frac{\partial B_n}{\partial \mathbf{q}_n} \vec{\mathbf{r}}_n = \begin{Bmatrix} 0 \\ 0 \\ -\hat{\rho}_n \beta_n \\ \{0\} \\ \{0\} \\ \{0\} \end{Bmatrix} \vec{\mathbf{r}}_n \quad . \tag{4.4}$$

It is clear that only $\mathbf{p}_n$ contributes to the mass matrix while $\mathbf{e}_n$ has no contribution in this regard.

Noting that $\vec{\mathbf{r}}_j, \vec{\mathbf{b}}_j$, and $\vec{\mathbf{r}}_{\mathbf{t}_j}$ are functions of $\mathbf{q}_j$ only [1], one can show that their second order time derivatives can be expressed as

$$\begin{aligned} \ddot{\vec{\mathbf{r}}}_j &= \boldsymbol{\mathcal{D}}_{\mathbf{r}_j}^T \ddot{\mathbf{q}}_j + \vec{\mathbf{d}}_{\mathbf{r}_j} \quad , \\ \ddot{\vec{\mathbf{b}}}_j &= \boldsymbol{\mathcal{D}}_{\mathbf{b}_j}^T \ddot{\mathbf{q}}_j + \vec{\mathbf{d}}_{\mathbf{b}_j} \quad , \\ \ddot{\vec{\mathbf{r}}}_{\mathbf{t}_j} &= \boldsymbol{\mathcal{D}}_{\mathbf{t}_j}^T \ddot{\mathbf{q}}_j + \vec{\mathbf{d}}_{\mathbf{t}_j} \quad . \end{aligned} \tag{4.5}$$

The first order time derivatives are included in $\vec{\mathbf{d}}_{\mathbf{r}_j}$, etc. Using Eq. (B.18) and the definition of $\boldsymbol{\mathcal{D}}_{B_j}$ in Eq. (4.4), we can write

$$\ddot{B}_j \vec{\mathbf{r}}_j = \boldsymbol{\mathcal{D}}_{B_j}^T \ddot{\mathbf{q}}_j + \vec{\mathbf{d}}_{B_j} \quad , \tag{4.6}$$

[1] Note that they are functions of the generalized coordinates corresponding to the j-th tether only.

where

$$\vec{\mathbf{d}}_{B_j} = -\rho_j \dot{\beta}_j \dot{\ell}_j \dot{\vec{\mathbf{r}}}_j \ . \tag{4.7}$$

Expressions for vectors $\vec{\mathbf{d}}_{\mathbf{r}_j}, \vec{\mathbf{d}}_{\mathbf{b}_j}$, and $\vec{\mathbf{d}}_{\mathbf{t}_j}$ are given in Appendix D.

Substituting for $\ddot{\vec{\mathbf{r}}}_j, \ddot{\vec{\mathbf{b}}}_j, \ddot{\vec{\mathbf{r}}}_{\mathbf{t}_j}$ and $\ddot{B}_j \vec{\mathbf{r}}_j$ from Eqs. (4.5) and (4.6) into Eq. (4.3) and performing some algebraic manipulations, $\mathbf{p}_n$ can be rewritten as

$$\mathbf{p}_n = \mathbf{h}_n + \sum_{j=1}^{N-1} \mathbf{M}_{nj} \ddot{\mathbf{q}}_j \ , \qquad n = 1, 2, \ldots, N-1 \ , \tag{4.8}$$

where $\mathbf{M}_{nj}$ is an $N_{q_n} \times N_{q_j}$ dimensional matrix given by

$$\begin{aligned} \mathbf{M}_{nj} = \delta_{nj} \hat{\rho}_n \int_0^{\ell_n} \mathcal{D}_{\mathbf{t}_n} \cdot \mathcal{D}_{\mathbf{t}_n}^T dx_n - A_{jn} \mathcal{D}_{\mathbf{r}_n} \cdot \mathcal{D}_{B_j}^T + (F_{jn} \mathcal{D}_{\mathbf{r}_n} + \bar{\mu}_n A_{nj} \mathcal{D}_{\mathbf{b}_n} \\ - A_{nj} \mathcal{D}_{B_n}) \cdot \mathcal{D}_{\mathbf{r}_j}^T + (\bar{\mu}_j A_{jn} \mathcal{D}_{\mathbf{r}_n} - \bar{\mu}_j \bar{\mu}_n \mathcal{D}_{\mathbf{b}_n} + \bar{\mu}_j \mathcal{D}_{B_n}) \cdot \mathcal{D}_{\mathbf{b}_j}^T \ , \end{aligned} \tag{4.9}$$

and $\mathbf{h}_n$ is given by

$$\begin{aligned} \mathbf{h}_n = \hat{\rho}_n \int_0^{\ell_n} \mathcal{D}_{\mathbf{t}_n} \cdot \vec{\mathbf{d}}_{\mathbf{t}_n} dx_n + \sum_{j=1}^{N-1} \Big[-A_{jn} \mathcal{D}_{\mathbf{r}_n} \cdot \vec{\mathbf{d}}_{B_j} + (F_{jn} \mathcal{D}_{\mathbf{r}_n} + \bar{\mu}_n A_{nj} \mathcal{D}_{\mathbf{b}_n} \\ - A_{nj} \mathcal{D}_{B_n} \vec{\mathbf{r}}_n) \cdot \vec{\mathbf{d}}_{\mathbf{r}_j} + (\bar{\mu}_j A_{jn} \mathcal{D}_{\mathbf{r}_n} - \bar{\mu}_j \bar{\mu}_n \mathcal{D}_{\mathbf{b}_n} + \bar{\mu}_j \mathcal{D}_{B_n} \vec{\mathbf{r}}_n) \cdot \vec{\mathbf{d}}_{\mathbf{b}_j} \Big] \ . \end{aligned} \tag{4.10}$$

Now we can rewrite Eq. (4.2) by substituting for $\mathbf{p}_n$. After some manipulation, equations of motion corresponding to $\mathbf{q}_n$ are given by

$$\sum_{j=1}^{N-1} \mathbf{M}_{nj} \ddot{\mathbf{q}}_j = \mathbf{f}_n \ , \qquad n = 1, 2, \ldots, N-1 \ , \tag{4.11}$$

where

$$\mathbf{f}_n = \frac{1}{m} \mathbf{Q}_n - \mathbf{e}_n - \mathbf{h}_n \ . \tag{4.12}$$

Note that $\mathbf{M}_{nj}$ is the submatrix representing the contribution of the j-th tether to the equations of motion corresponding to the generalized coordinates of the n-th tether, $\mathbf{q}_n$, while $\mathbf{f}_n$ is the N_{q_n} dimensional subvector of forcing array corresponding to these generalized coordinates.

For the station-keeping phase, which is examined extensively in the following sections, $\mathbf{f}_n$ is given by

$$\mathbf{f}_n = \frac{1}{m}\mathbf{Q}_n - \left\{ \sum_{j=1}^{N-1} \left[(F_{jn}\boldsymbol{\mathcal{D}}_{\mathbf{r}_n} + \bar{\mu}_n A_{nj}\boldsymbol{\mathcal{D}}_{\mathbf{b}_n}) \cdot \left[\vec{\mathbf{d}}_{\mathbf{r}_j} + \alpha_0^2 \left\{ \vec{\mathbf{r}}_j - 3(\hat{\mathbf{i}}_c \cdot \vec{\mathbf{r}}_j)\hat{\mathbf{i}}_c \right\} \right] \right. \right.$$
$$\left. + (\bar{\mu}_j A_{jn}\boldsymbol{\mathcal{D}}_{\mathbf{r}_n} - \bar{\mu}_j\bar{\mu}_n\boldsymbol{\mathcal{D}}_{\mathbf{b}_n}) \cdot \left[\vec{\mathbf{d}}_{\mathbf{b}_j} + \alpha_0^2 \left\{ \vec{\mathbf{b}}_j - 3(\hat{\mathbf{i}}_c \cdot \vec{\mathbf{b}}_j)\hat{\mathbf{i}}_c \right\} \right] \right]$$
$$+ \hat{\rho}_n \int_0^{\ell_n} \boldsymbol{\mathcal{D}}_{\mathbf{t}_n} \cdot \left[\vec{\mathbf{d}}_{\mathbf{t}_n} + \alpha_0^2 \left\{ \vec{\mathbf{r}}_{\mathbf{t}_n} - 3(\hat{\mathbf{i}}_c \cdot \vec{\mathbf{r}}_{\mathbf{t}_n})\hat{\mathbf{i}}_c \right\} \right] dx_n$$
$$\left. + \frac{EA_n}{2m} \int_0^{\ell_n} \frac{\partial \mathcal{E}_n}{\partial \mathbf{q}_n} dx_n \right\} \quad . \tag{4.13}$$

4.3 Equilibrium Configuration

A solution of the system , $\mathbf{q}^*(t)$, is a set of time functions which satisfy Eq. (4.1), i.e.

$$\mathbf{M}^*\ddot{\mathbf{q}}^* = \mathbf{f}^* \quad , \tag{4.14}$$

where

$$\mathbf{M}^* = \mathbf{M}(\mathbf{q}^*, t) \quad , \quad \mathbf{f}^* = \mathbf{f}(\mathbf{q}^*, \dot{\mathbf{q}}^*, t) \quad . \tag{4.15}$$

On the other hand, an equilibrium configuration of a system is a particular solution consisting of a set of constants, $q_i^e(t) = c_i$, $i = 1, 2, \ldots, N_q$. It is sometimes referred to as the *fixed point* of the system. It can be found, if there is any, by solving the equations of motion after putting $\dot{\mathbf{q}}^e = \{0\}$, $\ddot{\mathbf{q}}^e = \{0\}$, i.e. ,

$$\mathbf{f}^e(\mathbf{q}^e, \{0\}, t) = \{0\} \quad . \tag{4.16}$$

In addition to the above mathematical step a physical insight of the problem is needed to formulate the possible equilibrium configurations of the system. Following descriptions try to provide such an understanding of the problem.

In the deployment and retrieval stages of a tethered satellite system the reel mechanisms reel the tethers out or in, respectively. Hence the nominal lengths of the tethers, which are also some of the generalized coordinates of the system, do not remain constant. This implies that there is no static equilibrium state or fixed point in these stages. However during the station-keeping stage, where the nominal lengths of the tethers remain constant, one can expect a static equilibrium state depending on the applied forces and orbital motion of the system. In the case of a noncircular orbit there is again no equilibrium configuration.

If the forces acting on the system are only gravitational and internal elastic forces, a multi-body system has an infinite number of equilibrium points. In the case of a two-body system with a rigid tether, there are four configurations; two along the local vertical and two along the local horizontal. Those equilibrium states which are along the local vertical can be shown to be stable due to the gravity gradient, while the other two positions are unstable. In the case of three body systems, Amier and Misra [60] obtained the equilibrium configurations analytically. The stability of the system about these configurations was discussed in that study. For a general case it is very difficult to obtain all possible equilibrium configurations. However, the local vertical and horizontal configurations are equilibrium states even for a general multi-body tethered system.

If in addition to the gravitational force, there are environmental forces acting on the system, the whole situation is changed. First of all, in contrast to the case of no environmental forces, there are no equilibrium states for an inclined circular orbit because of the aerodynamic forces in a rotating atmosphere. The only possible equilibrium configurations exist in the case of an equatorial circular orbit. Furthermore, the equilibrium states are significantly affected by the aerodynamic forces acting on the bodies and the tethers.

Let us consider a two body tethered system which is located in an orbit close to the Earth. For the sake of argument let us also assume that the center of mass of the system is approximately coincident with that of the main satellite and the aerodynamic force on the main satellite as well as on the tether are negligible. The equilibrium configurations along the local vertical which were stable no longer remain along the local vertical and their stability depends on the system parameters. The lower position is displaced from the vertical line by an angle α, whose magnitude depends on the system parameters. In addition, the tether no longer has a straight shape in the lower equilibrium position. If the aerodynamic force on the tether is also included in the calculation, the equilibrium position, curvature of the tether, and the stability of the system are changed.

In the case where environmental forces are involved, the equilibrium state can be found analytically only for a very simple model, otherwise it must be obtained numerically. The situation becomes more complicated for a multi-body, multi-tethered system, and determining the equilibrium position of the system analytically is extremely difficult, if not impossible. Hence there is almost no way except using the numerical approach for this purpose.

4.3.1 Static Equilibrium Equations

Letting the lengths of the tethers remain constant and putting $\dot{\ell}_i = 0$, $\ddot{\ell}_i = 0$ in Eq. (2.71), lead to the equations of motion corresponding to the dynamics of the system in the station-keeping phase, given by

$$\sum_{j=1}^{N-1} \mathbf{P}_{nj} + \mathbf{S}_n = \frac{1}{m}\mathbf{Q}_n \quad , \tag{4.17}$$

where $\mathbf{P}_{nj}$ and $\mathbf{S}_n$ are defined by Eqs. (2.74) and (2.84), respectively, with the understanding that $\mathbf{L}_n$ appearing in Eq. (2.84) is a zero array in the station-keeping phase. To obtain the algebraic equations corresponding to the equilibrium states, two more steps must be taken;

- orbital motion is confined to a circular orbit, i.e. ,

$$\dot{\theta}_c = \alpha_0 = \Omega_c \quad , \quad R_c = \text{constant}. \tag{4.18}$$

- time derivative of the generalized coordinates are set to zero, i.e.

$$
\begin{aligned}
&\dot{\theta}_i = \ddot{\theta}_i = \dot{\phi}_i = \ddot{\phi}_i = 0 \quad , \\
&\dot{\xi}_i = \ddot{\xi}_i = \{0\} \quad , \quad \dot{\eta}_i = \ddot{\eta}_i = \{0\} \quad , \quad \dot{\nu}_i = \ddot{\nu}_i = \{0\} \quad . \qquad (4.19)
\end{aligned}
$$

Having done so, the desired equations can be written as

$$
\begin{aligned}
\frac{1}{m}\mathbf{Q}_n^e = \sum_{j=1}^{N-1} \Big\{ &\left(F_{jn}\mathcal{D}_{\mathbf{r}_n}^e + \bar{\mu}_n A_{nj}\mathcal{D}_{\mathbf{b}_n}^e\right) \cdot \left[\vec{\Omega}_j^e \times (\vec{\Omega}_j^e \times \vec{\mathbf{r}}_j^e) + \Omega_c^2\left\{\vec{\mathbf{r}}_j^e - 3(\hat{\mathbf{i}}_c \cdot \vec{\mathbf{r}}_j^e)\hat{\mathbf{i}}_c\right\}\right] \\
&+ \left(\bar{\mu}_j A_{jn}\mathcal{D}_{\mathbf{r}_n}^e - \bar{\mu}_j\bar{\mu}_n\mathcal{D}_{\mathbf{b}_n}^e\right) \cdot \left[\vec{\Omega}_j^e \times (\vec{\Omega}_j^e \times \vec{\mathbf{b}}_j^e) + \Omega_c^2\left\{\vec{\mathbf{b}}_j^e - 3(\hat{\mathbf{i}}_c \cdot \vec{\mathbf{b}}_j^e)\hat{\mathbf{i}}_c\right\}\right]\Big\} \\
&+ \bar{\rho}_n \int_0^{\ell_n} \mathcal{D}_{\mathbf{t}_n}^e \cdot \left[\vec{\Omega}_j^e \times (\vec{\Omega}_j^e \times \vec{\mathbf{r}}_{\mathbf{t}_n}^e) + \Omega_c^2\left\{\vec{\mathbf{r}}_{\mathbf{t}_n}^e - 3(\hat{\mathbf{i}}_c \cdot \vec{\mathbf{r}}_{\mathbf{t}_n}^e)\hat{\mathbf{i}}_c\right\}\right] dx_n \\
&+ \frac{EA_n}{2m}\int_0^{\ell_n} \frac{\partial \mathcal{E}_n^e}{\partial \mathbf{q}_n^e} dx_n \quad , \qquad (4.20)
\end{aligned}
$$

where now $\vec{\Omega}_j^e = \Omega_c\left(\sin\phi_j\hat{\mathbf{i}}_j + \cos\phi_j\hat{\mathbf{k}}_j\right)$.

In the following sections the static equilibrium equations are specialized for two cases: atmospheric missions when $\mathbf{Q}_A \neq \{0\}$, but $\mathbf{Q}_O = \{0\}$, and systems with no external forces, $\mathbf{Q}_O = \mathbf{Q}_A = \{0\}$.

Systems Used in Atmospheric Missions

As mentioned earlier, in the presence of atmospheric forces, a static equilibrium state can exist only in the equatorial plane. If only the aerodynamic drag on the bodies and tethers are considered and there are no other external forces, one can physically visualize that the only possible equilibrium configurations are in the orbital plane. The corresponding equations, after some manipulation, are given by

$$
\begin{aligned}
Q_{A_{\theta_n}}^e = -3m\Omega_c^2\, \hat{\mathbf{i}}_c \cdot \Big\{ &\sum_{j=1}^{N-1} \Big[\left(F_{jn}\hat{\mathbf{k}}_n \times \vec{\mathbf{r}}_n^e + \bar{\mu}_n A_{nj}\hat{\mathbf{k}}_n \times \vec{\mathbf{b}}_n^e\right)(\hat{\mathbf{i}}_c \cdot \vec{\mathbf{r}}_j^e) + \left(\bar{\mu}_j A_{jn}\hat{\mathbf{k}}_n \times \vec{\mathbf{r}}_n^e\right. \\
&\left. - \bar{\mu}_j\bar{\mu}_n\hat{\mathbf{k}}_n \times \vec{\mathbf{b}}_n^e\right)(\hat{\mathbf{i}}_c \cdot \vec{\mathbf{b}}_j^e)\Big] + \bar{\rho}_n\int_0^{\ell_n}(\hat{\mathbf{k}}_n \times \vec{\mathbf{r}}_{\mathbf{t}_n}^e)(\hat{\mathbf{i}}_c \cdot \vec{\mathbf{r}}_{\mathbf{t}_n}^e)dx_n\Big\} \quad ,
\end{aligned}
$$

$$\phi_n^e = 0 \quad ,$$

$$\mathbf{Q}^e_{A_{\boldsymbol{\xi}_n}} = -3m\Omega_c^2\ (\hat{\mathbf{i}}_c\cdot\hat{\mathbf{i}}_n)\left\{\sum_{j=1}^{N-1}\Big[(F_{jn}\mathbf{X}_{\ell n} + \hat{\rho}_n\ell_n A_{nj}\mathbf{X}_{*n})\,(\hat{\mathbf{i}}_c\cdot\vec{\mathbf{r}}_j^e) + (\bar{\mu}_j A_{jn}\mathbf{X}_{\ell n} - \bar{\mu}_j\hat{\rho}_n\ell_n\mathbf{X}_{*n})\,(\hat{\mathbf{i}}_c\cdot\vec{\mathbf{b}}_j^e)\ \Big] + \hat{\rho}_n\int_0^{\ell_n}(\hat{\mathbf{i}}_c\cdot\vec{\mathbf{r}}_{t_n}^e)\mathbf{X}_n dx_n\right\} + \frac{EA_n}{2}\int_0^{\ell_n}\left(\frac{\partial\mathcal{E}_n}{\partial\boldsymbol{\xi}_n}\right)^e dx_n \quad ,$$

$$\mathbf{Q}^e_{A\boldsymbol{\eta}_n} = -3m\Omega_c^2\ (\hat{\mathbf{i}}_c\cdot\hat{\mathbf{j}}_n)\left\{\sum_{j=1}^{N-1}\Big[\hat{\rho}_n\ell_n A_{nj}\mathbf{Y}_{*n}(\hat{\mathbf{i}}_c\cdot\vec{\mathbf{r}}_j^e) - \bar{\mu}_j\hat{\rho}_n\ell_n\mathbf{Y}_{*n}(\hat{\mathbf{i}}_c\cdot\vec{\mathbf{b}}_j^e)\Big] + \hat{\rho}_n\int_0^{\ell_n}(\hat{\mathbf{i}}_c\cdot\vec{\mathbf{r}}_{t_n}^e)\mathbf{Y}_n dx_n\right\} + \frac{EA_n}{2}\int_0^{\ell_n}\left(\frac{\partial\mathcal{E}_n}{\partial\boldsymbol{\eta}_n}\right)^e dx_n \quad ,$$

$$\mathbf{Q}^e_{A\boldsymbol{\nu}_n} = -3m\Omega_c^2\ (\hat{\mathbf{i}}_c\cdot\hat{\mathbf{k}}_n)\left\{\sum_{j=1}^{N-1}\Big[\hat{\rho}_n\ell_n A_{nj}\mathbf{Z}_{*n}(\hat{\mathbf{i}}_c\cdot\vec{\mathbf{r}}_j) - \bar{\mu}_j\hat{\rho}_n\ell_n\mathbf{Z}_{*n}(\hat{\mathbf{i}}_c\cdot\vec{\mathbf{b}}_j^e)\Big] + \hat{\rho}_n\int_0^{\ell_n}(\hat{\mathbf{i}}_c\cdot\vec{\mathbf{r}}_{t_n}^e)\mathbf{Z}_n dx_n\right\} + \frac{EA_n}{2}\int_0^{\ell_n}\left(\frac{\partial\mathcal{E}_n}{\partial\boldsymbol{\nu}_n}\right)^e dx_n \quad , \tag{4.21}$$

where after substitution for u_n, v_n and w_n, $\mathcal{E}_n$ is given by

$$\mathcal{E}_n = \frac{1}{2}\left(\frac{\partial\mathbf{X}_n}{\partial x_n}\boldsymbol{\xi}_n + \frac{1}{2}\left[\left(\frac{\partial\mathbf{Y}_n}{\partial x_n}\boldsymbol{\eta}_n\right)^2 + \left(\frac{\partial\mathbf{Z}_n}{\partial x_n}\boldsymbol{\nu}_n\right)^2\right]\right)^2 - \frac{1}{2}\left(\frac{\partial\mathbf{X}_n}{\partial x_n}\boldsymbol{\xi}_n\right)^2\left[\left(\frac{\partial\mathbf{Y}_n}{\partial x_n}\boldsymbol{\eta}_n\right)^2 + \left(\frac{\partial\mathbf{Z}_n}{\partial x_n}\boldsymbol{\nu}_n\right)^2\right] \quad . \tag{4.22}$$

Systems With No External Forces

In the absence of any external forces other than gravitational forces, it can be seen by inspection that $\theta_n^e = 0$, $\phi_n^e = 0$, $\boldsymbol{\eta}_n^e = \{0\}$, $\boldsymbol{\nu}_n^e = \{0\}$ satisfy the above equations, while $\boldsymbol{\xi}_n^e, n = 1, 2, \ldots, N-1$ are governed by the following equation

$$\sum_{j=1}^{N-1}\Big[(F_{jn}\mathbf{X}_{\ell n} + \hat{\rho}_n\ell_n A_{nj}\mathbf{X}_{*n})\,(\ell_j + \mathbf{X}_{\ell j}^T\boldsymbol{\xi}_j^e) + (\bar{\mu}_j A_{jn}\mathbf{X}_{\ell n} - \bar{\mu}_j\hat{\rho}_n\ell_n\mathbf{X}_{*n})\left(\ell_j^2/2\ell_0 + \mathbf{X}_{*j}^T\boldsymbol{\xi}_j^e\right)\ \Big] + \hat{\rho}_n\int_0^{\ell_n}\mathbf{X}_n(x_n + \mathbf{X}_n^T\boldsymbol{\xi}_n^e)dx_n - \frac{EA_n}{6m\Omega_c^2}\int_0^{\ell_n}\left(\frac{\partial\mathcal{E}_n}{\partial\boldsymbol{\xi}_n}\right)^e dx_n = \{0\} \quad , \tag{4.23}$$

which are a set of linear equations in terms of ξ_n^e's. Combining the equations corresponding to all n and performing some algebra, one can obtain ξ_n^e from the following vector equation:

$$\begin{bmatrix} \mathbf{A}_{11} & \mathbf{A}_{12} & \cdots & \mathbf{A}_{1(N-1)} \\ \mathbf{A}_{21} & \mathbf{A}_{22} & \cdots & \mathbf{A}_{2(N-1)} \\ \vdots & \vdots & \ddots & \vdots \\ \mathbf{A}_{(N-1)1} & \mathbf{A}_{(N-1)2} & \cdots & \mathbf{A}_{(N-1)(N-1)} \end{bmatrix} \begin{Bmatrix} \xi_1^e \\ \xi_2^e \\ \vdots \\ \xi_{N-1}^e \end{Bmatrix} = \begin{Bmatrix} \mathbf{c}_1 \\ \mathbf{c}_2 \\ \vdots \\ \mathbf{c}_{N-1} \end{Bmatrix} , \tag{4.24}$$

where $\mathbf{A}_{nj}$ is an $N_{q_n} \times N_{q_j}$ matrix given by

$$\begin{aligned} \mathbf{A}_{nj} = {} & \left(F_{jn}\mathbf{X}_{\ell n} + \hat{\rho}_n \ell_n A_{nj} \mathbf{X}_{*n}\right) \mathbf{X}_{\ell j}^T + \left(\bar{\mu}_j A_{jn} \mathbf{X}_{\ell n} - \bar{\mu}_j \hat{\rho}_n \ell_n \mathbf{X}_{*n}\right) \mathbf{X}_{*j}^T \\ & + \delta_{nj}\hat{\rho}_n \int_0^{\ell_n} \mathbf{X}_n \mathbf{X}_n^T dx_n - \delta_{nj} \frac{EA_n}{6m\Omega_c^2} \int_0^{\ell_n} \left(\frac{\partial \mathbf{X}_n}{\partial x_n}\right) \left(\frac{\partial \mathbf{X}_n}{\partial x_n}\right)^T dx_n \ , \end{aligned} \tag{4.25}$$

and $\mathbf{c}_n$ is an N_{q_n} vector given by

$$\begin{aligned} \mathbf{c}_n = {} & -\hat{\rho}_n \int_0^{\ell_n} \mathbf{X}_n x_n dx_n - \sum_{j=1}^{N-1} \left[\left(F_{jn}\mathbf{X}_{\ell n} + \hat{\rho}_n \ell_n A_{nj} \mathbf{X}_{*n}\right) \ell_j \right. \\ & \left. + \left(\bar{\mu}_j A_{jn} \mathbf{X}_{\ell n} - \bar{\mu}_j \hat{\rho}_n \ell_n \mathbf{X}_{*n}\right) \ell_j^2 / 2\ell_0 \right] \ . \end{aligned} \tag{4.26}$$

4.4 Linearization of the Equations of Motion

The equations of motion given by Eq. (4.1) are fully nonlinear and describe any motion of the system. Once a solution of the system, $\mathbf{q}^*$, is found, any other solution corresponding to small deviation from that solution, called the *nominal solution*, can be obtained using the linearized equations of motion rather than the nonlinear equations. The linearization is obviously carried out about the nominal solution.

Let us assume that $\mathbf{q}$ is a solution with small deviation from the nominal solution, $\mathbf{q}^*$, i.e. ,

$$\mathbf{q} = \mathbf{q}^* + \delta\mathbf{q} \tag{4.27}$$

Using Taylor expansion up to the first order, Eq. (4.1) can be rewritten as

$$\left[\mathbf{M}^* + \left(\frac{\partial \mathbf{M}}{\partial \mathbf{q}}\right)^* \delta\mathbf{q} + \mathcal{O}(\delta\mathbf{q}^2)\right](\ddot{\mathbf{q}}^* + \delta\ddot{\mathbf{q}}) = \mathbf{f}^* + \left(\frac{\partial \mathbf{f}}{\partial \mathbf{q}}\right)^* \delta\mathbf{q} + \left(\frac{\partial \mathbf{f}}{\partial \dot{\mathbf{q}}}\right)^* \delta\dot{\mathbf{q}} + \mathcal{O}(\delta\mathbf{q}^2, \delta\dot{\mathbf{q}}^2) \ . \tag{4.28}$$

Neglecting the second order terms and implementing Eq. (4.14), we obtain

$$\left[\left(\frac{\partial \mathbf{M}}{\partial \mathbf{q}}\right)^* \delta\mathbf{q}\right]\ddot{\mathbf{q}}^* + \mathbf{M}^*\delta\ddot{\mathbf{q}} = \left(\frac{\partial \mathbf{f}}{\partial \mathbf{q}}\right)^* \delta\mathbf{q} + \left(\frac{\partial \mathbf{f}}{\partial \dot{\mathbf{q}}}\right)^* \delta\dot{\mathbf{q}} \tag{4.29}$$

where a starred variable indicates the value of that variable at the nominal solution. Note that $\left[\left(\frac{\partial \mathbf{M}}{\partial \mathbf{q}}\right)^* \delta\mathbf{q}\right]$ is a matrix with its ij-th element equals to $\sum_{k=1}^{N_q}\left(\frac{\partial M_{ij}}{\partial q_k}\right)^* \delta q_k$, $i, j = 1, 2, \ldots, N_q$. Matrices $\frac{\partial \mathbf{f}}{\partial \mathbf{q}}$ and $\frac{\partial \mathbf{f}}{\partial \dot{\mathbf{q}}}$ are the Jacobian matrices of the force vector, $\mathbf{f}$, with respect to the vectors of generalized coordinates and speeds, respectively.

4.4.1 Linearization about the Equilibrium State

When an equilibrium state is chosen as the nominal solution about which linearization is carried out, Eq. (4.29) becomes

$$\mathbf{M}^e\delta\ddot{\mathbf{q}} = \left(\frac{\partial \mathbf{f}}{\partial \mathbf{q}}\right)^e \delta\mathbf{q} + \left(\frac{\partial \mathbf{f}}{\partial \dot{\mathbf{q}}}\right)^e \delta\dot{\mathbf{q}} \ , \tag{4.30}$$

where the mass matrix $\mathbf{M}$ and force vector $\mathbf{f}$ are defined in Section 4.2. Having the expression for $\mathbf{f}$, we can calculate the Jacobian matrices, $\frac{\partial \mathbf{f}}{\partial \mathbf{q}}$ and $\frac{\partial \mathbf{f}}{\partial \dot{\mathbf{q}}}$. They can be evaluated either numerically or analytically.

Since the static equilibrium states exist only for a system in a circular orbit and in the station-keeping stage, only the corresponding Jacobian matrices are given in the following sections. Because of the disadvantages of numerical differentiation (noise, etc.) they are obtained here analytically. For the sake of brevity, just the final forms are given. Note that in the station-keeping phase, lengths of the tethers are no longer part of the vector of generalized coordinates. Therefore the rows and columns corresponding to them are excluded from the Jacobian matrices that are given in Appendix D.

Matrix $\left[\dfrac{\partial \mathbf{f}}{\partial \mathbf{q}}\right]$

Matrix $\left[\dfrac{\partial \mathbf{f}}{\partial \mathbf{q}}\right]$ is composed of $(N-1)^2$ submatrices and can be written as follows:

$$\frac{\partial \mathbf{f}}{\partial \mathbf{q}} = \begin{bmatrix} \dfrac{\partial \mathbf{f}_1}{\partial \mathbf{q}_1} & \dfrac{\partial \mathbf{f}_1}{\partial \mathbf{q}_2} & \cdots & \dfrac{\partial \mathbf{f}_1}{\partial \mathbf{q}_{N-1}} \\ \dfrac{\partial \mathbf{f}_2}{\partial \mathbf{q}_1} & \dfrac{\partial \mathbf{f}_2}{\partial \mathbf{q}_2} & \cdots & \dfrac{\partial \mathbf{f}_2}{\partial \mathbf{q}_{N-1}} \\ \vdots & \vdots & \ddots & \vdots \\ \dfrac{\partial \mathbf{f}_{N-1}}{\partial \mathbf{q}_1} & \dfrac{\partial \mathbf{f}_{N-1}}{\partial \mathbf{q}_2} & \cdots & \dfrac{\partial \mathbf{f}_{N-1}}{\partial \mathbf{q}_{N-1}} \end{bmatrix} , \tag{4.31}$$

where $\dfrac{\partial \mathbf{f}_n}{\partial \mathbf{q}_k}$ is an $N_{q_n} \times N_{q_k}$ matrix in which *each row is the partial derivative of each element of the vector* $\mathbf{f}_n$ *with respect to the elements of the generalized coordinates corresponding to the tether* $k, \mathbf{q}_k$. It is given by

$$\begin{aligned}
\frac{\partial \mathbf{f}_n}{\partial \mathbf{q}_k} = &-\delta_{kn}\left\{\sum_{j=1}^{N-1}(F_{jn}\mathcal{J}_{\mathbf{r}_n} + \bar{\mu}_n A_{nj}\mathcal{J}_{\mathbf{b}_n})\cdot\left[\vec{\mathbf{d}}_{\mathbf{r}_j} + \Omega_c^2\left\{\vec{\mathbf{r}}_j - 3(\hat{\mathbf{i}}_c\cdot\vec{\mathbf{r}}_j)\hat{\mathbf{i}}_c\right\}\right]\right. \\
&\left. + (\bar{\mu}_j A_{jn}\mathcal{J}_{\mathbf{r}_n} - \bar{\mu}_j\bar{\mu}_n\mathcal{J}_{\mathbf{b}_n})\cdot\left[\vec{\mathbf{d}}_{\mathbf{b}_j} + \Omega_c^2\left\{\vec{\mathbf{b}}_j - 3(\hat{\mathbf{i}}_c\cdot\vec{\mathbf{b}}_j)\hat{\mathbf{i}}_c\right\}\right]\right\} \\
&-\delta_{kn}\left\{\hat{\rho}_n\int_0^{\ell_n}\left(\left[\mathcal{P}_{\mathbf{t}_n} + \Omega_c^2\left\{\mathcal{D}_{\mathbf{t}_n} - 3(\hat{\mathbf{i}}_c\cdot\mathcal{D}_{\mathbf{t}_n})\hat{\mathbf{i}}_c\right\}\right]\cdot\mathcal{D}_{\mathbf{t}_n}^T + \mathcal{J}_{\mathbf{t}_n}\cdot\left[\vec{\mathbf{d}}_{\mathbf{t}_n}\right.\right.\right. \\
&\left.\left.\left. + \Omega_c^2\left\{\vec{\mathbf{r}}_{\mathbf{t}_n} - 3(\hat{\mathbf{i}}_c\cdot\vec{\mathbf{r}}_{\mathbf{t}_n})\hat{\mathbf{i}}_c\right\}\right]\right)dx_n + \frac{EA_n}{2m}\int_0^{\ell_n}\frac{\partial}{\partial \mathbf{q}_n}\left(\frac{\partial \mathcal{E}_n}{\partial \mathbf{q}_k}\right)dx_n\right\} \\
&-\left\{(F_{kn}\mathcal{D}_{\mathbf{r}_n} + \bar{\mu}_n A_{nk}\mathcal{D}_{\mathbf{b}_n})\cdot\left[\mathcal{P}_{\mathbf{r}_k} + \Omega_c^2\left\{\mathcal{D}_{\mathbf{r}_k} - 3(\hat{\mathbf{i}}_c\cdot\mathcal{D}_{\mathbf{r}_k})\hat{\mathbf{i}}_c\right\}\right]^T\right. \\
&\left. + (\bar{\mu}_k A_{kn}\mathcal{D}_{\mathbf{r}_n} - \bar{\mu}_k\bar{\mu}_n\mathcal{D}_{\mathbf{b}_n})\cdot\left[\mathcal{P}_{\mathbf{b}_k} + \Omega_c^2\left\{\mathcal{D}_{\mathbf{b}_k} - 3(\hat{\mathbf{i}}_c\cdot\mathcal{D}_{\mathbf{b}_k})\hat{\mathbf{i}}_c\right\}\right]^T\right\} \\
&+\frac{1}{m}\frac{\partial \mathbf{Q}_n}{\partial \mathbf{q}_k} ,
\end{aligned} \tag{4.32}$$

where matrices $\mathcal{J}$ and column vectors $\mathcal{P}$ are defined as follows:

$$\begin{aligned}
\mathcal{J}_{\mathbf{r}_n} &= \frac{\partial \mathcal{D}_{\mathbf{r}_n}}{\partial \mathbf{q}_n} , \qquad & \mathcal{J}_{\mathbf{b}_n} &= \frac{\partial \mathcal{D}_{\mathbf{b}_n}}{\partial \mathbf{q}_n} , \qquad & \mathcal{J}_{\mathbf{t}_n} &= \frac{\partial \mathcal{D}_{\mathbf{t}_n}}{\partial \mathbf{q}_n} , \\
\mathcal{P}_{\mathbf{r}_k} &= \frac{\partial \vec{\mathbf{d}}_{\mathbf{r}_k}}{\partial \mathbf{q}_k} , \qquad & \mathcal{P}_{\mathbf{b}_k} &= \frac{\partial \vec{\mathbf{d}}_{\mathbf{b}_n}}{\partial \mathbf{q}_k} , \qquad & \mathcal{P}_{\mathbf{t}_k} &= \frac{\partial \vec{\mathbf{d}}_{\mathbf{t}_k}}{\partial \mathbf{q}_k} .
\end{aligned} \tag{4.33}$$

Expressions for these are given in Appendix D.

Matrix $\left[\frac{\partial \mathbf{f}}{\partial \dot{\mathbf{q}}}\right]$

Similarly Matrix $\left[\frac{\partial \mathbf{f}}{\partial \dot{\mathbf{q}}}\right]$ can be written as

$$\frac{\partial \mathbf{f}}{\partial \dot{\mathbf{q}}} = \begin{bmatrix} \frac{\partial \mathbf{f}_1}{\partial \dot{\mathbf{q}}_1} & \frac{\partial \mathbf{f}_1}{\partial \dot{\mathbf{q}}_2} & \cdots & \frac{\partial \mathbf{f}_1}{\partial \dot{\mathbf{q}}_{N-1}} \\ \frac{\partial \mathbf{f}_2}{\partial \dot{\mathbf{q}}_1} & \frac{\partial \mathbf{f}_2}{\partial \dot{\mathbf{q}}_2} & \cdots & \frac{\partial \mathbf{f}_2}{\partial \dot{\mathbf{q}}_{N-1}} \\ \vdots & \vdots & \ddots & \vdots \\ \frac{\partial \mathbf{f}_{N-1}}{\partial \dot{\mathbf{q}}_1} & \frac{\partial \mathbf{f}_{N-1}}{\partial \dot{\mathbf{q}}_2} & \cdots & \frac{\partial \mathbf{f}_{N-1}}{\partial \dot{\mathbf{q}}_{N-1}} \end{bmatrix} , \tag{4.34}$$

where

$$\begin{aligned} \frac{\partial \mathbf{f}_n}{\partial \dot{\mathbf{q}}_k} = & -\delta_{kn}\hat{\rho}_n \int_0^{\ell_n} \mathcal{D}_{\mathbf{t}_n} \cdot \mathcal{R}^T_{\mathbf{t}_n} dx_n - (F_{kn}\mathcal{D}_{\mathbf{r}_n} + \bar{\mu}_n A_{nk} \mathcal{D}_{\mathbf{b}_n}) \cdot \mathcal{R}^T_{\mathbf{r}_k} \\ & - (\bar{\mu}_k A_{kn} \mathcal{D}_{\mathbf{r}_n} - \bar{\mu}_k \bar{\mu}_n \mathcal{D}_{\mathbf{b}_n}) \cdot \mathcal{R}^T_{\mathbf{b}_k} + \frac{1}{m} \frac{\partial \mathbf{Q}_n}{\partial \dot{\mathbf{q}}_k} , \end{aligned} \tag{4.35}$$

and column vectors $\mathcal{R}$ are defined as

$$\mathcal{R}_{\mathbf{r}_n} = \frac{\partial \vec{\mathbf{d}}_{\mathbf{r}_n}}{\partial \dot{\mathbf{q}}_k} , \qquad \mathcal{R}_{\mathbf{b}_n} = \frac{\partial \vec{\mathbf{d}}_{\mathbf{b}_n}}{\partial \dot{\mathbf{q}}_k} , \qquad \mathcal{R}_{\mathbf{t}_n} = \frac{\partial \vec{\mathbf{d}}_{\mathbf{t}_n}}{\partial \dot{\mathbf{q}}_n} . \tag{4.36}$$

Their expressions can also be found in Appendix D.

Jacobian matrices $\frac{\partial \mathbf{Q}}{\partial \mathbf{q}}$ and $\frac{\partial \mathbf{Q}}{\partial \dot{\mathbf{q}}}$

Among the three components of the generalized forces $\mathbf{Q}_n$, defined in Eq. (3.1), the Jacobian matrices corresponding to $\mathbf{Q}_O$ can be calculated if the explicit expression of $\mathbf{Q}_O$ as a function of the generalized coordinates is provided. Jacobian matrices corresponding to the generalized aerodynamic forces $\mathbf{Q}_A$ for a general case, are very complicated to evaluate. Their calculations for a simple case, a two-body system, is given analytically in Chapter 6. For a more complex system they should be calculated numerically.

Using the previous formulation for the generalized forces due to the material damping, $\mathbf{Q}_D$, here we can express the corresponding Jacobian matrices in the explicit form. Let us rewrite $\mathbf{Q}_D$ defined in Eq. (3.39) as

$$\mathbf{Q}_D = \mathbf{C}\dot{\mathbf{q}} \quad , \tag{4.37}$$

where the matrix $\mathbf{C}$ is a function of the generalized coordinates only. Since at the equilibrium point $\dot{\mathbf{q}}^e = \{0\}$, it is very easy to see that

$$\left(\frac{\partial \mathbf{Q}_D}{\partial \mathbf{q}}\right)^e = \left(\frac{\partial \mathbf{C}}{\partial \mathbf{q}}\dot{\mathbf{q}}\right)^e = \{0\} \quad , \tag{4.38}$$

and

$$\left(\frac{\partial \mathbf{Q}_D}{\partial \dot{\mathbf{q}}}\right)^e = \left(\frac{\partial \mathbf{C}}{\partial \dot{\mathbf{q}}}\dot{\mathbf{q}}\right)^e + \left(\mathbf{C}\frac{\partial \dot{\mathbf{q}}}{\partial \dot{\mathbf{q}}}\right)^e = \mathbf{C}^e \quad . \tag{4.39}$$

Hence, the corresponding Jacobian matrices at the equilibrium point are simply given by

$$\begin{aligned} \left(\frac{\partial \mathbf{Q}_D}{\partial \mathbf{q}}\right)^e &= \{0\} \quad , \\ \left(\frac{\partial \mathbf{Q}_D}{\partial \dot{\mathbf{q}}}\right)^e &= \left[\frac{\partial}{\partial \mathbf{q}}\left(\frac{\partial U_E}{\partial \mathbf{q}}\right)\right]^e = \begin{bmatrix} \mathbf{C}_1^e & [0] & \dots & [0] \\ [0] & \mathbf{C}_2^e & \dots & [0] \\ \vdots & \vdots & \ddots & \vdots \\ [0] & [0] & \dots & \mathbf{C}_{N-1}^e \end{bmatrix} \quad , \end{aligned} \tag{4.40}$$

where

$$\mathbf{C}_n = \frac{EA_n}{2}\int_0^{\ell_n} \frac{\partial}{\partial \mathbf{q}_n}\left(\frac{\partial \mathcal{E}_n}{\partial \mathbf{q}_n}\right) dx_n \quad . \tag{4.41}$$

4.5 Eigenvalue Analysis

Once the equilibrium point and the linearized matrix equation of motion of the system about this particular solution are obtained, we can calculate the eigenfrequencis as well as the associated mode shapes governing the oscillations of the linear system. In fact these frequencies and mode shapes describe the motion of the nonlinear system in the vicinity of the equilibrium point, as long as the linearization is valid. By calculating the eigenvalues of the linearized system, one can analyze the stability of the system around the equilibrium point, in the linear sense. Clearly, this analysis is valid for the motion of the system in the close neighbourhood of this point. This approach is used to analyze the stability of a tethered satellite system used in atmospheric missions, in Chapter 6. To analyze the stability of the nonlinear system, one must utilize a nonlinear approach such as Lyapunov's second or indirect method, which is often very difficult to implement for a general case. With some assumptions, this method is applied in Chapter 7, to control the motion of the system during the inherent unstable retrieval stage.

Rewriting the linearized equations of motion, given by Eq. (4.30), in the following form

$$\mathbf{M}^e\delta\ddot{\mathbf{q}} + \mathbf{D}^e\delta\dot{\mathbf{q}} + \mathbf{K}^e\delta\mathbf{q} = \{0\} \quad , \tag{4.42}$$

eigenvalues of the system can be obtained from the following algebraic equation;

$$\det(\mathbf{A}\lambda - \mathbf{B}) = 0 \quad , \tag{4.43}$$

where

$$\mathbf{A} = \begin{bmatrix} \mathbf{M}^e & [0] \\ [0] & \mathbf{I} \end{bmatrix} \quad , \quad \mathbf{B} = \begin{bmatrix} -\mathbf{D}^e & -\mathbf{K}^e \\ \mathbf{I} & [0] \end{bmatrix} \quad . \tag{4.44}$$

Since the order of the matrices $\mathbf{A}$ and $\mathbf{B}$ are $2N_q$, Eq. (4.43) leads to a polynomial of order $2N_q$ in terms of λ, which in turn results in $2N_q$ solutions for λ. Corresponding to each $\lambda_n, n = 1, 2, \ldots, 2N_q$, there is an eigenvector $\mathbf{W}_n$ which is obtained from

$$(\mathbf{A}\lambda_n - \mathbf{B})\,\mathbf{W}_n = [0] \quad . \tag{4.45}$$

In general λ_n and $\mathbf{W}_n$ are complex variables and can be written as

$$\lambda_n = \eta_n + i\,\omega_n \quad , \qquad \mathbf{W}_n = \mathbf{U}_n + i\,\mathbf{V}_n \quad , \tag{4.46}$$

where $i = \sqrt{-1}$. For a mechanical system, such as ours the eigenvalues and eigenvectors are either real or in a complex conjugate pair.

The imaginary part of the n-th eigenvalue, ω_n, indicates the frequency of the corresponding mode and the real part, η_n, relates to the damping ratio of this mode. The stability of the linear system is evaluated by examining η_n's. The system is asymptotically stable if

$$\eta_n < 0 \ , \qquad n = 1, 2, \ldots, 2N_q \ , \tag{4.47}$$

is marginally stable if

$$\eta_n \leq 0 \ , \qquad n = 1, 2, \ldots, 2N_q \ , \tag{4.48}$$

and is unstable if at least one of the eigenvalues has positive real part, i.e. ,

$$\eta_j > 0 \ . \tag{4.49}$$

Chapter 5

NUMERICAL RESULTS OF THE UNCONTROLLED SYSTEM

5.1 Introductory Remarks

Based on the formulation developed in the previous chapters, a computer program was generated. It is capable of handling two kinds of problems: (i) numerical integration of the equations of motion and (ii) eigenvalue analysis for small motions of the system in the station-keeping phase. After discussing some aspects of the numerical procedures and programming, typical numerical results are presented in this Chapter. These results can be categorized in two groups; the first one is to *validate* the formulation while the second one is to get an insight into the general dynamical behaviour of multi-body tethered systems.

5.1.1 Comments on the Numerical Procedures

After obtaining an equilibrium state of the system, eigenvalue analysis is carried out by calculating the eigenvalues of the linearized system. The static equilibrium equations (Eqs. (4.20)) are solved using the Newton-Raphson method for a set of nonlinear algebraic equations. Once the equilibrium state has been obtained, matrices **A** and **B** in Eq. (4.44) can be calculated. Eigenvalues of the system are then evaluated from Eq. (4.45), using the QR algorithm. Computation of the eigenvalues was found to be fast. As an example, the eigenfrequencies of a 17-body system, in which every elastic tether was discretized using 6 shape functions, were obtained in 66 seconds on a 486-DX2-66 PC computer. Of course the execution time depends on different variables such as: proximity of the initial guess to the equilibrium state, system parameters, load distributions, etc.

Integration of the equations of motion was very time consuming, because of the following main reasons:

- The dynamical model involves many generalized coordinates. The computing time is dramatically increased with the increased number of generalized coordinates.
- The set of equations of motion is stiff in the numerical sense, because the time constants of the system vary by several orders of magnitude. For a multibody satellite system the vibrational frequencies are much higher than those of librational motion. The difference becomes larger during the initial period of deployment and final period of retrieval, when the lengths of the tethers are short. Therefore to handle the integration, the step size must be chosen to be very small to expect a correct result.
- Since the mass matrix, $\mathbf{M}$, and force vector, $\mathbf{f}$, are time and generalized coordinate dependent, Eq. (4.1) must be solved at each time step to obtain $\ddot{\mathbf{q}}$.

Not much can be done about these facts. One could try to model the system with as few degrees of freedom as possible to represent the actual dynamics of the system reasonably. Using appropriate shape functions is the best approach to reduce the order of the system.

In order to solve the set of equations given by Eq. (4.1), which are linear in terms of $\ddot{\mathbf{q}}$, an LU decomposition method is used first. Integration of the stiff differential equations is then accomplished by implementing Gear's method.

5.1.2 Remarks on the Programming

Prior to deriving the equations of motion of an N-body TSS system as outlined in Chapter 2, a symbolic program, using the symbolic manipulation language MAPLE-V, had been developed. This program is capable of deriving the governing equations of motion for the system under consideration symbolically and then transfer these equations to a FORTRAN code for simulation and numerical purposes. Although the program can be used for an arbitrary number of bodies in principle, because of available hardware restrictions, it encounters difficulties with a system with either a large number of bodies or a large number of elastic degrees of freedom. That is because all the algebraic tasks such as integration in the energy expressions and differentiation in the Lagrange's method, are left to the computer and MAPLE-V to handle. These tasks are very time consuming and need a reasonably high speed computer with an appropriate memory space, while all calculations for this thesis were carried out on a 486 PC.

Difficulties with the above-mentioned symbolic program motivated the present formulation and generation of a numerical program, written in the FORTRAN language. However the symbolic program was used to double check the results of the numerical program. This was done in addition to comparing the results of the numerical program with those of other investigators for some simple cases for validation purpose.

Evaluation of the integral terms associated with the tether mass and elasticity, appearing in the force vector (Eq. (4.10)), mass and Jacobian matrices (Eqs. (4.9), (4.32), and (4.35)), is the most challenging and time consuming part of the numerical task. For example, computation of the force vector and mass matrix of a three-body

TSS with 18 degrees of freedom for a given state takes 22.1 seconds on a 486/66 PC computer, if Simpson's rule with 128 divisions is used for numerical integration. This many divisions are needed to get six-digit accuracy. However it takes only 0.16 seconds if those integral terms are excluded. Thus one has to pay a heavy penalty for considering the small contributions from these integrals associated with the tether mass, if they are going to be evaluated by numerical routines.

Indeed this fact makes the numerical integration of the differential equations of motion very time consuming, if not impossible at times. It needs to be overcome somehow. The conventional way to tackle this difficulty is, if possible, to break the integrals into the summation of several smaller integrals, which need to be calculated only once. These smaller integrals are computed at the beginning of the program. However, that is almost impossible in the present case, because of the large number of these integrals, say over a hundred, and the very complicated and lengthy relations resulting from the breaking up the original integrals.

Hence, to solve this problem, advantage was taken of the 'translate' feature of MAPLE-V. Since the above mentioned integrals have similar form for all the tethers, one can calculate them for a general case analytically in MAPLE-V. Then the results are translated to some FORTRAN files, which are used as required subroutines in the numeric program. In order to make this calculation possible, the number of longitudinal and transverse degrees of freedom must be known. In fact this number is the corresponding maximum allowable number of elastic degrees of freedom of a tether in the numeric program. Here 2 is chosen as this maximum number in each direction. Although 2 elastic degrees of freedom in each direction is a reasonably practical number in dealing with a rigid-elastic system, it imposes a large restriction on the fidelity of modelling the tether flexibility. To remove this constraint one can increase it to a new number, say 3 or 4, and obtain the required FORTRAN subroutine by re-executing the MAPLE-V program, written for this purpose. However a larger number could not be chosen, because of the limitation of symbolic computation on a PC. To overcome this restriction, a numerical trick was used so that any large number of elastic degrees of freedom, say 10 in each direction, can be considered. It will be discussed in Section 5.2; case 3.

Although the output FORTRAN files resulting from the MAPLE-V program have large sizes, approximately 200 K-bytes, the computation time is much smaller than that for the numerical integration. For the example mentioned earlier, computation time of the force vector and the mass matrix decreases from 22.1 seconds to only 0.2 second, using this approach.

5.2 Eigenvalue Analysis

In this section results of several cases, considered by other researchers, are used to *validate the formulation* first. Then a couple of new cases, *that cannot be handled with the previous investigations*, are presented to show the *capability of the present work* to analyze a multi-tethered system with a large number of flexible tethers.

5.2.1 Validation

One cannot find in the literature results of an eigenvalue analysis corresponding to a multi-tethered system considering longitudinal as well as transverse oscillations of the tethers. Thus the following three cases are considered for comparison:

(i) eigenfrequencies of the librational motion (rigid-body motion) of a four-body system studied by Misra and Modi [65];

(ii) eigenfrequencies of a three-body tethered system undergoing transverse oscillations but no longitudinal motion, studied by Kumar et al. [64];

(iii) non-dimensional planar eigenfrequencies of a two-body tethered system obtained by Pasca and Pignataro [26] which include both longitudinal and transverse oscillations.

In all cases the system is in a circular orbit and in the station-keeping phase.

Case 1: Librational Frequencies of TECS

Table 5.1 shows the comparison between librational frequencies obtained from the present formulation and those of Misra and Modi [65] for a four-body TSS, called Tethered Elevator/Crawler System (TECS). The system shown in Fig. 5.1 consists of a Space-Station (m_2), lower and upper platforms (m_1 and m_4) and an elevator (m_3) between the Space-Station and the upper platform. The following parameters were chosen by Misra and Modi [65]: $m_1 = m_4 = 10^4$ kg, $m_2 = 10^5$ kg, $m_3 = 10^2$ kg, $\ell_1 = \ell_2 + \ell_3 = 10$ km; ℓ_2 was varied. Corresponding in-plane and out-of-plane frequencies are shown in Table 5.1. The frequencies have been non-dimensionalized by dividing them by the orbital frequency so that the results are valid for any orbital altitude. The second and third column of the Table show almost exact agreement of the results for the in-plane frequencies.

Misra and Modi have shown that the in-plane and out-of-plane librational frequencies are related by

$$\left(\frac{\omega_{O_j}}{\Omega_c}\right)^2 = \left(\frac{\omega_{I_j}}{\Omega_c}\right)^2 + 1 \tag{5.1}$$

where ω_{O_j} and ω_{I_j} are the j-th out-of-plane and in-plane frequencies, respectively, while Ω_c is the orbital frequency. This relation holds for the results obtained from the present formulation as shown in the last column of the Table.

Note that the lowest in-plane and out-of-plane non-dimensional frequencies are equal to 1.7321 ($= \sqrt{3}$) and 2, respectively, which are the same as those of the single-tether case. In fact, the tethers are aligned while oscillating with these frequencies and the system behaves like a single-tether system. It may also be noted that the third librational frequency is substantially higher than the other two and is associated primarily with the transverse motion of the light elevator.

Table 5.1: Non-dimensional librational frequencies of TECS; $m_1 = 10^4$ kg, $m_2 = 10^5$ kg, $m_3 = 10^2$ kg, $m_4 = 10^4$ kg, $\ell_1 = 10^4$ m, $\ell_2 + \ell_3 = 10^4$ m.

ℓ_2 m	ω_I		ω_O	$\frac{\omega_O^2-\omega_I^2}{\Omega^2}$
	[65]	Thesis	Thesis	Thesis
50	1.7321	1.7321	2.0000	1.0000
	1.8972	1.8972	2.1446	1.0000
	245.6908	245.6908	245.6928	1.0000
1000	1.7321	1.7321	2.0000	1.0000
	1.8974	1.8974	2.1448	1.0000
	57.7848	57.7849	57.7935	1.0000
2000	1.7321	1.7321	2.0000	1.0000
	1.8975	1.8975	2.1449	1.0000
	43.3548	43.3548	43.3663	1.0000
3000	1.7321	1.7321	2.0000	1.0000
	1.8977	1.8977	2.1450	1.0000
	37.8576	37.8576	37.8708	1.0000
4000	1.7321	1.7321	2.0000	1.0000
	1.8978	1.8978	2.1452	1.0000
	35.4264	35.4264	35.4405	1.0000
5000	1.7321	1.7321	2.0000	1.0000
	1.8979	1.8979	2.1452	1.0000
	34.7246	34.7246	34.7390	1.0000
6000	1.7321	1.7321	2.0000	1.0000
	1.8980	1.8980	2.1453	1.0000
	35.4552	35.4552	35.4693	1.0000
7000	1.7321	1.7321	2.0000	1.0000
	1.8981	1.8981	2.1454	1.0000
	37.9191	37.9191	37.9323	1.0000
8000	1.7321	1.7321	2.0000	1.0000
	1.8981	1.8981	2.1454	1.0000
	43.4605	43.4605	43.4720	1.0000
9000	1.7321	1.7321	2.0000	1.0000
	1.8981	1.8981	2.1455	1.0000
	57.9728	57.9728	57.9814	1.0000
9995	1.7321	1.7321	2.0000	1.0000
	1.8982	1.8982	2.1455	1.0000
	778.3286	778.3287	778.3293	1.0000

Table 5.2: In-plane dimensionless frequencies (ω/Ω_c) of a 3-body system ($\ell_1+\ell_2=10$ km, $m_1=10^5$ kg, $m_2=5\times10^3$ kg, $m_3=10^4$ kg, $\rho=6$ kg/m, $EA=61645$ N)

Mode	Case 1: $\ell_1/\ell_2=1/5$		Case 2: $\ell_1/\ell_2=1/3$		Case 3: $\ell_1/\ell_2=1/1$		Type
	Thesis	[64]	Thesis	[64]	Thesis	[64]	
1	1.725	1.732	1.725	1.732	1.724	1.732	Lib.
2	6.503	6.506	5.692	5.694	5.164	5.166	Lib.
3	22.084	–	21.959	–	21.094	–	Long.
4	80.535	–	70.817	–	63.867	–	Long.
5	81.807	81.756	89.291	90.484	133.075	134.088	Tran.
6	161.131	162.917	178.665	180.366	146.909	147.642	Tran.
7	244.424	243.821	271.027	269.843	266.356	267.580	Tran.
8	322.178	326.062	278.702	279.322	294.268	295.183	Tran.

Case 2: Eigenfrequencies of Transverse Oscillations of a Three-Body TSS

Table 5.2 compares the in-plane, non-dimensional eigenfrequencies (ω/Ω_c) of a three-body tethered system obtained by the present formulation, with the results of Kumar et al. [64]. The system consists of three point masses, $m_1=10^5$ kg, $m_2=5000$ kg, $m_3=10^4$ kg, the two tethers having a linear mass density of $\rho_1=\rho_2=6$ kg/km and axial stiffness $EA_1=EA_2=61645$ N. Three different cases of length configurations are considered, assuming $\ell_1+\ell_2=10$ km.

Although the linearized in-plane librations and elastic oscillations of the system are coupled and every eigenfrequency contributes to the motion of all the generalized coordinates, the coupling is fairly weak so that each frequency can be associated exclusively with either libration or one longitudinal or one in-plane transverse mode. This can be verified by observing the corresponding eigenvector. Thus the modes are easily identifiable and are shown by the label 'Type' in the last column of Table 5.2.

Since Kumar et al. [64] did not consider longitudinal elastic oscillations of the tethers in their analysis, they have no eigenfrequencies corresponding to these modes of the system. Although the results of the present formulation are in good agreement with those of Ref. [64], the small differences can be explained as follows: ignoring the longitudinal elastic oscillations leads to omitting the gyroscopic effects in the linearized form of in-plane transverse motion.

Case 3: Eigenfrequencies of a Two-Body Tethered Satellite System

Tables 5.3 and 5.4 compare the non-dimensional planar eigenfrequencies of different cases of a two-body tethered system obtained from the present formulation with those of Pasca and Pignataro [26]. The results are for single-tether systems, however, there is a very interesting point to note, showing the capabilities of the present formulation for multi-tether systems.

As was mentioned in the previous section, the number of elastic modes of a tether in each direction was limited to two in the computation due to symbolic manipulation limitation. It means that each tether at most could have six elastic DOFs. With this limitation, one can expect to obtain only the first two longitudinal and the first two transverse eigenfrequencies of the in-plane motion of a two-body (single-tether) system, and the higher frequencies of the system can not be calculated. However, using what we call a *segmented-tether model*, i.e., by breaking the tethers to a number of smaller tethers and putting a very small mass at the connection points of the smaller tethers, one can obtain the higher frequencies of the system to whatever order one desires, limited only by the numerical computation capability of the facility being used. This in fact shows the very powerful feature of the present formulation in handling multi-tether systems.

Table 5.3 compares the results of Ref. [26] and the present formulation, employing a segmented-tether model, for a two-body tethered system with tether density, $\rho = 5.76$ kg/km, longitudinal stiffness, $EA = 2.8 \times 10^5$ N, and various tether length and mass combinations. The orbit is a circular one with orbital radius, $R_c = 6657$ km. As an example, the two-body tethered system in the first case ($\ell = 100$ km, $m_1 = 10^5$

Table 5.3: In-plane dimensionless frequencies (ω/Ω_c) of a 2-body system (ρ = 5.76 kg/km, $EA = 2.8 \times 10^5$ N)

Mode	$\ell = 100$ km $m_1 = 10^5$ kg $m_2 = 500$ kg		$\ell = 20$ km $m_1 = \infty$ $m_2 = 576$ kg		$\ell = 20$ km $m_1 = \infty$ $m_2 = 115.2$ kg		Type
	Thesis	[26]	Thesis	[26]	Thesis	[26]	
1	1.731	1.794	1.732	1.733	1.732	1.742	Lib.
2	6.389	6.905	12.777	12.780	6.709	6.750	Tran.
3	12.059	12.457	25.245	25.241	12.747	12.811	Tran.
4	17.879	18.269	37.795	37.771	18.929	19.014	Tran.
5	23.742	24.143	50.369	50.319	25.148	25.256	Tran.
10	53.344	53.807					Tran.
11	54.541	54.559					Long.
12	59.337	59.758					Tran.

kg, m_2 = 500 kg) is represented as a 21-body system with $m_1 = 10^5 kg$, $m_i = .001$ kg,$i = 2,\ldots,20$, m_{21} = 500 kg, and ρ_i = 5.76 kg/km, ℓ_i = 5 km,$i = 1,\ldots,20$. In addition to the three rigid DOFs, three elastic DOFs (one longitudinal, one in-plane transverse, and one out-of-plane transverse elastic DOF) are considered for each segment. In total, the system has 120 DOFs of which 20, corresponding to the tether lengths, are not involved in the eigenvalue problem since the system is in the station-keeping phase. It takes only 80 seconds to find the fixed point and the eigenfrequencies of this system on a 486/66 PC computer.

The first column of Table 5.3 shows the order of the eigenfrequencies, while the last column represents the type of the modes. As can be seen the results for the second case (ℓ = 20 km, $m_1 = \infty, m_2$ = 576 kg) agree better than the two other cases, because the parameter $\gamma = \rho\ell/m_2$ defined in Ref. [26], which has an important role in their analysis and the employed perturbation method, has a much lower value in this case than the other cases. As mentioned by the authors in Ref. [26], their results are more accurate for smaller γ, which agree better with the present results.

Table 5.4: In-plane dimensionless frequencies (ω/Ω_c) of a 2-body system ($\ell = 20$ km, $\rho = 5.76$ kg/km, $EA = 2.8 \times 10^5$ N)

Mode	$m_1 = 10^5$ kg $m_2 = 500$ kg		$m_1 = 10^5$ kg $m_2 = 10^5$ kg		$m_1 = 500$ kg $m_2 = 500$ kg		Type
	Thesis	[26]	Thesis	[26]	Thesis	[26]	
1	1.732	1.738	1.715	1.728	1.732	1.742	Lib.
2	11.956	11.993	14.432		8.486	8.341	Tran.
3	23.578	23.644	113.430	113.385	16.507	16.191	Tran.
4	35.286	35.368	227.023	226.736	24.637	24.155	Tran.
5	47.019	47.112	340.934	340.095	32.799	32.142	Tran.
6			455.167	453.455			Tran.

Table 5.4 shows the effect of the mass-ratio of the end-bodies on the in-plane eigenfrequencies of a typical two-body tethered system. Since γ has reasonably small values in these cases, the results given in [26] are accurate and are in good agreement with those of the thesis. However, in one of the cases, the second mode, which is a longitudinal mode, has somehow been missed in Ref. [26].

5.2.2 New Results for Multi-Tether Systems

Vibrational Frequencies of TECS

Table 5.5 presents the eigenvalues of the TECS in both the absence and presence of material damping of the tethers. Here the mass of the end-bodies and lengths of the tethers are slightly different from those of the previous case (i.e. Table 5.1). In addition, the tethers are considered to be elastic and massive. The new parameters are chosen as follows: $m_1 = 10^4$ kg, $m_2 = 3 \times 10^5$ kg, $m_3 = 5000$ kg, $m_4 = 10^4$ kg, $\ell_1 = 10.5$ km, $\ell_2 = 1$ km, $\ell_3 = 9$ km. The tethers have a linear mass density of $\rho_1 = \rho_2 = \rho_3 = 6$ kg/km and an axial stiffness of $EA_1 = EA_2 = EA_3 = 61575.2$ N. The system is in a circular orbit at an altitude of 450 km, and is in the station-keeping phase. The elastic oscillations of each tether are represented by 3 elastic DOFs, one longitudinal, one in-plane and one out-of-plane transverse elastic mode.

Table 5.5: Eigenvalues and nominal stretches of the tethers of TECS ($m_1 = 10^4$ kg, $m_2 = 3 \times 10^5$ kg, $m_3 = 5000$ kg, $m_4 = 10^4$ kg, $\ell_1 = 10.5$ km, $\ell_2 = 1$ km, $\ell_3 = 9$ km, $\rho = 6$ kg/km, $EA = 61575.2$ N)

Mode	In the absence of material damping	In the presence of material damping	Type
	System eigenvalues		
1	0 ± 1.7247 i	-0.00001 ± 1.7247 i	I.P. Lib.
2	0 ± 1.7839 i	-0.00001 ± 1.7839 i	I.P. Lib.
3	0 ± 2.0000 i	0 ± 2.0000 i	O.P. Lib.
4	0 ± 2.0512 i	0 ± 2.0512 i	O.P. Lib.
5	0 ± 8.4160 i	-0.00001 ± 8.4160 i	I.P. Lib.
6	0 ± 8.4768 i	0 ± 8.4768 i	O.P. Lib.
7	0 ± 21.7990 i	-0.26528 ± 21.7974 i	Long.
8	0 ± 22.7067 i	-0.28789 ± 22.7048 i	Long.
9	0 ± 68.8932 i	0 ± 68.8932 i	I.P. Tran.
10	0 ± 68.9004 i	0 ± 68.9004 i	O.P. Tran.
11	0 ± 78.4984 i	-0.00000 ± 78.4984 i	I.P. Tran.
12	0 ± 78.5047 i	0 ± 78.5047 i	O.P. Tran.
13	0 ± 105.3134 i	-6.20478 ± 105.1304 i	Long.
14	0 ± 723.1814 i	0 ± 723.1814 i	I.P. Tran.
15	0 ± 723.1821 i	0 ± 723.1821 i	O.P. Tran.
Tether Stretches: $\xi_{11}^e = 67.835$ m, $\xi_{21}^e = 6.464$ m, $\xi_{31}^e = 55.351$ m			

Therefore the complete attitude motion of the system is described by 15 DOFs. The effect of material damping of the tethers on the response of the system is studied by introducing a damping ratio of $\xi = 1.2\%$ based on the first natural frequency of the longitudinal elastic oscillation of the system.

Eigenvalues of the system in the absence and presence of material damping of the tethers are given in Table 5.5. At the bottom, the longitudinal stretches of the tethers in the equilibrium position of the system are given. The material damping affects the in-plane longitudinal modes strongly, but the in-plane transverse modes through a weaker coupling. Thus the eigenvalues associated with the transverse oscillations have much smaller damping (negative real parts). That is because the steady state longitudinal is non-zero. This can also be observed in the dynamical response of the system given in Section 5.3.2. Since the material damping affects the longitudinal oscillations of the tethers through first order terms, while the in-plane and out-of-plane motions are completely decoupled in the linear sense, the material damping has no effect on the out-of-plane frequencies. Also one can notice that the material damping, here, has almost no effect on the natural frequencies of the system (imaginary parts), but has a greater effect on the real parts of the eigenvalues associated with the higher modes of the system.

Case 1: Eigenfrequencies of a Ten-Tethered TSS

Table 5.6 presents some results for a 10-probe tethered system deployed from the Shuttle and compares the first ten longitudinal and the first ten transverse frequencies with those of a single-probe case. The two-body system is exactly the same as the first case of Table 5.3, while the multi-body system consists of $m_1 = 10^5$ kg, $m_i = 500$ kg,$i = 2, \ldots, 11$, $\rho_i = 5.76$ kg/km, $EA_i = 2.8 \times 10^5$ N,$i = 1, \ldots, 10$, $\ell_1 = 55$ km, $\ell_i = 5$ km,$i = 2, \ldots, 10$. Thus the total tether length is the same (100 km). Both systems have the same orbital motion. One can observe many more low-frequency elastic modes for the 10-probe system. It is also noted that the in-plane and out-of-plane transverse frequencies are related by $(\omega_O/\Omega_c)_i^2 \approx (\omega_I/\Omega_c)_i^2 + 1$. Note that because of coupling between elastic oscillations and librations of the tethers, this relation, which is exact in the case of rigid tethers, turns to be an approximation.

5.3 Transient Dynamics

Several simulations of three-dimensional transient dynamics of three-body and four-body tethered systems were carried out using the nonlinear equations of motion (Eq. (4.1)) derived in the previous chapters. Among them some were chosen so as to verify the formulation and the integration program.

Table 5.6: The first ten non-dimensional longitudinal and transverse frequencies (ω/Ω_c) of a 2-body TSS and an 11-body TSS (ρ = 5.76 kg/km, $EA = 2.8 \times 10^5$ N).

Mode	Case 1: Single-Probe TSS $m_1 = 10^5$ kg, $m_2 = 500$ kg $\ell = 100$ km				Case 2: Ten-Probe TSS $m_1 = 10^5$ kg, $m_i = 500$ kg $\ell_1 = 55$ km, $\ell_i = 5$km			
	Longit.	Transverse ω_I	Transverse ω_O	$\frac{\omega_O^2-\omega_I^2}{\Omega_c^2}$	Longit.	Transverse ω_I	Transverse ω_O	$\frac{\omega_O^2-\omega_I^2}{\Omega_c^2}$
1	54.541	1.731	2.000	1.002	24.209	1.726	2.000	1.010
2	208.026	6.388	6.466	1.002	93.781	4.882	4.984	1.005
3	389.134	12.059	12.101	1.002	174.065	8.356	8.416	1.005
4	577.896	17.879	17.907	1.002	251.930	11.940	11.982	1.005
5	771.800	23.742	23.763	1.002	321.395	15.605	15.638	1.006
6	971.095	29.627	29.643	1.002	370.592	19.331	19.358	1.006
7	1176.628	35.528	35.542	1.002	412.193	23.039	23.061	1.007
8	1389.404	41.445	41.458	1.002	463.049	26.241	26.260	1.008
9	1610.410	47.383	47.393	1.002	508.205	28.699	28.716	1.008
10	1840.492	53.344	53.354	1.002	542.257	32.367	32.383	1.008

5.3.1 Verification: Librational Dynamics of a Three-Body TSS

Transient dynamics of two different three-body tethered satellite systems with rigid and massless tethers are considered here, in order to verify the formulation.

Case 1: Constant Lengths

The first system is the same as the one that Misra and Modi [65] considered. It is in the station-keeping phase and has the following parameters; $m_1 = 10^5$ kg, $m_2 = 500$ kg, $m_3 = 10^4$ kg, $\ell_1 = 200$ m, $\ell_2 = 300$ m. It is known that the motion of the system about the local vertical is composed of stable oscillations involving various natural frequencies. These natural frequencies for the present system are as follows:

$$\text{In-plane frequencies: } \frac{\omega_{I_1}}{\Omega_c} = 1.7321 \;, \qquad \frac{\omega_{I_2}}{\Omega_c} = 15.2139 \;,$$
$$\text{Out-of-plane frequencies: } \frac{\omega_{O_1}}{\Omega_c} = 2 \;, \qquad \frac{\omega_{O_2}}{\Omega_c} = 15.2467 \;,$$

where they are nondimensionalized using the orbital frequency, Ω_c. Figure 5.2-a shows the response corresponding to small initial deviations from the local vertical: $\theta_1 = 2°, \theta_2 = 5°, \phi_1 = 5°, \phi_2 = 4°$. The oscillations are stable and identical to those obtained by Misra and Modi [65], thus validating the present formulation.

Figure 5.2-b shows the response of the above system to the following set of initial conditions: $\theta_1 = -89.95°, \theta_2 = -89.95°, \phi_1 = 2.9°, \phi_2 = 2.3°$. In fact these initial conditions are small deviations from the local horizontal equilibrium state, which is an unstable one. One might think that the system will move to the stable vertical configuration, which is not the case. It is true only for a specific energy level; otherwise, end to end tumbling takes place. As can be noticed in Fig. 5.2-b the nonlinear system keeps on rotating in the orbital plane, while the out-of-plane motion remains small.

Case 2: Variable Lengths

The second system is the system that Monshi et al. [50] studied. They obtained numerical simulation results for uncontrolled exponential retrieval of the system. Here in addition to exponential retrieval, exponential deployment is also considered. In order to compare the results with those of Monshi et al. [50], the length rate was chosen as:

$$\dot{\ell}_j = c_j \Omega_c \ell_j \tag{5.2}$$

where c_j is the exponential rate corresponding to the j-th tether. The negative value for c_j results in retrieval of the j-th tether while the positive value corresponds to its deployment.

The system consists of three bodies with the following masses; $m_1 = 10^5$ kg , $m_2 = 5 \times 10^3$ kg, and $m_3 = 10^4$ kg. In the deployment case the exponential rates, c_j's were chosen as $c_1 = c_2 = 0.3$, while for retrieval they were chosen as $c_1 = -0.1$ and

$c_2 = -0.5$. The corresponding initial configuration of the system is given in the figure captions. Figures 5.3 and 5.4 show the pitch and roll angles as well as the length variation of the two tethers during the deployment and retreival phases, respectively. The pitch motion during retrieval are compatible with those of Monshi et al. [50], while the other results were not obtained by them. As can be noticed, the system is stable in the deployment case, while it is highly unstable in the retrieval one.

5.3.2 Numerical Simulation of TECS

With some confidence that the formulation and coding are correct, a four-body system (TECS) is now considered.

Case 1: Constant Lengths

Simulation up to 17000 sec ($\sim$ 3 orbits) of the station-keeping phase of TECS was carried out with a set of initial conditions which perturb the system from its equilibrium position and excite its general dynamics. The system parameters are exactly the same as those used to determine the system vibrational frequencies in Section 5.2.2. The initial conditions were chosen as follows:

$$\theta_1 = .07 \text{ rad}(4.01^\circ), \quad \phi_1 = .05 \text{ rad}(2.86^\circ), \quad \xi_{11} = 64.0 \text{ m}, \quad \eta_{11} = 10.0 \text{ m}, \quad \nu_{11} = 0.0 \text{ m}$$
$$\theta_2 = .03 \text{ rad}(1.72^\circ), \quad \phi_2 = .04 \text{ rad}(2.29^\circ), \quad \xi_{21} = 6.00 \text{ m}, \quad \eta_{21} = 0.0 \text{ m}, \quad \nu_{21} = 0.0 \text{ m}$$
$$\theta_3 = .03 \text{ rad}(1.72^\circ), \quad \phi_3 = .04 \text{ rad}(2.29^\circ), \quad \xi_{31} = 52.0 \text{ m}, \quad \eta_{31} = 0.0 \text{ m}, \quad \nu_{31} = 5.0 \text{ m}$$

Figure 5.5 shows the time history of some of the generalized coordinates of the system in both the absence and presence of material damping . The effect of material damping on the longitudinal oscillations of the tethers is quite evident. However, as has been mentioned before, it has almost no effect on the transverse oscillations of the tethers. It can be seen that some higher frequencies of the transverse oscillations of the tethers are damped out even in the absence of material damping. One might explain this in terms of numerical damping, arising from the numerical procedures.

Case 2: Variable Lengths

Figures 5.6 and 5.7 display simulation results up to 18 orbits for librational motion and 2.5 orbits for vibrational motion of the tethers for a two-phase operation: deployment of the elevator in approximately one orbit followed by the station-keeping phase. The elevator (m_3) is deployed from the space-station by increasing the second tether length. The following strategy was used for this operation;

$$\begin{cases} \ell_2 = (\ell_2)_0 + \dfrac{\Delta\ell_2}{T}\left(t - \dfrac{T}{2\pi}sin(\dfrac{2\pi t}{T})\right) & t \leq T \\ \ell_2 = (\ell_2)_f = (\ell_2)_0 + \Delta\ell_2 & t > T \\ m_2 = (m_2)_0 - \rho_2\left[\ell_2 - (\ell_2)_0\right] & \end{cases} \tag{5.3}$$

where $(\ell_2)_0 = 1$ km, $\Delta\ell_2 = 9$ km, and $T = 5600$ s for the present case. The same parameters were chosen as in the station-keeping phase and the initial conditions were set as follows:

$\theta_1 = .07$ rad$(4.01°)$, $\phi_1 = .05$ rad$(2.86°)$, $\xi_{11} = 64.0$ m, $\eta_{11} = 50.0$ m, $\nu_{11} = 10.0$ m

$\theta_2 = .03$ rad$(1.72°)$, $\phi_2 = .04$ rad$(2.29°)$, $\xi_{21} = 6.00$ m, $\eta_{21} = 10.0$ m, $\nu_{21} = 5.00$ m

$\theta_3 = .03$ rad$(1.72°)$, $\phi_3 = .04$ rad$(2.29°)$, $\xi_{31} = 52.0$ m, $\eta_{31} = 50.0$ m, $\nu_{31} = 10.0$ m

The deployment strategy is shown in Figs. 5.6-a,b while the Hamiltonian of the system is shown in Fig. 5.6-c. Note that during the station-keeping phase the Hamiltonian is conserved which gives some confidence in the formulation and numerical analysis. Examining the results shown in Figs. 5.6 and 5.7, one can see that the deployment here has a greater effect on the librational and vibrational motion of tethers 2 and 3 rather than on the first tether. It can be explained by a very small effect of deployment on the position of the centre of mass and consequently on that of the lower platform. The Coriolis effect on the librational motions can be seen clearly from Figs. 5.6-e,f. It can be seen that during the accelerating period these motion tend to grow, while it is the converse for the decelerating period. Therefore it is evident that the librational motion can become very large, even in the deployment phase, for some deploying rates. Because of the very close librational frequencies of the system in the final station-keeping phase, there is a beat phenomenon between the librational motion of the first tether and the other two tethers, which can be seen in Figs. 5.6-d,e,f

Fig. 5.7-a shows the longitudinal oscillations of the tethers. It can be seen that during deployment, the longitudinal stretches of tethers 2 and 3 are affected more than that of tether 1. This is because of increasing tension in these two tethers due to the deployment of m_3 and m_4 to large distances from the centre of mass. Typical transverse vibrations of the tethers, usually oscillatory motions with high frequencies are shown in Fig. 5.7-b. The shorter the tether length, the higher the frequency.

5.4 Microgravity Evaluation

A variety of experiments, dealing with material processing, pharmaceutical research, have been proposed for the Space-Station microgravity laboratory. The threshold levels of acceleration noise for such experiments range from 10^{-2} to 10^{-8} g. Tether Elevator/Crawler System (TECS) can be used for this purpose. Microgravity experiments can be carried out onboard a stationary microgravity laboratory (SML) that is attached to the Space-Station. In order to minimize the gravity gradient acceleration onboard this laboratory, the centre of mass of the system must be as close as possible to the stationary microgravity laboratory. The above range of microgravity can be achieved by crawling the elevator between the Space-Station and the upper platform and controlling the tether lengths.

Microgravity acceleration of body i located at $\vec{\mathbf{R}}_i$ measured in the orbital frame is defined as the difference between the absolute acceleration of the body and the acceleration acting on the body resulting from the Earth's gravity, i.e.

$$\vec{a}_i = \ddot{\vec{\mathbf{R}}}_c + \ddot{\vec{\mathbf{R}}}_i + \frac{GM}{|\vec{\mathbf{R}}_c + \vec{\mathbf{R}}_i|^3}\left(\vec{\mathbf{R}}_c + \vec{\mathbf{R}}_i\right) \tag{5.4}$$

Note that for a circular orbit, when $\vec{\mathbf{R}}_i$ becomes zero, i.e. the i-th body is located at the origin of the orbital frame which is assumed to be coincident with the centre of mass, the microgravity acceleration becomes zero.

Here microgravity fluctuation of the TECS, which is initially located at its equilibrium position along the local vertical, due to application of thrusters of the Space-Station is studied. The system parameters are exactly the same as those of Section 5.3.2. The thruster exerts the following thrust in this operation;

$$\begin{aligned}
\vec{T} &= \vec{0} && t < t_0 \,, \\
\vec{T} &= T_0 \cos\frac{\pi(t-t_0)}{t_1-t_0}\hat{\mathbf{j}}_1 && t_0 < t < t_1 \,, \\
\vec{T} &= \vec{0} && t_1 < t < t_2 \,, \\
\vec{T} &= \frac{T_0}{20}\cos\frac{\pi(t-t_2)}{t_3-t_2}\hat{\mathbf{k}}_1 && t_2 < t < t_3 \,, \\
\vec{T} &= \vec{0} && t > t_3 \,,
\end{aligned}$$

where $T_0 = 5000$ N, $t_0 = 720$ s, $t_1 = 840$ s, $t_2 = 1440$ s, and $t_4 = 1560$ s.

Figures 5.8 and 5.9 show the librational and some of the vibrational motions of the tethers, respectively. Microgravity variation at the Space-Station as well as the elevator level is shown in Fig. 5.10. As can be seen the system is initially at rest, as far as the attitude motion is concerned. Because of the thruster force, the librational motion as well as the vibrational motions of the tethers are excited. Consequently, microgravity acceleration at the body levels fluctuate.

One can appreciate the value of this formulation when needs to compare the results for the case in which the elasticity of the tethers are ignored with those when it is considered. In Figs. 5.8 and 5.10 the solid-lines represent the flexible tether case while the dotted-lines correspond to the rigid tether case. Comparing the microgravity acceleration at the Space-Station and elevator levels, we can say that the closer to the centre of mass of the system, the more affected is the microgravity by the flexibility of the tethers. It can be seen that at the Space-Station level, where the laboratory is located, the radial component of the microgravity acceleration (x-component), is more affected by the tether oscillations than those of the transverse components (y and z-components). That is because, in general, the transverse components of microgravity acceleration are mostly influenced by the librational as well as the vibrational motions of the tethers, but at this level the transverse oscillations of the tethers are small and have no significant effects on the transverse component of microgravity. However, as can be seen the x-component, which is the most important component in the microgravity experiments is highly affected by the longitudinal oscillations of the tethers. Hence we can conclude that ignoring the flexibility of the tethers in evaluating the microgravity accelerations leads to inaccurate results.

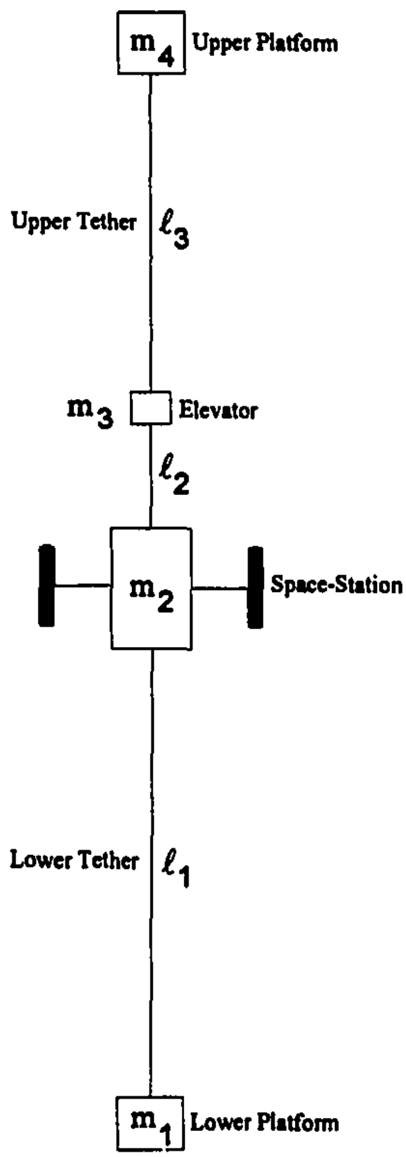

Figure 5.1: Tether Elevator/Crawler System (TECS)

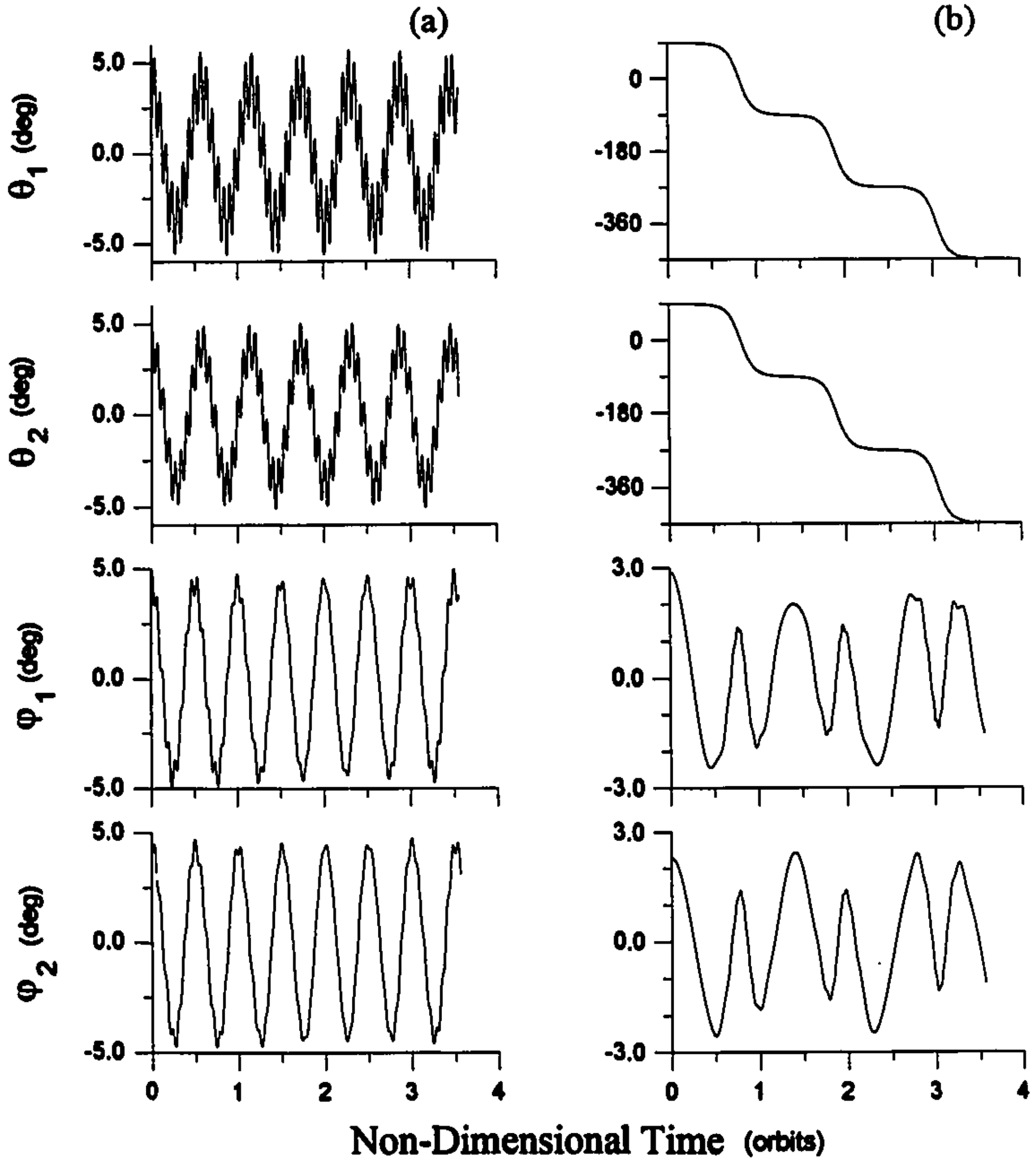

Figure 5.2: Transient response of a three-body TSS, station-keeping: **(a)** $\theta_1(0) = 2°, \theta_2(0) = 5°, \phi_1(0) = 5°, \phi_2(0) = 4°$; **(b)** $\theta_1(0) = -89.95°, \theta_2(0) = -89.95°, \phi_1(0) = 2.9°, \phi_2(0) = 2.3°$.

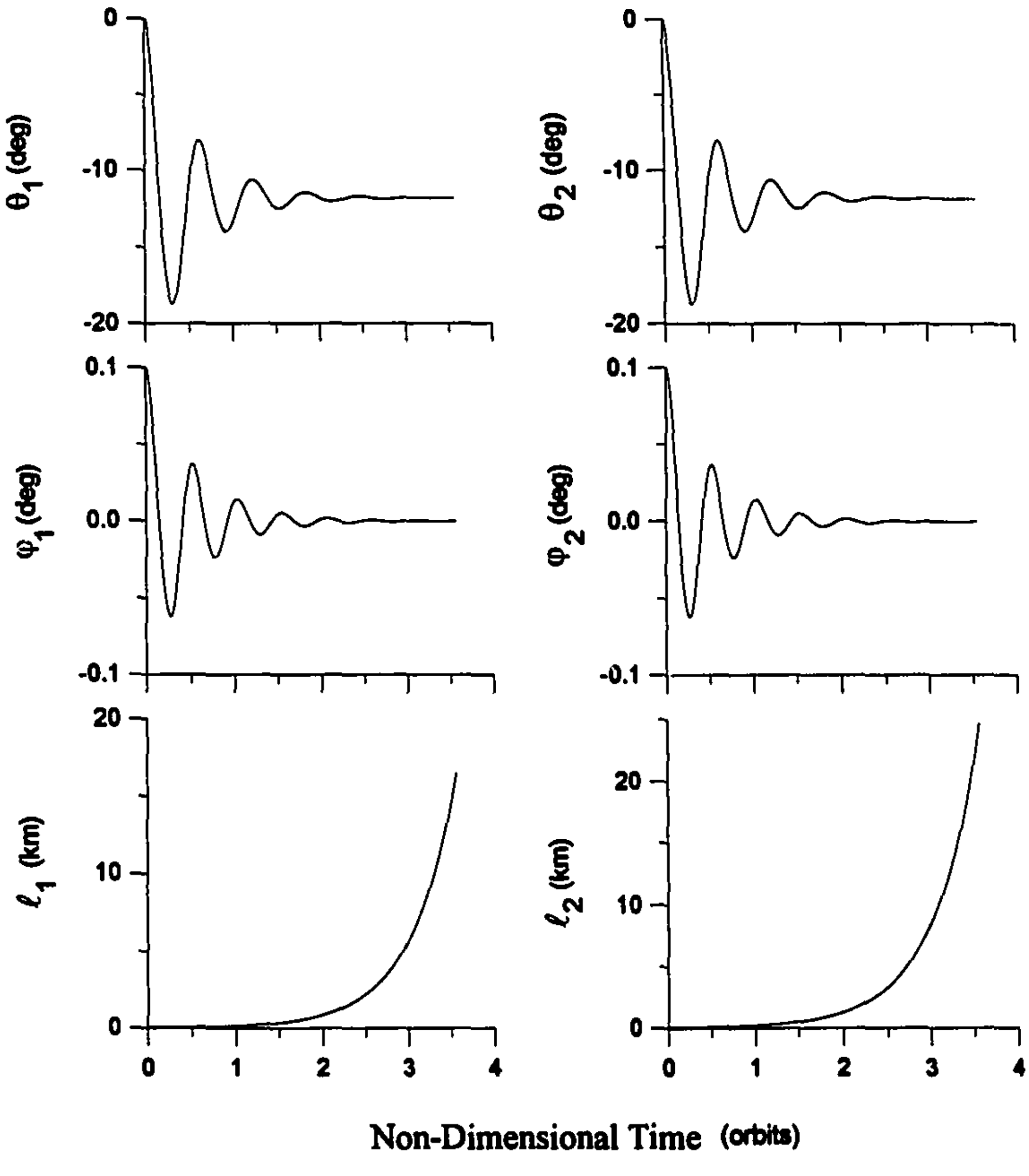

Figure 5.3: Transient response of a three-body TSS, deployment: $\ell_1(0) = 20$ m, $\ell_2(0) = 30$ m, $\theta_1(0) = \theta_2(0) = 0$, $\phi_1(0) = \phi_2(0) = 0.1°$; $c_1 = c_2 = 0.3$.

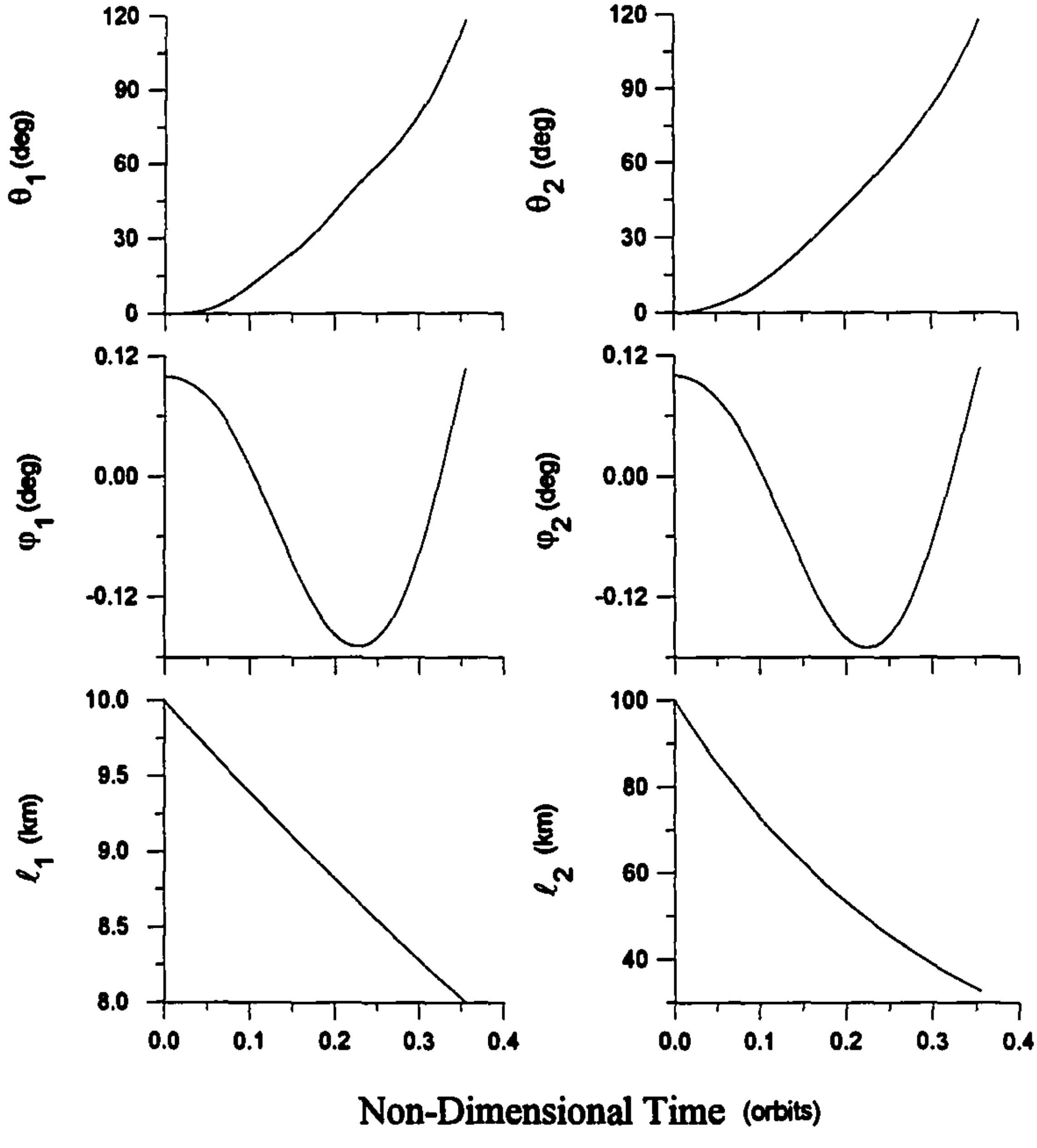

Figure 5.4: Transient response of a three-body TSS, retrieval: $\ell_1(0) = 10$ km, $\ell_2(0) = 100$ km, $\theta_1(0) = \theta_2(0) = 0, \phi_1(0) = \phi_2(0) = 0.1°$; $c_1 = -0.1, c_2 = -0.5$.

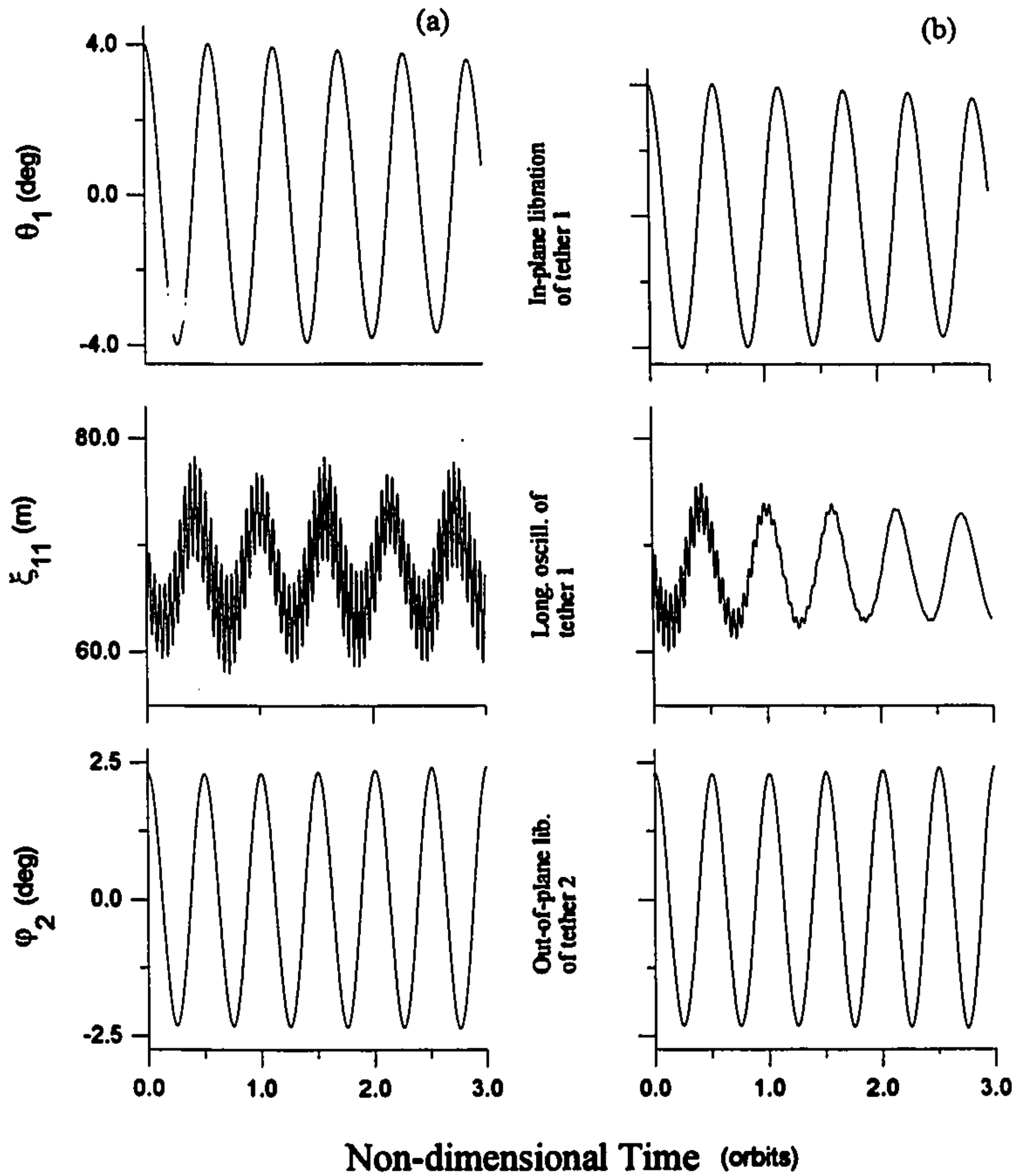

Figure 5.5: Typical dynamic response of TECS with constant length: **(a)** in the absence of material damping; **(b)** in the presence of material damping.

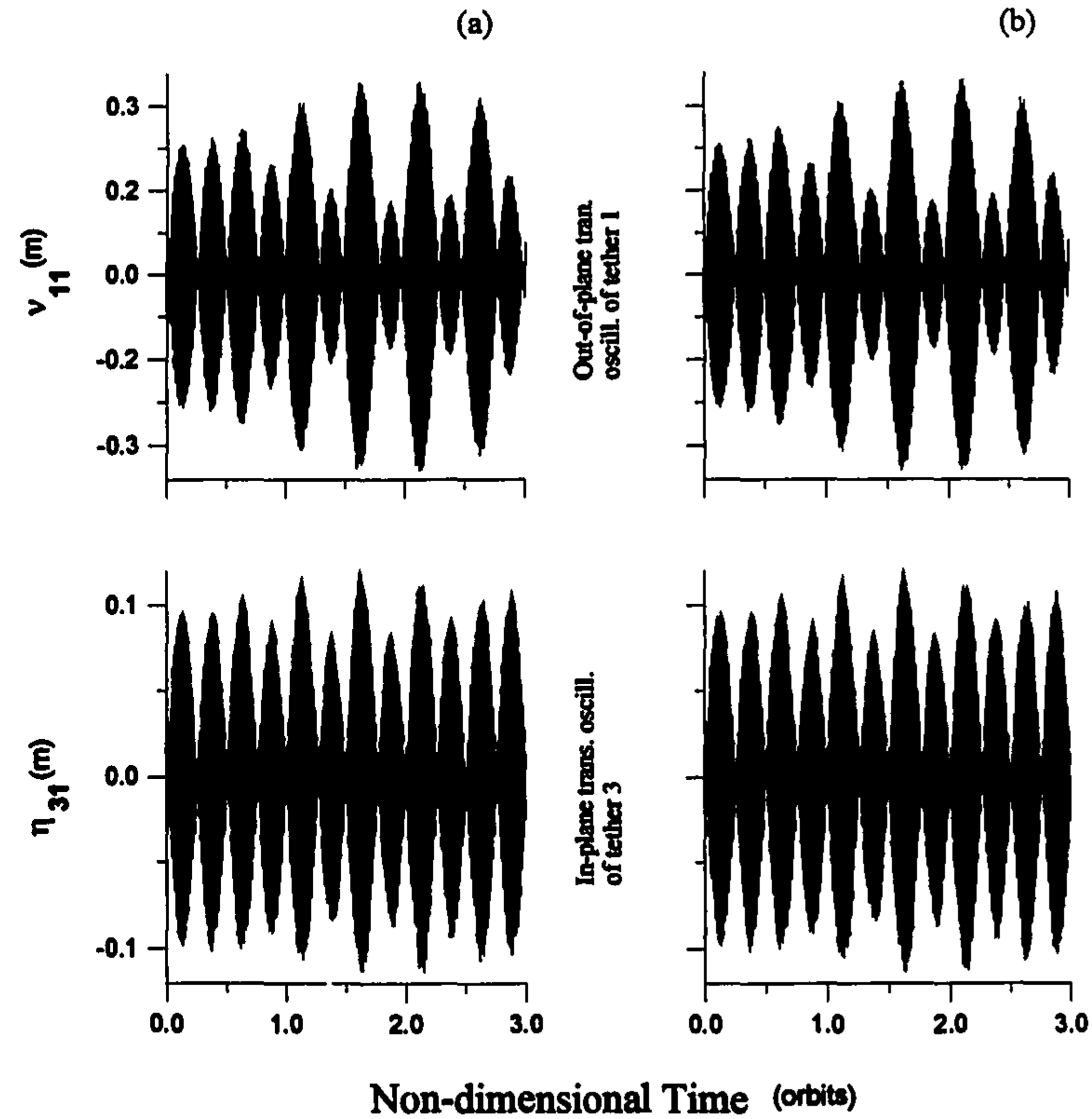

Figure 5.5: Contd.

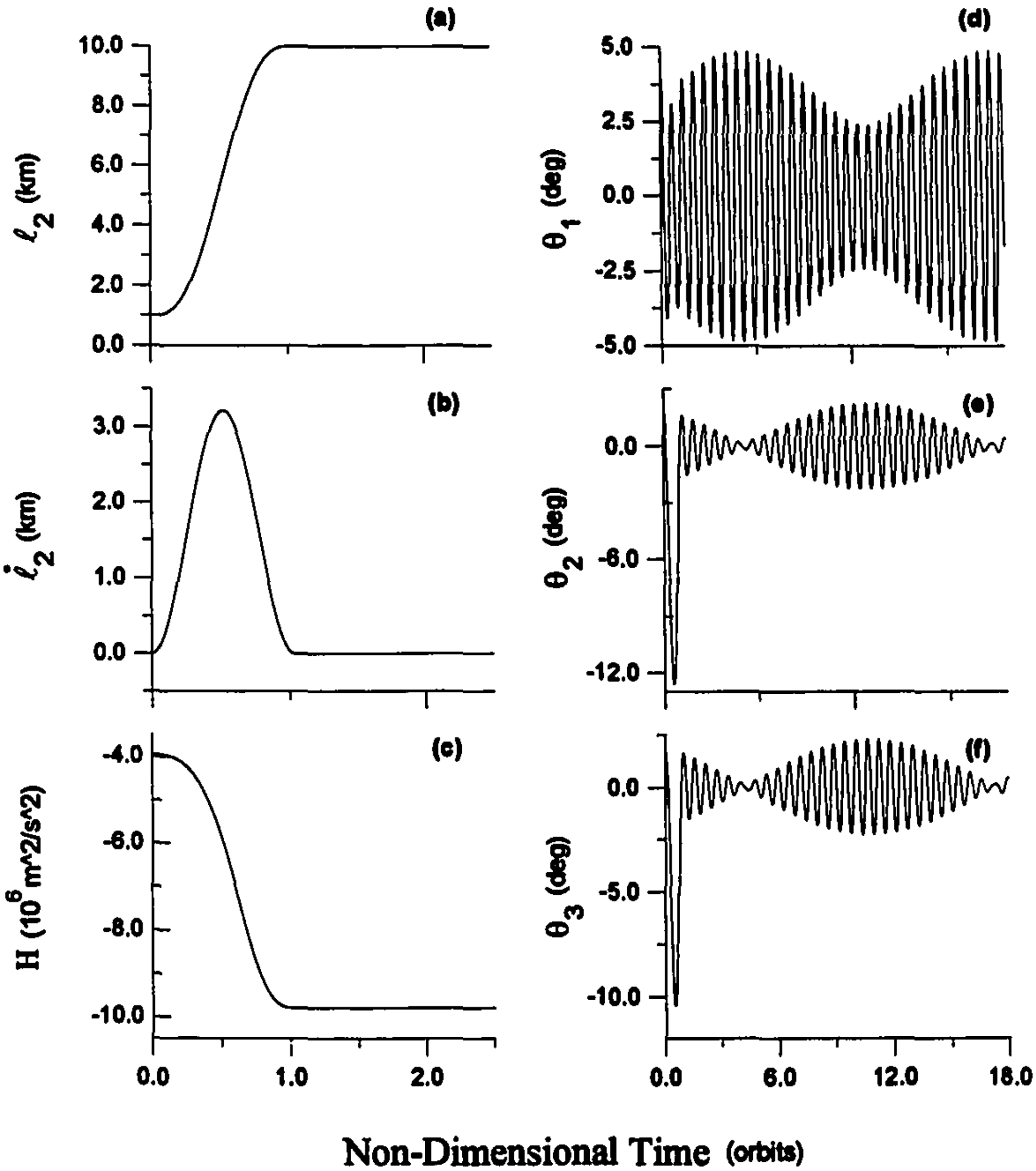

Figure 5.6: Typical dynamic response of TECS with variable length: **(a)** length variation of tether 2; **(b)** deployment rate of tether 2; **(c)** Hamiltonian of the system; **(d)** in-plane libration of the tether 1; **(e)** in-plane libration of the tether 2; **(f)** in-plane libration of the tether 3.

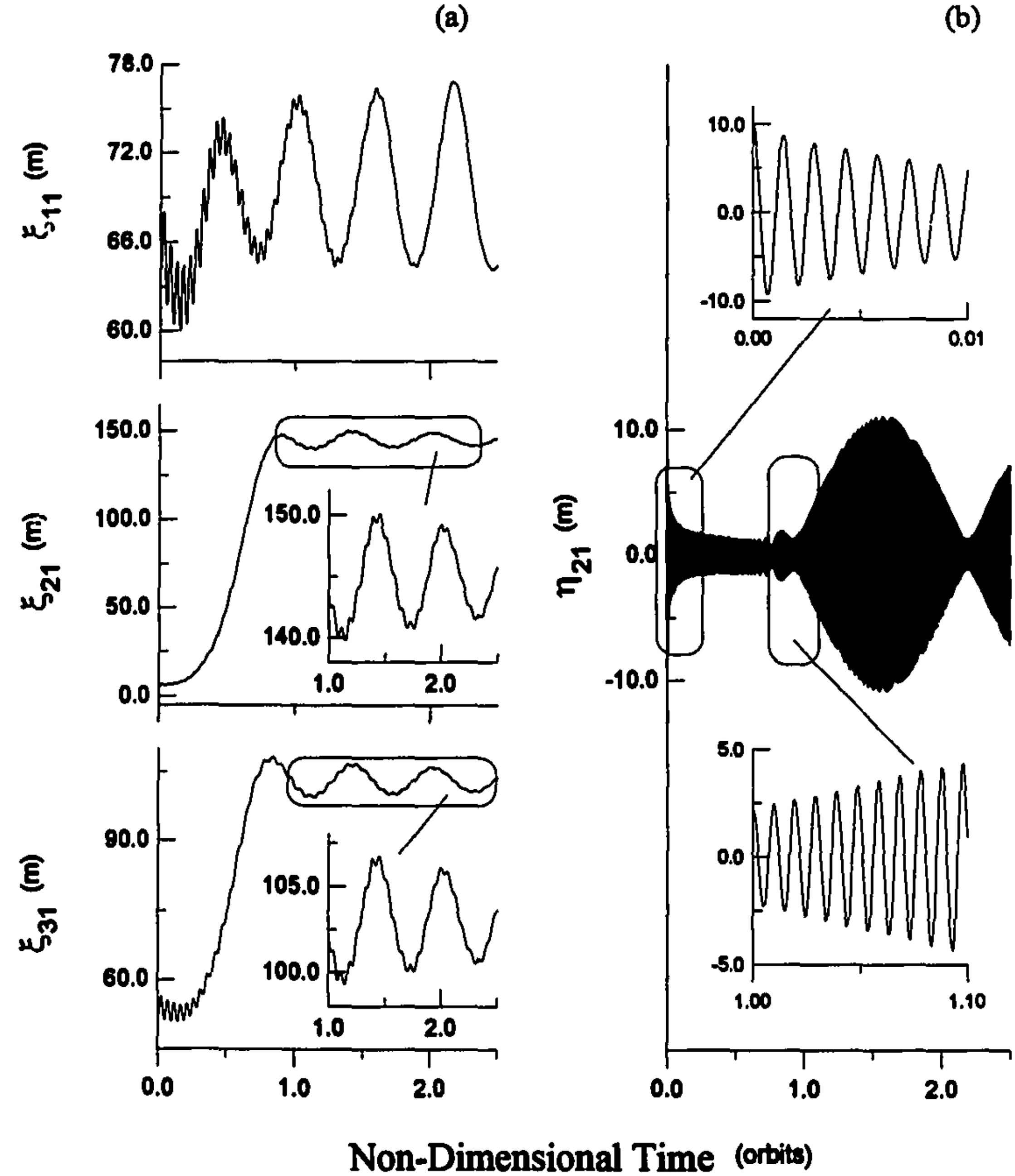

Figure 5.7: Typical dynamic response of TECS with variable length: (a) longitudinal oscillation of the tethers; (b) in-plane transverse oscillation of tether 2.

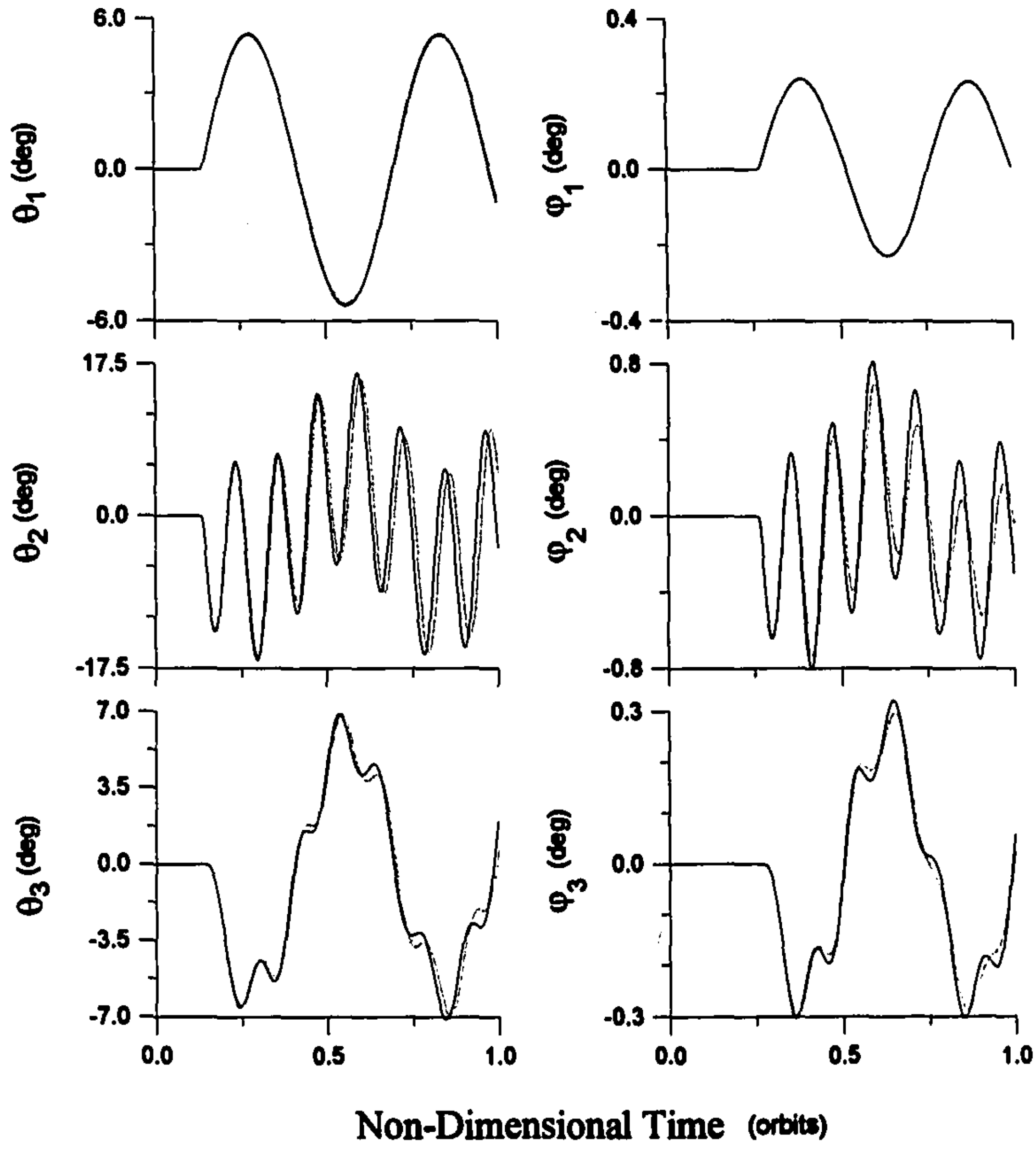

Figure 5.8: Librational motion of TECS due to the thruster force: —– rigid-tether model, ... flexible-tether model

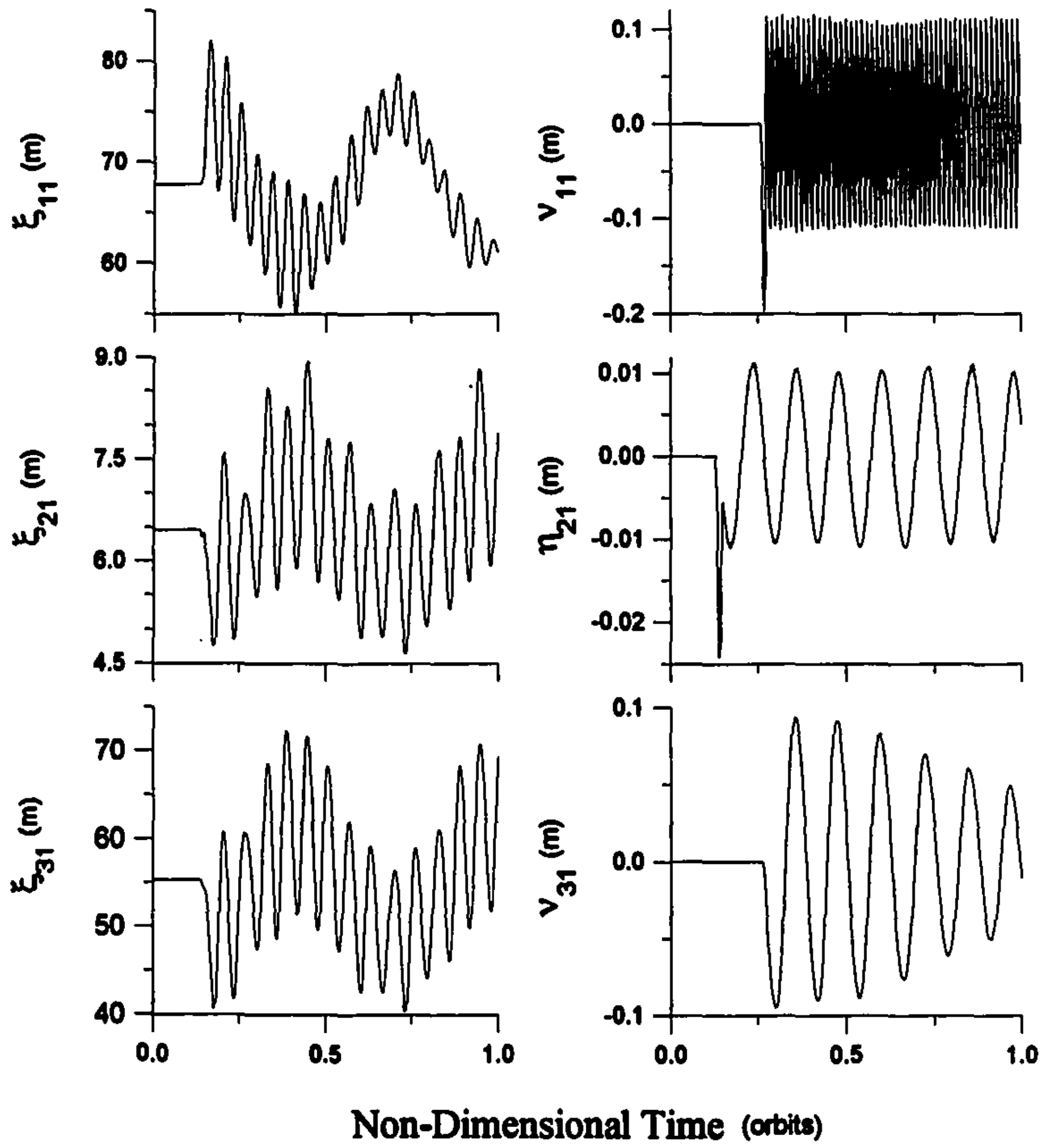

Figure 5.9: Typical vibrational motion of TECS due to the thruster force.

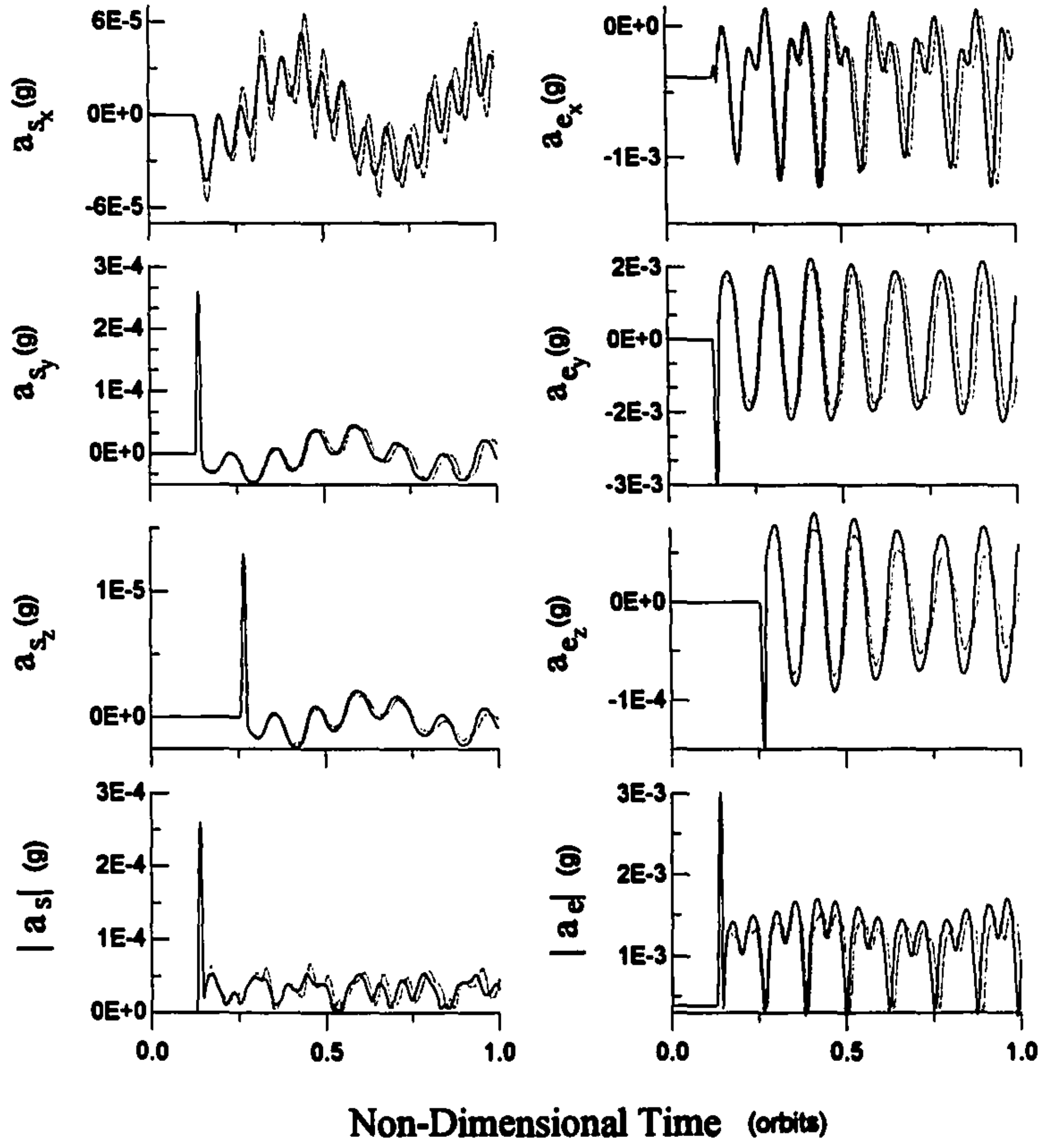

Figure 5.10: Microgravity acceleration components and magnitude of TECS at the Space-Station and Elevator level: —— rigid-tether model, ... flexible-tether model

Chapter 6

STABILITY ANALYSIS OF SYSTEMS IN ATMOSPHERIC MISSIONS

6.1 Introductory Remarks and Assumptions

As mentioned in Section 1.4, a tethered satellite system, which is normally stable or marginally stable in the absence of any external forces other than gravitational force, can become unstable due to the combined effects of the stiffness of the tethers and the atmospheric density gradient. It is observed that there is no instability if one of these two factors is ignored. So far the researchers have examined the role of aerodynamic drag in their analysis and no study can be found that analyzed systematically the role played by aerodynamic lift in the uncontrolled motion.

In this chapter, to start with, the stability problem for a single-tether system is reviewed, considering only the aerodynamic drag on the system. It is then extended to multi-tethered systems. The effects of aerodynamic lift on the stability of the system is studied next. Since our objective is to examine the qualitative behaviour, only a two-body, i.e. , a single-tether system is considered for this part of analysis. It is expected that a multi-tether system will behave similarly. It is assumed that the system is in the station-keeping phase and moves in an equatorial circular orbit around the spherical Earth.

6.2 Stability Analysis of Single-Tether Systems

6.2.1 Equations of Motion

In order to conduct our discussion here, let us assume that the system, shown in Fig. 6.1, has a massless and straight but not rigid tether. Thus one has to use only the first longitudinal mode shape, given in Eq. (2.56), to model the elastic motion of the tether, i.e., [1]

$$u(x,t) = \left(\frac{x}{L}\right)\xi \quad , \tag{6.1}$$

where, L is the nominal length of the tether and is constant. Since the system is a single-tether one and is in the station-keeping phase, it has only three degrees of freedom. The vector of generalized coordinates is then defined by

$$\mathbf{q} = \{\theta, \phi, \xi\}^T \quad , \tag{6.2}$$

where θ and ϕ represent the in-plane and out-of-plane librational angles of the tether, respectively, while ξ represents the total stretch of the tether.

Identifying different terms in Eq. (2.71) for the present system, defining the longitudinal strain

$$\epsilon = \frac{\xi}{L} \quad , \tag{6.3}$$

as a new elastic generalized coordinate instead of ξ, and performing some algebra, the equations of motion can be obtained as follows:

$$\begin{aligned}
&\ddot{\epsilon} - (1+\epsilon)\left[\dot{\phi}^2 + \cos^2\phi\left(\Omega_c + \dot{\theta}\right)^2 + \Omega_c^2\left(3\cos^2\theta\cos^2\phi - 1\right)\right] + \frac{EA}{m_* L}\epsilon = \frac{Q_\epsilon}{m_* L^2} \quad , \\
&\ddot{\theta} - 2\tan\phi\left(\Omega_c + \dot{\theta}\right)\dot{\phi} + \frac{2\left(\Omega_c + \dot{\theta}\right)\dot{\epsilon}}{1+\epsilon} + 3\Omega_c^2\sin\theta\cos\theta = \frac{Q_\theta}{m_* L^2(1+\epsilon)^2\cos^2\phi} \quad , \\
&\ddot{\phi} + \frac{2\dot{\epsilon}\dot{\phi}}{1+\epsilon} + \left[\left(\Omega_c + \dot{\theta}\right)^2 + 3\Omega_c^2\cos^2\theta\right]\sin\phi\cos\phi = \frac{Q_\phi}{m_* L^2(1+\epsilon)^2} \quad ,
\end{aligned} \tag{6.4}$$

[1] Note that since the system has only one tether, all subscripts corresponding to the tether number are omitted in this section.

where m_* is the equivalent mass defined by

$$m_* = \frac{m_1 m_2}{m_1 + m_2} \quad , \tag{6.5}$$

and Q_θ, Q_ϕ and Q_ϵ stand for the generalized aerodynamic forces corresponding to the generalized coordinates, θ, ϕ, and ϵ, respectively. Using Eq. (3.22) they can be written as

$$\begin{aligned} Q_\theta &= -(1+\epsilon)\cos\phi \; \vec{\tau}\cdot\hat{\mathbf{j}}_t \quad , \\ Q_\phi &= (1+\epsilon) \; \vec{\tau}\cdot\hat{\mathbf{k}}_t \quad , \\ Q_\epsilon &= -\vec{\tau}\cdot\hat{\mathbf{i}}_t \quad , \end{aligned} \tag{6.6}$$

where $\hat{\mathbf{i}}_t, \hat{\mathbf{j}}_t, \hat{\mathbf{k}}_t$ are the unit vectors along the tether coordinate system and $\vec{\tau}$ is the resultant aerodynamic torque about the centre of mass and is given by

$$\vec{\tau} = -(L - \ell_*)\vec{f}_1 + \ell_* \vec{f}_2 + \int_{-(L-\ell_*)}^{\ell_*} x_* \, d\vec{f}_t \quad . \tag{6.7}$$

In Eq. (6.7) $\vec{f}_1, \vec{f}_2$ and $d\vec{f}_t$ represent aerodynamic forces acting on the end-bodies and an element of the tether, respectively, $\ell_* = \dfrac{m_1 L}{m_1 + m_2}$ is the nominal distance of the subsatellite with respect to the centre of mass and x_* is the distance measured from the centre of mass of the system along the unstretched tether *downward*. The aerodynamic forces $\vec{f}_1, \vec{f}_2$ and $d\vec{f}_t$ are calculated using Eq. (3.8).

To write the generalized aerodynamic forces explicitly, which is needed for any further analysis, the geometrical configuration of the bodies must be known. For the sake of simplicity the following is assumed:

- The main satellite is at a higher altitude and above the sensible atmosphere such that the aerodynamic force acting on it can be ignored.
- The aerodynamic force on the tether is negligible.
- The subsatellite consists of a sphere with an attached lifting panel.

6.2.2 Linearized Equations of motion

In order to have the linearized equations of motion in the explicit form, only two dimensional (in-plane) motion of the system is considered here. Nonlinear equations of planar motion is simply obtained by removing the last line of Eqs. (6.4) and (6.6) and substituting zero for $\dot{\phi}$ and ϕ in the other equations. Using Eq. (4.21) for a single-tether system with the above-mentioned assumptions and the definitions of ϵ and Q_ϵ, one can find the equilibrium states of the system from the following set of nonlinear equations:

$$\begin{aligned}
&\frac{EA}{m_* L}\epsilon_e - 3(1+\epsilon_e)\Omega_c^2\cos^2\theta_e = \frac{Q_{\epsilon_e}}{m_* L^2} \ , \\
&\frac{3}{2}\Omega_c^2 \sin 2\theta_e = \frac{Q_{\theta_e}}{m_* L^2(1+\epsilon_e)^2} \ ,
\end{aligned} \tag{6.8}$$

where the subscript e denotes the magnitude of a variable at the equilibrium point. Using Eqs. (3.10) and (3.11) the magnitude of the generalized aerodynamic forces at the equilibrium point are given by

$$\begin{aligned}
Q_{\epsilon_e} &= \rho_e \ell_* \left(A_s V_e u_e + A_p |V_{t_e}| V_{t_e} \cos\psi\right) \ , \\
Q_{\theta_e} &= \rho_e \ell_* \left(A_s V_e v_e + A_p |V_{t_e}| V_{t_e} \sin\psi\right)(1+\epsilon_e) \ ,
\end{aligned} \tag{6.9}$$

where

$$\begin{aligned}
\rho_e &= \rho_0 \exp\left[\ell_*(1+\epsilon_e)\cos\theta_e / H_0\right] \ , \\
u_e &= R_c(\Omega_c - \Lambda)\sin\theta_e \ , \\
v_e &= (\Omega_c - \Lambda)\left[R_c\cos\theta_e - \ell_*(1+\epsilon_e)\right] \ , \\
V_e &= \sqrt{{u_e}^2 + {v_e}^2} \ , \\
V_{t_e} &= u_e\cos\psi + v_e\sin\psi \ ,
\end{aligned} \tag{6.10}$$

while ψ represents the angle between the lifting panel and normal to the tether, as shown in Fig. 6.1-b.

Substituting for Q_{θ_e} and performing some algebra in conjunction with some approximation, one can show that the steady state angle θ_e is obtained from the solution of the transcendental equation

$$\sin 2\theta_e \approx \frac{2}{3m_2 L\Omega_c^2}\rho_0 R_c^2(\Omega_c - \Lambda)^2 \exp\left(\ell_* \cos\theta_e / H_0\right)\left[A_s \cos\theta_e \right.$$
$$\left. + A_p|\sin(\theta_e + \psi)|\sin(\theta_e + \psi)\sin\psi\right] \quad . \tag{6.11}$$

Furthermore, the steady state strain is approximately given by

$$\epsilon_e \approx \frac{m_*}{m_2(EA - 3m_* L\Omega_c^2\cos^2\theta_e)}\left\{\rho_0 R_c^2(\Omega_c - \Lambda)^2 \exp\left(\ell_* \cos\theta_e / H_0\right)\left[A_s \sin\theta_e \right.\right.$$
$$\left.\left. + A_p|\sin(\theta_e + \psi)|\sin(\theta_e + \psi)\cos\psi\right] + 3m_2 L\Omega_c^2\cos^2\theta_e\right\} \quad . \tag{6.12}$$

Considering small motion about the equilibrium point (θ_e, ϵ_e), i.e.

$$\theta = \theta_e + \delta\theta \quad , \quad \epsilon = \epsilon_e + \delta\epsilon \quad , \tag{6.13}$$

the linearized equations of motion of the system are given by:

$$\dot{\mathbf{u}} = (\mathbf{B} + \mathbf{A})\,\mathbf{u} \tag{6.14}$$

where $\mathbf{u}$ is the state vector defined by

$$\mathbf{u} = \left\{\delta\dot{\theta}, \delta\dot{\epsilon}, \delta\theta, \delta\epsilon\right\}^T \quad . \tag{6.15}$$

$\mathbf{B}$ is the Jacobian matrix of the system in the absence of aerodynamic forces, while $\mathbf{A}$ is the contribution of aerodynamic forces in the Jacobian matrix. Matrix $\mathbf{B}$ can be calculated either directly from Eq. (6.4) or from the general form of the linearized equations of motion, Eqs. (4.30)-(4.36). Those matrices can be written as:

$$\mathbf{A} = \begin{bmatrix} Z_{11}Z_5 & Z_{10}Z_3 & Z_9 Z_1 + Z_{10}Z_4 + Z_{11}Z_6 & Z_9 Z_2 + Z_{11}Z_7 + Z_{12}Z_8 \\ Z_{15}Z_5 & Z_{14}Z_3 & Z_{13}Z_1 + Z_{14}Z_4 + Z_{15}Z_6 & Z_{13}Z_2 + Z_{15}Z_7 \\ 0 & 0 & 0 & 0 \\ 0 & 0 & 0 & 0 \end{bmatrix} ,$$

$$\mathbf{B} = \begin{bmatrix} 0 & -2\dfrac{\Omega_c}{Z_0} & -3\Omega_c^2\cos 2\theta_e & -3\dfrac{\Omega_c^2}{Z_0}\sin 2\theta_e \\ 2Z_0 & 0 & -3Z_0\Omega_c^2\sin 2\theta_e & -\dfrac{EA}{m_* L} + 3\Omega_c^2\cos^2\theta_e \\ 1 & 0 & 0 & 0 \\ 0 & 1 & 0 & 0 \end{bmatrix} , \tag{6.16}$$

where

$$
\begin{aligned}
Z_0 &= (1+\epsilon_e) \ , \\
Z_1 &= -\rho_e \ell_*(1+\epsilon_e)\sin\theta_e/H_0 \ , \\
Z_2 &= \rho_e \ell_* \cos\theta_e/H_0 \ . \\
Z_3 &= -\ell_* \ , \\
Z_4 &= R_c(\Omega_c - \Lambda)\cos\theta_e \ , \\
Z_5 &= -\ell_*(1+\epsilon_e) \ , \\
Z_6 &= -R_c(\Omega_c - \Lambda)\sin\theta_e \ , \\
Z_7 &= -(\Omega_c - \Lambda)\ell_* \ , \\
Z_8 &= 1 \ , \\
Z_9 &= (A_s V_e v_e + A_p|V_{t_e}|V_{t_e}\sin\psi)/m_2 L(1+\epsilon_e) \ , \\
Z_{10} &= \rho_e (A_s v_e u_e/V_e + 2A_p|V_{t_e}|\cos\psi\sin\psi)/m_2 L(1+\epsilon_e) \ , \\
Z_{11} &= \rho_e \left(A_s {v_e}^2/V_e + 2A_p|V_{t_e}|\sin^2\psi + A_s V_e\right)/m_2 L(1+\epsilon_e) \ , \\
Z_{12} &= \rho_e (A_s V_e v_e + A_p|V_{t_e}|V_{t_e}\sin\psi)/m_2 L(1+\epsilon_e)^2 \ , \\
Z_{13} &= (A_s V_e u_e + A_p|V_{t_e}|V_{t_e}\cos\psi)/m_2 L \ , \\
Z_{14} &= \rho_e \left(A_s {u_e}^2/V_e + 2A_p|V_{t_e}|\cos^2\psi + A_s V_e\right)/m_2 L \ , \\
Z_{15} &= \rho_e (A_s v_e u_e/V_e + 2A_p|V_{t_e}|\cos\psi\sin\psi)/m_2 L \ .
\end{aligned} \tag{6.17}
$$

6.2.3 Eigenvalue Analysis

The formulation results for various cases in the absence of aerodynamic forces were validated in Section 5.2. In this Section, we extend the validation to the formulation with aerodynamic forces by comparing the results obtained here (suppressing the out-of-plane motion) with those of No and Cochran [36] and Onada and Watanabe [15] for a spherical subsatellite (that is with no lift). The following data have been used in their studies:

- radius of orbit $\qquad R_c = 6.6 \times 10^6$ (m)

Table 6.1: Comparison of Results with other researchers

L (km)	Thesis	No and Cochran [36]	Onada and Watanabe [15]
100	$4.35 \times 10^{-5} \pm 2.26 \times 10^{-3}i$	$4.38 \times 10^{-5} \pm 2.28 \times 10^{-3}i$	$4.15 \times 10^{-5} \pm 2.23 \times 10^{-3}i$
16	$6.98 \times 10^{-13} \pm 2.04 \times 10^{-3}i$	$6.41 \times 10^{-13} \pm 2.04 \times 10^{-3}i$	-
14	$-1.80 \times 10^{-12} \pm 2.04 \times 10^{-3}i$	$-1.83 \times 10^{-12} \pm 2.04 \times 10^{-3}i$	-

- subsatellite mass $m_2 = 500$ (kg)
- angular velocity of the atmosphere $\Lambda = 7 \times 10^{-5}$ (rad/sec)
- tether stiffness $EA = 10^4$ (N)
- drag coefficient $C_D = 2.2$
- aerodynamic effective surface $A_{eff} = 10$ (m^2)
- reference atmosphere density at R_c $\rho_0 = 1.38 \times 10^{-14}$ (kg/m^3)
- scale height $H_0 = 6700$ (m)

The same data are used here, excepting A_{eff} and C_D. Since $C_D = 2$ for a sphere in this formulation, we compensate for the difference by choosing $A_s = 11$, so that the product $C_D A_s$ remains the same. Also to make the comparison possible A_p is set to zero and it is assumed that $m_* = \dfrac{m_1 m_2}{m_1 + m_2} \approx m_2$. The results obtained here and those of the above mentioned researchers are given in Table 6.1. It can be seen that the eigenvalue results are in good agreement.

Effects of EA, L, and R_c on the stability of the system for different radii of the spherical subsatellite ($R_s = 0.25 - 3.0$ m) are shown in Figs. 6.2 and 6.3. Note that the eigenvalues are nondimensionalized with respect to the orbital rate. The results confirm what Onada and Watanabe [15] concluded in their paper. The system loses stability if the tether stiffness falls below a certain value or if the subsatellite is placed at a sufficiently low altitude by either increasing L or decreasing R_c.

6.2.4 Simulation Results

To obtain a better understanding of the problem some simulation results for in-plane librational motion of a single-tether system are presented here. The system has the following parameters:

$$R_c = 6590\,\text{km},\ m_* \approx m_2 = 500\,\text{kg},\ \ell_* \approx L = 100\,\text{km},\ A_s = 10\,\text{m}^2\ ,$$
$$\rho_0 = 6.139 \times 10^{-14}\,\text{kg/m}^3 \text{ at } R_c,\ H_0 = 6700\,\text{m}\ \ .$$

and four different cases are considered:

- case 1: rigid tether with no aerodynamic force;
- case 2: rigid tether with aerodynamic drag on the subsatellite;
- case 3: elastic tether with aerodynamic drag on the subsatellite ($EA = 10^5$ N);
- case 4: same as case 3 but with $EA = 4 \times 10^4$ N.

Figure 6.4 shows the librational motion of the system due to small deviation from its equilibrium point [2]. It can be seen that the system is marginally stable in case 1. Adding aerodynamic effects to case 1 results in a new equilibrium point and asymptotical stability of the system. However, the system can be unstable, depending on the stiffness of the tether, if elasticity of the tether is included (case 3 is stable, while case 4 with a smaller EA is unstable).

6.3 Stability Analysis of Multi-Tethered Systems

Similar behaviour can be observed in the dynamics of a multi-tethered system that is moving in a low Earth orbit. In the following, the eigenvalues and simulation results for two different three-body systems are presented. The systems differ only in their

[2]Note that the equilibrium point differs from case to case because of the aerodynamic and elasticity effects.

tether stiffness. The system parameters are as follows:

$R_c = 6600\,\text{km},\ m_1 = 10^5\ \text{kg},\ m_2 = 100\,\text{kg},\ m_3 = 50\,\text{kg},\ \ell_1 = 90\,\text{km},\ \ell_2 = 10\,\text{km},$

$A_{s_1} = A_{s_2} = 3\,\text{m}^2,\ \rho_0 = 1.38 \times 10^{-14}\,\text{kg/m}^3$ at R_c, $H_0 = 6.7\,\text{km},\ \rho_1 = \rho_2 = 6\text{kg/km}.$

The mass of the tethers as well as their transverse oscillations are considered in the analysis. For the first case, the tether stiffness is taken as $EA_1 = EA_2 = 10^4$ N, while for the second one it is $EA_1 = EA_2 = 10^5$ N. Here only the in-plane motion is studied and one longitudinal and one transverse mode are considered for each tether.

The equilibrium configuration and the eigenvalues are given in Tables 6.2 and 6.3 respectively, for the two cases. Eigenfrequencies of the system in the absence of aerodynamic forces are also given in these tables. It can be seen that the systems are marginally stable, when aerodynamic forces are not taken into account. Including the air density gradient and the resultant aerodynamic forces leads to the instability of system 1, in which the modulus of elasticity of the tethers is much lower than that of system 2. Examining the eigenvectors of the unstable system, one can find that most of the instability is predominant in the librational motion of the tethers. This can be seen clearly in Fig. 6.5-a which shows the time history of librational motion of tether 1 of the two systems. Typical time histories of transverse oscillation of tethers 1 and 2 of the second system is shown in Fig. 6.5-b, which are stable.

6.4 Investigation of The Aerodynamic Lift Effects

The same configuration as that of Onada and Watanabe is used in this investigation, except that a lifting panel is attached to the spherical subsatellite (Fig. 6.1-b), in order to study the effects of the aerodynamic lift on the system stability. The comparison is done by examining the real part of the critical eigenvalue (the one with the lowest imaginary part), which is usually related to the swinging motion of the

Table 6.2: Eigenvalues of system 1 ($EA = 10^4$ N)

In the absence of aerodynamic forces	In the present of aerodynamic forces
$0 \pm 1.7150i$	$\underline{+1.0472 \times 10^{-02} \pm 1.7611i}$
$0 \pm 5.0510i$	$-3.0389 \times 10^{-03} \pm 5.1246i$
$0 \pm 7.6318i$	$-8.0668 \times 10^{-03} \pm 7.7847i$
$0 \pm 14.408i$	$-1.2325 \times 10^{-02} \pm 14.449i$
$0 \pm 22.196i$	$-2.2157 \times 10^{-03} \pm 25.668i$
$0 \pm 116.30i$	$-5.6389 \times 10^{-03} \pm 117.31i$
Equilibrium Point	
$\theta_{1_e} = 0.0^\circ$, $\theta_{2_e} = 0.0^\circ$	$\theta_{1_e} = 3.26^\circ$, $\theta_{2_e} = 12.03^\circ$
$\epsilon_{11_e} = 1350.5\,\mathrm{m}$, $\epsilon_{21_e} = 33.07\,\mathrm{m}$	$\epsilon_{11_e} = 1344.3\,\mathrm{m}$, $\epsilon_{21_e} = 26.37\,\mathrm{m}$
$\eta_{11_e} = 0.0$, $\eta_{21_e} = 0.0$	$\eta_{11_e} = 319.6\,\mathrm{m}$, $\eta_{21_e} = 121.5\,\mathrm{m}$

Table 6.3: Eigenvalues of system 2 ($EA = 10^5$ N)

In the absence of aerodynamic forces	In the present of aerodynamic forces
$0 \pm 1.7304i$	$-3.8775 \times 10^{-04} \pm 1.7643i$
$0 \pm 5.0195i$	$-2.8754 \times 10^{-03} \pm 5.1541i$
$0 \pm 7.5930i$	$-6.2044 \times 10^{-03} \pm 7.7690i$
$0 \pm 22.057i$	$-1.8583 \times 10^{-03} \pm 34.433i$
$0 \pm 45.456i$	$-2.0467 \times 10^{-03} \pm 45.579i$
$0 \pm 367.76i$	$-4.2271 \times 10^{-03} \pm 369.17i$
Equilibrium Point	
$\theta_{1_e} = 0.0^\circ$, $\theta_{2_e} = 0.0^\circ$	$\theta_{1_e} = 2.81^\circ$, $\theta_{2_e} = 10.26^\circ$
$\epsilon_{11_e} = 133.3\,\mathrm{m}$, $\epsilon_{21_e} = 3.27\,\mathrm{m}$	$\epsilon_{11_e} = 129.6\,\mathrm{m}$, $\epsilon_{21_e} = 0.24\,\mathrm{m}$
$\eta_{11_e} = 0.0$, $\eta_{21_e} = 0.0$	$\eta_{11_e} = 267.0\,\mathrm{m}$, $\eta_{21_e} = 78.8\,\mathrm{m}$

tether. The following parameters, which are more or less the same as those in the previous cases are used in this analysis, while the other parameters vary as indicated in the graphs:

$$m_s \approx m_2 = 500\,\text{kg},\ \Lambda = 7 \times 10^{-5}\,\text{rad/s},\ H_0 = 6667\,\text{m},\ \rho_0 = 1.13 \times 10^{-14}\,\text{kg/m}^3,$$

where ρ_0 is the air density at R_c = 6600 km. Since the aerodynamic force on the tether changes the results only marginally, it has been ignored in the following.

Figure 6.6 shows the effects of the added panel and the surface area ratio, A_p/A_s, on the real part of the critical eigenvalue of the system, $Re(\lambda_1)$, and its equilibrium librational angle, θ_e, for two different values of ψ, which is the angle between the panel and the normal to the tether. Here A_p and A_s represent the surface area of the panel and projected area of the sphere (πR_s^2) , respectively. Each curve in the graphs represents a typical value of A_s . Clearly, the system is unstable $[R_e(\lambda) > 0]$ in the absence of the panel ($A_p/A_s = 0$), but it becomes stable when A_p/A_s is sufficiently large. The minimum value of A_p/A_s required for the stabilization depends on the radius of the spherical subsatellite. Comparing Figs. 6.6-a and 6.6-b, one observes that the effects of the lifting panel change with ψ. For $\psi = 145°$ the stabilizing effect is larger than that for $\psi = 90°$, while the changes in the equilibrium librational angle are just the opposite, which is desirable.

Effects of ψ on the equilibrium librational angle of the tether and the real part of the critical eigenvalue are shown in Fig. 6.7 for a typical value of ψ, and for two different values of σ (0 and 0.8). Similar trends are seen in both cases. For a small value of ψ, the lifting panel makes the system more unstable. This is because the panel produces a lift force which is more or less along the tether and increases the tether tension. For larger ψ this component reduces the tether tension and makes the system stable. There is a jump point at $\psi = 160°$, where the lifting panel is along the relative velocity. The most appropriate value of ψ lies between 130° and 150° where the stabilizing effect is greater and changes in θ_e are smaller.

The effect of changing the parameters EA, R_c, and L, in the case of a sphere with an added panel is shown in Fig. 6.8. Figure 6.8-a shows that the stabilization effect of the aerodynamic panel is greater when the main satellite is located at a lower altitude. Comparing the curves in Fig. 6.8-b, one concludes that the more flexible the tether, the greater is the stabilization effect. Also, it is concluded from Fig. 6.8-c that the stabilization effect is usually larger for a longer tether.

Simulation results, shown in Fig. 6.9, support the above discussion. Time histories of the swinging motion and elastic oscillation of the tether for the case of a spherical subsatellite without any lifting panel are given in Fig. 6.9-a. The effect of adding a panel is shown in Fig. 6.9-b, where the system has been stabilized without much change in its equilibrium point.

Aerodynamic lift also strongly affects the stability of the system in the case of non-spherical subsatellites. Figure 6.10 shows this for a cylindrical subsatellite rigidly fixed to a tether, making an angle ψ with the tether (Fig. 6.10-d). Each curve represents a different H_{cyl}/R_{cyl} (height/radius) ratio, while $A_c = 2H_{cyl}R_{cyl}$ is kept constant. For a given angle ψ , decreasing H_{cyl}/R_{cyl} means producing more lift and consequently increasing the stability of the system, which can be seen in Fig. 6.10-a,b,c.

Since the in-plane and out-of-plane motions are decoupled in the linearized case, one expects the in-plane characteristics of the system to remain unchanged when the out-of-plane motion is added to the two dimensional case. Comparison of the results shown in Fig. 6.11-a for the three-dimensional case to that of Fig. 6.6-a corresponding to planar motion of the same system confirms this. However, it should be emphasized that the out-of-plane motion affects the in-plane motion if the orbit is either elliptical or non-equatorial, or if oblateness of the Earth is taken into account. Although the out-of-plane motion does not affect the planar characteristics in the present case, the out-of-plane oscillation frequency ($Im(\lambda_2)$ in Fig. 6.11-b) decreases from 2 due to the aerodynamic force effects.

6.5 Physical Interpretation

In the absence of aerodynamic force and elasticity of the tether, any deviation from the equilibrium position, local vertical, is restored by the component of the gravitational force on the subsatellite normal to the tether. Aerodynamic drag which is almost perpendicular to the tether, causes a slight deviation of the steady-state position from the local vertical. The new position is obtained from the equilibrium between the normal components of the aerodynamic drag and the gravitational force. In the absence of tether elasticity, any positive deviation from the steady-state configuration puts the subsatellite at a higher altitude. Since the air density decreases *exponentially* with an increase in the altitude while the gravitational force decreases with *inverse square* of $|\vec{r}|$, the normal component of the net force opposes the swinging motion of the subsatellite and returns it towards its equilibrium point. The same effect is observed for a negative deviation.

In the presence of tether elasticity, a positive deviation from the steady-state position causes the centrifugal force to increase and the tether elongates, and therefore, the altitude of the subsatellite decreases. In this case, the normal component of the resultant force is in the direction of the deviation and excites the swinging motion. Similarly, the reverse holds true for a negative deviation.

Adding the lifting panel to the subsatellite imposes a new aerodynamic force on the subsatellite, which can be decomposed into two components, normal and tangential to the tether. Each of these two components can be used to stabilize the swinging motion of the subsatellite in a different way. The normal component shifts the equilibrium point to a higher altitude such that the destabilizing effect is less. The tangential component opposes the centrifugal force and decreases the tether elongation thereby reducing the aerodynamic force, and therefore stabilizes the swinging motion. The magnitude and direction of these components are changed by changing the position of the lifting panel on the subsatellite.

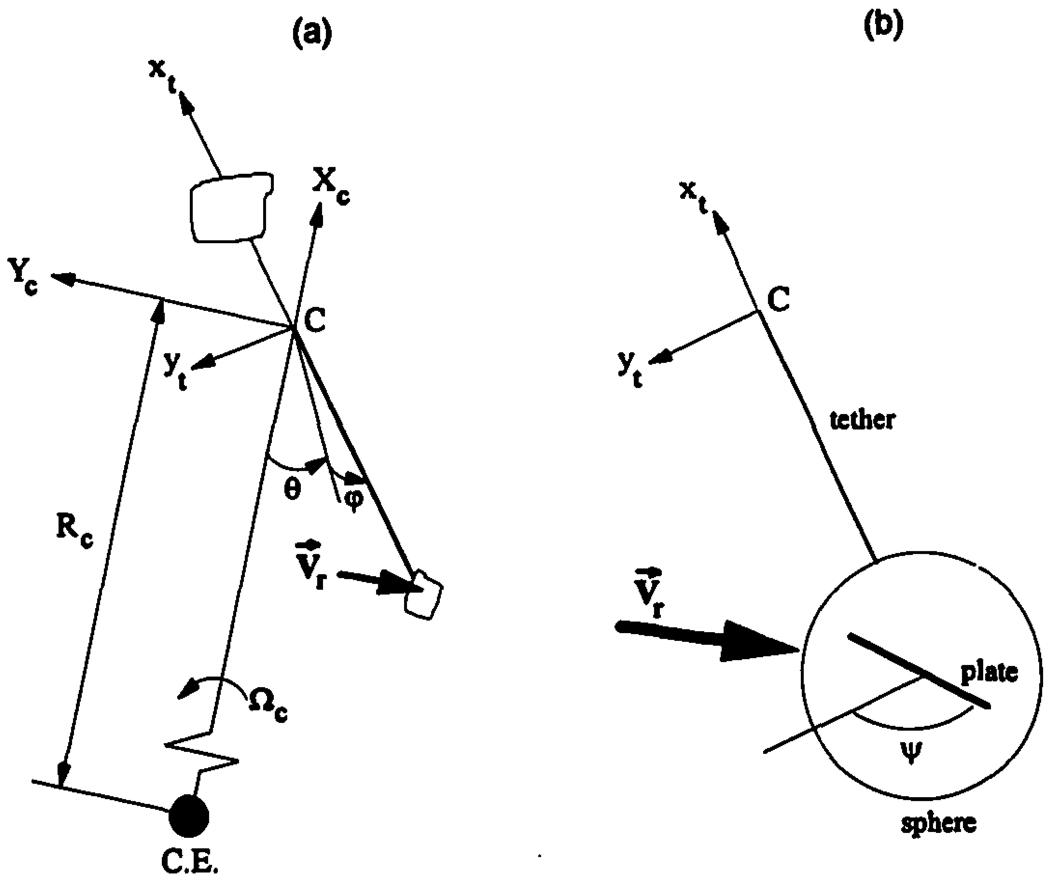

Figure 6.1: Tethered subsatellite system: a): system configuration ($X_c - Y_c$ is the orbital plane, b): spherical subsatellite with an added lifting panel.

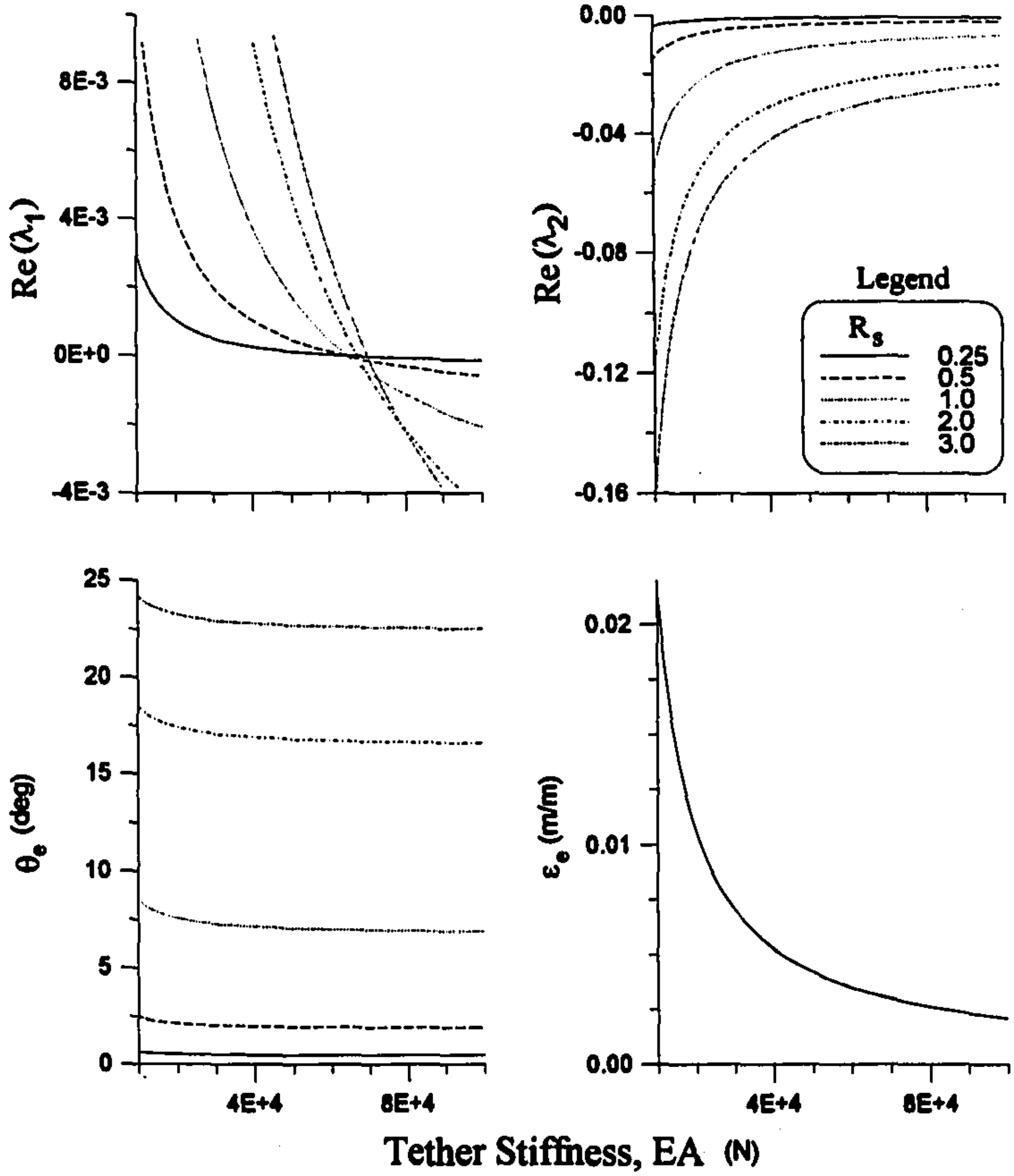

Figure 6.2: Effects of the tether stiffness on the system stability and equilibrium configuration in the absence of aerodynamic lift ($R_c = 6.59 \times 10^3$ km, $L = 100$ km).

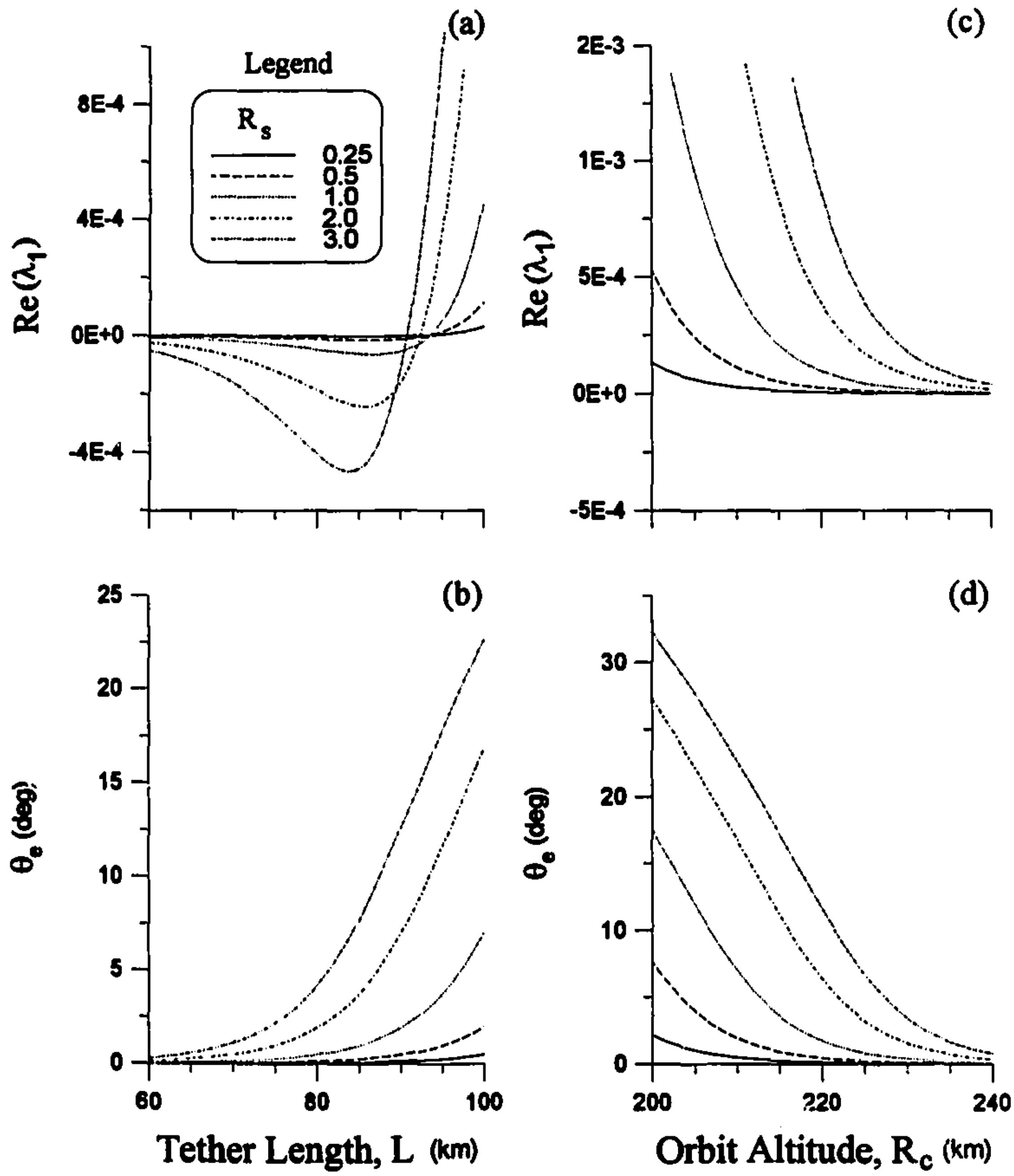

Figure 6.3: Effect of the tether length and orbit altitude on the system stability and equilibrium librational angle in the absence of aerodynamic lift.

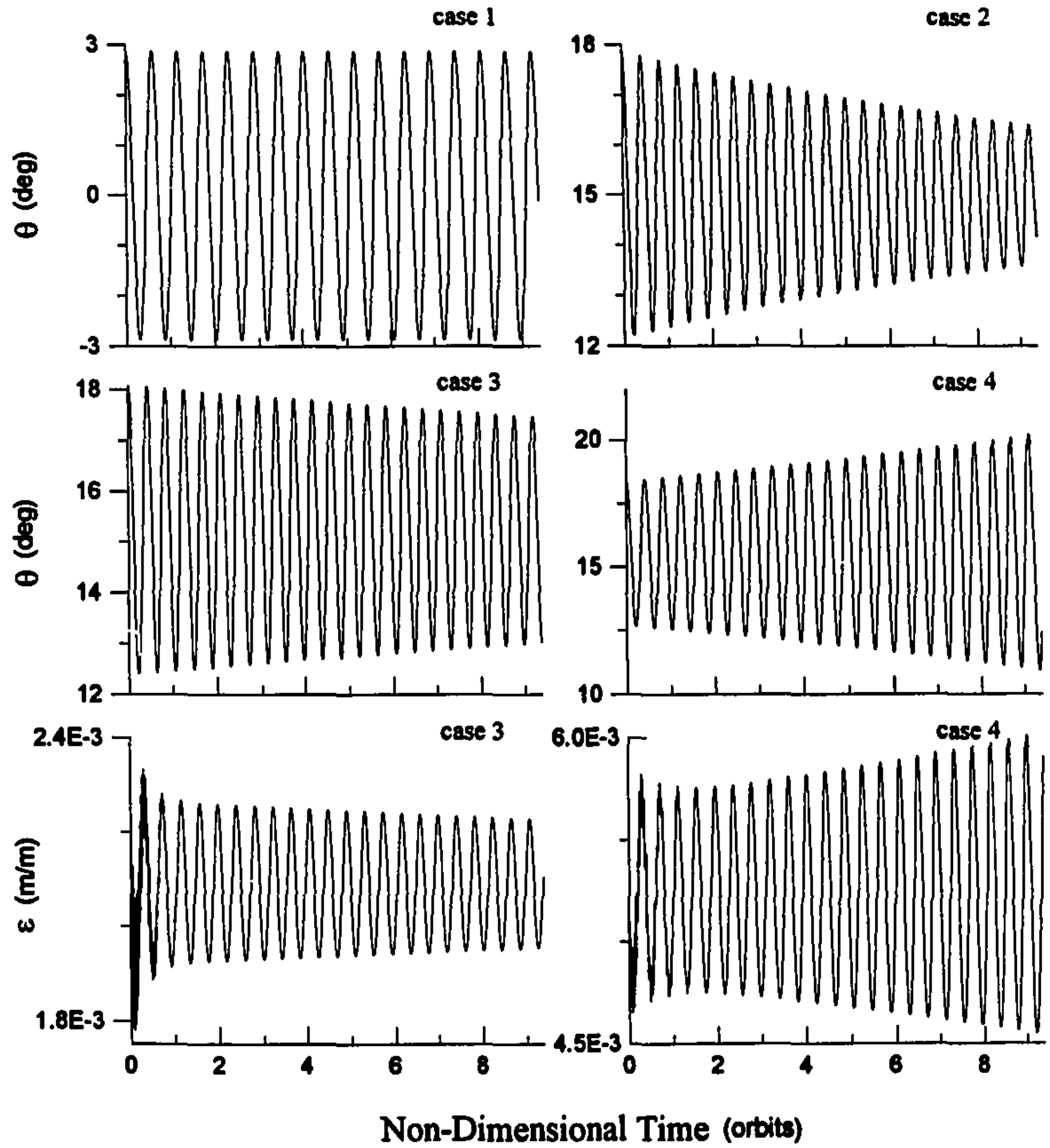

Figure 6.4: Transient response of a single-tethered system: case 1: system with a rigid tether in the absence of atmospheric drag; case 2: system with a rigid tether in the presence of aerodynamic drag, case 3: system with a flexible tether in the presence of aerodynamic drag ($EA = 10^5$ N); case 4: system with a flexible tether in the presence of aerodynamic drag ($EA = 4 \times 10^4$ N).

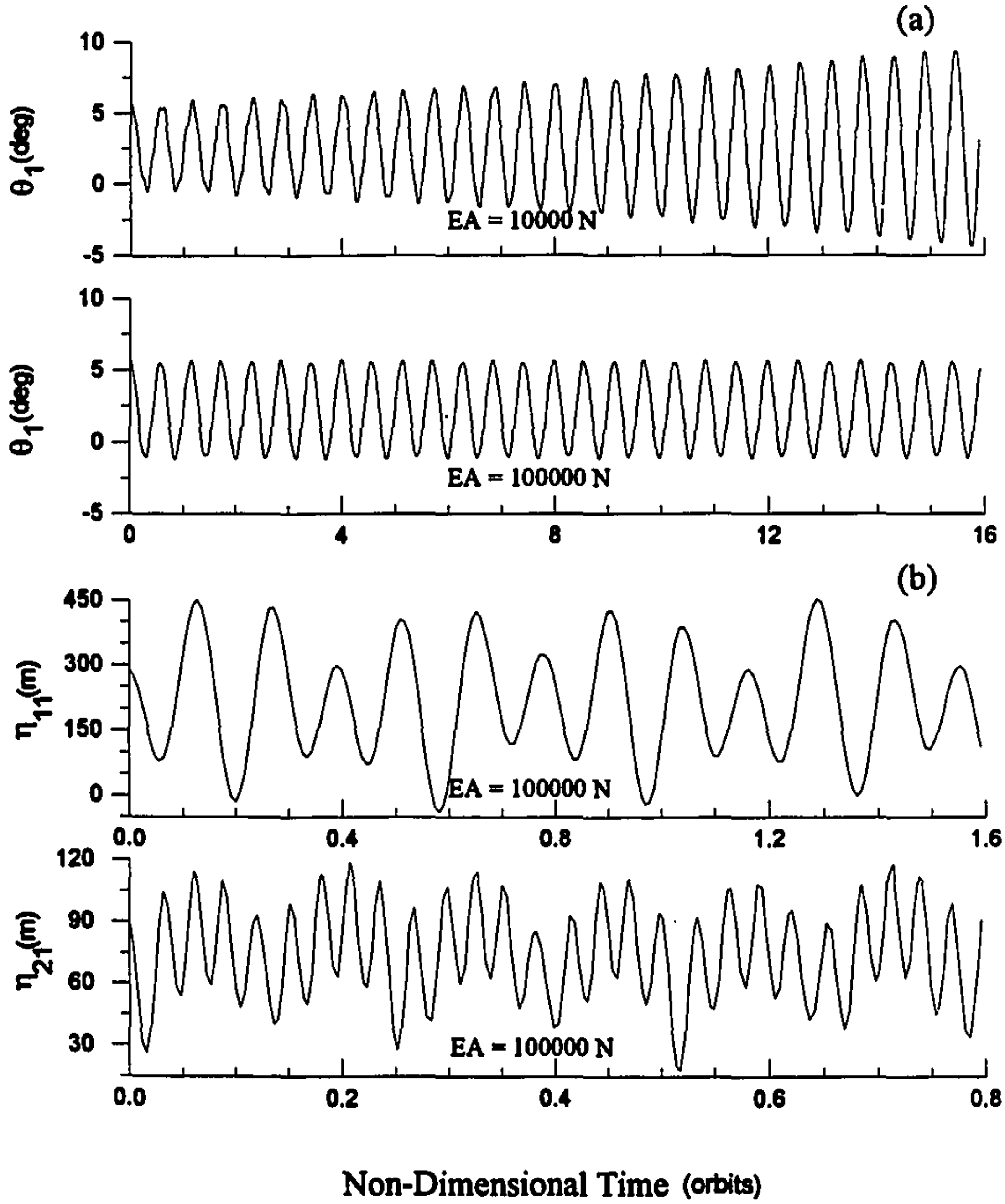

Figure 6.5: Time history of: **(a)** librational motion of tether 1 of the two systems; **(b)** transverse displacement of the two tethers of system 2.

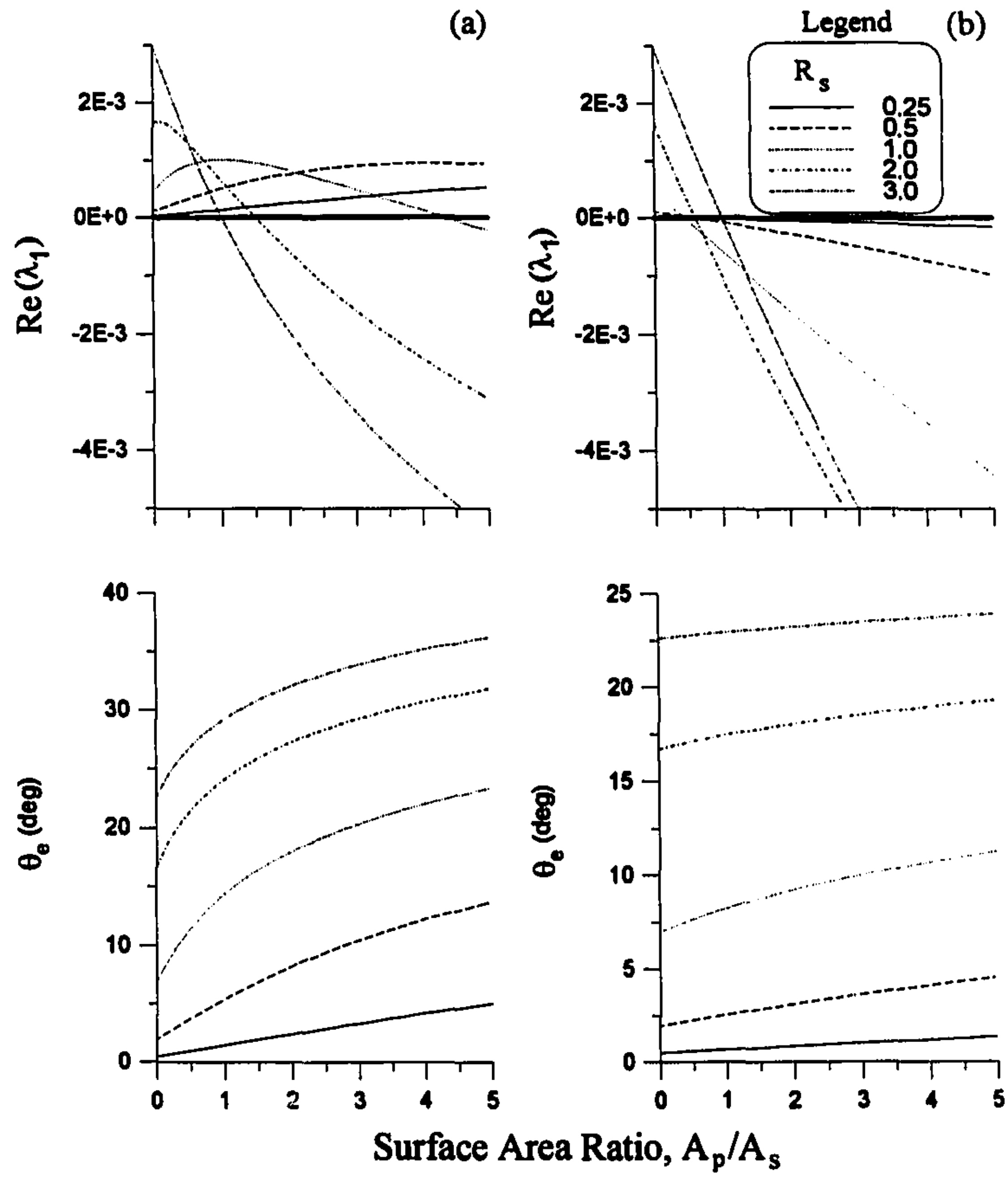

Figure 6.6: Effects of a lifting panel on the system stability and equilibrium point ($EA = 6 \times 10^4$ N, $R_c = 6.59 \times 10^3$ km, $L = 100$ km, $\sigma = 0$: (a) $\psi = 90°$; (b) $\psi = 145°$.

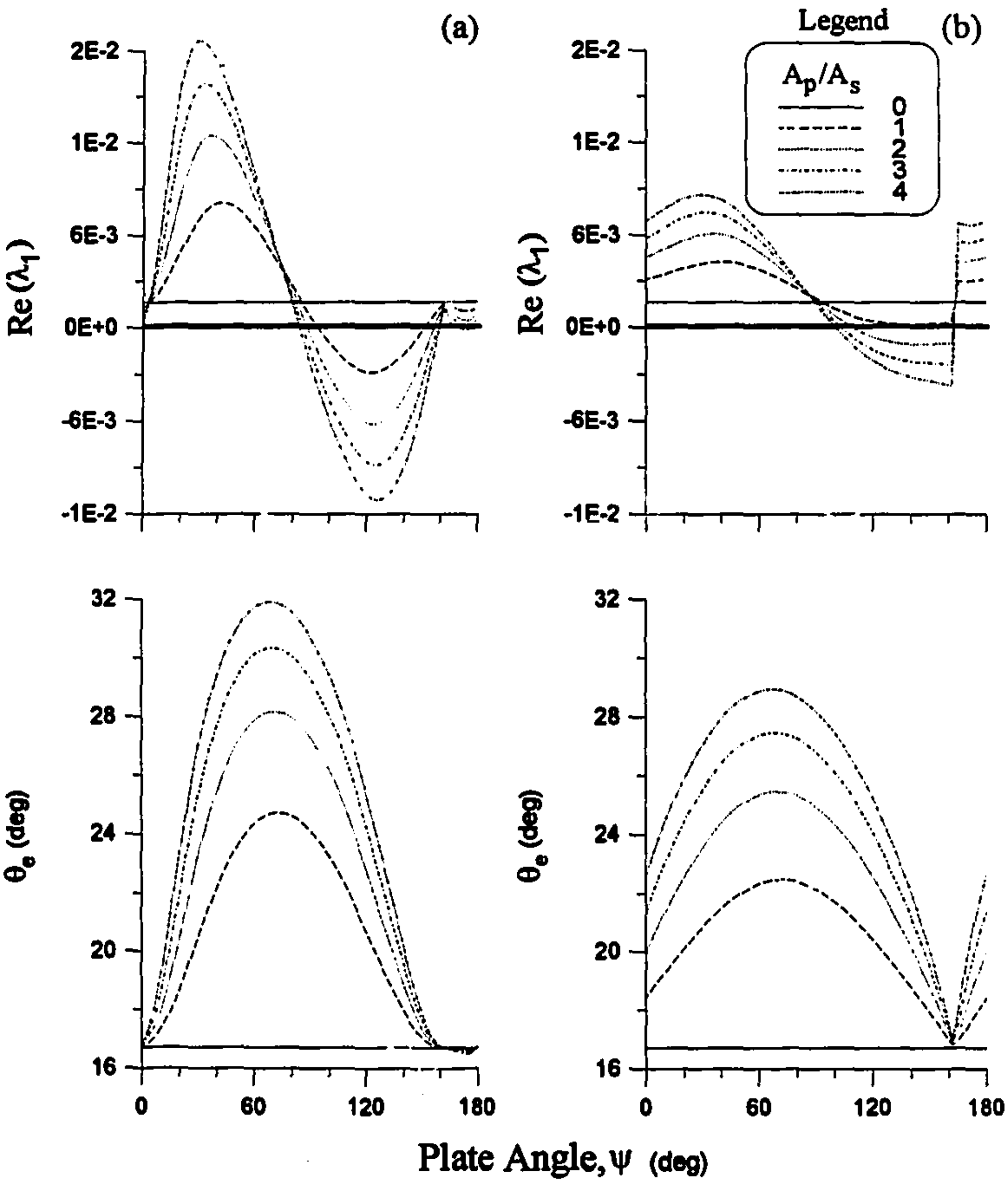

Figure 6.7: Effects of the panel angle on the system stability and equilibrium point ($EA = 6 \times 10^4$ N, $R_c = 6.59 \times 10^3$ km, $L = 100$ km, $R_s = 2$ m : **(a)**$\sigma = 0$; **(b)** $\sigma = 0.8$.

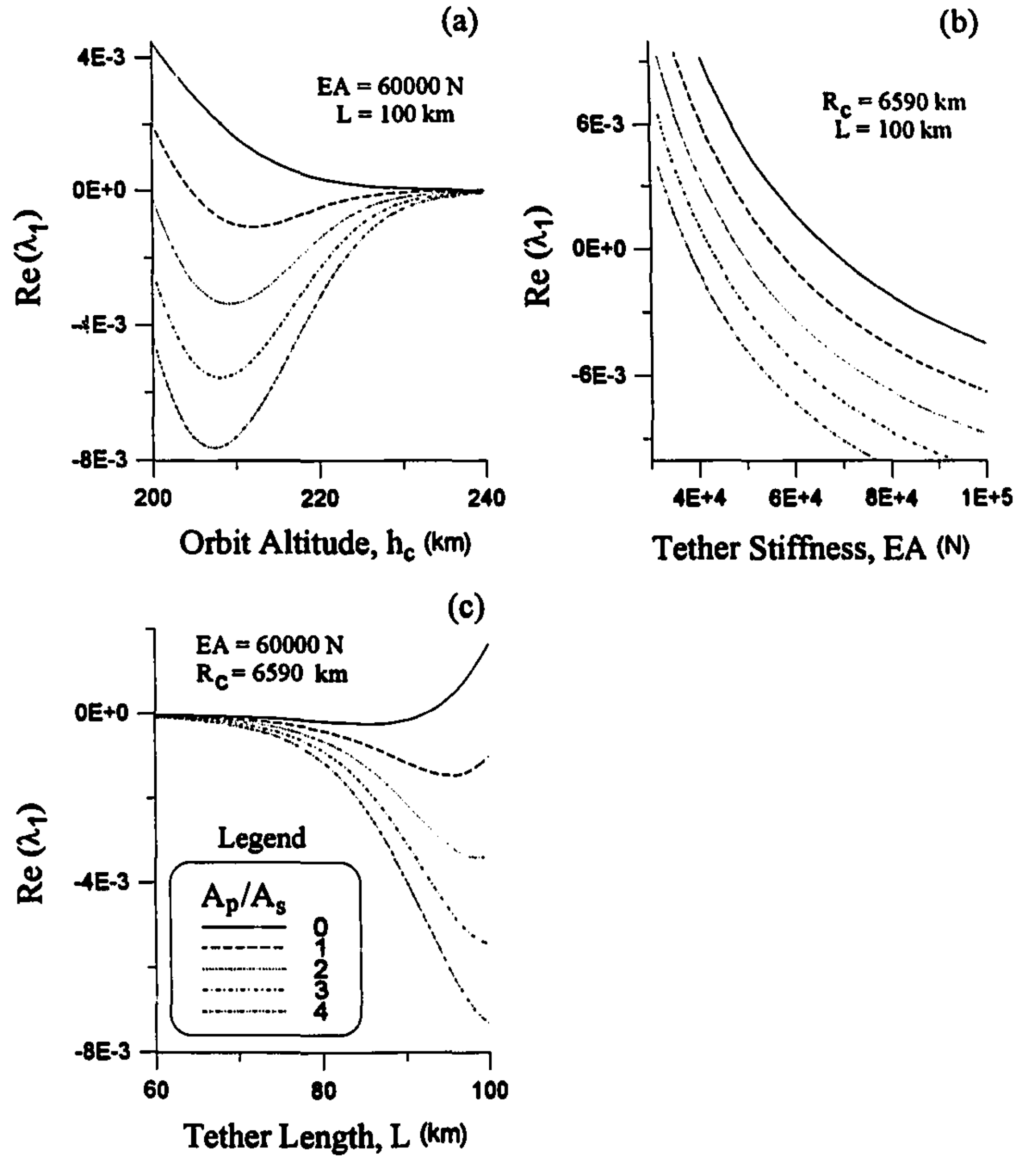

Figure 6.8: Effects of a lifting panel on the stability of the system ($\psi = 145°$, $\sigma = 0$, $R_s = 2\,\mathrm{m}$.

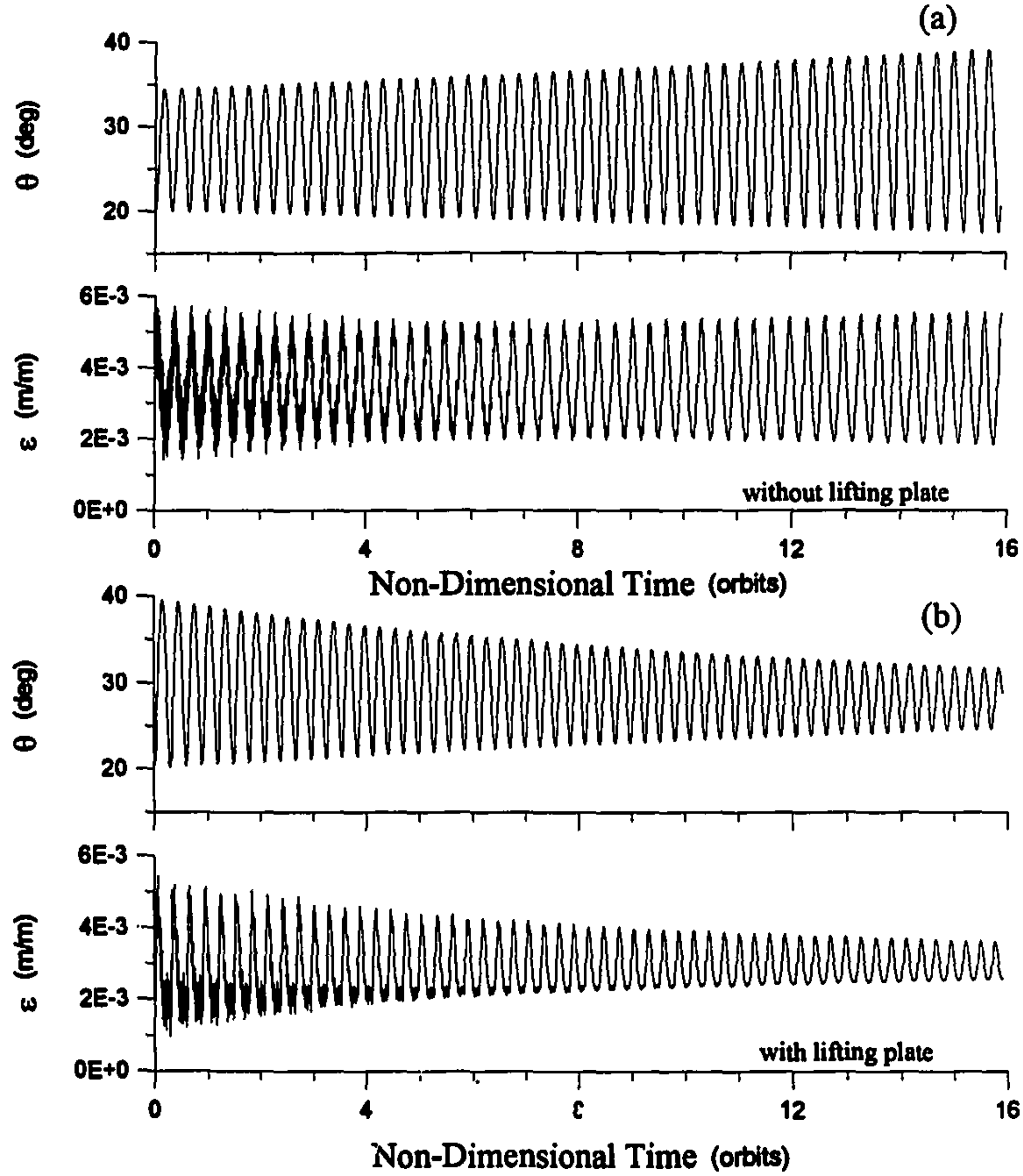

Figure 6.9: Simulation results ($EA = 6 \times 10^4$ N, $R_c = 6.59 \times 10^3$ km, $L = 100$ km, $R_s = 4$ m, $\psi = 145°$, $\sigma = 0$): **(a)** spherical subsatellite with no lifting panel $A_p/A_s = 0$; **(b)** subsatellite with a lifting panel, $A_p/A_s = 4$.

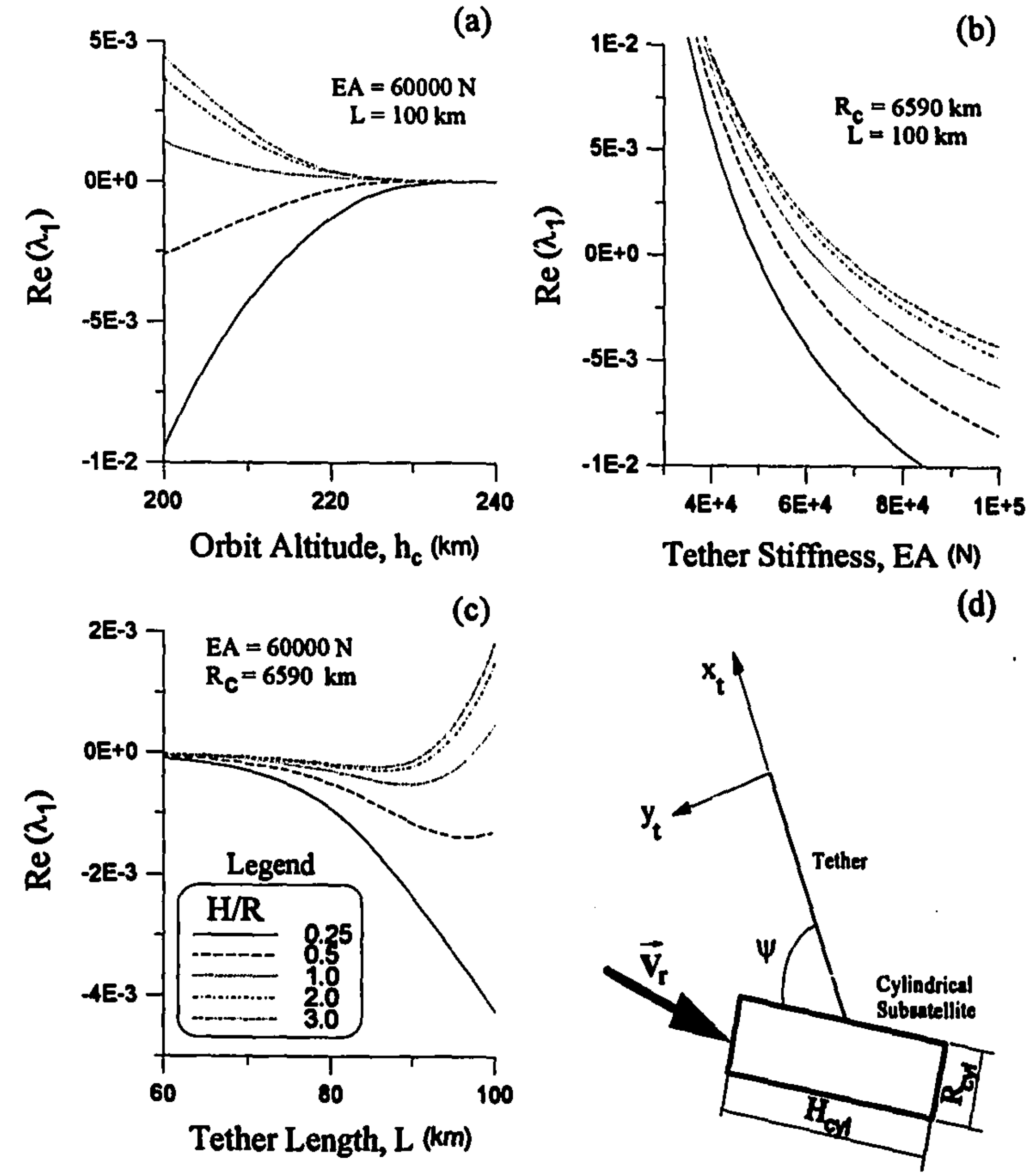

Figure 6.10: Effects of the cylinder aspect ratio on the stability of the system ($A_c = 11\,\mathrm{m}^2$, $EA = 6 \times 10^4\,\mathrm{N}$, $R_c = 6.59 \times 10^3\,\mathrm{km}$, $L = 100\,\mathrm{km}, \psi = 145°, \sigma = 0.8$).

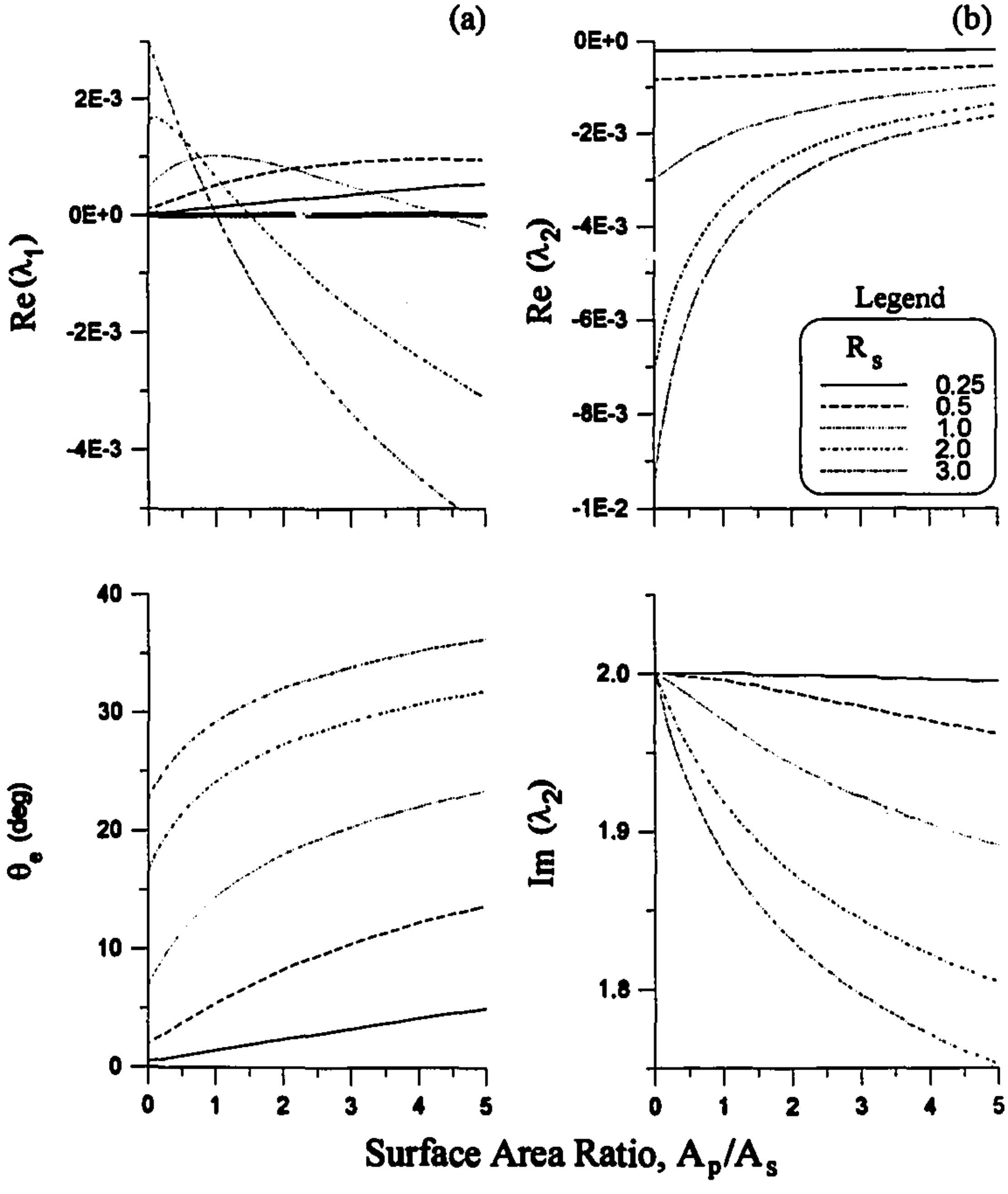

Figure 6.11: Effects of a lifting panel on the system stability and equilibrium point in three dimensional motion ($EA = 6 \times 10^4$ N, $R_c = 6.59 \times 10^3$ km, $L = 100$ km, $\psi = 90°, \sigma = 0.8$).

Chapter 7

CONTROL SYNTHESIS; LYAPUNOV APPROACH

7.1 Introductory Remarks

The idea of using Lyapunov's stability theory to control attitude motion of a spacecraft goes back to 1968, when Mortenson [74] used this method to control the dynamics of an arbitrary rigid body. Since then many investigators have used this method for analyzing the control problems associated with spacecraft attitude maneuvers, among which one can mention the works such as [75, 76, 77, 78, 79]

As far as tethered satellite systems are concerned, a Lyapunov type approach was used to synthesize a tension control law for deployment/retrieval by Fujii and Ishijima [47]. They used what they called a 'mission function' for this synthesis. Using basically the same dynamical model, two other control laws were introduced by Vadali [80]. The model was initially quite simple and similar to the one used by Rupp [81]. However Fujii et al. [82] and Vadali and Kim [48, 45] extended their work to three dimensional motion of two-body systems with massive but rigid tethers and obtained various tension and reel rate control laws . Using the Lyapunov approach, Moushi et al. [50] came up with a reel rate control law to control the motion of a two-body satellite system with massless and rigid tethers.

All of the above works, based on Lyapunov's stability theory, considered single tether systems. No study has been conducted to control the dynamics of multi-tethered systems, even a three-body system, using the Lyapunov approach. Extension from a single to a multi-tether system is difficult because of the complexity of the dynamics. In this chapter we attempt to do this. Using the formulation presented in Chapter 2, we initially derive the control law for a multi-tether system with rigid and massless tethers. Then the work is extended to systems with massive and flexible tethers.

7.2 Lyapunov's Second Method

The idea behind Lyapunov's direct method, which is also known as Lyapunov's second method, is to answer the stability question without actually solving the equations of motion. The method consists of finding a suitable scalar function for the dynamical system, called *Lyapunov function*, defined in the state space, and using it in conjunction with the differential equations in order to test the stability of the system. Except for linear autonomous systems, for which a Lyapunov function can be obtained by solving a set of simultaneous algebraic equations, there is no systematic way of producing a Lyapunov function for a general dynamical system. There is no unique Lyapunov function for a given system, and indeed there is a large degree of flexibility in the selection of a Lyapunov function.

In the following a brief description of Lyapunov's stability theory is presented for an n-degree-of-freedom autonomous system governed by a set of 2n-first-order differential equations

$$\dot{\mathbf{z}} = \mathbf{Z}(\mathbf{z}) \quad , \tag{7.1}$$

where $\mathbf{z}$ and $\mathbf{Z}$ are real 2n-vectors.

Let us assume that the origin is a singular point of the system, $\mathbf{Z}(\{0\}) = \{0\}$. Next let us consider a real continuous scalar function $\mathcal{L}(\mathbf{z})$ whose first partial derivatives with respect to $\mathbf{z}$ exist and the function vanishes at the origin, i.e. , $\mathcal{L}(\{0\}) = 0$. Now the stability criteria according to Lyapunov's theory are as follows [83]:

> If there exists a positive definite scalar function of the state variables, $\mathcal{L}(\mathbf{z}) > 0$, whose total time derivative is negative definite or semidefinite, $\dot{\mathcal{L}}(\mathbf{z}) \leq 0$, along every trajectory of the system governed by Eq. (7.1), then the trivial solution $\mathbf{z} = \{0\}$ is stable, i.e. the system is stable at the origin of the state space. The trivial solution is asymptotically stable, if $\dot{\mathcal{L}}(\mathbf{z})$ is negative definite along every trajectory.

This method is very powerful and has two salient features: (1) The method can examine the stability of nonlinear systems for large motion. (2) It can reveal the stability of the system by utilizing the differential equations of the system, but without actually solving them. On the other hand, the main disadvantage of this method is the practical difficulties in applying. It requires constructing a Lyapunov function which may not be always possible. Hence Lyapunov's direct method should be regarded as more of a philosophy of approach than a method. The fact that for a particular case an appropriate Lyapunov function cannot be found gives no indication of the system's stability or instability.

7.3 Hamiltonian of the System as a Suitable Candidate

The Lagrangian of a mechanical system, in general, is given by

$$L = T - V = T_2 + T_1 + T_0 - U \quad , \tag{7.2}$$

where T_2 is the non-negative quadratic function of the generalized speeds, T_1 is a linear homogenous function in the generalized speeds, and T_0 is a non-negative function of the generalized coordinates and time. The potential energy, U, of the system corresponding to the conservative forces, is also a scalar function of the generalized coordinates and time. The *Hamiltonian* of the system is defined by

$$H = \left(\sum_{k=1}^{N_q} \dot{q}_k \frac{\partial L}{\partial \dot{q}_k}\right) - L \quad , \tag{7.3}$$

which, with the help of Eq. (7.2), can be expressed as

$$H = T_2 - T_0 + U \quad . \tag{7.4}$$

Using Eq. (7.3), together with Lagrange's equations of motion,

$$\frac{d}{dt}\left(\frac{\partial L}{\partial \dot{q}_k}\right) - \frac{\partial L}{\partial q_k} = Q_k \quad , \qquad k = 1, 2, \ldots, N_q \quad , \tag{7.5}$$

the total time derivative of the Hamiltonian can be obtained as

$$\dot{H} = \frac{dH}{dt} = \sum_{k=1}^{N_q} \dot{q}_k Q_k - \frac{\partial L}{\partial t} \quad . \tag{7.6}$$

When time does not appear explicitly in the Lagrangian, such as the system under consideration, the last term in the right hand side vanishes, and the time derivative of the Hamiltonian is given by

$$\dot{H} = \sum_{k=1}^{N_q} \dot{q}_k Q_k \quad . \tag{7.7}$$

Usually, for a mechanical system starting from the Hamiltonian of the system, one can find some indications to establish an appropriate Lyapunov function. For a single tether system with a massless and rigid tether moving in a circular orbit, the Hamiltonian is given by

$$H = m_e \left\{ \ell^2 \left[\dot{\phi}^2 + \dot{\theta}^2 \cos^2\phi + \Omega_c^2 \left(3\sin^2\theta\cos^2\phi + 4\sin^2\phi - 3 \right) \right] + \dot{\ell}^2 \right\} \quad . \tag{7.8}$$

The Lyapunov function used by Vadali and Kim [48] was

$$\mathcal{L} = C \left[\dot{\phi}^2 + \dot{\theta}^2 \cos^2\phi + \Omega_c^2 \left(3\sin^2\theta\cos^2\phi + 4\sin^2\phi \right) \right] + \frac{1}{2} K (\lambda - \lambda_f)^2 \quad , \tag{7.9}$$

where λ represents a nondimensional length equal to ℓ/ℓ_f and C and K are two arbitrary positive constants. Using this Lyapunov function they obtained a tension control law to control the nonlinear dynamics of the system. Monshi et al. [50] used a more or less similar Lyapunov function:

$$\mathcal{L} = C\left[\dot{\phi}^2 + \dot{\theta}^2\cos^2\phi + \Omega_c^2\left(3\sin^2\theta\cos^2\phi + 4\sin^2\phi\right)\right] + \ln\left(\frac{\ell}{\ell_f}\right) \quad , \tag{7.10}$$

and derived a reel rate control law to control the system in the retrieval stage.

As can be seen, the two Lyapunov functions are constructed starting from the Hamiltonian of the system. In fact in the following sections a similar approach is used to obtain the control law for a multi-tether system.

7.4 Hamiltonian of the Multi-Tether System

Since the equations of motion for the general case are very complicated, while implementing the Lyapunov method is rather difficult, a special case is considered. It is assumed here that the system is moving in a circular orbit and is influenced by no external forces except the gravitational ones. Transverse oscillations of the tethers are assumed to be negligible. As far as the mass and flexibility of the tethers are concerned, initially they are assumed to be negligible. However, subsequently these assumptions are removed one by one.

For the system under consideration the Hamiltonian of the system, Eq. (7.4), can be re-written as

$$H = (T_2 + U_E + U_{G_1}) - (T_0 + U_{G_0}) \quad , \tag{7.11}$$

where T_2 and T_0 are as described earlier, U_E is the elastic potential energy, U_{G_1} and U_{G_0} are two components of the gravitational potential energy which are defined later.

Examining Eq. (2.26) one obtains

$$T_2 = \frac{m}{2}\left\{\sum_{i=1}^{N}\sum_{n=1}^{N_q}\sum_{k=1}^{N_q}\dot{q}_n\dot{q}_k\left[\mu_i\frac{\partial\vec{\mathbf{R}}_i}{\partial q_n}\cdot\frac{\partial\vec{\mathbf{R}}_i}{\partial q_k} + \hat{\rho}_i\int_0^{\ell_i}\frac{\partial\vec{\mathbf{R}}_{t_i}}{\partial q_n}\cdot\frac{\partial\vec{\mathbf{R}}_{t_i}}{\partial q_k}dx_i\right]\right\} \quad ,$$

$$T_0 = \frac{m}{2}\left\{\sum_{i=1}^{N}\left(\mu_i\frac{\partial\vec{\mathbf{R}}_i}{\partial t}\cdot\frac{\partial\vec{\mathbf{R}}_i}{\partial t} + \hat{\rho}_i\int_0^{\ell_i}\frac{\partial\vec{\mathbf{R}}_{t_i}}{\partial t}\cdot\frac{\partial\vec{\mathbf{R}}_{t_i}}{\partial t}dx_i\right)\right\} \quad . \tag{7.12}$$

It is clear that both T_2 and T_0 are non-negative scalars. Performing similar algebra as in Chapter 2, T_0 can be rewritten as

$$T_0 = \frac{m}{2}\left\{\sum_{n=1}^{N-1}\sum_{k=1}^{N-1}F_{nk}\frac{\partial\vec{\mathbf{r}}_n}{\partial t}\cdot\frac{\partial\vec{\mathbf{r}}_k}{\partial t} - \bar{\mu}_n\bar{\mu}_k\frac{\partial\vec{\mathbf{b}}_n}{\partial t}\cdot\frac{\partial\vec{\mathbf{b}}_k}{\partial t} + 2\bar{\mu}_nA_{nk}\frac{\partial\vec{\mathbf{r}}_k}{\partial t}\cdot\frac{\partial\vec{\mathbf{b}}_n}{\partial t}\right.$$
$$\left. + \delta_{nk}\hat{\rho}_n\int_0^{\ell_n}\frac{\partial\vec{\mathbf{r}}_{t_n}}{\partial t}\cdot\frac{\partial\vec{\mathbf{r}}_{t_n}}{\partial t}dx_n\right\} \quad . \tag{7.13}$$

Since transverse oscillations of the tethers are ignored, the displacement vectors, $\vec{\mathbf{r}}_n, \vec{\mathbf{b}}_n$ and $\vec{\mathbf{r}}_{t_n}$ can be written as

$$\vec{\mathbf{r}}_n = (\ell_n + u_{\ell_n})\,\hat{\mathbf{i}}_n = r_n\hat{\mathbf{i}}_n \quad ,$$
$$\vec{\mathbf{r}}_{t_n} = (x_n + u_n)\,\hat{\mathbf{i}}_n = r_{t_n}\hat{\mathbf{i}}_n \quad ,$$
$$\vec{\mathbf{b}}_n = \frac{1}{\ell_0}\int_0^{\ell_n}\vec{\mathbf{r}}_{t_n}dx_n = b_n\hat{\mathbf{i}}_n \quad , \tag{7.14}$$

where u_n is the longitudinal stretch at any arbitrary point of the n-th tether, while u_{ℓ_n} is that of the whole tether. Recalling that the system is moving in a circular orbit, partial derivatives of these vectors with respect to time are given by

$$\frac{\partial\vec{\mathbf{r}}_n}{\partial t} = r_n\frac{\partial\hat{\mathbf{i}}_n}{\partial t} = r_n\Omega_c\cos\phi_n\hat{\mathbf{j}}_n \quad ,$$
$$\frac{\partial\vec{\mathbf{r}}_{t_n}}{\partial t} = r_{t_n}\frac{\partial\hat{\mathbf{i}}_n}{\partial t} = r_{t_n}\Omega_c\cos\phi_n\hat{\mathbf{j}}_n \quad ,$$
$$\frac{\partial\vec{\mathbf{b}}_n}{\partial t} = b_n\frac{\partial\hat{\mathbf{i}}_n}{\partial t} = b_n\Omega_c\cos\phi_n\hat{\mathbf{j}}_n \quad .$$

Substituting back the above equations in Eq. (7.13) results in

$$T_0 = \frac{m\Omega_c^2}{2}\sum_{n=1}^{N-1}\sum_{k=1}^{N-1}\cos\phi_n\cos\phi_k[F_{nk}r_nr_k - \bar{\mu}_n\bar{\mu}_kb_nb_k + 2\bar{\mu}_nA_{nk}r_kb_n$$
$$+ \delta_{nk}\hat{\rho}_n\int_0^{\ell_n}r_{t_n}r_{t_n}dx_n]\hat{\mathbf{j}}_n\cdot\hat{\mathbf{j}}_k \quad . \tag{7.15}$$

Using Eq. (2.39), the gravitational potential energy of the system can be written as the difference of two non-negative functions as follows

$$U_G = U_{G_1} - U_{G_0} \quad , \tag{7.16}$$

where

$$U_{G_1} = \frac{m\Omega_c^2}{2}\left\{\sum_{i=1}^{N}\mu_i\left[\vec{\mathbf{R}}_i\cdot\vec{\mathbf{R}}_i - \left(\hat{\mathbf{i}}_c\cdot\vec{\mathbf{R}}_i\right)^2\right] + \hat{\rho}_i\int_0^{\ell_i}\left[\vec{\mathbf{R}}_{t_i}\cdot\vec{\mathbf{R}}_{t_i} - \left(\hat{\mathbf{i}}_c\cdot\vec{\mathbf{R}}_{t_i}\right)^2\right]dx_i\right\} \quad ,$$

$$U_{G_0} = m\Omega_c^2\left\{\sum_{i=1}^{N}\mu_i\left(\hat{\mathbf{i}}_c\cdot\vec{\mathbf{R}}_i\right)^2 + \hat{\rho}_i\int_0^{\ell_i}\left(\hat{\mathbf{i}}_c\cdot\vec{\mathbf{R}}_{t_i}\right)^2 dx_i\right\} \quad . \tag{7.17}$$

Similar to T_0, U_{G_0} can be written as

$$\begin{aligned} U_{G_0} = m\Omega_c^2\sum_{n=1}^{N-1}\sum_{k=1}^{N-1}[F_{nk}r_n r_k - \bar{\mu}_n\bar{\mu}_k b_n b_k + 2\bar{\mu}_n A_{nk} r_k b_n \\ + \delta_{nk}\hat{\rho}_n\int_0^{\ell_n} r_{t_n} r_{t_n} dx_n]\,(\hat{\mathbf{i}}_c\cdot\hat{\mathbf{i}}_n)(\hat{\mathbf{i}}_c\cdot\hat{\mathbf{i}}_k) \quad . \end{aligned} \tag{7.18}$$

Recalling Eq. (7.11), we can express the Hamiltonian of the system as the difference of two non-negative scalar functions

$$H = P_1 - P_0 \quad , \tag{7.19}$$

where

$$\begin{aligned} P_1 &= T_2 + U_{G_1} + U_E \quad , \\ P_0 &= T_0 + U_{G_0} \quad . \end{aligned} \tag{7.20}$$

P_1 and P_0 are non-negative because all the components T_2, T_0, U_E, U_{G_1}, and U_{G_0} are non-negative scalar functions. To construct a Lyapunov function based on the Hamiltonian of the system, it is enough to compensate for P_0 which appears with a negative sign in the Hamiltonian expression. Substituting for U_{G_0} and T_0, the expression of P_0 is given by

$$\begin{aligned} P_0 = \frac{m\Omega_c^2}{2}\sum_{n=1}^{N-1}\sum_{k=1}^{N-1}[F_{nk}r_n r_k - \bar{\mu}_n\bar{\mu}_k b_n b_k + 2\bar{\mu}_n A_{nk} r_k b_n \\ + \delta_{nk}\hat{\rho}_n\int_0^{\ell_n} r_{t_n} r_{t_n} dx_n]\left\{\cos\phi_n\cos\phi_k\hat{\mathbf{j}}_n\cdot\hat{\mathbf{j}}_k + 2(\hat{\mathbf{i}}_c\cdot\hat{\mathbf{i}}_n)(\hat{\mathbf{i}}_c\cdot\hat{\mathbf{i}}_k)\right\} \quad . \end{aligned} \tag{7.21}$$

In the absence of all non-conservative external forces the only generalized force appearing in the equations of motion, is $Q_{\ell_n} = -T_n$, $n = 1, 2, \ldots, N-1$, where T_n denotes the tension in the n-th tether. Hence, since time does not appear explicitly in the Lagrangian expression in the present case, the total time derivative of the Hamiltonian, Eq. (7.7), is given by

$$\dot{H} = \sum_{n=1}^{N-1} \left(-\dot{\ell}_n T_n\right) \quad . \tag{7.22}$$

7.5 Tension Control Laws

7.5.1 Systems with Rigid Massless Tethers

Ignoring the mass of the tethers, P_0 given by Eq. (7.21) can be simplified to

$$P_0 = \frac{m\Omega_c^2}{2} \sum_{n=1}^{N-1} \sum_{k=1}^{N-1} F_{nk} r_n r_k \left\{ \cos\phi_n \cos\phi_k \hat{\mathbf{j}}_n \cdot \hat{\mathbf{j}}_k + 2(\hat{\mathbf{i}}_c \cdot \hat{\mathbf{i}}_n)(\hat{\mathbf{i}}_c \cdot \hat{\mathbf{i}}_k) \right\} \quad , \tag{7.23}$$

where in the absence of elasticity of the tethers r_n is given by

$$r_n = \ell_n \quad . \tag{7.24}$$

Hence P_0 is simply given by

$$P_0 = \frac{m\Omega_c^2}{2} \sum_{n=1}^{N-1} \sum_{k=1}^{N-1} F_{nk} \ell_n \ell_k \left\{ \cos\phi_n \cos\phi_k \hat{\mathbf{j}}_n \cdot \hat{\mathbf{j}}_k + 2(\hat{\mathbf{i}}_c \cdot \hat{\mathbf{i}}_n)(\hat{\mathbf{i}}_c \cdot \hat{\mathbf{i}}_k) \right\} \quad . \tag{7.25}$$

Let us introduce the following Lyapunov function

$$\mathcal{L} = H + 3S + \sum_{n=1}^{N-1} \frac{1}{2} C'_n (\ell_n - \ell_{c_n})^2 = P_1 - P_0 + 3S + \sum_{n=1}^{N-1} \frac{1}{2} C'_n (\ell_n - \ell_{c_n})^2 \quad , \tag{7.26}$$

where S, defined by

$$S = \frac{m\Omega_c^2}{2} \sum_{n=1}^{N-1} \sum_{k=1}^{N-1} F_{nk} \ell_n \ell_k \quad , \tag{7.27}$$

is introduced to overcome the negative part of the Hamiltonian, $-P_0$, while ℓ_{c_n} is the command length. In the above, C'_n is an arbitrary positive constant. First we must show that $\mathcal{L}$ is always a non-negative function.

Since P_1 and the last term in Eq. (7.26) are always non-negative, it would be sufficient if we show that $3S - P_0$ is always non-negative. It is clear that

$$\begin{aligned} |\cos\phi_n \cos\phi_k| &\leq 1 \quad , \\ |\hat{\mathbf{j}}_n \cdot \hat{\mathbf{j}}_k| &\leq 1 \quad , \\ |\hat{\mathbf{i}}_n \cdot \hat{\mathbf{i}}_c| &\leq 1 \quad , \\ |\hat{\mathbf{i}}_k \cdot \hat{\mathbf{i}}_c| &\leq 1 \quad . \end{aligned} \tag{7.28}$$

This results in

$$\cos\phi_n \cos\phi_k \hat{\mathbf{j}}_n \cdot \hat{\mathbf{j}}_k + 2(\hat{\mathbf{i}}_c \cdot \hat{\mathbf{i}}_n)(\hat{\mathbf{i}}_c \cdot \hat{\mathbf{i}}_k) \leq 3 \quad . \tag{7.29}$$

Since ℓ_n is always positive one concludes that

$$\ell_n \ell_k \left[\cos\phi_n \cos\phi_k \hat{\mathbf{j}}_n \cdot \hat{\mathbf{j}}_k + 2(\hat{\mathbf{i}}_c \cdot \hat{\mathbf{i}}_n)(\hat{\mathbf{i}}_c \cdot \hat{\mathbf{i}}_k)\right] \leq 3\,\ell_n \ell_k \quad . \tag{7.30}$$

Consequently since the F_{jk}'s are all positive, it is clear that

$$3S - P_0 \geq 0 \quad , \tag{7.31}$$

and hence, $\mathcal{L}$ is always non-negative.

Differentiating Eq. (7.26) with respect to time gives us

$$\dot{\mathcal{L}} = \dot{H} + 3\dot{S} + \sum_{n=1}^{N-1} C_n'(\dot{\ell}_n - \dot{\ell}_{c_n})(\ell_n - \ell_{c_n}) \quad . \tag{7.32}$$

Substituting for $\dot{H}$ from Eq. (7.22) and for $\dot{S}$ from time derivative of Eq. (7.27), we can write

$$\dot{\mathcal{L}} = \sum_{n=1}^{N-1} \left(-\dot{\ell}_n T_n\right) + 3m\Omega_c^2 \sum_{n=1}^{N-1}\sum_{k=1}^{N-1} F_{nk}\dot{\ell}_n \ell_k + \sum_{n=1}^{N-1} C_n'(\dot{\ell}_n - \dot{\ell}_{c_n})(\ell_n - \ell_{c_n}) \quad . \tag{7.33}$$

Note that F_{nk}'s are symmetric with respect to the indices n and k and in the case of massless tethers they are constant.

Usually the command length, ℓ_{c_n} is chosen either as the final length or a function of the present length. As we will see later, they basically represent the same command.

Let us consider the following function for the command length

$$\ell_{c_n} = \varepsilon_n \ell_n + \sigma_n \quad . \tag{7.34}$$

where ε_n and σ_n are two positive constants. Differentiating the above relation and substituting back in Eq. (7.33), we obtain

$$\dot{\mathcal{L}} = \sum_{n=1}^{N-1} \dot{\ell}_n \left[-T_n + C_n'(1-\varepsilon_n)(\ell_n - \ell_{c_n}) + 3m\Omega_c^2 \sum_{k=1}^{N-1} F_{nk}\ell_k \right] \quad . \tag{7.35}$$

Selecting the tension in the tethers such that $\dot{\mathcal{L}}$ becomes always non-positive leads to the control law that guarantees the stability of the system in every trajectory of the system. Let us set the tensions as

$$T_n = C_n'(1-\varepsilon_n)(\ell_n - \ell_{c_n}) + 3m\Omega_c^2 \sum_{k=1}^{N-1} F_{nk}\ell_k + K_{\ell_n}\dot{\ell}_n \quad , \tag{7.36}$$

where K_{ℓ_n} is another arbitrary positive constant, then $\dot{\mathcal{L}}$ reduces to

$$\dot{\mathcal{L}} = \sum_{n=1}^{N-1} \left(-K_{\ell_n}\dot{\ell}_n^2 \right) \quad . \tag{7.37}$$

Substituting for ℓ_{c_n} from Eq. (7.34) into Eq. (7.36) and defining the following constants

$$\begin{aligned} \ell_{f_n} &= \frac{\sigma_n}{1-\varepsilon_n} \quad , \\ C_n &= C_n'(1-\varepsilon_n)^2 \quad , \end{aligned} \tag{7.38}$$

the tension control law is given by

$$T_n = K_{\ell_n}\dot{\ell}_n + C_n(\ell_n - \ell_{f_n}) + 3m\Omega_c^2 \sum_{k=1}^{N-1} F_{nk}\ell_k \qquad n = 1, 2, \ldots, N-1 \quad . \tag{7.39}$$

If one chooses $\ell_{f_n} < \ell_n$, the final length is less than the present length, i.e. the control law forces the length of any tether to a smaller value, which is nothing but retrieving the subsatellites. Setting $\ell_{f_n} = 0$ leads to a complete retrieval.

7.5.2 Systems with Rigid Massive Tethers

A procedure similar to that in the previous case is followed to obtain the control law for a system with massive but rigid tethers. In this case,

$$
\begin{aligned}
r_n &= \ell_n \quad , \\
r_{t_n} &= x_n \quad , \\
b_n &= \frac{\ell_n^2}{2\ell_0} \quad ,
\end{aligned}
\tag{7.40}
$$

and P_0, after performing some algebra, is given by

$$
\begin{aligned}
P_0 = \frac{m\Omega_c^2}{2}\sum_{n=1}^{N-1}\sum_{k=1}^{N-1}\ell_n\ell_k\Bigg[F_{nk} &- \frac{\bar{\mu}_n\bar{\mu}_k}{4\ell_0^2}\ell_n\ell_k + \frac{2\bar{\mu}_n}{2\ell_0}A_{nk}\ell_n \\
&+ \frac{\delta_{nk}\hat{\rho}_n}{3}\ell_n\Bigg]\left\{\cos\phi_n\cos\phi_k\,\hat{\mathbf{j}}_n\cdot\hat{\mathbf{j}}_k + 2(\hat{\mathbf{i}}_c\cdot\hat{\mathbf{i}}_n)(\hat{\mathbf{i}}_c\cdot\hat{\mathbf{i}}_k)\right\} \quad .
\end{aligned}
\tag{7.41}
$$

Since $\bar{\mu}_n = \hat{\rho}_n\ell_0$, the above equation can be rewritten as

$$
P_0 = \frac{m\Omega_c^2}{2}\sum_{n=1}^{N-1}\sum_{k=1}^{N-1}D_{nk}\ell_n\ell_k\left\{\cos\phi_n\cos\phi_k\,\hat{\mathbf{j}}_n\cdot\hat{\mathbf{j}}_k + 2(\hat{\mathbf{i}}_c\cdot\hat{\mathbf{i}}_n)(\hat{\mathbf{i}}_c\cdot\hat{\mathbf{i}}_k)\right\} \quad , \tag{7.42}
$$

where D_{nk} is a dimensionless mass coefficient defined by

$$
D_{nk} = F_{nk} - \frac{\hat{\rho}_n\hat{\rho}_k}{4}\ell_n\ell_k + \hat{\rho}_n A_{nk}\ell_n + \frac{\delta_{nk}\hat{\rho}_n}{3}\ell_n \quad . \tag{7.43}
$$

As can be seen, in contrast to F_{nk} in the previous case, D_{nk} is time dependent and is not symmetric with respect to the indices n and k. However D_{nk} is always positive.

Next a similar Lyapunov function as before is introduced for the present case, i.e.

$$
\mathcal{L} = H + 3S + \sum_{n=1}^{N-1}\frac{1}{2}C_n(\ell_n - \ell_{f_n})^2 \quad , \tag{7.44}
$$

where C_n and ℓ_{f_n} are as defined earlier, but S is now defined by

$$
S = \frac{m\Omega_c^2}{2}\sum_{n=1}^{N-1}\sum_{k=1}^{N-1}D_{nk}\ell_n\ell_k \quad . \tag{7.45}
$$

Since D_{nk} like F_{nk} is always positive it is clear that

$$
\mathcal{L} \geq 0 \quad . \tag{7.46}
$$

Because of the time dependence and asymmetry of D_{nk}. $\dot{\mathcal{L}}$ obtained has a slightly different form from the case of rigid and massless tethers. It is now given by

$$\dot{\mathcal{L}} = \sum_{n=1}^{N-1}\left(-\dot{\ell}_n T_n\right) + \frac{3m\Omega_c^2}{2}\sum_{n=1}^{N-1}\sum_{k=1}^{N-1}\left[D_{nk}\left(\dot{\ell}_n\ell_k + \ell_n\dot{\ell}_k\right) + \dot{D}_{nk}\ell_n\ell_k\right] + \sum_{n=1}^{N-1} C_n\dot{\ell}_n(\ell_n - \ell_{f_n}) \ . \tag{7.47}$$

Using the definition of D_{nk}, its derivative with respect to time can be written as

$$\dot{D}_{nk} = \dot{F}_{nk} - \frac{\hat{\rho}_n\hat{\rho}_k}{4}(\dot{\ell}_n\ell_k + \ell_n\dot{\ell}_k) + \hat{\rho}_n\left(\dot{A}_{nk}\ell_n + A_{nk}\dot{\ell}_n\right) + \frac{\delta_{nk}\hat{\rho}_n}{3}\dot{\ell}_n \ . \tag{7.48}$$

For the sake of simplicity let us assume that $\dot{B}_n$ in Eq. (B.16) is zero, i.e. body $i+1$ is reeled in/out only from body i; however, the following procedure can be easily extended to the general case. With this assumption, Eq. (7.48) can be simplified to

$$\dot{D}_{nk} = -\frac{\hat{\rho}_n\hat{\rho}_k}{4}\left(\dot{\ell}_n\ell_k + \ell_n\dot{\ell}_k\right) + \hat{\rho}_n A_{nk}\dot{\ell}_n + \frac{\delta_{nk}\hat{\rho}_n}{3}\dot{\ell}_n \ . \tag{7.49}$$

Substituting for $\dot{D}_{nk}$ in Eq. (7.47) and performing some algebra, we obtain

$$\dot{\mathcal{L}} = \frac{3m\Omega_c^2}{2}\sum_{n=1}^{N-1}\sum_{k=1}^{N-1}\left\{(D_{nk} + D_{kn})\dot{\ell}_n\ell_k - \left(\frac{\hat{\rho}_n\hat{\rho}_k}{2}\dot{\ell}_n\ell_k - \hat{\rho}_n A_{nk}\dot{\ell}_n - \frac{\delta_{nk}\hat{\rho}_n}{3}\dot{\ell}_n\right)\ell_n\ell_k\right\} + \sum_{n=1}^{N-1}\left(-\dot{\ell}_n T_n\right) + \sum_{n=1}^{N-1} C_n\dot{\ell}_n(\ell_n - \ell_{f_n}) \ . \tag{7.50}$$

Next let us define a new dimensionless mass coefficient, G_{nk} as

$$\begin{aligned} G_{nk} &= \frac{1}{2}\left(D_{nk} + D_{kn} - \frac{\hat{\rho}_n\hat{\rho}_k}{2}\ell_n\ell_k + \hat{\rho}_n A_{nk}\ell_n + \frac{\delta_{nk}\hat{\rho}_n}{3}\ell_n\right) \\ &= \frac{1}{2}\left(2F_{nk} - \hat{\rho}_n\hat{\rho}_k\ell_n\ell_k + 2\hat{\rho}_n A_{nk}\ell_n + \hat{\rho}_k A_{kn}\ell_k + \delta_{nk}\hat{\rho}_n\ell_n\right) \ . \end{aligned} \tag{7.51}$$

Then we can write $\dot{\mathcal{L}}$ as

$$\dot{\mathcal{L}} = \sum_{n=1}^{N-1}\dot{\ell}_n\left[-T_n + C_n(\ell_n - \ell_{f_n}) + 3m\Omega_c^2\sum_{k=1}^{N-1} G_{nk}\ell_k\right] \ . \tag{7.52}$$

Similar to the previous case, if the tension in the tethers are chosen according to the following law

$$T_n = K_{\ell_n}\dot{\ell}_n + C_n(\ell_n - \ell_{f_n}) + 3m\Omega_c^2\sum_{k=1}^{N} G_{nk}\ell_k \qquad n = 1, 2, \ldots, N-1 \ , \tag{7.53}$$

the stability of the controlled motion would be guaranteed. Note that in contrast to the case of massless and rigid tethers, the tension control law here is not a linear function of the lengths of the tethers. That is because G_{nk} is itself a function of the lengths of the tethers.

7.5.3 Systems with Flexible and Massless Tethers

In many cases, flexibility of the tethers cannot be ignored. However if one considers all elastic oscillations, transverse and longitudinal, it is difficult, if not impossible to construct a Lyapunov function. Hence, only the most important elastic motion of the system, the longitudinal oscillations of the tethers will be considered in constructing the Lyapunov function. Furthermore, the mass of the tethers will be neglected in this Section. It will be considered later.

Since the tethers are assumed to be massless, only the first longitudinal mode of each tether can be taken into account. Considering the admissible function defined in Eq. (2.56), we can write

$$r_n = \ell_n + \xi_n \quad , \tag{7.54}$$

where ξ_n is the longitudinal stretch of the n-th tether and clearly less than ℓ_n. substituting for r_n, P_0 is given by

$$P_0 = \frac{m\Omega_c^2}{2}\sum_{n=1}^{N-1}\sum_{k=1}^{N-1} F_{nk}(\ell_n + \xi_n)(\ell_k + \xi_k)\left\{\cos\phi_n \cos\phi_k \hat{\mathbf{j}}_n\cdot\hat{\mathbf{j}}_k + 2(\hat{\mathbf{i}}_c\cdot\hat{\mathbf{i}}_n)(\hat{\mathbf{i}}_c\cdot\hat{\mathbf{i}}_k)\right\} \quad . \tag{7.55}$$

Let us assume that

$$\xi_n < \varrho\ell_n \quad , \qquad n = 1, 2, \ldots, N-1 \quad , \tag{7.56}$$

where ϱ is a positive number. In practice, it is a small number. It is then clear that

$$P_0 < \frac{m\Omega_c^2}{2}\sum_{n=1}^{N-1}\sum_{k=1}^{N-1} F_{nk}(1+\varrho)^2\ell_n\ell_k\left\{\cos\phi_n \cos\phi_k \hat{\mathbf{j}}_n\cdot\hat{\mathbf{j}}_k + 2(\hat{\mathbf{i}}_c\cdot\hat{\mathbf{i}}_n)(\hat{\mathbf{i}}_c\cdot\hat{\mathbf{i}}_k)\right\} \quad . \tag{7.57}$$

As before the following function is chosen as the Lyapunov function:

$$\mathcal{L} = H + 3S + \sum_{n=1}^{N-1}\frac{1}{2}C_n(\ell_n - \ell_{f_n})^2 \quad , \tag{7.58}$$

where S is now defined by

$$S = \frac{m\Omega_c^2}{2}\sum_{n=1}^{N-1}\sum_{k=1}^{N-1}(1+\varrho)^2 F_{nk}\ell_n\ell_k \quad . \tag{7.59}$$

Once again one can easily show that

$$3S - P_0 \geq 0 \quad . \tag{7.60}$$

Proceeding in a similar manner as in the case of rigid and massless tethers, the control law for the present case is given by

$$T_n = K_{\ell_n}\dot{\ell}_n + C_n(\ell_n - \ell_{f_n}) + 3(1+\varrho)^2 m\Omega_c^2\sum_{k=1}^{N-1}F_{nk}\ell_k \ , \quad n = 1,2,\ldots,N-1 \quad . \tag{7.61}$$

7.5.4 Systems with Flexible and Massive Tethers

Extending the Lyapunov method to control a tethered satellite system with flexible and massive tethers even for a two-body system is a very complicated job, if not impossible. To the best of the author's knowledge such a study has not been conducted yet. In order to account for the mass of the tethers to the previous case once again we assume that the transverse oscillations of the tethers are negligible, compared to the longitudinal ones, therefore can be ignored.

With the above assumptions the following relations for the displacements are obtained:[1]

$$\begin{aligned} r_n &= \ell_n + u_{\ell_n} \quad , \\ r_{t_n} &= x_n + u_n \quad , \\ b_n &= \frac{1}{\ell_0}\int_0^{\ell_n}(x_n + u_n)dx_n \quad . \end{aligned} \tag{7.62}$$

As in the previous case let us assume that

$$u_n < \varrho x_n \ , \quad u_{\ell_n} < \varrho\ell_n \ , \quad n = 1,2,\ldots,N-1 \quad . \tag{7.63}$$

[1]Note that here u_n is the longitudinal stretch of tether n and contains all longitudinal elastic degrees of freedom corresponding to the n-th tether.

It implies that

$$
\begin{aligned}
r_n &< \ell_n(1+\varrho) \ , \\
r_{t_n} &< x_n(1+\varrho) \ , \\
b_n &< \frac{\ell^2}{2\ell_0}(1+\varrho)dx_n \ .
\end{aligned} \tag{7.64}
$$

Using these relations, Eq. (7.21), and the definition of D_{nk} given in Eq. (7.43), one can see that

$$
P_0 < \frac{m\Omega_c^2}{2}\sum_{n=1}^{N-1}\sum_{k=1}^{N-1}(1+\varrho)^2 D_{nk}\ell_n\ell_k\left\{\cos\phi_n\cos\phi_k\,\hat{\mathbf{j}}_n\cdot\hat{\mathbf{j}}_k + 2(\hat{\mathbf{i}}_c\cdot\hat{\mathbf{i}}_n)(\hat{\mathbf{i}}_c\cdot\hat{\mathbf{i}}_k)\right\} \ . \tag{7.65}
$$

Based on the previous experience a proper Lyapunov function is then chosen as

$$
\mathcal{L} = H + 3S + \sum_{n=1}^{N-1}\frac{1}{2}C_n(\ell_n - \ell_{f_n})^2 \ , \tag{7.66}
$$

where

$$
S = \frac{m\Omega_c^2}{2}\sum_{n=1}^{N-1}\sum_{k=1}^{N-1}(1+\varrho)^2 D_{nk}\ell_n\ell_k \ . \tag{7.67}
$$

Subsequently one obtains the tension control law as the following

$$
T_n = K_{\ell_n}\dot{\ell}_n + C_n(\ell_n - \ell_{f_n}) + 3(1+\varrho)^2 m\Omega_c^2\sum_{k=1}^{N-1}G_{nk}\ell_k \qquad n = 1,2,\ldots,N-1 \ , \tag{7.68}
$$

where G_{nk} and D_{nk} are as defined in Eqs. (7.51) and (7.43), respectively.

7.5.5 Some Results and Discussion

Two different systems, a two-body and a three-body tethered systems are considered to apply the tension control laws obtained in this Section to control the dynamics of the system in the retrieval stage. These cases are considered to show that those control laws can stabilize the unstable motion of the system in the retrieval stage. Optimizing the performance of the controller is a separate issue that one can practice while selecting the most appropriate gains or using a hybrid controller.

The Two Body-System

The system consists of a main-satellite undergoing a circular orbit connected with a long tether, initially 50 km, to a subsatellite. The subsatellite is being retrieved towards the main-satellite. The parameters of the system are as follows:

$$m_1 = 3 \times 10^5\,\text{kg},\ m_2 = 10^3\,\text{kg},\ \rho_1 = 6\,\text{kg/km},\ EA_1 = 61575.2\,\text{N},\ R_c = 6828\,\text{km},$$

and the initial conditions of the system are set as follows:

$$\theta_1(0) = 10°,\ \phi_1(0) = 5°,\ \ell_1(0) = 50\,\text{km},\ \xi_1(0) = 167.7\,\text{m}.$$

Three different cases are considered: (i) rigid and massless tether; (ii) rigid and massive tether; and (iii) massive and flexible, but straight tether. The longitudinal oscillation of the tether is represented by its first mode, i.e. strain is constant along the tether. The following parameters are selected for the control laws given in Eqs. (7.39), (7.53), and (7.68):

$$K_{\ell_1} = 6.266\,\text{N.s/m}\ C_1 = 3.51 \times 10^{-4}\text{N/m},\ \ell_{f_1} = 0,\ \varrho = 0.01\ .$$

It is well known that the retrieval phase of the uncontrolled system is unstable. Results presented in this section show the effectiveness of the tension control laws in stabilizing the system. Figure 7.1 compares the simulation results of the controlled system with rigid and massless tether with those of the system with rigid but massive tether. The dotted-lines represent the system with massless tether, while the solid-lines represent the massive one. In the figure $\dot{\ell}_1, T_1$, and P_1 are retrieval rate, tension in the tether, and the required power to retrieve the subsatellite, respectively. As can be seen, mass of the tether has a small effect on the performance of the system. The differences are so small that it can hardly be seen in the plots. Note that when the length of the tether is large and mass of the tether is comparable to that of the subsatellite, the tension in the tether (Fig. 7.1-c), and subsequently the power required (Fig. 7.1-f) are quite different. However, this difference diminishes when the tether becomes short.

Effect of the flexibility of the tether on the dynamics of the controlled system is shown in Fig. 7.2. The dotted-lines correspond to the system with no flexibility, while the solid-lines represent the system with flexible tether. Since the controller gains are selected similarly in both cases, comparing the results, one can conclude that including the flexibility of the tether leads to a faster retrieval at the cost of larger librational motion. It can be seen that the tension in the tethers in the flexible case are slightly smaller than those of the rigid case. However the power required (P) is reverse. This is in agreement with the physical understanding of the problem. The longitudinal oscillation of the tether for the system with flexible tether is shown in Fig. 7.2-c. As can be seen ξ, the longitudinal stretch of the tether, is always positive. It assures us that the tether does not become slack.

The Three-Body System

The three-body system is also in a circular orbit. It consists of a main-satellite and two subsatellites. The main-satellite retrieves the first subsatellite. At the same time the second satellite is reeled in by the first satellite. As in the case of the two-body system, the longitudinal oscillations of the tethers are modelled by their first modes. The system parameters are as follows:

$$m_1 = 3 \times 10^5\,\mathrm{kg},\ m_2 = 10^3\,\mathrm{kg},\ m_3 = 500\,\mathrm{kg},\ \rho_1 = \rho_2 = 6\,\mathrm{kg/km},$$
$$EA_1 = EA_2 = 61575.2\,\mathrm{N},\ R_c = 6828\,\mathrm{km},$$

and the initial conditions are set as

$$\theta_1(0) = \theta_2(0) = 10^\circ,\ \phi_1(0) = \phi_2(0) = 5^\circ,\ \ell_1(0) = 50\,\mathrm{km},\ \ell_2(0) = 20\,\mathrm{km},$$
$$\xi_1(0) = 296.5\,\mathrm{m},\ \xi_2(0) = 47.4\,\mathrm{m}\,.$$

Similar to the two-body system, three different cases are considered here: (i) rigid and massless tethers; (ii) rigid and massive tethers; and (iii) massive and flexible, but straight tethers.

Figure 7.3 compares the dynamics response of the system with massless tethers with those of the system with massive tethers. The dotted-lines represent the massless tether case while the solid-lines are corresponding to the massive tether case. The controller gains are as follows:

$$K_{\ell_1} = 6.714\,\text{N.s/m},\ K_{\ell_2} = 2.965\,\text{N.s/m},\ C_1 = 5.26 \times 10^{-4}\,\text{N/m},$$
$$C_2 = 1.75 \times 10^{-4}\,\text{N/m},\ \ell_{f_1} = \ell_{f_2} = 0.$$

Results of the system with massive and rigid tethers are compared with those of the flexible tether case in Fig. 7.4. Since the preceding gains result in an undesirable performance, the controller gains are chosen slightly different from the previous gains. They are chosen as follows:

$$K_{\ell_1} = 13.43\,\text{N.s/m},\ K_{\ell_2} = 5.93\,\text{N.s/m},\ C_1 = 6.31 \times 10^{-4}\,\text{N/m},$$
$$C_2 = 2.1 \times 10^{-4}\,\text{N/m},\ \ell_{f_1} = \ell_{f_2} = 0,\ \varrho = .01\ .$$

Comparing the results shown in these two figures, one can draw similar conclusions as those for the two-body system. Note that simulating the flexible system is more challenging and time consuming than the rigid case. That is because as the tethers become shorter, the tension in the tethers reduce and the governing equations become stiffer in the numerical sense.

7.6 Hybrid Control Laws

Results presented in the previous Section show the capability of the tension control laws in stabilizing the system in the retrieval phase. However, one can see that these control laws do not have the desired performance. Generally, it can be said that the controllers perform much better in the initial stage of the retreival than the final stage. The tension control law seems to be slow. In fact a fast retrieval with bounded librations, specially out-of-plane librations, cannot be achieved using these control laws. The faster is the retrieval, the larger are the librational motions. That is because in these control laws only lengths of the tethers and their rates are fed-back.

To improve the performance of the controller, one option is to use a hybrid control law. In this Section a thruster augmented control law using Lyapunov's stability theory is developed. One will appreciate the improvement of the performance when the results of the hybrid control laws are compared with those of the tension control laws. For the sake of brevity, the analysis is presented only for a multi-body system with massless and rigid tethers. However, the analysis can be extended to other cases similar to those in Section 7.5. In the numerical results, a system with massive and flexible tethers is considered to show the effectiveness of the hybrid control laws.

Without any loss of generality, let us assume that body 1 is the main-satellite. In order to control the librations of the system, a thruster is located at each subsatellite. Let us denote the force of the thruster on body $i+1$ $(i = 1, 2, \ldots, N-1)$ by $\vec{F}_i$. Using Eq. (3.40), one can easily show that the generalized forces are now given by

$$
\begin{aligned}
Q_{\theta_n} &= P_{y_n} \ell_n \cos\phi_n \quad , \\
Q_{\phi_n} &= P_{z_n} \ell_n \quad , \\
Q_{\ell_n} &= -T_n + P_{x_n} \quad ,
\end{aligned}
\tag{7.69}
$$

where $P_{x_n}, P_{y_n}, P_{z_n}$ are the components of the resultant force $\vec{P}$ in the n-th tether coordinate system, defined by

$$
\vec{P} = P_{x_n}\hat{\mathbf{i}}_n + P_{y_n}\hat{\mathbf{j}}_n + P_{z_n}\hat{\mathbf{k}}_n = \sum_{i=1}^{N-1} A_{i+1,n}\vec{F}_i \quad . \tag{7.70}
$$

Now let us select a similar Lyapunov function as the one given in Eq. (7.26) for the present case. Time derivative of this function is then given by

$$\dot{\mathcal{L}} = \sum_{i=1}^{N-1} \dot{\ell}_n \left[-T_n + P_{x_n} + C_n(\ell_n - \ell_{f_n}) + 3m\Omega_c^2 \sum_{k=1}^{N-1} F_{nk}\ell_k \right]$$
$$+ \sum_{n=1}^{N-1} \left[\dot{\theta}_n (P_{y_n} \ell_n \cos\phi_n) + \dot{\phi}_n (P_{z_n} \ell_n) \right] \quad . \tag{7.71}$$

Selecting

$$\begin{aligned} P_{x_n} &= 0 \quad , \\ P_{y_n} &= -K_{\theta_n}\dot{\theta}_n / \cos\phi_n \quad , \\ P_{z_n} &= -K_{\phi_n}\dot{\phi}_n \quad , \\ T_n &= P_{x_n} + K_{\ell_n}\dot{\ell}_n + C_n(\ell_n - \ell_{f_n}) + 3m\Omega^2 \sum_{k=1}^{N-1} F_{nk}\ell_k \quad , \end{aligned} \tag{7.72}$$

where K_{ℓ_n}, K_{θ_n}, and K_{ϕ_n} are arbitrary positive constants, one obtains

$$\dot{\mathcal{L}} = \sum_{n=1}^{N-1} - \left(K_{\ell_n}\dot{\ell}_n^2 + K_{\theta_n}\ell_n\dot{\theta}_n^2 + K_{\phi_n}\ell_n\dot{\phi}_n^2 \right) \quad . \tag{7.73}$$

Since ℓ_n is always positive, it is clear that $\dot{\mathcal{L}}$ is always non-positive. Eq. (7.72) describes the hybrid control law.

The forces of the thrusters, $\vec{\boldsymbol{F}}_i$, $i = 1, 2, \ldots, N-1$, required to implement the control law, are obtained from the components of $\vec{\boldsymbol{P}}_n$'s forces. Let us define column vectors $\mathbf{P}_n$ and $\mathbf{F}_n$ as

$$\mathbf{P}_n = \{P_{x_n}, P_{y_n}, P_{z_n}\}^T \quad , \quad \mathbf{F}_n = \{F_{x_n}, F_{y_n}, F_{z_n}\}^T \quad , \tag{7.74}$$

where $P_{x_n}, P_{y_n}, P_{z_n}$ and $F_{x_n}, F_{y_n}, F_{z_n}$ are the components of $\vec{\boldsymbol{P}}_n$ and $\vec{\boldsymbol{F}}_n$ in the n-th tether coordinate frame. Denoting the rotation matrix of the n-th tether frame with respect to the orbital frame by $\mathbf{R}_n$ and using Eq. (7.70), one can show that

$$\begin{bmatrix} A_{21}\mathbf{R}_1\mathbf{R}_1^T & A_{31}\mathbf{R}_1\mathbf{R}_2^T & \dots & A_{N1}\mathbf{R}_1\mathbf{R}_{N-1}^T \\ A_{22}\mathbf{R}_2\mathbf{R}_1^T & A_{32}\mathbf{R}_2\mathbf{R}_2^T & \dots & A_{N2}\mathbf{R}_2\mathbf{R}_{N-1}^T \\ \vdots & \vdots & \ddots & \vdots \\ A_{2,N-1}\mathbf{R}_{N-1}\mathbf{R}_1^T & A_{3,N-1}\mathbf{R}_{N-1}\mathbf{R}_2^T & \dots & A_{N,N-1}\mathbf{R}_{N-1}\mathbf{R}_{N-1}^T \end{bmatrix} \begin{Bmatrix} \mathbf{F}_1 \\ \mathbf{F}_2 \\ \vdots \\ \mathbf{F}_{N-1} \end{Bmatrix}$$

$$= \begin{Bmatrix} \mathbf{P}_1 \\ \mathbf{P}_2 \\ \vdots \\ \mathbf{P}_{N-1} \end{Bmatrix} . \tag{7.75}$$

Hence $\mathbf{F}_1, \mathbf{F}_2, \dots, \mathbf{F}_{N-1}$ are obtained by solving the above set of linear equations.

For a two-body system, Eq. (7.75) results in

$$F_{x_1} = P_{x_1}/A_{21} = 0, \quad F_{y_1} = P_{y_1}/A_{21}, \quad F_{z_1} = P_{z_1}/A_{21} \quad . \tag{7.76}$$

It means that the thruster force has no component along the tether. However, for a multi-tethered system, even by setting P_{x_n}'s zero, generally one should expect thruster forces with non-zero component along the tetherline, i.e. $F_{x_n} \neq 0$, $n = 1, 2, \dots N-1$.

7.6.1 Numerical Results

Figures 7.5 - 7.7 show the effectiveness of the hybrid control law in achieving a desirable performance for the controlled system. In Figs. 7.5 and 7.6 the results of a two-body system are shown, while in Fig. 7.7 a three-body system is considered. For the two-body system all the different cases, massless tether, massive but rigid tether, and massive and flexible tether, are considered. However, in the case of the three-body system the results are compared between massless-tether and massive-tether systems only. The flexibility of the tethers are not taken into account in this case. The parameters and the initial conditions of the systems are exactly as those considered while studying the tension control law (Figs. 7.1 - 7.4).

The following gains are used to retrieve the subsatellite in the case of the two-body system:

$$K_{\ell_1} = 2.239\,\mathrm{N.s/m},\ K_{\theta_1} = K_{\phi_1} = 10^4\,\mathrm{N.s/rad},\ C_1 = 4.211 \times 10^{-4}\,\mathrm{N/m},$$
$$\ell_{f_1} = 0,\ \varrho = 0.01\ .$$

Figure 7.5 compares the results of the massless-tether system with those of the massive-tether system, while in Fig. 7.6 the results of rigid-tether system and flexible-tether system are compared. From these figures one can observe that the retrieval duration is significantly reduced by using the hybrid control law compared to that in Figs. 7.1 and 7.2. At the same time the out-of-plane librational motion is bounded to a small magnitude, which is desirable. Of course faster retrieval and smaller out-of-plane motion can be obtained for the cost of a larger thruster force.

For the three-body system the following controller gains are chosen:

$$K_{\ell_1} = 2.821\,\mathrm{N.s/m},\ K_{\ell_2} = 1.364\,\mathrm{N.s/m},\ K_{\theta_1} = K_{\phi_1} = K_{\theta_2} = K_{\phi_2} = 10^4\,\mathrm{N.s/rad},$$
$$C_1 = 4.74 \times 10^{-4}\,\mathrm{N/m},\ C_2 = 1.44 \times 10^{-4}\,\mathrm{N/m},\ \ell_{f_1} = \ell_{f_2} = 0.$$

Figure 7.7 compares the motion as well as the time history of the forces of the massless-tether system with those of the massive-tether system. The effectiveness of the hybrid control law is quite evidence when the present results are compared with those of the tension control law given in Fig. 7.3. Note that in contrast to the two-body case the x-components of the thrusters are not zero. Comparing the results for the two-body and three-body systems, one observes a fairly similar behaviour in the dynamics of the controlled systems.

As far as the effects of mass and flexibility of the tethers are concerned, similar conclusion to those of the tension control law can be drawn. Looking at the results shown in this Chapter, one can conclude that using a tension control law alone results in somewhat poor performance: therefore a hybrid control law should be used to obtain a good performance. Furthermore, ignoring the elasticity of the tethers leads to poor results: hence they should be included in the analysis.

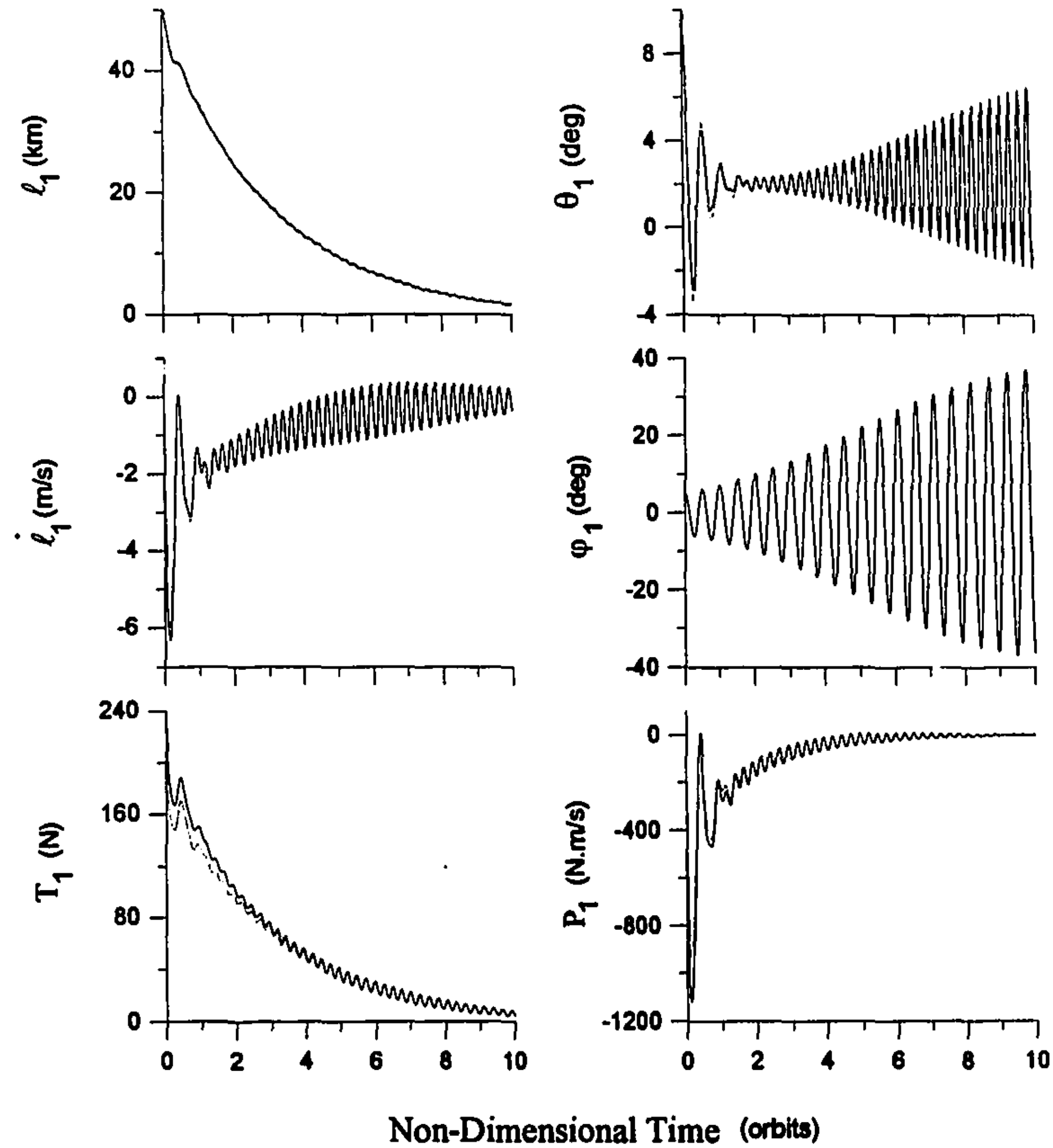

Figure 7.1: Dynamical response of a controlled two-body system (tension control law): ... system with rigid and massless tether , —— system with rigid and massive tether.

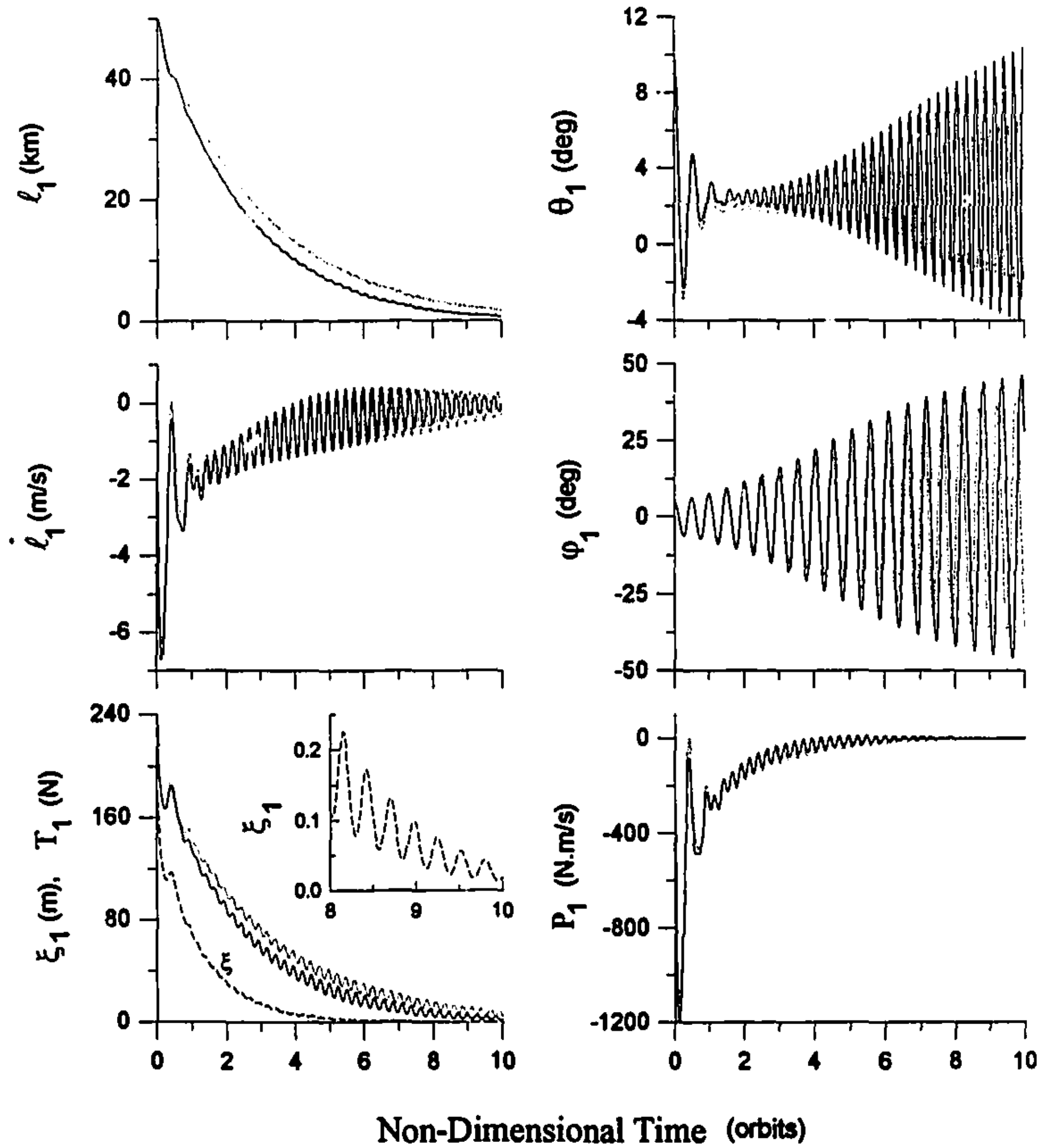

Figure 7.2: Dynamical response of a controlled two-body system (tension control law): . . . system with rigid and massive tether , —— system with massive and flexible tether.

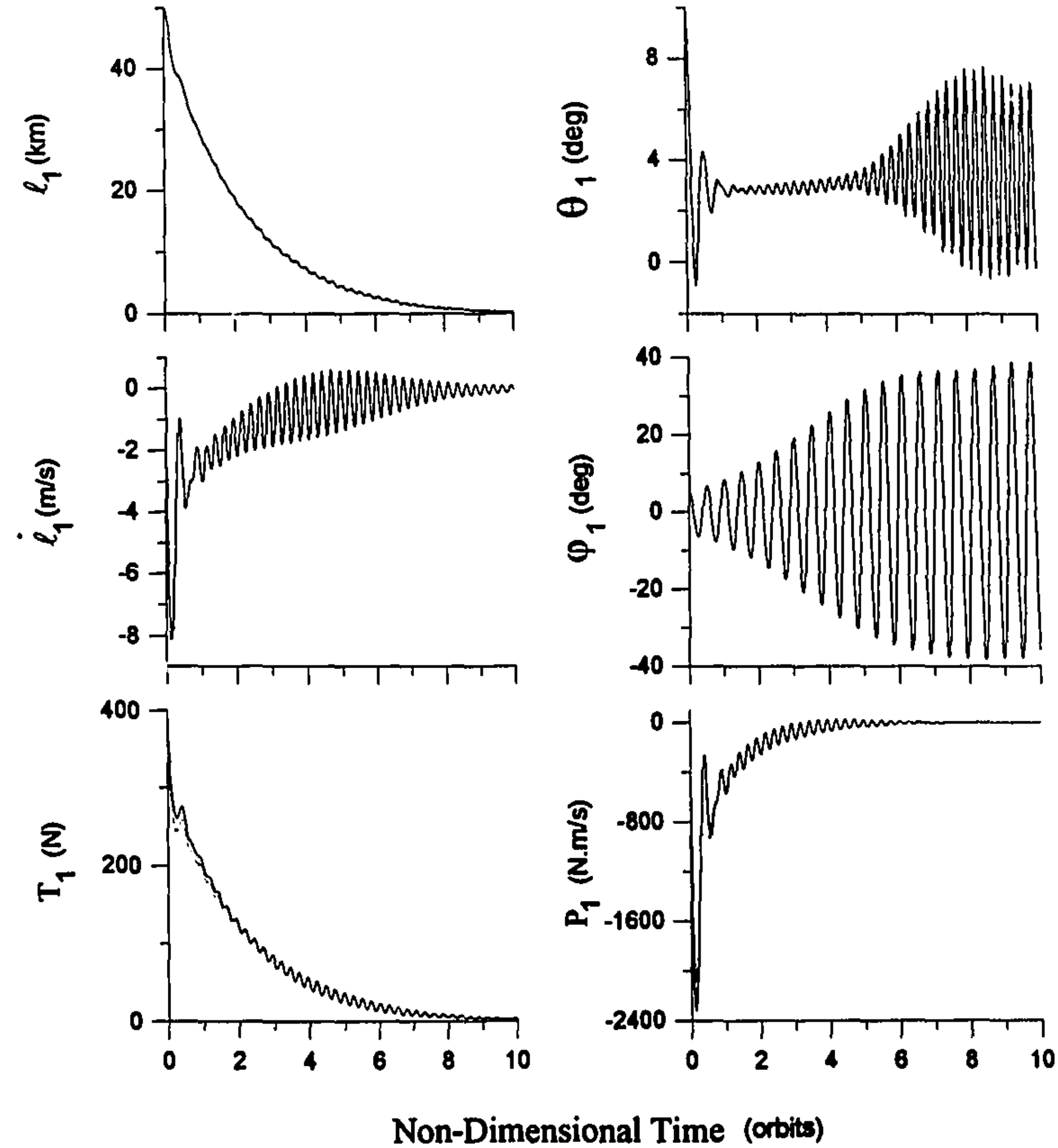

Figure 7.3: Dynamical response of a controlled three-body system (tension control law): ... system with rigid and massless tether , — system with rigid and massive tether.

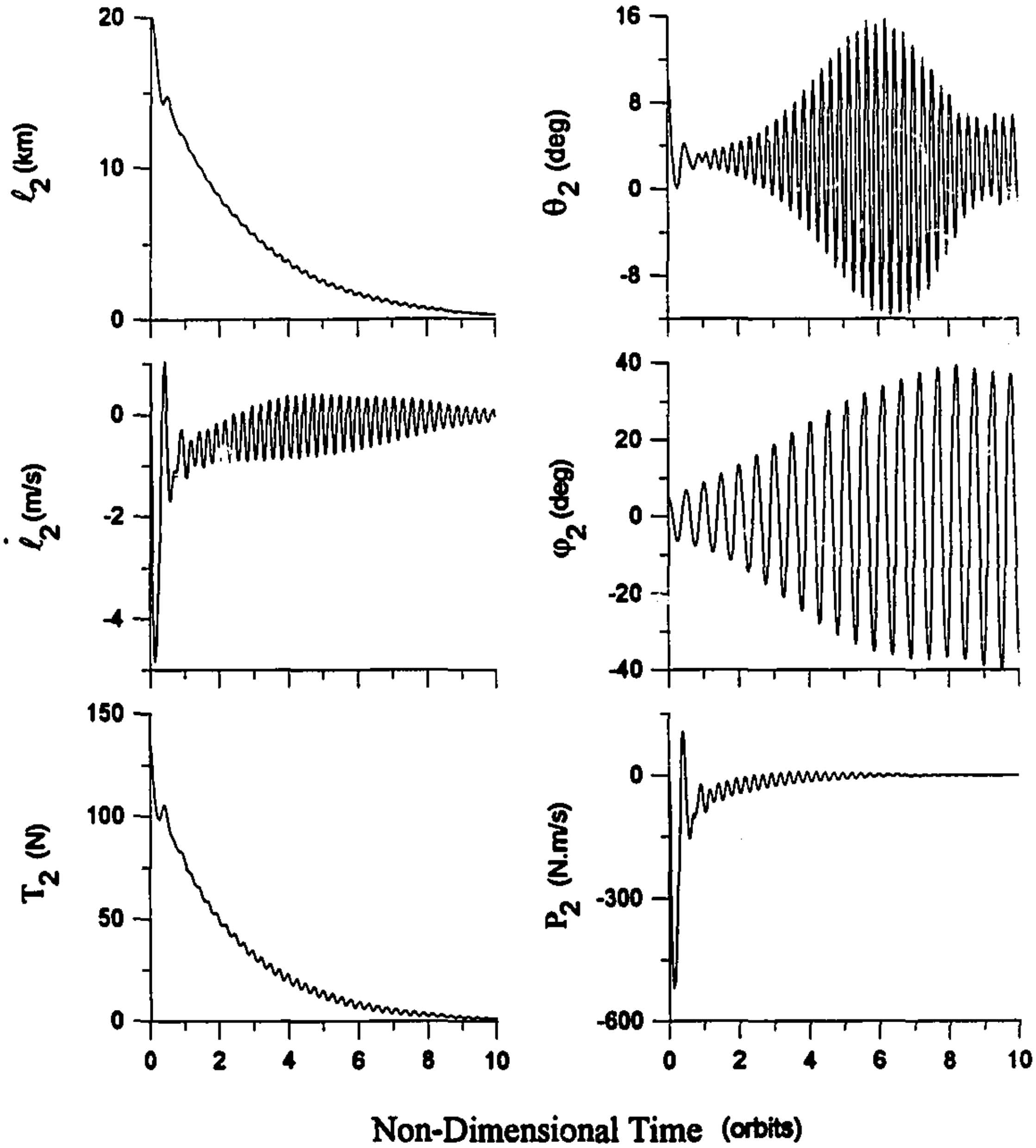

Figure 7.3: Contd.

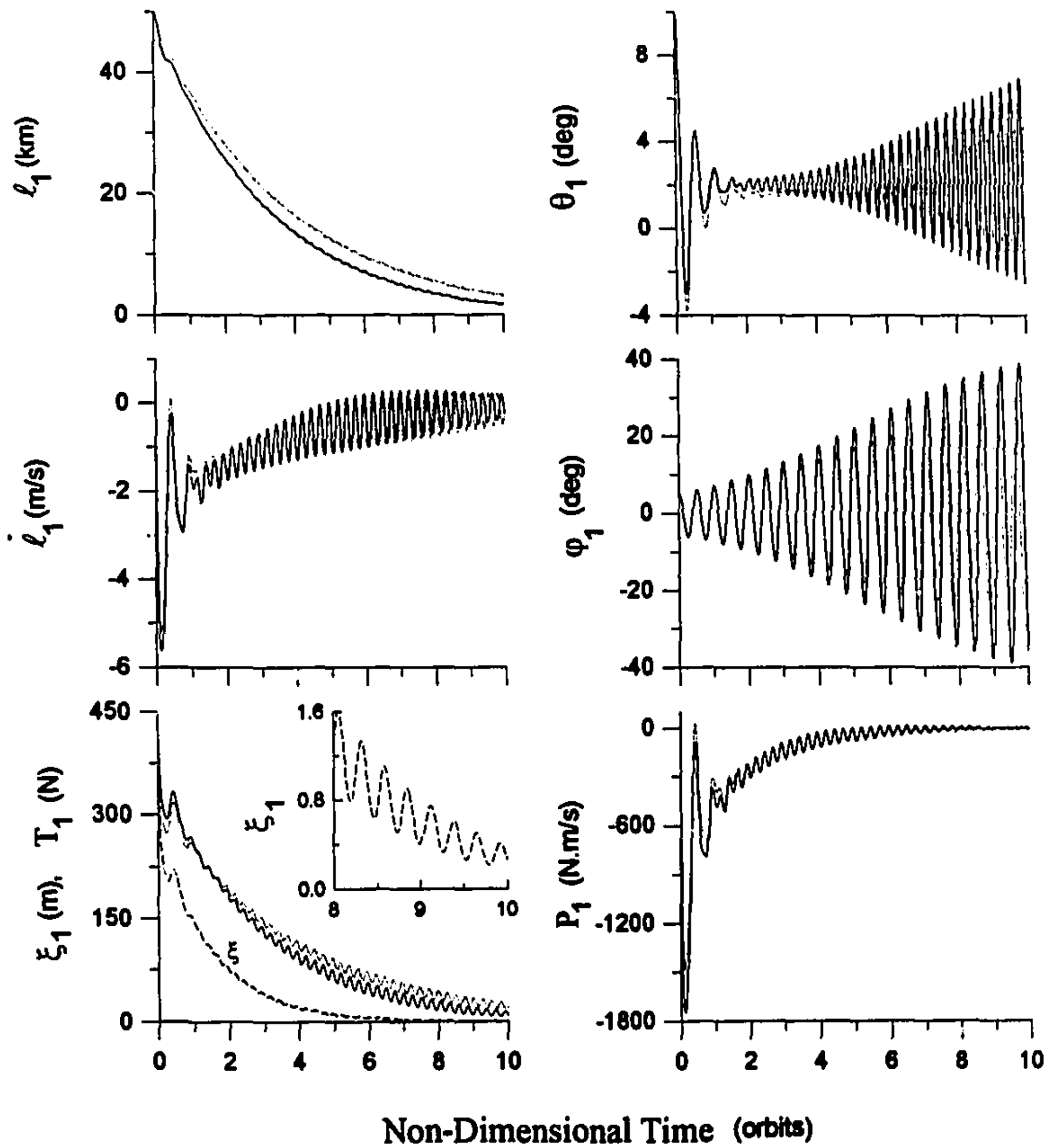

Figure 7.4: Dynamical response of a controlled three-body system (tension control law): ... system with rigid and massive tether , —– system with massive and flexible tether.

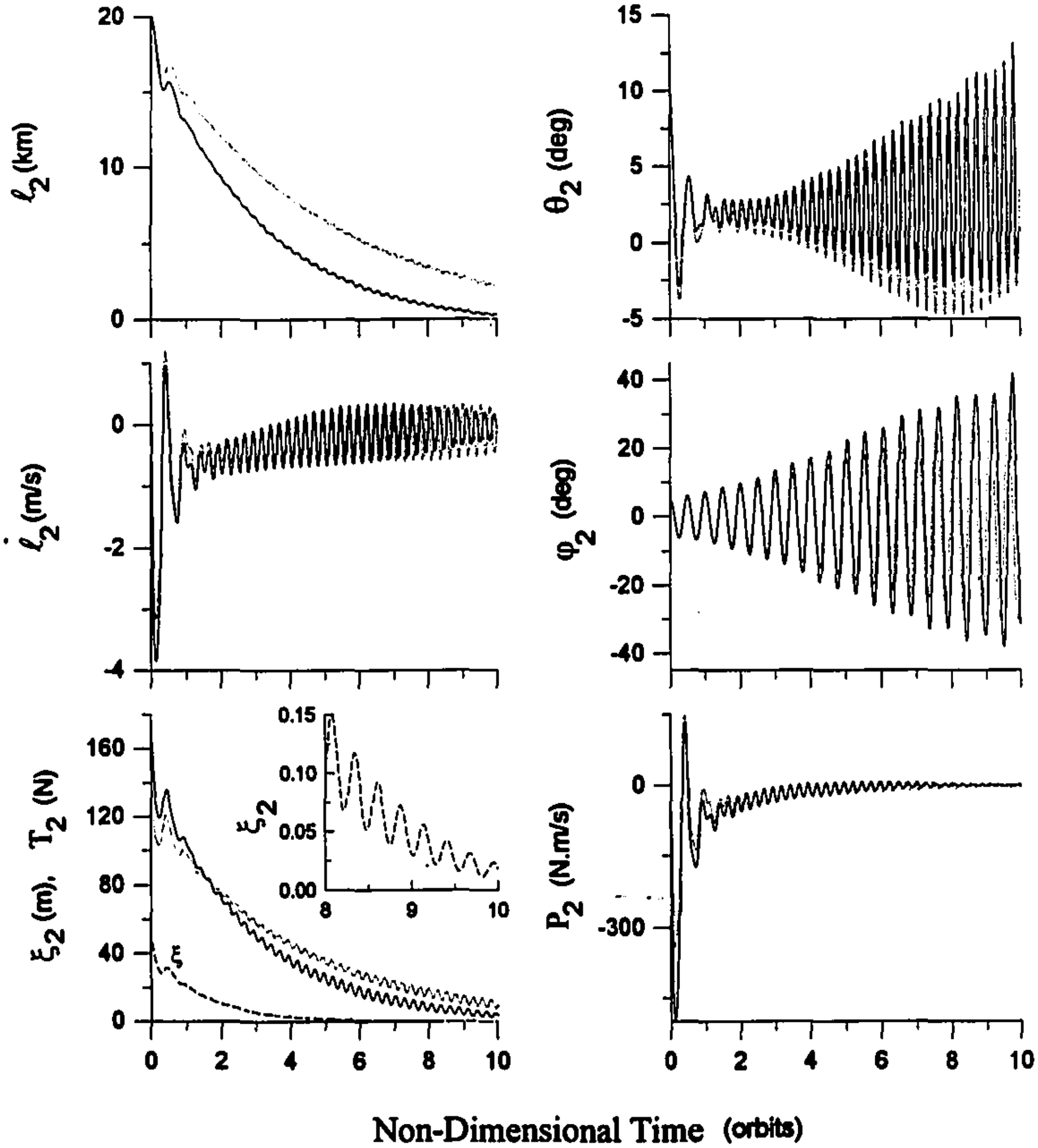

Figure 7.4: Contd.

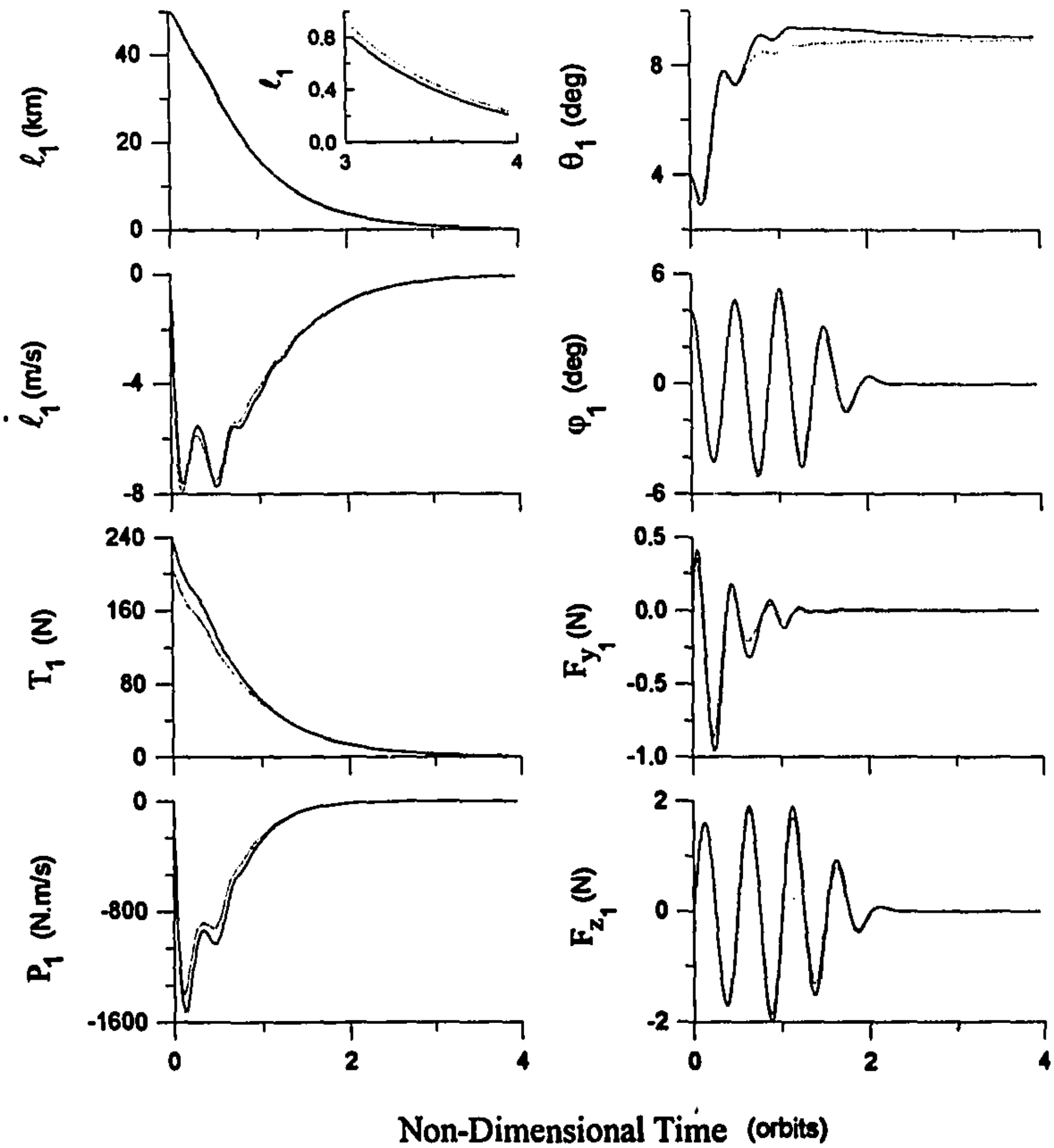

Figure 7.5: Dynamical response of a controlled two-body system (hybrid control law): ... system with rigid and massless tether , —— system with rigid and massive tether. Parameters are the same as those in Fig. 7.1 .

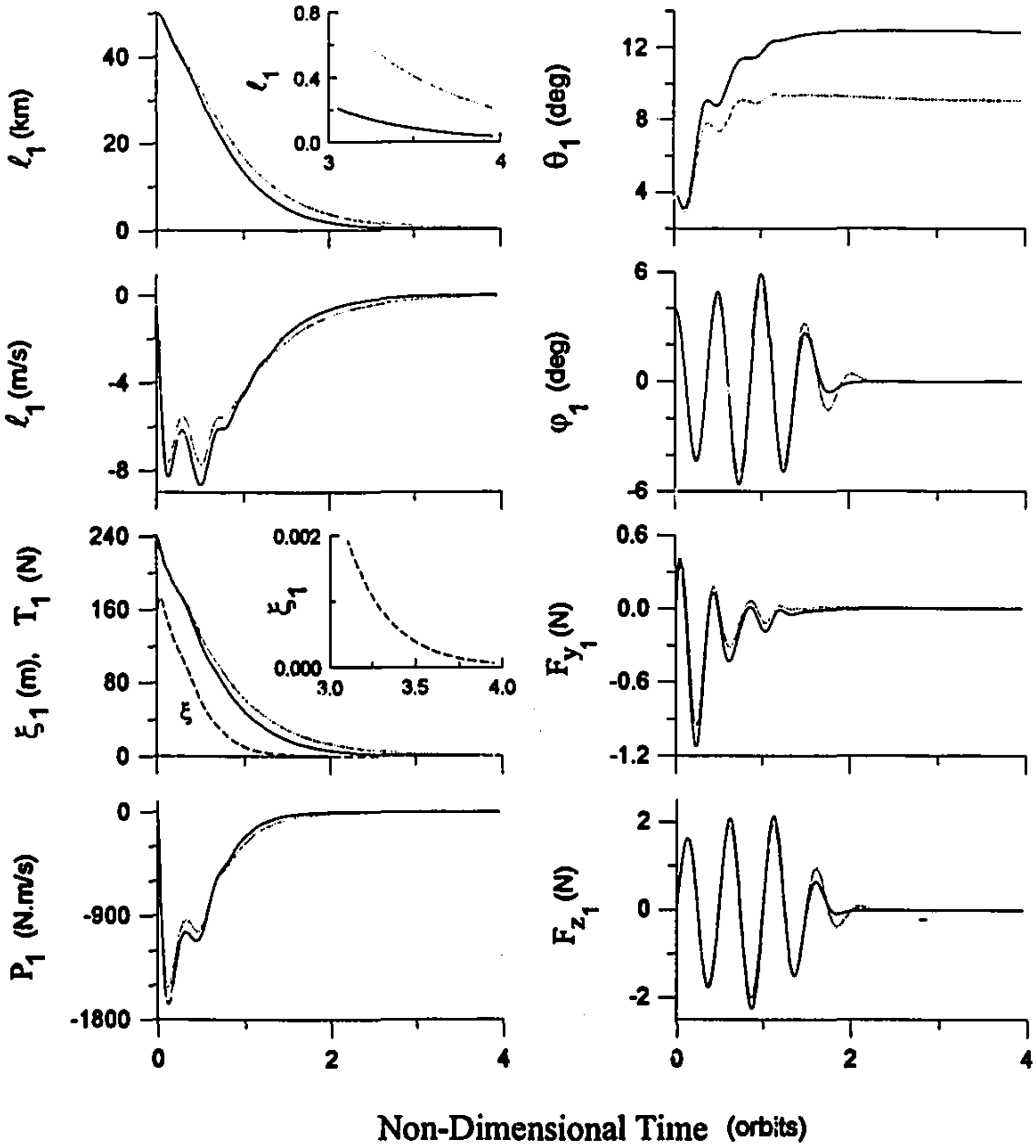

Figure 7.6: Dynamical response of a controlled two-body system (hybrid control law): ... system with rigid and massive tether, —— system with massive and flexible tether. Parameters are the same as those in Fig. 7.2 .

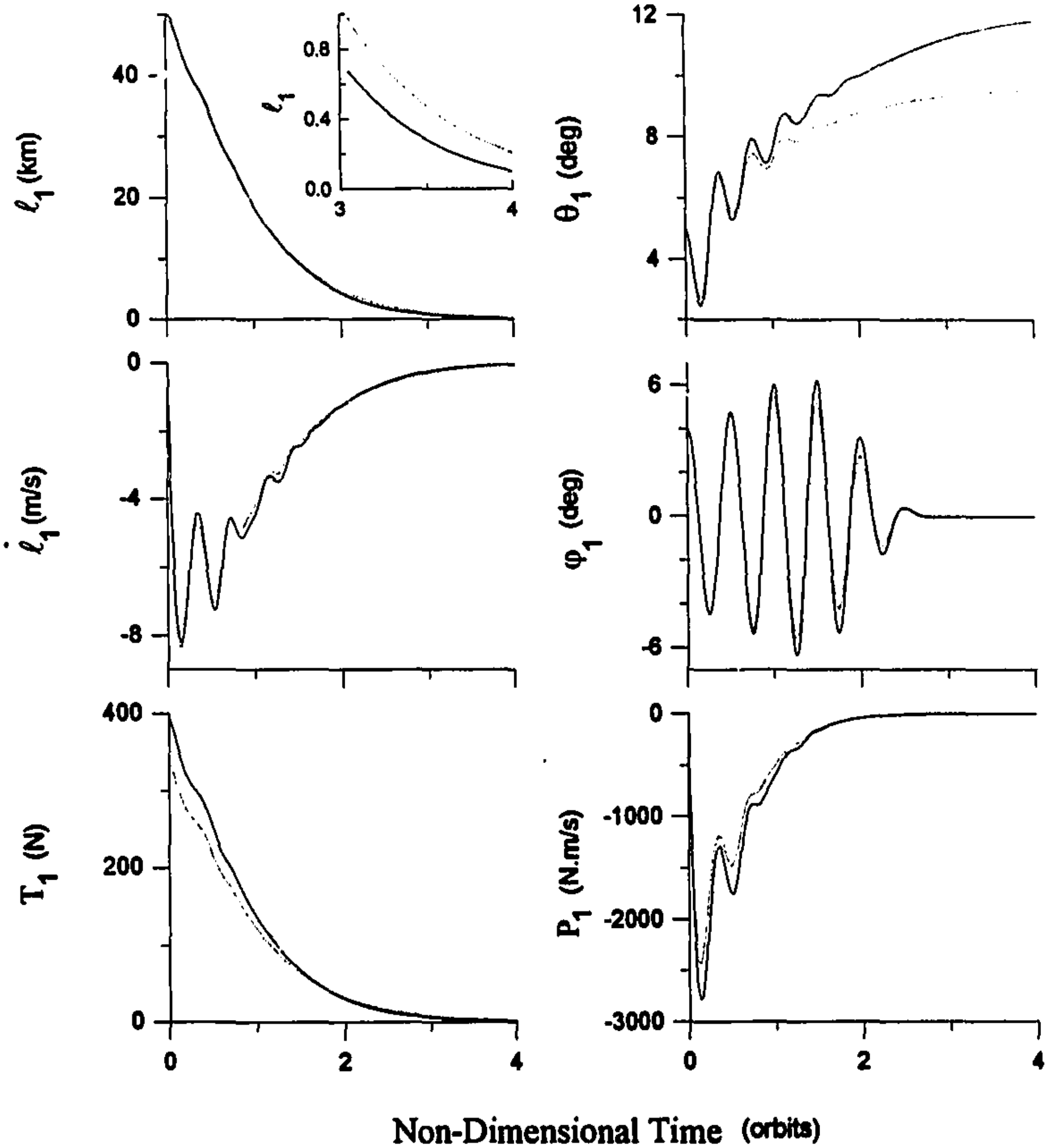

Figure 7.7: Dynamical response of a controlled three-body system (hybrid control law): ... system with rigid and massless tether , — system with rigid and massive tether. Parameters are the same as those in Fig. 7.3 .

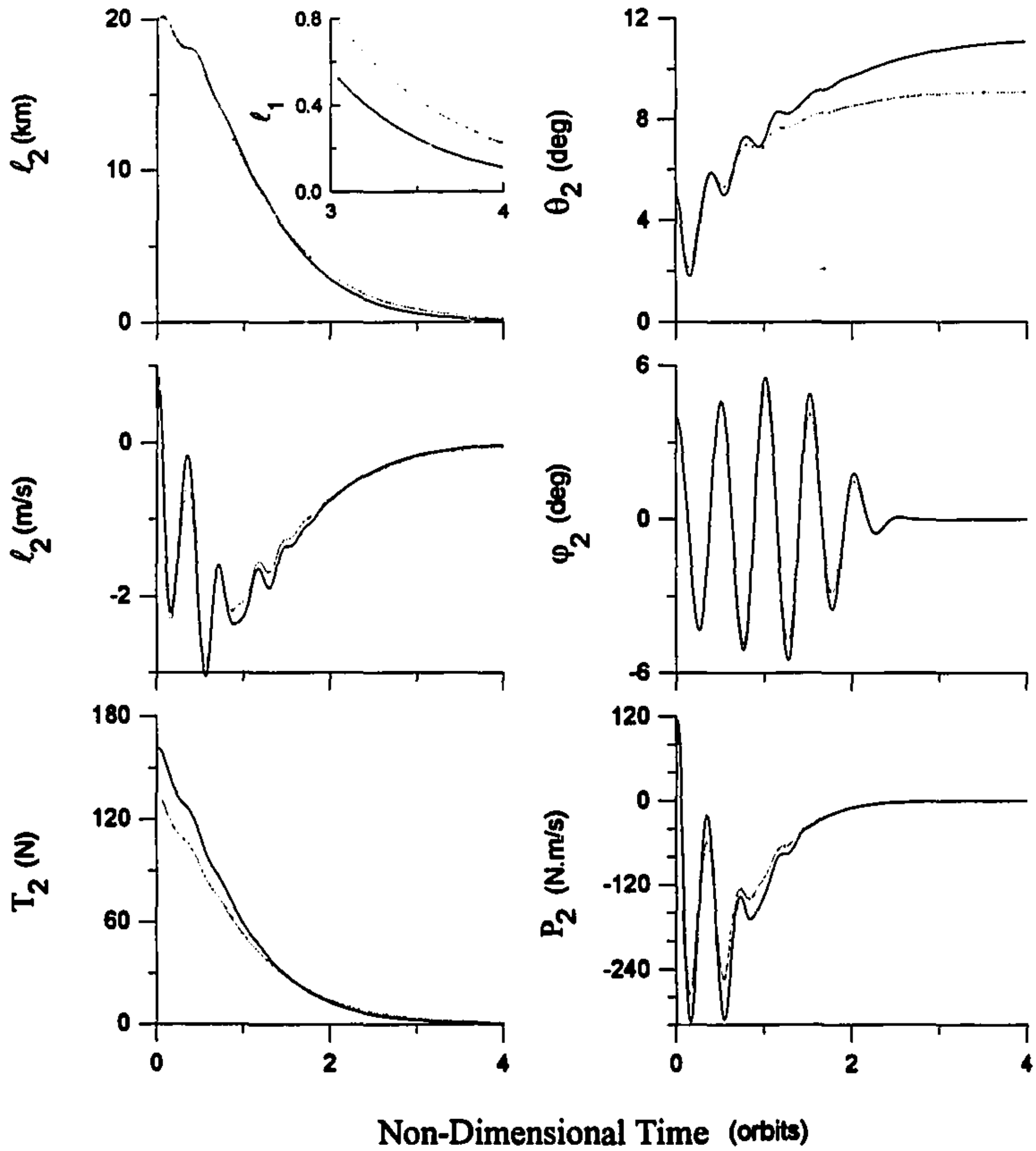

Figure 7.7: Contd.

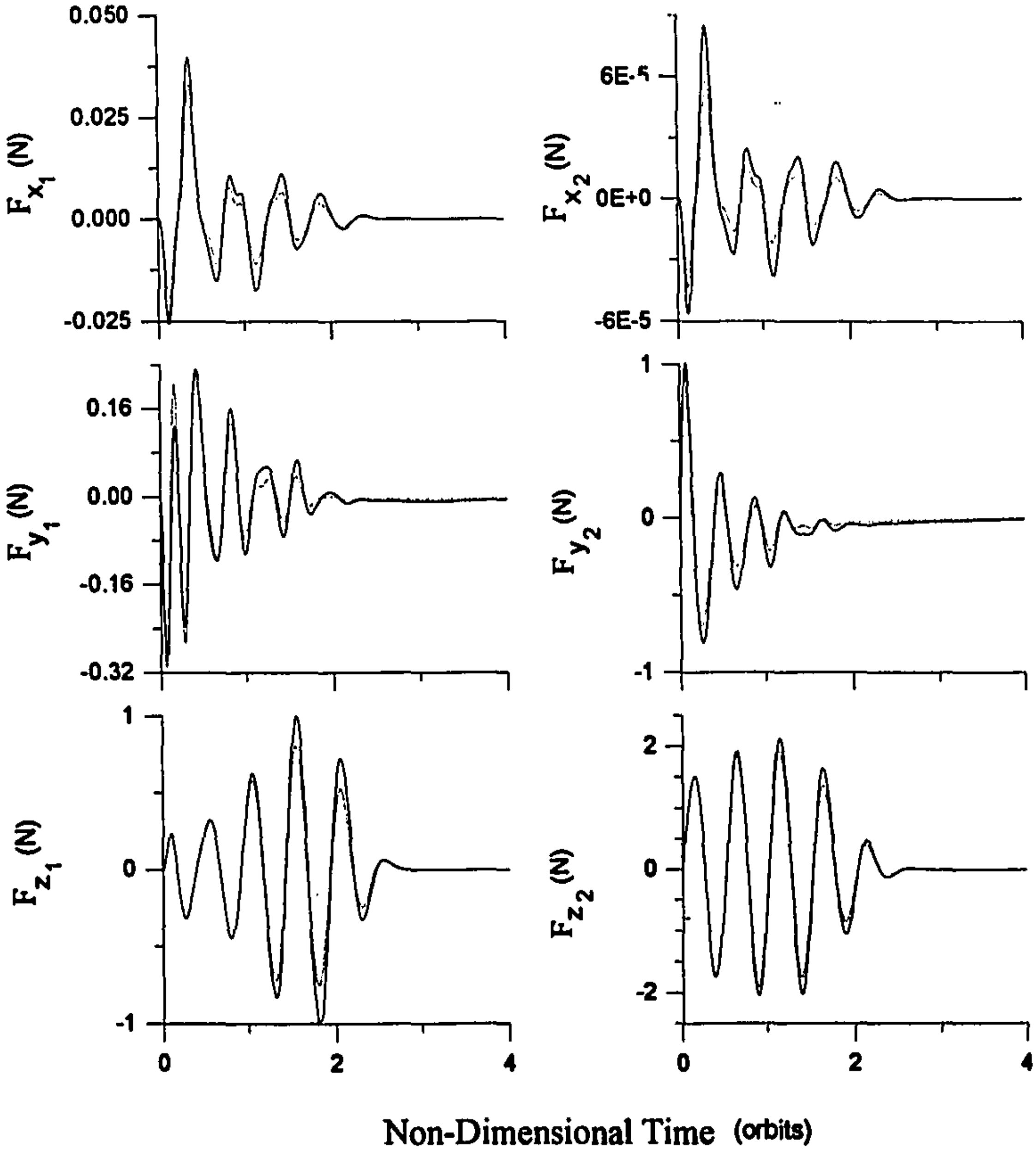

Figure 7.8: Contd.: Thruster forces

Chapter 8

CONCLUSIONS

8.1 Summary of Finding

Throughout this thesis, the main objective of the investigation has been the dynamical analysis of multi-body tethered satellite systems: their modelling, analysis of their stability in low-altitude missions, and control synthesis using Lyapunov's stability theory. Both dynamical analysis and control synthesis of these systems are extremely complex problems. The two problems are closely related so that developing a good dynamical model makes the control synthesis easier. Rather than presenting a massive amount of data, the emphasis has been on the modelling and understanding of the problem.

Discretizing the tethers using the assumed modes method, a set of ordinary differential equations describing the rotational motion as well as the vibrations of the tethers has been derived. An analytical procedure has been used to linearize the equations obtained from the discretized model to analyze the eigenvalues and stability of the system. Aerodynamic forces on the system have been calculated using the free molecular flow model to study their effects on the stability of the system used for atmospheric missions. In the absence of external forces, an analytical solution is obtained for the static equilibrium equations.

Ignoring the transverse vibrational motion of the tethers, a nonlinear tension control law has been developed to control the system during the retrieval stage. The control law has been obtained using Lyapunov's direct method by analyzing the Hamiltonian of the system in several steps. The control law was then validated by numerical analysis of some sample cases. A hybrid control law has been proposed to improve the performance of the controller system.

The important conclusions derived from this study are summarized below.

(i) The dynamical model of multi-body tethered satellite systems must consider the elastic vibrations of the tethers. Similar to the librational motion of the tethers, their longitudinal as well as the transverse vibrational motion tend to grow during the retrieval stage.

(ii) Longitudinal and transverse vibrations of the tethers are strongly coupled, particularly when the tethers are short. The dynamical model must consider the nonlinear term in the strain expression caused by transverse vibrations, since there can be a significant difference between the linear and nonlinear results. During the retrieval process, the tension in the tethers becomes weaker and weaker and the nonlinear strain term becomes more and more significant.

(iii) Dynamics and stability of the system in low-altitude missions are significantly affected by aerodynamic forces on the end-bodies as well as the tethers. Changing the geometry of the bodies changes the aerodynamic forces and consequently the stability of the system. Stability behaviour as well as equilibrium configurations of the system change if the bodies are changed from those with no lift to bodies with lift. Consideration of the general aerodynamical model rather than only the aerodynamic drag is indispensable for proper design of low-altitude orbital missions.

(iv) The elasticity of the tethers plays an important role in the dynamics, stability, and control of multi-body tethered satellite systems. Combined effect of the tether flexibility and the atmospheric density gradient can lead to instability of the system. Although it makes the dynamical analysis as well as control synthesis more challenging, the tether elasticity must be included in the analysis to derive more reliable results.

(v) The material damping present in the tethers affects their longitudinal oscillations. However they have very negligible effect on the transverse oscillations and the librations of the tethers. On the other hand, the material damping has a great effect on the computation time; in fact it may be reduced significantly by damping.

(vi) The retrieval phase is the critical phase of the mission as far as stability and control of the system are concerned. Among the different well-known control methods for tethered satellite systems, tension control laws and reel rate control laws are easy to implement and more practical. The reel rate of the tethers $(\dot{\ell}_i/\ell_i)$ or tension affects the in-plane libration of the tethers more than the out-of-plane motion. Therefore controlling the latter with unaided reel rate or tension control law is a demanding task. That is because the coupling between the in-plane and out-of-plane rotations is a weak nonlinear one.

(vii) Lyapunov's direct method is a very powerful method, since it is applicable to the motion of the system in large and it can reveal the stability of the system just by using the equations of motion without actually solving them. However constructing a proper Lyapunov function is a very challenging and strenuous task. Using the Hamiltonian of the system and then compensating for the negative terms to form a Lyapunov function, a tension control law and a hybrid control law have been formulated that stabilize the in-plane and out-of-plane librations in the sense of Lyapunov. The control laws are linear in terms of length of the tethers, if mass of the tethers are ignored; but they are highly nonlinear if these masses are included. Fast retrieval and bounded out-of-plane librational motion cannot be achieved through a tension control law alone. One has to use other schemes or a hybrid control law such as the one proposed in this thesis. In the control analysis it was found that ignoring the elasticity of the tethers can completely lead to incorrect results.

8.2 Recommendation for Future Work

There are many possibilities for extension of the present investigation. Only some of them are mentioned below.

(i) The attitude dynamics of the end-bodies are not considered in the present dynamical model. Further research should include these motions as well.

(ii) Spinning of the tether(s) along its (their) nominal tetherline is not included in this study. It can result in further instability for high spinning rates, particularly in the transverse oscillations of the tethers.

(iii) Dynamics of the reeling system may be modelled in more detail to avoid any confusion about the interactive force due to the change of mass of the tethers.

(iv) A more complete and realistic aerodynamic model could be developed for further studies, particularly for the control synthesis using aerodynamic forces.

(v) The perturbing effects of other environmental forces such as solar radiation pressure and electrodynamic forces on the motion of multi-body tethered systems can be investigated, for applications in which these effects are significant.

(vi) The proposed control laws must be verified by experiments.

(vii) Control synthesis using the Lyapunov approach may be extended to include both longitudinal as well as transverse vibrations of the tethers.

(viii) Further studies can be conducted on dynamics and control of multi-tethered systems with a non-chain configuration.

(ix) Methods similar to those employed in this thesis can be used to study the dynamics and control of deployment of multiple beam type appendages, solar panels, etc.

(x) Other control synthesis such as LQR or feedback linearization can be used to devise the desired control laws.

Statement of Originality and Contribution to Knowledge

Original contributions made in this thesis to the knowledge on tethered satellite systems may be summarized as follows:

(i) A fairly general dynamical model of N-body tethered satellite systems has been proposed. Both types of vibrations (longitudinal and transverse) of tethers in multi-tethered systems have been considered simultaneously for the first time in the dynamical analysis.

(ii) Analytically linearized equations of motion have been presented for eigenvalue as well as stability analysis.

(iii) Effects of aerodynamic lift of the end-bodies on the stability and dynamics of low-altitude missions have been studied in detail. It has been found that they can change system stability significantly. Passive stabilization of a low-altitude tethered subsatellite using aerodynamic panels has been investigated.

(iv) Lyapunov approach has been used to control the nonlinear system and various nonlinear tension control laws have been developed. Longitudinal elasticity and mass of the tethers have been considered in the control synthesis.

(v) A hybrid control law, using thruster and tension control law, has been developed to achieve the desired performance in controlling multi-tethered systems.

Bibliography

[1] Tsiolkovksy, K.E., "Grezy O. Zemie i nebe (i) Na Veste (Speculations between Earth and Sky, and on Vesta; Science Fiction Works)," *Moscow, izd-vo AN SSSR*, p. 35, 1959.

[2] Artsutanov, Y., "V. Kosmos na Elektrovoze," *Komsomolskaya Pravda*, July 1960.

[3] Starly, W.H. and Adlhoch R.W., "Study of the Retrieval of an Astronaut from an Extra-Vehicular Assignment," *TMC Report No. S-356*, November 1963.

[4] Eades, J.B. and Wolf, H., "Tethered Body Problems and Relative Motion Orbit Determination," *Final Report, Contract NASA S-21453, Analytical Mechanics Associates, Inc.*, August 1972.

[5] Lang, D.L. and Nolting, R.K., "Operations with Tethered Space Vehicles," *NASA SP-138, Gemini Summary Conference*, February 1967.

[6] Colombo, G., Gaposchkin, E.M., Grossi, M.D. and Weiffenbach, G.C., "Shuttle borne Skyhook: a new tool for low-orbital-altitude research," *Smithsonian Institution Astrophysical Observatory, Reports in Geoastronomy, No. 1*, September 1974.

[7] Bekey, I., "Tethers Open New Space Options," *Astronautics and Aeronautics*, vol. 21, pp. 32–40, 1983.

[8] Misra, A.K. and Modi, V.J., "A Survey on the dynamics and Control of Tethered Satellite Systems," *Advances in the Astronautical Sciences*, vol. 62, pp. 667–719, 1987.

[9] Beletsky V.V. and Levin E.M., "Dynamics of Space Tether Systems," *Advances in the Astronautical Sciences*, vol. 83, 1993.

[10] von Tiesenhausen, G., "Tethers in Space: Birth and Growth of a New Avenue to Space Utilization," *NASA, TM-82571*, February 1984.

[11] Penzo, P.A. and Ammann, P.W., "Tethers In Space Handbook," *NASA office of Space Flight, Advanced Program Development*, May 1989.

[12] Modi, V.J. and Misra, A.K., "Orbital Perturbation of Tethered Satellite Systems," *The Journal of the Astronautical Sciences*, vol. 25, pp. 271–278, 1977.

[13] Rupp, C.C., "A Tether Tension Control Law for Tethered Subsatellite Deployed Along Vertical," *NASA TMX-64963*, September 1975.

[14] Baker, W.P, Dunkin, j.A., Galaboff, Z.J., Johnston, K.D., Kissel, R.R., Rheinfurth, M.H., and Siebel, M.P.L., "Tethered Subsatellite Study," *NASA TMX-73314*, 1976.

[15] Onada, J. and Watanabe, N., "Tethered Subsatellite Swinging from Atmospheric Gradient," *Journal of Guidance, Control, and Dynamics*, vol. 11, pp. 447–479, 1988.

[16] Kalaghan, P.N., Arnold, D.A. Colombo, G., Grossi, M.D., Kirschner, L.R., and Orringer, O., "Study of Dynamics of Tethered Satellite System (Skyhook)," *Final Report, Contract NAS8-32199, Smithsonian Institution, Astrophysical Observary*, March 1978.

[17] Bainum, P.M. and Kumar, V.K., "Optimal Control of the Shuttle-Tethered System," *Acta Astronautica*, vol. 7, pp. 1333–1348, 1980.

[18] Kulla, P., "Dynamics of Tethered Satellites," *Proceedings of the Symposium on Dynamics and Control of Non-Rigid Spacecraft*, pp. 349–354, May 1976.

[19] Buckens, F., "On the Motion Stability of Tethered Satellites Configurations," *Proceedings of the 12-th International Symposium on Space Technology and Science*, pp. 351–358, 1977.

[20] Kohler, P., Maag, W., Wehrli, R., Weber, R., and Brauchli, H., "Dynamics of a System of Two Satellites Connected by a Deployable and Extensible Tether of Finite Mass," *Contract Report, ESTEC Contract No. 2992/76/NL/AK(SC)*, vol. 1 and 2, October 1978.

[21] Modi, V.J. and Misra, A.K., "Deployment Dynamics of a Tethered Satellite System," *AIAA/AAS Astrodynamics Conference*, Paper No. 78-1398, August 1978.

[22] Xu, D.M, *The Dynamics and Control of the Shuttle Supported Tethered Satellite Systems*. PhD thesis, Mech. Eng. Dept., McGill University, November 1984.

[23] Modi, V.J. and Misra, A.K., "On the Deployment Dynamics of Tethered Connected Two-Body Systems," *Acta Astronautica*, vol. 6, pp. 1183–1197, 1979.

[24] Glaese, J.R. and Pastrick, H.L., "Modal Synthesis Simulation of the Shuttle Orbiter Tethered Satellite System," *AIAA/AAS Astrodynamics Conference*, Paper No. AIAA-82-1424, August 1982.

[25] von Flotow, A.H., "Some approximation for the dynamics of Spacecraft Tethers," *Journal of Guidance, Control, and Dynamics*, vol. 11, pp. 357–364, 1988.

[26] Pasca, M., Pignataro, M., and Luongo, A., "Three-Dimensional Vibrations of Tethered Satellite Systems," *Journal of Guidance, Control, and Dynamics*, vol. 14, pp. 312–320, 1991.

[27] Pasca, M. and Lorenzini E., "Collection of Martian Atmospheric Dust With a Low Attitude Tethered Probe," *AAS/AIAA Spaceflight Mechanics Meeting*, Paper No. AAS-91-178, February 1991.

[28] Beletsky V.V. and Levin E.M., "Dynamics of the Orbital Cable System," *Acta Astronautica*, vol. 12, pp. 285–291, 1985.

[29] Matteis, G. and Socio, L.M., "Equilibrium of a Tether-Subsatellite System," *European Journal of Mechanics, A/Solids*, vol. 9, pp. 207–224, 1990.

[30] Kim, E. and Vadali, S.R., "Modelling Issues Related to Retrieval of Flexible Tethered Satellite Systems," *Proceeding of the AIAA/AAS Astrodynamics Conference*, August 1992.

[31] Misra, A.K. and Modi, V.J., "A General Dynamical Model for the Space Shuttle Based Tethered Satellite," *Advances in the Astronautical Sciences*, vol. 40, Part II, pp. 537–557, 1979.

[32] Banerjee, A.K. and Kane, T.R., "Tethered Satellite Retrieval with Thruster Augmented Control," *AIAA/AAS Astrodynamics Conference*, Paper No. AIAA-82-1421, August 1982.

[33] Xu, D.M, Misra, A.K., and Modi, V.J., "Thruster-Augmented Active Control of a Tethered Subsatellite System During Its Retrieval," *Journal of Guidance, Control, and Dynamics*, vol. 9, pp. 663–672, 1986.

[34] Tyc, G., Han, R.P.S., Vigneron, F.R., Jablonski, A.M., Modi, V.J., and Misra, A.K., "Dynamics and Stability of a Spinning Tethered Spacecraft with Flexible Appendages," *AAS/AIAA Astrodynamics Specialist Conference*, Paper No. AAS-93-736, August 1993.

[35] No, T.S. and Cochran, J.E.Jr., "Dynamic and Control of a Tethered Flight Vehicle," *AAS/AIAA Astrodynamics Conference*, Paper No. AAS-91-554, August 1991.

[36] No, T.S. and Cochran, J.E.Jr., "Dynamic and Stability analysis of an Orbiter-Tether-Maneuverable subsatellite System," *AAS/AIAA Spaceflight Mechanics Meeting*, Paper No. AAS-91-172, February 1991.

[37] Quadrelli, B.M., Lorenzini, E.C., "Dynamics and Stability of a Tethered Centrifuge in Low Earth Orbit," *The Journal of the Astronautical Sciences*, vol. 40, pp. 3–25, 1992.

[38] Berry, T., "Dynamics of Spinning Tethers," *Bristol Aerospace Report.*

[39] Banerjee, A.K. and Kane, T.R., "Tethered Deployment Dynamics," *The Journal of the Astronautical Sciences*, vol. 30, pp. 347–365, 1982.

[40] Bainum, P.M., Diarra, C.M., and Kumar, V.K., "Shuttle-Tethered Subsatellite System Stability with Flexible Massive Tether," *Journal of Guidance, Control, and Dynamics*, vol. 8, pp. 230–234, 1985.

[41] Lang, D.L, "GTOSS Manual," *David L. Lang and Associates.*

[42] Netzer, E. and Kane, T.R., "An Alternative Approach to Space Missions Involving a Long Tether," *The Journal of the Astronautical Sciences*, vol. 40, pp. 313–327, 1992.

[43] Puig-Suari, J. and Longuski, J.M., "Aerocapture with a Flexible Tether," *Proceeding of the AIAA/AAS Astrodynamics Conference*, August 1992.

[44] Banerjee, A.K., "Order-n Formulation of Extrusion of a Beam with Large Bending and Rotation," *Journal of Guidance, Control, and Dynamics*, vol. 15, pp. 121–127, 1992.

[45] Kim E.S. and Vadali, S.R., "Nonlinear Feedback Deployment and Retrieval of Tethered Satellite Systems," *Journal of Guidance, Control, and Dynamics*, vol. 15, pp. 28–34, 1992.

[46] Modi, V.J., Chang-Fu, G., Misra, A.K., and Xu, D.M., "On the Control of the Space Shuttle Based Tethered Systems," *Acta Astronautica*, vol. 9, pp. 437–443, 1982.

[47] Fujii, H. and Ishijima, S., "Mission Function Control for Deployment and Retrieval of a Subsatellite," *Journal of Guidance, Control, and Dynamics*, vol. 12, pp. 243–247, 1989.

[48] Vadali, S.R. and Kim E.S., "Feedback Control of Tethered Satellites Using Lyapunov Stability Theory," *Journal of Guidance, Control, and Dynamics*, vol. 14, pp. 729–735, 1991.

[49] Misra, A.K. and Modi, V.J., "Deployment and Retrieval of Shuttle Supported Tethered Satellite," *Journal of Guidance, Control, and Dynamics*, vol. 5, pp. 278–285, 1982.

[50] Monshi, N. ,Misra, A.K., and Modi, V.J., "On the Reel Rate Control of Retrieval Dynamics of Tethered Satellite Systems," *AAS/AIAA Spaceflight Mechanics Meeting*, Paper No. AAS-91-175, February 1991.

[51] Lorenzini, E., Arnold, D.A., Grossi, M.D., Gullahorn, G.E., Harrold, W., and Parker, L., "The Investigation of Tethered Satellite System Dynamics," *Smithsonian Institution Astrophysical Observatory, Contract Report NASA-36160*, September 1985.

[52] Fleurisson, E.J., Pines, D.J. and von Flotow, A.H., "Trajectory Design Feedforward and Feedback Stabilization of Tethered Spacecraft Retrieval," *AAS/AIAA Spaceflight Mechanics Meeting*, Paper No. AAS-91-176, February 1991.

[53] Lakshmanan, P.K., Modi, V.J., and Misra, A.K., "Dynamics and Control of the Tethered Satellite System in the Presence of Offsets," *Acta Astronautica*, vol. 19, pp. 145–160, 1989.

[54] Modi, V.J., Lakshmanan, P.K., and Misra, A.K., "Offset Control of Tethered Satellite Systems: Analysis and Experimental Verification," *Acta Astronautica*, vol. 21, pp. 283–294, 1990.

[55] Modi, V.J., Lakshmanan, P.K., and Misra, A.K., "Offset Control Strategy for the Space Station Based Tethered Payload," *The Journal of the Astronautical Sciences*, vol. 39, pp. 205–232, 1991.

[56] Pradhan, S., Modi, V.J., and Misra, A.K., "Dynamics and Control of the Space Platform Based Tethered Satellite Systems," *AAS/AIAA Astrodynamics Specialist Conference*, Paper No. AAS-93-732, August 1993.

[57] Liu, F.C., "On Dynamical Formulation of a Tethered Satellite System with Mass Transfer," *AIAA 23-rd Aerospace Science Meeting*, Paper No. 85-0117, January 1985.

[58] Lorenzini, E.C., "Analytical Investigation of the Dynamics of Tethered Constellation in Earth Orbit," *Smithsonian Institution Astrophysical Observatory, Final Report for NASA/MSFC under Contract NAS8-35497*, December 1984.

[59] Lorenzini, E.C., "A Three-Mass Tethered System for Micro-g/Variable-g Applications," *Journal of Guidance, Control, and Dynamics*, vol. 10, pp. 242–249, 1987.

[60] Misra, A.K., Amier Z.E., and Modi, V.J., "Attitude Dynamics of Three-Body Tethered Systems," *Acta Astronautica*, vol. 17, pp. 1059–1068, 1988.

[61] Lorenzini, E.C., Cosmo, M., Vetrella, S., and Moccia A., "Acceleration Levels on Board the Space Station and a Tethered Elevator for Micro and Variable-Gravity

Applications," *Proceeding of the NASA/PSN/AIAA Second International Conference on Tethers in Space*, pp. 513–522, October 1987.

[62] Cosmo, M., Lorenzini, E.C., Vetrella, S., and Moccia A., "Transient Dynamics of the Tether Elevator/Crawler System," *Proceeding of AIAA/AAS Astrodynamics Conference*, pp. 480–489, August 1988.

[63] Bachmann, S., Modi, V.J., and Misra, A.K., "Dynamic and Control of a Space Station Based Tethered Elevator System," *AAS/AIAA Spaceflight Mechanics Meeting*, Paper No. AAS-91-177, February 1991.

[64] Kumar, K., Jha, O.N., Misra, A.K., and Yan., Y., "Transverse Elastic Oscillations of Three-Body Tethered Systems," *Advances in the Astronautical Sciences*, vol. 76, pp. 2383–2396, 1991.

[65] Misra, A.K. and Modi, V.J., "Three-Dimensional Dynamics and Control of Tether Connected N-Body Systems," *Acta Astronautica*, vol. 26, pp. 77–84, 1992.

[66] Kim, E., *Dynamics and Control of Tethered Satellite Systems*. PhD thesis, Aerospace Engineering, Texas A&M University, May 1993.

[67] Meirovitch, L., *Computational Methods in Structural Dynamics*. Sijthoff & Noordhoff, 1980.

[68] Tsien, H.S., "Superaerodynamics, Mechanics of Rarefied Gases," *Journal of Aeronautical Sciences*, vol. 13, pp. 653–664, 1949.

[69] Siegel, K.M., "Boundaries of Fluid Mechanics," *Journal of Aeronautical Sciences*, vol. 17, pp. 191–192, 1950.

[70] Hayes, W.D. and Probstein, R.F., "Viscous Hypersonic Similitude," *Report No. 59-63, Inst. of Aero. Sci.*, 1959.

[71] Hughes, P.C., *Spacecraft Attitude Dynamics*. New York: John Wiley & Sons. 1986.

[72] NASA, "Models of Earth's Atmosphere (120-1000 km)," *NASA SP-8024*. May 1969.

[73] Geying, F.T. and Westerman, H.R., *Introduction to Orbital Mechanics*. Addison-Wesley Publishing Company, 1971.

[74] Mortenson, R.E., "A Globally Stable Linear Attitude Regulator," *International Journal of Control*, vol. 8, pp. 297–302, 1968.

[75] Vadali, S.R. and Junkins J.L., "Optimal Open Loop and Stable Feedback Control of Rigid Spacecraft Attitude Maneuvers," *The Journal of the Astronautical Sciences*, vol. 32, pp. 105–122, 1984.

[76] Wie, B. and Barba, P.M., "Quaternion Feedback for Spacecraft Large Angle Maneuvers," *Journal of Guidance, Control, and Dynamics*, vol. 8, pp. 360–365, 1985.

[77] Fujii, H. and Ishijima, S., "Mission Function Control Applied to Slew Maneuvers," *38-th Congress of the IAF*, pp. 471–473, October Paper 87-354, 1987.

[78] Lee, B. and Grantham, W.J., "Aeroassisted Orbital Maneuvering Using Lyapunov Optimal Feedback Control," *Journal of Guidance, Control, and Dynamics*, vol. 12, pp. 237–242, 1989.

[79] Junkins, J.L., Rahman, Z., and Bang, H., "Near Minimum-Time Maneuvers of Flexible Vehicles: A Lyapunov Control Design Method," *Mechanics and Control of Large Space Structure*, Published by AIAA, 1990.

[80] Vadali, S.R., "Feedback Tether Deployment and Retrieval," *Journal of Guidance, Control, and Dynamics*, vol. 14, pp. 469–470, 1991.

[81] Rupp, C.C. et al., "Shuttle/Tethered Satellite System Conceptual Design Study," *NASA TMX-73365*, December 1976.

[82] Fujii, H., Uchiyama, K., and Kokubun, K., "Mission Function Control of Tethered Subsatellite Deployment/Retrieval: In-plane and Out-of-Plane Motion," *Journal of Guidance, Control, and Dynamics*, vol. 14, pp. 471–473, 1991.

[83] Meirovitch, L., *Methods of Analytical Dynamics*. New York: McGraw-Hill, 1970.

[84] Shames, I.H., *Mechanics of Fluids*. New York: McGraw Hill, 1982.

[85] McIver, D.B., "Hamilton's Principle for Systems of Changing Mass," *Journal of Engineering Mathematics*, vol. 7, pp. 249–261, 1973.

[86] Laithier, B, *The Dynamics of Timoshinko Tubular Beams Conveying Fluid*. PhD thesis, Mech. Eng. Dept., McGill University, July 1979.

Appendix A

Leibnitz's Integral

In some cases, we need to evaluate time derivative of an integral with time-dependent limits. In fact in this thesis, they have the following form

$$I = \frac{d}{dt}\int_0^{\ell_i} f(x_i, t)\ dx_i \quad , \tag{A.1}$$

where $f(x_i, t)$ can be a scalar or a vector. Using Leibnitz's rule, we obtain

$$I = \int_0^{\ell_i} \frac{\partial}{\partial t} f(x_i, t)\ dx_i + f(\ell_i, t)\dot{\ell}_i \quad . \tag{A.2}$$

Here in our problem, body i reels out tether i at a rate $\alpha_i\dot{\ell}_i$. It implies that $\dot{x}_i = \dfrac{dx_i}{dt} = \alpha_i\dot{\ell}_i$ and is constant along x_i. We can then write

$$\begin{aligned}
I &= \int_0^{\ell_i} \frac{\partial}{\partial t} f(x_i, t)\ dx_i + \alpha_i\dot{\ell}_i f(\ell_i, t) + (1-\alpha_i)\dot{\ell}_i f(\ell_i, t) + \alpha_i\dot{\ell}_i f(0, t) - \alpha_i\dot{\ell}_i f(0, t) \\
&= \int_0^{\ell_i} \frac{\partial}{\partial t} f(x_i, t)\ dx_i + \alpha_i\dot{\ell}_i \left[f(x_i, t)\right]_0^{\ell_i} + (1-\alpha_i)\dot{\ell}_i f(\ell_i, t) + \alpha_i\dot{\ell}_i f(0, t) \\
&= \int_0^{\ell_i} \frac{\partial}{\partial t} f(x_i, t)\ dx_i + \dot{x}_i \left[f(x_i, t)\right]_0^{\ell_i} + (1-\alpha_i)\dot{\ell}_i f(\ell_i, t) + \alpha_i\dot{\ell}_i f(0, t) \quad .
\end{aligned} \tag{A.3}$$

Carrying the constant $\dot{x}_i$ inside the integral leads to

$$I = \int_0^{\ell_i} \left[\frac{\partial}{\partial t} f(x_i, t) + \dot{x}_i \frac{\partial}{\partial x_i} f(x_i, t)\right] dx_i + (1-\alpha_i)\dot{\ell}_i f(\ell_i, t) + \alpha_i\dot{\ell}_i f(0, t) \quad . \tag{A.4}$$

Since $\alpha_i - \beta_i = 1$, we obtain

$$\frac{d}{dt}\int_0^{\ell_i} f(x_i, t)\ dx_i = \int_0^{\ell_i} \frac{d}{dt} f(x_i, t)\ dx_i - \beta_i\dot{\ell}_i f(\ell_i, t) + \alpha_i\dot{\ell}_i f(0, t) \quad , \tag{A.5}$$

where in some cases $f(0, t)$ vanishes and in some cases does not.

Appendix B

Mass Coefficients

Using the definitions of B_j, A_{ij}, and F_{ij}, given in Eqs. (2.14) and (2.32), and the fact that total mass of the system is constant, i.e.

$$\sum_{i=1}^{N} \mu_i = 1 \quad , \tag{B.1}$$

we obtain the following relations which have been used in simplifying the algebra in the formulation.

1. Using Eq. (2.14) we can write

$$\sum_{i=1}^{N} \mu_i A_{ij} = \sum_{i=1}^{N} \mu_i \left[B_j - H(j-i)\right] = B_j \sum_{i=1}^{N} \mu_i - \sum_{i=1}^{N} \mu_i H(j-i) = B_j - B_j \quad . \tag{B.2}$$

   Thus

$$\sum_{i=1}^{N} \mu_i A_{ij} = 0 \quad . \tag{B.3}$$

2. Differentiating Eq. (B.1) with respect to time, t, and generalized coordinate q_r, results in

$$\sum_{i=1}^{N} \dot{\mu}_i = 0 \quad , \qquad \sum_{i=1}^{N} \frac{\partial \mu_i}{\partial q_r} = 0 \quad . \tag{B.4}$$

3. Time differentiation of Eq. (2.14) leads to

$$\dot{A}_{ij} = \frac{d}{dt}\left[B_j - H(j-i)\right] = \dot{B}_j \quad , \tag{B.5}$$

   since $H(j-i)$ is constant.

4. Using the definitions of A_{ij} and B_j, we have

$$\sum_{i=1}^{N}\dot{\mu}_i A_{ij} = \sum_{i=1}^{N}\dot{\mu}_i \left(B_j - H(j-i)\right) = B_j\sum_{i=1}^{N}\dot{\mu}_i - \sum_{i=1}^{N}\dot{\mu}_i H(j-i) = 0 - \dot{B}_j \quad . \tag{B.6}$$

Hence

$$\sum_{i=1}^{N}\dot{\mu}_i A_{ij} = -\dot{B}_j \quad . \tag{B.7}$$

5. Differentiating of Eq. (2.32) with respect to time, we obtain

$$\dot{F}_{ij} = \sum_{k=1}^{N}\frac{d}{dt}\left(\mu_k A_{ki} A_{kj}\right) = \sum_{k=1}^{N}\left(\dot{\mu}_k A_{ki} A_{kj} + \mu_k \dot{B}_i A_{kj} + \mu_k A_{ki}\dot{B}_j\right) \quad . \tag{B.8}$$

Taking out $\dot{B}_i$ and $\dot{B}_j$ from the summation and using Eq. (B.3), we get

$$\begin{aligned}
\dot{F}_{ij} &= \sum_{k=1}^{N}\dot{\mu}_k A_{ki} A_{kj} = \sum_{k=1}^{N}\dot{\mu}_k \left[B_i - H(i-k)\right]\left[B_j - H(j-k)\right] \\
&= B_i B_j \sum_{k=1}^{N}\dot{\mu}_k - B_i\sum_{k=1}^{N}\dot{\mu}_k H(j-k) - B_j\sum_{k=1}^{N}\dot{\mu}_k H(i-k) \\
&\quad + \sum_{k=1}^{N}\dot{\mu}_k H(i-k)H(j-k) \\
&= -B_i\dot{B}_j - B_j\dot{B}_j + \sum_{k=1}^{N}\dot{\mu}_k H(i-k)H(j-k) \quad .
\end{aligned} \tag{B.9}$$

For the last term we can write

$$\sum_{k=1}^{N}\dot{\mu}_k H(i-k)H(j-k) = \begin{cases} \sum_{k=1}^{j}\dot{\mu}_k H(j-k) = \dot{B}_j & \text{if} \quad j < i \\ \sum_{k=1}^{i}\dot{\mu}_k H(i-k) = \dot{B}_i & \text{if} \quad j \geq i \end{cases} \quad . \tag{B.10}$$

Combining these two cases, we have

$$\sum_{k=1}^{N}\dot{\mu}_k H(i-k)H(j-k) = \dot{B}_j H(i-j) + \dot{B}_i H(j-i) - \delta_{ij}\dot{B}_i \quad . \tag{B.11}$$

Backsubstituing in Eq. (B.9) and using the definition of A_{ij}, we obtain

$$\dot{F}_{ij} = -\dot{B}_j A_{ji} - \dot{B}_i A_{ij} - \delta_{ij}\dot{B}_i \quad . \tag{B.12}$$

6. Similarly differentiation of Eq. (2.32) with respect to q_r leads to

$$\frac{\partial F_{ij}}{\partial q_r} = -\frac{\partial B_j}{\partial q_r}A_{ji} - \frac{\partial B_i}{\partial q_r}A_{ij} - \delta_{ij}\frac{\partial B_i}{\partial q_r} \quad . \tag{B.13}$$

7. Differentiating Eq. (2.1) with respect to time implies that

$$\dot{\mu}_i = \frac{\dot{m}_i + \dot{\bar{m}}_i}{m} = \frac{\left(\rho_{i-1}\beta_{i-1}\dot{\ell}_{i-1} - \rho_i\alpha_i\dot{\ell}_i\right) + \rho_i\dot{\ell}_i}{m} = \hat{\rho}_{i-1}\beta_{i-1}\dot{\ell}_{i-1} - \hat{\rho}_i\beta_i\dot{\ell}_i \ , \quad \text{(B.14)}$$

since $\alpha_i - \beta_i = 1$ and $\hat{\rho}_i = \frac{\rho_i}{m}$. Using this result, we can write

$$\dot{B}_j = \sum_{i=1}^{j}\dot{\mu}_j = \sum_{i=1}^{j}\left(\hat{\rho}_{i-1}\beta_{i-1}\dot{\ell}_{i-1} - \hat{\rho}_i\beta_i\dot{\ell}_i\right) = \hat{\rho}_0\beta_0\dot{\ell}_0 - \hat{\rho}_j\beta_j\dot{\ell}_j \ . \quad \text{(B.15)}$$

Since there is no tether number 0, we get

$$\dot{B}_j = -\hat{\rho}_j\beta_j\dot{\ell}_j \ . \quad \text{(B.16)}$$

8. From Eq. (B.16) we conclude that

$$\frac{\partial B_j}{\partial \ell_k} = \frac{\partial \dot{B}_j}{\partial \dot{\ell}_k} = \begin{cases} 0 \ , & k \neq j \ , \\ -\hat{\rho}_j\beta_j \ , & k = j \ , \end{cases} \quad \text{(B.17)}$$

and

$$\ddot{B}_j = -\hat{\rho}_j\left(\dot{\beta}_j\dot{\ell}_j + \beta_j\ddot{\ell}_j\right) \ . \quad \text{(B.18)}$$

Appendix C

Proof to Equation (2.23)

Differentiating Eq. (2.4) with respect to time, we get

$$\frac{d}{dt}\left[\sum_{i=1}^{N} m_i \vec{\mathbf{R}}_i + \sum_{i=1}^{N-1} \rho_i \int_0^{\ell_i} \vec{\mathbf{R}}_{\mathbf{t}_i}\, dx_i\right] = \vec{\mathbf{0}} \ . \tag{C.1}$$

Substituting for $\vec{\mathbf{R}}_{\mathbf{t}_i}$ from Eq. (2.5) we have

$$\sum_{i=1}^{N} (\dot{m}_i + \dot{\bar{m}}_i)\, \vec{\mathbf{R}}_i + \sum_{i=1}^{N} (m_i + \bar{m}_i)\, \dot{\vec{\mathbf{R}}}_i + \sum_{i=1}^{N-1} \rho_i \frac{d}{dt} \int_0^{\ell_i} \vec{\mathbf{r}}_{\mathbf{t}_i}\, dx_i = \vec{\mathbf{0}} \ . \tag{C.2}$$

Using Eq. (A.5) derived in Appendix A and the fact that $\vec{\mathbf{r}}_{\mathbf{t}_i}(0,t) = 0$ and $\vec{\mathbf{r}}_{\mathbf{t}_i}(\ell_i, t) = \vec{\mathbf{r}}_i$, we can rewrite the above relation as

$$\sum_{i=1}^{N} (\dot{m}_i + \dot{\bar{m}}_i)\, \vec{\mathbf{R}}_i + \sum_{i=1}^{N} (m_i + \bar{m}_i)\, \dot{\vec{\mathbf{R}}}_i + \sum_{i=1}^{N-1} \left(\rho_i \int_0^{\ell_i} \dot{\vec{\mathbf{r}}}_{\mathbf{t}_i}\, dx_i - \beta_i \dot{\ell}_i \vec{\mathbf{r}}_i\right) = \vec{\mathbf{0}} \ . \tag{C.3}$$

Since $\dot{\vec{\mathbf{R}}}_i$ is not function of x_i, it can be taken inside the integral sign. Using the definition of $\vec{\mathbf{R}}_{\mathbf{t}_i}$, we obtain

$$\sum_{i=1}^{N} (\dot{m}_i + \dot{\bar{m}}_i)\, \vec{\mathbf{R}}_i - \sum_{i=1}^{N-1} \rho_i \beta_i \dot{\ell}_i \vec{\mathbf{r}}_i + \left[\sum_{i=1}^{N} m_i \dot{\vec{\mathbf{R}}}_i + \sum_{i=1}^{N-1} \rho_i \int_0^{\ell_i} \dot{\vec{\mathbf{R}}}_{\mathbf{t}_i}\, dx_i\right] = \vec{\mathbf{0}} \ . \tag{C.4}$$

Hence

$$\sum_{i=1}^{N} m_i \dot{\vec{\mathbf{R}}}_i + \sum_{i=1}^{N-1} \rho_i \int_0^{\ell_i} \dot{\vec{\mathbf{R}}}_{\mathbf{t}_i}\, dx_i = -\sum_{i=1}^{N} (\dot{m}_i + \dot{\bar{m}}_i)\, \vec{\mathbf{R}}_i + \sum_{i=1}^{N-1} \rho_i \beta_i \dot{\ell}_i \vec{\mathbf{r}}_i \ . \tag{C.5}$$

The right hand side can be simplified by substituting for $\vec{\mathbf{R}}_i$ from Eq. (2.5) and for $\rho_i \beta_i \dot{\ell}_i$ from Eq. (B.16) and changing the index in the last summation:

$$\sum_{i=1}^{N} m_i \dot{\ddot{\mathbf{R}}}_i + \sum_{i=1}^{N-1} \rho_i \int_0^{\ell_i} \dot{\ddot{\mathbf{R}}}_{\mathbf{t}_i} \, dx_i = -m \left[\sum_{i=1}^{N} \dot{\mu}_i \left(\sum_{j=1}^{N-1} A_{ij} \vec{\mathbf{r}}_j - \bar{\mu}_j \vec{\mathbf{b}}_j \right) \right] - \sum_{j=1}^{N-1} \dot{B}_j \vec{\mathbf{r}}_j$$

$$= m \sum_{j=1}^{N-1} \left[\bar{\mu}_j \left(\sum_{i=1}^{N} \dot{\mu}_i \right) \vec{\mathbf{b}}_j - \left(\sum_{i=1}^{N} \dot{\mu}_i A_{ij} \right) \vec{\mathbf{r}}_j - \dot{B}_j \vec{\mathbf{r}}_j \right] \quad . \tag{C.6}$$

Finally using Eqs. (B.4) and (B.7), we would get

$$\sum_{i=1}^{N} m_i \dot{\ddot{\mathbf{R}}}_i + \sum_{i=1}^{N-1} \rho_i \int_0^{\ell_i} \dot{\ddot{\mathbf{R}}}_{\mathbf{t}_i} \, dx_i = m \sum_{j=1}^{N-1} \left(\dot{B}_j \vec{\mathbf{r}}_j - \dot{B}_j \vec{\mathbf{r}}_j \right) = \vec{\mathbf{0}} \quad . \tag{C.7}$$

Appendix D

Definition of Column Arrays and Matrices

Before expressing the desired vectors, column arrays and matrices, the following variables, which are used extensively in this appendix, are defined to shorten the formulation. Recalling the definitions of the admissible functions, $\mathbf{X}_i(s_i), \mathbf{Y}_i(s_i), \mathbf{Z}_i(s_i)$, we define:

$$
\begin{aligned}
&\mathbf{X}_{\ell i} = \mathbf{X}_i(s_i = 1) \quad , \\
&\mathbf{X}_{*i} = \int_0^1 \mathbf{X}_i ds_i \quad , \quad \mathbf{Y}_{*i} = \int_0^1 \mathbf{Y}_i ds_i \quad , \quad \mathbf{Z}_{*i} = \int_0^1 \mathbf{Z}_i ds_i \quad , \\
&\mathbf{X}'_i = \frac{d\mathbf{X}_i}{ds_i} \quad , \quad \mathbf{Y}'_i = \frac{d\mathbf{Y}_i}{ds_i} \quad , \quad \mathbf{Z}'_i = \frac{d\mathbf{Z}_i}{ds_i} \quad , \\
&\mathbf{X}''_i = \frac{d^2\mathbf{X}_i}{ds_i^2} \quad , \quad \mathbf{Y}''_i = \frac{d^2\mathbf{Y}_i}{ds_i^2} \quad , \quad \mathbf{Z}''_i = \frac{d^2\mathbf{Z}_i}{ds_i^2} \quad ,
\end{aligned}
\tag{D.1}
$$

Using the above definitions a set of vectors which are resulted from the elasticity of the tethers, is defined here as follows:

$$
\begin{aligned}
\vec{\vartheta}_i &= \mathbf{X}_i^T \boldsymbol{\xi}_i \, \hat{\mathbf{i}}_i + \mathbf{Y}_i^T \boldsymbol{\eta}_i \, \hat{\mathbf{j}}_i + \mathbf{Z}_i^T \boldsymbol{\nu}_i \, \hat{\mathbf{k}}_i \quad , \\
\vec{\vartheta}_{*i} &= \mathbf{X}_{*i}^T \boldsymbol{\xi}_i \, \hat{\mathbf{i}}_i + \mathbf{Y}_{*i}^T \boldsymbol{\eta}_i \, \hat{\mathbf{j}}_i + \mathbf{Z}_{*i}^T \boldsymbol{\nu}_i \, \hat{\mathbf{k}}_i \quad , \\
\vec{\zeta}_i &= \mathbf{X}_i^T \dot{\boldsymbol{\xi}}_i \, \hat{\mathbf{i}}_i + \mathbf{Y}_i^T \dot{\boldsymbol{\eta}}_i \, \hat{\mathbf{j}}_i + \mathbf{Z}_i^T \dot{\boldsymbol{\nu}}_i \, \hat{\mathbf{k}}_i \quad , \\
\vec{\zeta}_{*i} &= \mathbf{X}_{*i}^T \dot{\boldsymbol{\xi}}_i \, \hat{\mathbf{i}}_i + \mathbf{Y}_{*i}^T \dot{\boldsymbol{\eta}}_i \, \hat{\mathbf{j}}_i + \mathbf{Z}_{*i}^T \dot{\boldsymbol{\nu}}_i \, \hat{\mathbf{k}}_i \quad , \\
\vec{\varsigma}_i &= \mathbf{X'}_i^T \boldsymbol{\xi}_i \, \hat{\mathbf{i}}_i + \mathbf{Y'}_i^T \boldsymbol{\eta}_i \, \hat{\mathbf{j}}_i + \mathbf{Z'}_i^T \boldsymbol{\nu}_i \, \hat{\mathbf{k}}_i \quad , \\
\vec{\varrho}_i &= \mathbf{X''}_i^T \boldsymbol{\xi}_i \, \hat{\mathbf{i}}_i + \mathbf{Y''}_i^T \boldsymbol{\eta}_i \, \hat{\mathbf{j}}_i + \mathbf{Z''}_i^T \boldsymbol{\nu}_i \, \hat{\mathbf{k}}_i \quad ,
\end{aligned}
$$

$$\vec{\kappa}_i = \mathbf{X}'^T_i \dot{\boldsymbol{\xi}}_i \, \hat{\mathbf{i}}_i + \mathbf{Y}'^T_i \dot{\boldsymbol{\eta}}_i \, \hat{\mathbf{j}}_i + \mathbf{Z}'^T_i \dot{\boldsymbol{\nu}}_i \, \hat{\mathbf{k}}_i \quad . \tag{D.2}$$

Another set of vectors, corresponding to the rotation of the tethers, is defined as:

$$\begin{aligned}
\vec{\boldsymbol{A}}_i &= \left[\dot{\varphi}_i \left(\dot{\theta}_0 + \dot{\theta}_i\right) \cos\phi_i + \ddot{\theta}_0 \sin\phi_i\right] \hat{\mathbf{i}}_i + \left[-\dot{\phi}_i \left(\dot{\theta}_0 + \dot{\theta}_i\right) \sin\varphi_i + \ddot{\theta}_0 \cos\phi_i\right] \hat{\mathbf{k}}_i \quad , \\
\vec{\boldsymbol{\alpha}}_i &= \left(\dot{\theta}_0 + \dot{\theta}_i\right) \cos\phi_i \hat{\mathbf{i}}_i - \left(\dot{\theta}_0 + \dot{\theta}_i\right) \sin\phi_i \hat{\mathbf{k}}_i \quad , \\
\vec{\boldsymbol{\beta}}_i &= \left[-\dot{\phi}_i \left(\dot{\theta}_0 + \dot{\theta}_i\right) \sin\varphi_i + \ddot{\theta}_0 \cos\varphi_i\right] \hat{\mathbf{i}}_i + \left[-\dot{\varphi}_i \left(\dot{\theta}_0 + \dot{\theta}_i\right) \cos\varphi_i - \ddot{\theta}_0 \sin\varphi_i\right] \hat{\mathbf{k}}_i \quad , \\
\vec{\gamma}_i &= \sin\phi_i \hat{\mathbf{i}}_i + \cos\phi_i \hat{\mathbf{k}}_i \quad , \\
\vec{\boldsymbol{\sigma}}_i &= \dot{\phi}_i (\cos\phi_i \hat{\mathbf{i}}_i - \sin\phi_i \hat{\mathbf{k}}_i) \quad .
\end{aligned} \tag{D.3}$$

D.1 Position Vectors, $\vec{\mathbf{r}}_i, \vec{\mathbf{b}}_i, \vec{\mathbf{r}}_{\mathbf{t}_i}$

Local position vectors $\vec{\mathbf{r}}_i, \vec{\mathbf{r}}_{\mathbf{t}_i}$, and $\vec{\mathbf{b}}_i$ in tether coordinate system are defined as:

$$\begin{aligned}
\vec{\mathbf{r}}_i &= \left(\ell_i + \mathbf{X}_{\ell_i}^T \boldsymbol{\xi}_i\right) \hat{\mathbf{i}}_i \quad , \\
\vec{\mathbf{r}}_{\mathbf{t}_i} &= x_i \hat{\mathbf{i}}_i + \vec{\boldsymbol{\vartheta}}_i \quad , \\
\vec{\mathbf{b}}_i &= \frac{1}{\ell_0} \int_0^{\ell_i} \vec{\mathbf{r}}_{\mathbf{t}_i} dx_i = \frac{\ell_i^2}{2\ell_0} \hat{\mathbf{i}}_i + \frac{\ell_i}{\ell_0} \vec{\boldsymbol{\vartheta}}_{*i} \quad .
\end{aligned} \tag{D.4}$$

D.2 Velocity Vectors, $\dot{\vec{\mathbf{r}}}_i, \dot{\vec{\mathbf{b}}}_i, \dot{\vec{\mathbf{r}}}_{\mathbf{t}_i}$

The time derivatives of the position vectors in the inertial frame are related to those of tether frame through the following equations;

$$\begin{aligned}
\dot{\vec{\mathbf{r}}}_i &= \mathring{\vec{\mathbf{r}}}_i + \vec{\boldsymbol{\Omega}}_i \times \vec{\mathbf{r}}_i \quad , \\
\dot{\vec{\mathbf{b}}}_i &= \mathring{\vec{\mathbf{b}}}_i + \vec{\boldsymbol{\Omega}}_i \times \vec{\mathbf{b}}_i \quad , \\
\dot{\vec{\mathbf{r}}}_{\mathbf{t}_i} &= \mathring{\vec{\mathbf{r}}}_{\mathbf{t}_i} + \vec{\boldsymbol{\Omega}}_i \times \vec{\mathbf{r}}_{\mathbf{t}_i} \quad ,
\end{aligned} \tag{D.5}$$

where $\vec{\boldsymbol{\Omega}}_i$ is defined earlier and the local time derivatives are given by

$$\begin{aligned}
\mathring{\vec{\mathbf{r}}}_i &= \left(\dot{\ell}_i + \mathbf{X}_{\ell_i}^T \dot{\boldsymbol{\xi}}_i\right) \hat{\mathbf{i}}_i \quad , \\
\mathring{\vec{\mathbf{b}}}_i &= \frac{\ell_i \dot{\ell}_i}{\ell_0} \hat{\mathbf{i}}_i + \frac{\dot{\ell}_i}{\ell_0} \vec{\boldsymbol{\vartheta}}_{*i} + \frac{\ell_i}{\ell_0} \vec{\boldsymbol{\zeta}}_{*i} \quad , \\
\mathring{\vec{\mathbf{r}}}_{\mathbf{t}_i} &= \dot{\ell}_i \hat{\mathbf{i}}_i + \dot{s}_i \vec{\boldsymbol{\varsigma}}_i + \vec{\boldsymbol{\zeta}}_i \quad .
\end{aligned} \tag{D.6}$$

D.3 Vectors $\vec{\mathbf{d}}_{\mathbf{r}_i}, \vec{\mathbf{d}}_{\mathbf{b}_i}, \vec{\mathbf{d}}_{\mathbf{t}_i}$

Vectors $\vec{\mathbf{d}}_{\mathbf{r}_i}, \vec{\mathbf{d}}_{\mathbf{b}_i}, \vec{\mathbf{d}}_{\mathbf{t}_i}$, used in Eq. (4.5), are defined as

$$
\begin{aligned}
\vec{\mathbf{d}}_{\mathbf{r}_i} &= 2\vec{\Omega}_i \times \overset{\circ}{\vec{\mathbf{r}}}_i + \vec{\Omega}_i \times (\vec{\Omega}_i \times \vec{\mathbf{r}}_i) + \vec{\Lambda}_i \times \vec{\mathbf{r}}_i \ , \\
\vec{\mathbf{d}}_{\mathbf{b}_i} &= \frac{\dot{\ell}_i^2}{\ell_0}\hat{\mathbf{i}}_i + \frac{2\dot{\ell}_i}{\ell_0}\vec{\zeta}_{*i} + 2\vec{\Omega}_i \times \overset{\circ}{\vec{\mathbf{b}}}_i + \vec{\Omega}_i \times (\vec{\Omega}_i \times \vec{\mathbf{b}}_i) + \vec{\Lambda}_i \times \vec{\mathbf{b}}_i \ , \\
\vec{\mathbf{d}}_{\mathbf{t}_i} &= \frac{-2\dot{s}_i\dot{\ell}_i}{\ell_i}\vec{\varsigma}_i + \dot{s}_i^2\vec{\varrho}_i + 2\dot{s}_i\vec{\zeta}_i + 2\vec{\Omega}_i \times \overset{\circ}{\vec{\mathbf{r}}}_{\mathbf{t}_i} + \vec{\Omega}_i \times (\vec{\Omega}_i \times \vec{\mathbf{r}}_{\mathbf{t}_i}) + \vec{\Lambda}_i \times \vec{\mathbf{r}}_{\mathbf{t}_i} \ , \qquad \text{(D.7)}
\end{aligned}
$$

where $\dot{s}_i = \dfrac{\dot{\ell}_i}{\ell_i}(\alpha_i - s_i)$, and α_i as defined earlier is the reeling rate of tether i from the i-th body.

D.4 Column Vectors $\mathcal{D}$'s

The column vectors $\mathcal{D}_{\mathbf{r}_i}, \mathcal{D}_{\mathbf{b}_i}$, and $\mathcal{D}_{\mathbf{t}_i}$ are in fact partial derivatives of vectors $\vec{\mathbf{r}}_i, \vec{\mathbf{b}}_i$, and $\vec{\mathbf{r}}_{\mathbf{t}_i}$ with respect to the elements of generalized coordinates corresponding to the i-th tether, $\mathbf{q}_i$, respectively. They are given by

$$
\mathcal{D}_{\mathbf{r}_i} = \begin{Bmatrix} \vec{\gamma}_i \times \vec{\mathbf{r}}_i \\ -\hat{\mathbf{j}}_i \times \vec{\mathbf{r}}_i \\ \hat{\mathbf{i}}_i \\ \mathbf{X}_{\ell i}\,\hat{\mathbf{i}}_i \\ \{\vec{0}\} \\ \{\vec{0}\} \end{Bmatrix}, \quad
\mathcal{D}_{\mathbf{b}_i} = \begin{Bmatrix} \vec{\gamma}_i \times \vec{\mathbf{b}}_i \\ -\hat{\mathbf{j}}_i \times \vec{\mathbf{b}}_i \\ \dfrac{1}{\ell_i}\vec{\mathbf{b}}_i + \dfrac{\ell_i}{2\ell_0}\hat{\mathbf{i}}_i \\ \ell_i\mathbf{X}_{*i}\,\hat{\mathbf{i}}_i/\ell_0 \\ \ell_i\mathbf{Y}_{*i}\,\hat{\mathbf{j}}_i/\ell_0 \\ \ell_i\mathbf{Z}_{*i}\,\hat{\mathbf{k}}_i/\ell_0 \end{Bmatrix}, \quad
\mathcal{D}_{\mathbf{t}_i} = \begin{Bmatrix} \vec{\gamma}_i \times \vec{\mathbf{r}}_{\mathbf{t}_i} \\ -\hat{\mathbf{j}}_i \times \vec{\mathbf{r}}_{\mathbf{t}_i} \\ \hat{\mathbf{i}}_i + \dfrac{1-s_i}{\ell_i}\vec{\varsigma}_i \\ \mathbf{X}_i\,\hat{\mathbf{i}}_i \\ \mathbf{Y}_i\,\hat{\mathbf{j}}_i \\ \mathbf{Z}_i\,\hat{\mathbf{k}}_i \end{Bmatrix}, \qquad \text{(D.8)}
$$

D.5 Column Vectors $\mathcal{P}$'s

The column vectors $\mathcal{P}_{\mathbf{r}_i}, \mathcal{P}_{\mathbf{b}_i}$, and $\mathcal{P}_{\mathbf{t}_i}$ which are partial derivatives of position vectors $\vec{\mathbf{d}}_{\mathbf{r}_i}, \vec{\mathbf{d}}_{\mathbf{b}_i}$, and $\vec{\mathbf{d}}_{\mathbf{t}_i}$, respectively, with respect to the elements of $\mathbf{q}_i$ are given by

$$
\mathcal{P}_{\mathbf{r}_i} = \left\{ \begin{array}{c}
\vec{\gamma}_i \times \vec{\mathbf{d}}_{\mathbf{r}_i} \\[2ex]
-\hat{\mathbf{j}}_i \times \vec{\mathbf{d}}_{\mathbf{r}_i} + 2\vec{\alpha}_i \times \overset{\circ}{\vec{\mathbf{r}}}_i + \vec{\Omega}_i \times (\vec{\alpha}_i \times \vec{\mathbf{r}}_i) \\
+\vec{\alpha}_i \times (\vec{\Omega}_i \times \vec{\mathbf{r}}_i) + \vec{\beta}_i \times \vec{\mathbf{r}}_i \\[2ex]
\mathbf{X}_{\ell_i}[\vec{\Omega}_i \times (\vec{\Omega}_i \times \hat{\mathbf{i}}_i) + \vec{\Lambda}_i \times \hat{\mathbf{i}}_i] \\[2ex]
\left\{\vec{0}\right\} \\[2ex]
\left\{\vec{0}\right\}
\end{array} \right\},
$$

$$
\mathcal{P}_{\mathbf{b}_i} = \left\{ \begin{array}{c}
\vec{\gamma}_i \times \vec{\mathbf{d}}_{\mathbf{b}_i} \\[2ex]
-\hat{\mathbf{j}}_i \times \vec{\mathbf{d}}_{\mathbf{b}_i} + 2\vec{\alpha}_i \times \overset{\circ}{\vec{\mathbf{b}}}_i + \vec{\Omega}_i \times (\vec{\alpha}_i \times \vec{\mathbf{b}}_i) \\
+\vec{\alpha}_i \times (\vec{\Omega}_i \times \vec{\mathbf{b}}_i) + \vec{\beta}_i \times \vec{\mathbf{b}}_i \\[2ex]
\mathbf{X}_{*i}\left\{2\dot{\ell}_i(\vec{\Omega}_i \times \hat{\mathbf{i}}_i) + \ell_i[\vec{\Omega}_i \times (\vec{\Omega}_i \right. \\
\left. \times \hat{\mathbf{i}}_i)] + \ell_i(\vec{\Lambda}_i \times \hat{\mathbf{i}}_i)\right\}/\ell_0 \\[2ex]
\mathbf{Y}_{*i}\left\{2\dot{\ell}_i(\vec{\Omega}_i \times \hat{\mathbf{j}}_i) + \ell_i[\vec{\Omega}_i \times (\vec{\Omega}_i \right. \\
\left. \times \hat{\mathbf{j}}_i)] + \ell_i(\vec{\Lambda}_i \times \hat{\mathbf{j}}_i)\right\}/\ell_0 \\[2ex]
\mathbf{Z}_{*i}\left\{2\dot{\ell}_i(\vec{\Omega}_i \times \hat{\mathbf{k}}_i) + \ell_i[\vec{\Omega}_i \times (\vec{\Omega}_i \right. \\
\left. \times \hat{\mathbf{k}}_i)] + \ell_i(\vec{\Lambda}_i \times \hat{\mathbf{k}}_i)\right\}/\ell_0
\end{array} \right\},
$$

$$
\mathcal{P}_{\mathbf{t}_i} = \left\{ \begin{array}{l}
\vec{\gamma}_i \times \vec{\mathbf{d}}_{\mathbf{t}_i} \\[2ex]
-\hat{\mathbf{j}}_i \times \vec{\mathbf{d}}_{\mathbf{t}_i} + 2\vec{\alpha}_i \times \overset{\circ}{\vec{\mathbf{r}}}_{\mathbf{t}_i} + \vec{\Omega}_i \times (\vec{\alpha}_i \times \vec{\mathbf{r}}_{\mathbf{t}_i}) \\
+\vec{\alpha}_i \times (\vec{\Omega}_i \times \vec{\mathbf{r}}_{\mathbf{t}_i}) + \vec{\beta}_i \times \vec{\mathbf{r}}_{\mathbf{t}_i} \\[2ex]
\dot{s}_i \left\{ [-2\dfrac{\dot{\ell}_i}{\ell_i}\mathbf{X}'_i + \dot{s}_i\mathbf{X}''_i]\hat{\mathbf{i}}_i + 2\mathbf{X}'_i(\vec{\Omega}_i \times \hat{\mathbf{i}}_i) \right\} \\
+ \mathbf{X}_i[\vec{\Omega}_i \times (\vec{\Omega}_i \times \hat{\mathbf{i}}_i) + (\vec{\Lambda}_i \times \hat{\mathbf{i}}_i)] \\[2ex]
\dot{s}_i \left\{ [-2\dfrac{\dot{\ell}_i}{\ell_i}\mathbf{Y}'_i + \dot{s}_i\mathbf{Y}''_i]\hat{\mathbf{j}}_i + 2\mathbf{Y}'_i(\vec{\Omega}_i \times \hat{\mathbf{j}}_i) \right\} \\
+ \mathbf{Y}_i[\vec{\Omega}_i \times (\vec{\Omega}_i \times \hat{\mathbf{j}}_i) + (\vec{\Lambda}_i \times \hat{\mathbf{j}}_i)] \\[2ex]
\dot{s}_i \left\{ [-2\dfrac{\dot{\ell}_i}{\ell_i}\mathbf{Z}'_i + \dot{s}_i\mathbf{Z}''_i]\hat{\mathbf{k}}_i + 2\mathbf{Z}'_i(\vec{\Omega}_i \times \hat{\mathbf{k}}_i) \right\} \\
+ \mathbf{Z}_i[\vec{\Omega}_i \times (\vec{\Omega}_i \times \hat{\mathbf{k}}_i) + (\vec{\Lambda}_i \times \hat{\mathbf{k}}_i)]
\end{array} \right\} . \qquad \text{(D.9)}
$$

D.6 Column Vectors $\mathcal{R}$'s

The column vectors $\mathcal{R}_{\mathbf{r}_i}, \mathcal{R}_{\mathbf{b}_i}$, and $\mathcal{R}_{\mathbf{t}_i}$ are partial derivatives of vectors $\vec{\mathbf{d}}_{\mathbf{r}_i}, \vec{\mathbf{d}}_{\mathbf{b}_i}$, and $\vec{\mathbf{d}}_{\mathbf{t}_i}$ with respect to the elements of generalized speeds, $\dot{\mathbf{q}}_i$, respectively. They are given by

$$
\mathcal{R}_{\mathbf{r}_i} = \left\{ \begin{array}{c}
2\vec{\gamma}_i \times \overset{\circ}{\vec{\mathbf{r}}}_i + \vec{\Omega}_i \times (\vec{\gamma}_i \times \vec{\mathbf{r}}_i) + \vec{\gamma}_i \times (\vec{\Omega}_i \times \vec{\mathbf{r}}_i) + \vec{\sigma}_i \times \vec{\mathbf{r}}_i \\[2ex]
-2\hat{\mathbf{j}}_i \times \overset{\circ}{\vec{\mathbf{r}}}_i - \vec{\Omega}_i \times (\hat{\mathbf{j}}_i \times \vec{\mathbf{r}}_i) - \hat{\mathbf{j}}_i \times (\vec{\Omega}_i \times \vec{\mathbf{r}}_i) + \vec{\alpha}_i \times \vec{\mathbf{r}}_i \\[2ex]
2\mathbf{X}_{\ell i}(\vec{\Omega}_i \times \hat{\mathbf{i}}_i) \\[2ex]
\{\vec{0}\} \\[2ex]
\{\vec{0}\}
\end{array} \right\} ,
$$

$$
\mathcal{R}_{\mathbf{b}_i} = \left\{ \begin{array}{c}
2\vec{\gamma}_i \times \overset{\circ}{\vec{\mathbf{b}}}_i + \vec{\Omega}_i \times (\vec{\gamma}_i \times \vec{\mathbf{b}}_i) + \vec{\gamma}_i \times (\vec{\Omega}_i \times \vec{\mathbf{b}}_i) + \vec{\sigma}_i \times \vec{\mathbf{b}}_i \\[2ex]
-2\hat{\mathbf{j}}_i \times \overset{\circ}{\vec{\mathbf{b}}}_i - \vec{\Omega}_i \times (\hat{\mathbf{j}}_i \times \vec{\mathbf{b}}_i) - \hat{\mathbf{j}}_i \times (\vec{\Omega}_i \times \vec{\mathbf{b}}_i) + \vec{\alpha}_i \times \vec{\mathbf{b}}_i \\[2ex]
\dfrac{2}{\ell_0} \mathbf{X}_{*i} (\dot{\ell}_i \hat{\mathbf{i}}_i + \ell_i \vec{\Omega}_i \times \hat{\mathbf{i}}_i) \\[2ex]
\dfrac{2}{\ell_0} \mathbf{Y}_{*i} (\dot{\ell}_i \hat{\mathbf{j}}_i + \ell_i \vec{\Omega}_i \times \hat{\mathbf{j}}_i) \\[2ex]
\dfrac{2}{\ell_0} \mathbf{Z}_{*i} (\dot{\ell}_i \hat{\mathbf{k}}_i + \ell_i \vec{\Omega}_i \times \hat{\mathbf{k}}_i)
\end{array} \right\} ,
$$

$$
\mathcal{R}_{\mathbf{t}_i} = \left\{ \begin{array}{c}
2\vec{\gamma}_i \times \overset{\circ}{\vec{\mathbf{r}}}_{\mathbf{t}_i} + \vec{\Omega}_i \times (\vec{\gamma}_i \times \vec{\mathbf{r}}_{\mathbf{t}_i}) + \vec{\gamma}_i \times (\vec{\Omega}_i \times \vec{\mathbf{r}}_{\mathbf{t}_i}) + \vec{\sigma}_i \times \vec{\mathbf{r}}_{\mathbf{t}_i} \\[2ex]
-2\hat{\mathbf{j}}_i \times \overset{\circ}{\vec{\mathbf{r}}}_{\mathbf{t}_i} - \vec{\Omega}_i \times (\hat{\mathbf{j}}_i \times \vec{\mathbf{r}}_{\mathbf{t}_i}) - \hat{\mathbf{j}}_i \times (\vec{\Omega}_i \times \vec{\mathbf{r}}_{\mathbf{t}_i}) + \vec{\alpha}_i \times \vec{\mathbf{r}}_{\mathbf{t}_i} \\[2ex]
2\mathbf{X}_i (\vec{\Omega}_i \times \hat{\mathbf{i}}_i) + 2\dot{s}_i \mathbf{X}'_i \hat{\mathbf{i}}_i \\[2ex]
2\mathbf{Y}_i (\vec{\Omega}_i \times \hat{\mathbf{j}}_i) + 2\dot{s}_i \mathbf{Y}'_i \hat{\mathbf{j}}_i \\[2ex]
2\mathbf{Z}_i (\vec{\Omega}_i \times \hat{\mathbf{k}}_i) + 2\dot{s}_i \mathbf{Z}'_i \hat{\mathbf{k}}_i
\end{array} \right\} , \tag{D.10}
$$

D.7 Matrices $\mathcal{J}$'s

Matrices $\mathcal{J}_{\mathbf{r}_i}, \mathcal{J}_{\mathbf{b}_i}, \mathcal{J}_{\mathbf{t}_i}$, defined in Eq. (4.33), are indeed Jacobian matrices of position vectors $\vec{\mathbf{r}}_i, \vec{\mathbf{b}}_i, \vec{\mathbf{r}}_{\mathbf{t}_i}$ with respect to $\mathbf{q}_i$, respectively, i.e.

$$
\mathcal{J}_{\mathbf{r}_i} = \frac{\partial}{\partial \mathbf{q}_i} \left(\frac{\partial \vec{\mathbf{r}}_i}{\partial \mathbf{q}_i} \right) , \quad \mathcal{J}_{\mathbf{b}_i} = \frac{\partial}{\partial \mathbf{q}_i} \left(\frac{\partial \vec{\mathbf{b}}_i}{\partial \mathbf{q}_i} \right) , \quad \mathcal{J}_{\mathbf{t}_i} = \frac{\partial}{\partial \mathbf{q}_i} \left(\frac{\partial \vec{\mathbf{r}}_{\mathbf{t}_i}}{\partial \mathbf{q}_i} \right) . \tag{D.11}
$$

Since they are symmetric matrices, only the lower triangular part of the matrices are presented here.

$$\mathcal{J}_{\mathbf{r}_i} = \begin{bmatrix} \vec{\gamma}_i \times (\vec{\gamma}_i \times \vec{\mathbf{r}}_i) & * & * & * & * \\ (\hat{\mathbf{j}}_i \times \vec{\mathbf{r}}_i) \times \vec{\gamma}_i & \hat{\mathbf{j}}_i \times (\hat{\mathbf{j}}_i \times \vec{\mathbf{r}}_i) & * & * & * \\ \mathbf{X}_{\ell i} \cos\phi_i \hat{\mathbf{j}}_i & \mathbf{X}_{\ell i}\hat{\mathbf{k}}_i & \left[\vec{\mathbf{0}}\right] & * & * \\ \left\{\vec{\mathbf{0}}\right\} & \left\{\vec{\mathbf{0}}\right\} & \left[\vec{\mathbf{0}}\right] & \left[\vec{\mathbf{0}}\right] & * \\ \left\{\vec{\mathbf{0}}\right\} & \left\{\vec{\mathbf{0}}\right\} & \left[\vec{\mathbf{0}}\right] & \left[\vec{\mathbf{0}}\right] & \left[\vec{\mathbf{0}}\right] \end{bmatrix} .$$

$$\mathcal{J}_{\mathbf{b}_i} = \frac{1}{\ell_0} \begin{bmatrix} \ell_0 \vec{\gamma}_i \times (\vec{\gamma}_i \times \vec{\mathbf{b}}_i) & * & * & * & * \\ \ell_0 (\hat{\mathbf{j}}_i \times \vec{\mathbf{b}}_i) \times \vec{\gamma}_i & \ell_0 \hat{\mathbf{j}}_i \times (\hat{\mathbf{j}}_i \times \vec{\mathbf{b}}_i) & * & * & * \\ \ell_i \mathbf{X}_{\bullet i} \cos\phi_i \hat{\mathbf{j}}_i & \ell_i \mathbf{X}_{\bullet i} \hat{\mathbf{k}}_i & \left[\vec{\mathbf{0}}\right] & * & * \\ \ell_i \mathbf{Y}_{\bullet i}(\sin\phi_i \hat{\mathbf{k}}_i - \cos\phi_i \hat{\mathbf{i}}_i) & \left\{\vec{\mathbf{0}}\right\} & \left[\vec{\mathbf{0}}\right] & \left[\vec{\mathbf{0}}\right] & * \\ -\ell_i \mathbf{Z}_{\bullet i} \sin\phi_i \hat{\mathbf{j}}_i & -\ell_i \mathbf{Z}_{\bullet i} \hat{\mathbf{i}}_i & \left[\vec{\mathbf{0}}\right] & \left[\vec{\mathbf{0}}\right] & \left[\vec{\mathbf{0}}\right] \end{bmatrix} ,$$

$$\mathcal{J}_{\mathbf{t}_i} = \begin{bmatrix} \vec{\gamma}_i \times (\vec{\gamma}_i \times \vec{\mathbf{r}}_{\mathbf{t}_i}) & * & * & * & * \\ (\hat{\mathbf{j}}_i \times \vec{\mathbf{b}}_i) \times \vec{\gamma}_i & \hat{\mathbf{j}}_i \times (\hat{\mathbf{j}}_i \times \vec{\mathbf{r}}_{\mathbf{t}_i}) & * & * & * \\ \mathbf{X}_i \cos\phi_i \hat{\mathbf{j}}_i & \mathbf{X}_i \hat{\mathbf{k}}_i & \left[\vec{\mathbf{0}}\right] & * & * \\ \mathbf{Y}_i(\sin\phi_i \hat{\mathbf{k}}_i - \cos\phi_i \hat{\mathbf{i}}_i) & \left\{\vec{\mathbf{0}}\right\} \hat{\mathbf{i}}_i & \left[\vec{\mathbf{0}}\right] & \left[\vec{\mathbf{0}}\right] & * \\ -\mathbf{Z}_i \sin\phi_i \hat{\mathbf{j}}_i & -\mathbf{Z}_i \hat{\mathbf{i}}_i & \left[\vec{\mathbf{0}}\right] & \left[\vec{\mathbf{0}}\right] & \left[\vec{\mathbf{0}}\right] \end{bmatrix} . \quad \text{(D.12)}$$

Appendix E

Rigid Longitudinal Equation of Motion

In the case of length equation, $q_r = \ell_n$, one should exercise care to carry out the differentiation of integrals with length-dependent limits. Let us substitute ℓ_n for $\mathbf{q}_n$ in $\mathbf{S}_n$ defined in Eq. (2.75) and rewrite it as

$$S_{\ell_n} = \frac{EA_n}{m}\frac{\partial}{\partial \ell_n}\left(\int_0^{\ell_n} \mathcal{E}_n dx_n\right) + \hat{\rho}_n \alpha_0^2 \frac{\partial}{\partial \ell_n}\int_0^{\ell_n} \frac{1}{2}\left\{\vec{\mathbf{r}}_{\mathbf{t}_n} - 3(\hat{\mathbf{i}}_c \cdot \vec{\mathbf{r}}_{\mathbf{t}_n})\hat{\mathbf{i}}_c\right\} \cdot \vec{\mathbf{r}}_{\mathbf{t}_n} dx_n$$
$$+ \hat{\rho}_n \left(\frac{d}{dt}\frac{\partial}{\partial \dot{\ell}_n} - \frac{\partial}{\partial \ell_n}\right)\left(\int_0^{\ell_n} \frac{1}{2}\dot{\vec{\mathbf{r}}}_{\mathbf{t}_n} \cdot \dot{\vec{\mathbf{r}}}_{\mathbf{t}_n} dx_n\right) \quad . \tag{E.1}$$

Since all the integrands are functions of ℓ_n as well as x_n, because of the way the admissible functions were defined, we should use Leibnitz's rule to carry out the differentiation inside the integrals. Having done so, we would get

$$S_{\ell_n} = \frac{(EA)_n}{m}\int_0^{\ell_n} \frac{\partial \mathcal{E}_n}{\partial \ell_n} dx_n + \frac{(EA)_n}{m}\left(\mathcal{E}_n\right)_{x_n=\ell_n} + \hat{\rho}_n \alpha_0^2 \int_0^{\ell_n} \frac{\partial}{\partial \ell_n}\left[\frac{1}{2}\left\{\vec{\mathbf{r}}_{\mathbf{t}_n}\right.\right.$$
$$\left.\left. - 3(\hat{\mathbf{i}}_c \cdot \vec{\mathbf{r}}_{\mathbf{t}_n})\hat{\mathbf{i}}_c\right\} \cdot \vec{\mathbf{r}}_{\mathbf{t}_n}\right] dx_n + \frac{1}{2}\hat{\rho}_n \alpha_0^2 \left[\left\{\vec{\mathbf{r}}_{\mathbf{t}_n} - 3(\hat{\mathbf{i}}_c \cdot \vec{\mathbf{r}}_{\mathbf{t}_n})\hat{\mathbf{i}}_c\right\} \cdot \vec{\mathbf{r}}_{\mathbf{t}_n}\right]_{x_n=\ell_n}$$
$$+ \hat{\rho}_n \left(\frac{d}{dt}\frac{\partial}{\partial \dot{\ell}_n} - \frac{\partial}{\partial \ell_n}\right)\int_0^{\ell_n} \frac{1}{2}\dot{\vec{\mathbf{r}}}_{\mathbf{t}_n} \cdot \dot{\vec{\mathbf{r}}}_{\mathbf{t}_n} dx_n \quad . \tag{E.2}$$

In order to compute S_{ℓ_n}, let us first deal with the term

$$I = \frac{d}{dt}\int_0^{\ell_n} \frac{\partial}{\partial \dot{\ell}_n}\left(\frac{1}{2}\dot{\vec{\mathbf{r}}}_{\mathbf{t}_n} \cdot \dot{\vec{\mathbf{r}}}_{\mathbf{t}_n}\right) dx_n - \frac{\partial}{\partial \ell_n}\int_0^{\ell_n} \frac{1}{2}\dot{\vec{\mathbf{r}}}_{\mathbf{t}_n} \cdot \dot{\vec{\mathbf{r}}}_{\mathbf{t}_n} dx_n \quad . \tag{E.3}$$

Since $\vec{\mathbf{r}}_{\mathbf{t}_n}$ is a function of the spatial coordinate x_n, tether length ℓ_n, and time t, i.e. $\vec{\mathbf{r}}_{\mathbf{t}_n} = \vec{\mathbf{r}}_{\mathbf{t}_n}(x_n, \ell_n, t)$, then we can write[1]

$$\dot{\vec{\mathbf{r}}}_{\mathbf{t}_n} = \dot{x}_n \frac{\partial \vec{\mathbf{r}}_{\mathbf{t}_n}}{\partial x_n} + \dot{\ell}_n \frac{\partial \vec{\mathbf{r}}_{\mathbf{t}_n}}{\partial \ell_n} + \frac{\partial \vec{\mathbf{r}}_{\mathbf{t}_n}}{\partial t} \quad . \tag{E.4}$$

Since $\dot{x}_n = \dot{\ell}_n$ we get

$$\frac{\partial \dot{\vec{\mathbf{r}}}_{\mathbf{t}_n}}{\partial \dot{\ell}_n} = \frac{\partial \vec{\mathbf{r}}_{\mathbf{t}_n}}{\partial x_n} + \frac{\partial \vec{\mathbf{r}}_{\mathbf{t}_n}}{\partial \ell_n} \quad . \tag{E.5}$$

Note that this is not consistent with

$$\frac{\partial \dot{\vec{\mathbf{r}}}}{\partial \dot{q}} = \frac{\partial \vec{\mathbf{r}}}{\partial q} \quad , \tag{E.6}$$

because of the convective term $\dot{x}_n \dfrac{\partial \vec{\mathbf{r}}_{\mathbf{t}_n}}{\partial x_n}$.

Using Eqs. (E.5) and (A.5), I can be rewritten as

$$\begin{aligned} I = {} & \int_0^{\ell_n} \left[\ddot{\vec{\mathbf{r}}}_{\mathbf{t}_n} \cdot \left(\frac{\partial \vec{\mathbf{r}}_{\mathbf{t}_n}}{\partial x_n} + \frac{\partial \vec{\mathbf{r}}_{\mathbf{t}_n}}{\partial \ell_n} \right) + \dot{\vec{\mathbf{r}}}_{\mathbf{t}_n} \cdot \left(\frac{\partial \dot{\vec{\mathbf{r}}}_{\mathbf{t}_n}}{\partial x_n} + \frac{\partial \dot{\vec{\mathbf{r}}}_{\mathbf{t}_n}}{\partial \ell_n} \right) \right] dx_n \\ & - \frac{\partial}{\partial \ell_n} \int_0^{\ell_n} \frac{1}{2} \dot{\vec{\mathbf{r}}}_{\mathbf{t}_n} \cdot \dot{\vec{\mathbf{r}}}_{\mathbf{t}_n} dx_n - \beta_n \dot{\ell}_n \left[\dot{\vec{\mathbf{r}}}_{\mathbf{t}_n} \cdot \left(\frac{\partial \vec{\mathbf{r}}_{\mathbf{t}_n}}{\partial x_n} + \frac{\partial \vec{\mathbf{r}}_{\mathbf{t}_n}}{\partial \ell_n} \right) \right]_{x_n = \ell_n} \\ & + \alpha_n \dot{\ell}_n \left[\dot{\vec{\mathbf{r}}}_{\mathbf{t}_n} \cdot \left(\frac{\partial \vec{\mathbf{r}}_{\mathbf{t}_n}}{\partial x_n} + \frac{\partial \vec{\mathbf{r}}_{\mathbf{t}_n}}{\partial \ell_n} \right) \right]_{x_n = 0} \quad . \end{aligned} \tag{E.7}$$

But

$$\int_0^{\ell_n} \dot{\vec{\mathbf{r}}}_{\mathbf{t}_n} \cdot \frac{\partial \dot{\vec{\mathbf{r}}}_{\mathbf{t}_n}}{\partial x_n} dx_n = \left[\frac{1}{2} \dot{\vec{\mathbf{r}}}_{\mathbf{t}_n} \cdot \dot{\vec{\mathbf{r}}}_{\mathbf{t}_n} \right]_{x_n = 0}^{\ell_n} \quad , \tag{E.8}$$

and

$$\int_0^{\ell_n} \dot{\vec{\mathbf{r}}}_{\mathbf{t}_n} \cdot \frac{\partial \dot{\vec{\mathbf{r}}}_{\mathbf{t}_n}}{\partial \ell_n} dx_n = \frac{\partial}{\partial \ell_n} \int_0^{\ell_n} \frac{1}{2} \dot{\vec{\mathbf{r}}}_{\mathbf{t}_n} \cdot \dot{\vec{\mathbf{r}}}_{\mathbf{t}_n} dx_n - \left[\frac{1}{2} \dot{\vec{\mathbf{r}}}_{\mathbf{t}_n} \cdot \dot{\vec{\mathbf{r}}}_{\mathbf{t}_n} \right]_{x_n = \ell_n} \quad , \tag{E.9}$$

[1] Note that it is convenient to write $\vec{\mathbf{r}}_{\mathbf{t}_n}$ as a function of the spatial coordinate x_n and time, thus in the usual way, $\dot{\vec{\mathbf{r}}}_{\mathbf{t}_n}$ is given by

$$\dot{\vec{\mathbf{r}}}_{\mathbf{t}_n} = \dot{x}_n \frac{\partial \vec{\mathbf{r}}_{\mathbf{t}_n}}{\partial x_n} + \frac{\partial \vec{\mathbf{r}}_{\mathbf{t}_n}}{\partial t} \quad .$$

However, here ℓ_n is considered as a separate variable. This means $\dfrac{\partial}{\partial t}$ in the above equation is equivalent to $\dot{\ell}_n \dfrac{\partial}{\partial \ell_n} + \dfrac{\partial}{\partial t}$ in Eq. (E.4).

by using Leibnitz's rule conversely. Substituting these relations in Eq. (E.7) and collecting similar terms, we obtain

$$I = \int_0^{\ell_n} \ddot{\vec{\mathbf{r}}}_{\mathbf{t}_n} \cdot \left(\frac{\partial \vec{\mathbf{r}}_{\mathbf{t}_n}}{\partial x_n} + \frac{\partial \vec{\mathbf{r}}_{\mathbf{t}_n}}{\partial \ell_n} \right) dx_n - \beta_n \dot{\ell}_n \left[\dot{\vec{\mathbf{r}}}_{\mathbf{t}_n} \cdot \left(\frac{\partial \vec{\mathbf{r}}_{\mathbf{t}_n}}{\partial x_n} + \frac{\partial \vec{\mathbf{r}}_{\mathbf{t}_n}}{\partial \ell_n} \right) \right]_{x_n = \ell_n}$$
$$+ \alpha_n \dot{\ell}_n \left[\dot{\vec{\mathbf{r}}}_{\mathbf{t}_n} \cdot \left(\frac{\partial \vec{\mathbf{r}}_{\mathbf{t}_n}}{\partial x_n} + \frac{\partial \vec{\mathbf{r}}_{\mathbf{t}_n}}{\partial \ell_n} \right) \right]_{x_n = 0} - \left[\frac{1}{2} \dot{\vec{\mathbf{r}}}_{\mathbf{t}_n} \cdot \dot{\vec{\mathbf{r}}}_{\mathbf{t}_n} \right]_{x_n = 0} . \tag{E.10}$$

From the definition of $\vec{\mathbf{r}}_{\mathbf{t}_n}$ and admissible function, one can see that

$$\dot{\ell}_n \left[\frac{\partial \vec{\mathbf{r}}_{\mathbf{t}_n}}{\partial x_n} + \frac{\partial \vec{\mathbf{r}}_{\mathbf{t}_n}}{\partial \ell_n} \right]_{x_n = 0} = \left[\dot{\vec{\mathbf{r}}}_{\mathbf{t}_n} \right]_{x_n = 0} . \tag{E.11}$$

and

$$\dot{\ell}_n \left[\frac{\partial \vec{\mathbf{r}}_{\mathbf{t}_n}}{\partial x_n} + \frac{\partial \vec{\mathbf{r}}_{\mathbf{t}_n}}{\partial \ell_n} \right]_{x_n = \ell_n} = \dot{\ell}_n \hat{\mathbf{i}}_n , \qquad \left[\dot{\vec{\mathbf{r}}}_{\mathbf{t}_n} \right]_{x_n = \ell_n} = \dot{\vec{\mathbf{r}}}_n . \tag{E.12}$$

Hence I can be simplified as:

$$I = \int_0^{\ell_n} \ddot{\vec{\mathbf{r}}}_{\mathbf{t}_n} \cdot \left(\frac{\partial \vec{\mathbf{r}}_{\mathbf{t}_n}}{\partial x_n} + \frac{\partial \vec{\mathbf{r}}_{\mathbf{t}_n}}{\partial \ell_n} \right) dx_n - \beta_n \dot{\ell}_n \dot{\vec{\mathbf{r}}}_n \cdot \hat{\mathbf{i}}_n + \left(\alpha_n - \frac{1}{2} \right) \left[\dot{\vec{\mathbf{r}}}_{\mathbf{t}_n} \cdot \dot{\vec{\mathbf{r}}}_{\mathbf{t}_n} \right]_{x_n = 0} . \tag{E.13}$$

Finally we can write S_{ℓ_n} in the following form by substituting back the above relation into Eq. (E.2)

$$S_{\ell_n} = \frac{(EA)_n}{m} \int_0^{\ell_n} \frac{\partial \mathcal{E}_n}{\partial \ell_n} dx_n + \frac{(EA)_n}{m} (\mathcal{E}_n)_{x_n = \ell_n} + \hat{\rho}_n \int_0^{\ell_n} \left\{ \ddot{\vec{\mathbf{r}}}_{\mathbf{t}_n} \cdot \frac{\partial \vec{\mathbf{r}}_{\mathbf{t}_n}}{\partial x_n} \right.$$
$$\left. + \left[\ddot{\vec{\mathbf{r}}}_{\mathbf{t}_n} + \alpha_0^2 \left\{ \vec{\mathbf{r}}_{\mathbf{t}_n} - 3(\hat{\mathbf{i}}_c \cdot \vec{\mathbf{r}}_{\mathbf{t}_n}) \hat{\mathbf{i}}_c \right\} \right] \cdot \frac{\partial \vec{\mathbf{r}}_{\mathbf{t}_n}}{\partial \ell_n} dx_n \right\} + \frac{1}{2} \hat{\rho}_n \left[\alpha_0^2 \left\{ \vec{\mathbf{r}}_{\mathbf{t}_n} \right. \right.$$
$$\left. \left. - 3(\hat{\mathbf{i}}_c \cdot \vec{\mathbf{r}}_{\mathbf{t}_n}) \hat{\mathbf{i}}_c \right\} \cdot \vec{\mathbf{r}}_{\mathbf{t}_n} \right]_{x_n = \ell_n} - \beta_n \hat{\rho}_n \dot{\ell}_n \dot{\vec{\mathbf{r}}}_n \cdot \hat{\mathbf{i}}_n + \hat{\rho}_n \left(\alpha_n - \frac{1}{2} \right) \left[\dot{\vec{\mathbf{r}}}_{\mathbf{t}_n} \cdot \dot{\vec{\mathbf{r}}}_{\mathbf{t}_n} \right]_{x_n = 0} \tag{E.14}$$

Since $\vec{\mathbf{r}}_{\mathbf{t}_n} = \vec{\mathbf{0}}$ at $x_n = 0$, after some manipulation we obtain

$$S_{\ell_n} = \hat{\rho}_n \int_0^{\ell_n} \left[\ddot{\vec{\mathbf{r}}}_{\mathbf{t}_n} + \alpha_0^2 \left\{ \vec{\mathbf{r}}_{\mathbf{t}_n} - 3(\hat{\mathbf{i}}_c \cdot \vec{\mathbf{r}}_{\mathbf{t}_n}) \hat{\mathbf{i}}_c \right\} \right] \cdot \left(\frac{\partial \vec{\mathbf{r}}_{\mathbf{t}_n}}{\partial \ell_n} + \frac{\partial \vec{\mathbf{r}}_{\mathbf{t}_n}}{\partial x_n} \right) dx_n$$
$$+ \dot{B}_n \dot{\vec{\mathbf{r}}}_n \cdot \hat{\mathbf{i}}_n + \frac{(EA)_n}{m} \int_0^{\ell_n} \frac{\partial \mathcal{E}_n}{\partial \ell_n} dx_n + \frac{(EA)_n}{m} (\mathcal{E}_n)_{x_n = \ell_n}$$
$$+ \hat{\rho}_n \left(\alpha_n - \frac{1}{2} \right) \left[\dot{\vec{\mathbf{r}}}_{\mathbf{t}_n} \cdot \dot{\vec{\mathbf{r}}}_{\mathbf{t}_n} \right]_{x_n = 0} . \tag{E.15}$$

Appendix F

Comments on the Analytical Mechanics Approaches

Use of the analytical mechanics approaches to derive the equations of motion has been a controversial subject for a system with a changing mass. Similar to Newton's second law

$$\vec{F} = \frac{d\vec{P}}{dt} \quad , \tag{F.1}$$

the extended Hamilton's principle

$$\int_{t_1}^{t_2} (\delta \mathcal{L} + \delta W)\, dt = 0 \quad , \tag{F.2}$$

can be applied only to a system with a constant mass. In the case of a system with a changing mass, one has to use a modified form of these equations. Newton's second law was extended for a system of changing mass, in the early stage of the development of fluid mechanics [84]. Using the idea of open and closed control volume, McIver [85], modified the extended Hamilton's principle for a system of variable mass. In a general form it is written as

$$\int_{t_1}^{t_2} \left[(\delta \mathcal{L}_o + \delta W) + \oint_{B_o} \rho (\dot{\mathbf{r}} \cdot \delta \mathbf{r})(\vec{V} - \dot{\mathbf{r}}) \cdot \hat{n}\, dA \right] dt = 0 \quad , \tag{F.3}$$

where at position $\mathbf{r}$ and time t the particle has the density and velocity of ρ and $\dot{\mathbf{r}}$, respectively. B_o is the boundary of the open control volume, $\vec{V}$, $\mathcal{L}_o$ and δW are the velocity of this boundary, Lagrangian of the open system and the virtual work performed on the same system due to the virtual displacement $\delta\mathbf{r}$, respectively. In fact $\rho(\bar{V} - \dot{\mathbf{r}})dA$ is the mass flow rate crossing the boundary surface element dA.

Using the modified form of the extended Hamilton's principle researches like McIver [85] and Laithier [86], showed that similar equations can be obtained as that of Newton's method for a system of changing mass such as the rocket problem and vibrations of a tube conveying fluid internally.

In the following an illustrative example is considered to compare the equations of motion using Newton's second law with those of an analytical method for a tethered satellite system. It can be seen that one can arrive at similar equations of motion using either of approaches. However, based on different assumptions made during the modelling, one can come up with different equations.

F.1 An Illustrative Example

The system, which models a tethered satellite system in a very simple form, consists of a mass m suspended through a hole by an inextensible tether with a mass density of ρ per unit length. In this model, point A represents the attachment point of the tether to the reel mechanism, and F is the tension force applied by the reel mechanism at this point. It is assumed that there is no force acting on the system other than F. The upper part of the tether (d) models the unreeled part, while the reeled part is modelled by the lower part (ℓ).

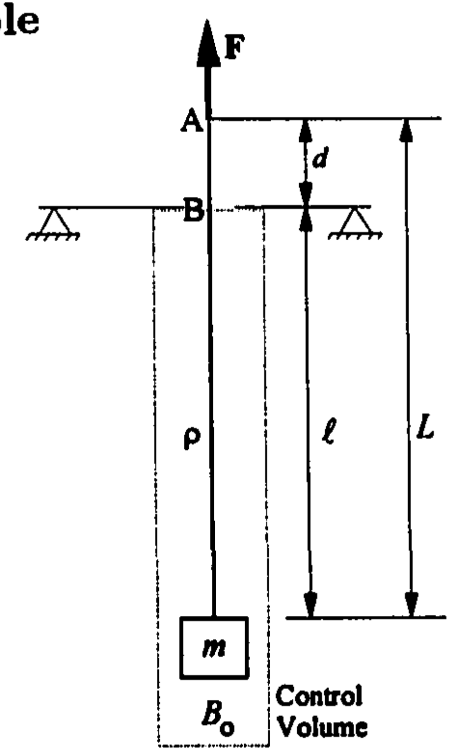

Figure F.1: Illustrative example

The equation of motion is obtained for three different cases: (a) the upper part is assumed to be moving with the same velocity as the lower part; (b) the upper part has no motion and the velocity change takes place suddenly; and (c) most of the upper part has no motion and the velocity change takes place within a small portion of the upper part of the tether such that no energy is lost in this process.

F.1.1 Case 1: The Upper Part Moves with the Same Velocity As the Lower Part

In this case we are dealing with a rigid body system moving with respect to the inertial frame with the displacement d. From Newton's method, we have

$$F = (m + \rho L)\ddot{d} \ , \quad T = (m + \rho \ell)\ddot{d} \ . \tag{F.4}$$

Since $d + \ell = L =$ constant, we can write

$$F = -(m + \rho L)\ddot{\ell} \ , \quad T = -(m + \rho \ell)\ddot{\ell} \ . \tag{F.5}$$

Similar equations can be obtained using Lagrange's method along with Lagrange multiplier or extended Hamilton's principle.

These relations show that the tension at point A, the point that the tether is really attached to the reel mechanism, in general, is different from that of point B, if it is assumed the upper part has moving. They are approximately equal only when $d \ll \ell$. In other words there is an inconsistency if one assumes that the unreeled part of the tether has the same velocity as the reeled part and uses the tension at point B as the regulating tension applied by the reel mechanism and controller.

F.1.2 Case 2: The Upper Part Has No Motion and the Velocity Changes Suddenly

Assuming that the upper part has no motion and the velocity change takes place suddenly between the upper part and the lower part and using the Newton's method for a control volume, one obtains

$$T = -(m + \rho \ell)\ddot{\ell} - \rho \dot{\ell}^2 \quad . \tag{F.6}$$

The term $\rho \dot{\ell}^2$ in the right hand side is the transport momentum across the control volume.

To apply the modified form of the extended Hamilton's principle, Eq. (F.3), let us assume that our closed control volume is the box shown in Figure F.1 with the dotted-lines and the open control volume is coincident on the closed control volume instantaneously. Let us give a virtual displacement $\delta\ell$ and figure out the different terms in Eq. (F.3).

At the boundary, $\dot{\mathbf{r}}$ is zero, therefore the closed integral over the boundary vanishes. Lagrangian of the open system is given by

$$\mathcal{L}_o = \frac{1}{2} M \dot{\ell}^2 \quad , \tag{F.7}$$

where $M = m + \rho\ell$ is the total mass inside the open control volume. Performing the δ operator, we would get

$$\delta\mathcal{L}_o = \frac{1}{2}\delta(M)\dot{\ell}^2 + M\dot{\ell}\delta(\dot{\ell}) = M\dot{\ell}\delta(\dot{\ell}) \quad , \tag{F.8}$$

since $\delta(M) = 0$ is a constraint of the open system. Hence we can write

$$\delta\mathcal{L}_o = M\dot{\ell}\delta(\dot{\ell}) = \frac{d}{dt}(M\dot{\ell}\delta\ell) - (\frac{dM}{dt}\dot{\ell} + M\ddot{\ell})\delta\ell \quad , \tag{F.9}$$

For the present system $\dfrac{dM}{dt} = \rho\dot{\ell}$, thus

$$\delta\mathcal{L}_o = \frac{d}{dt}(M\dot{\ell}\delta\ell) - (\rho\dot{\ell}^2 + M\ddot{\ell})\delta\ell \quad . \tag{F.10}$$

The virtual work on the open system is simply given by

$$\delta W = -T\delta\ell \quad . \tag{F.11}$$

Substituting for $\delta\mathcal{L}_o$ and δW, performing some algebra, and implementing $\delta\ell = 0$ at t_1 and t_2, we obtain

$$\int_{t_1}^{t_2} \left[-T - \rho\dot{\ell}^2 - (m + \rho\ell)\ddot{\ell}\right] \delta\ell dt = 0 \ . \tag{F.12}$$

Since $\delta\ell$ is any arbitrary virtual motion, one concludes that

$$T = -(m + \rho\ell)\ddot{\ell} - \rho\dot{\ell}^2 \ , \tag{F.13}$$

which is identical with the result of Newton's method.

F.1.3 Case 3: The Upper Part Has No Motion and the Velocity Changes Smoothly Within a Small Portion of the Tether

In this case we assume that the velocity changes smoothly between the upper and the lower parts within a small portion of the tether, such that: first there is no energy lost due to the momentum transfer; and second this portion is so small that its kinetic energy is negligible. It is equivalent to assuming that the incoming tether enters the closed control volume with the average velocity, $\frac{1}{2}\dot{\ell}$. Using Newton's second law or the extended Hamilton's principle for the open system, the equation of motion corresponding to ℓ is given by

$$T = -(m + \rho\ell)\ddot{\ell} - \frac{1}{2}\rho\dot{\ell}^2 \ . \tag{F.14}$$

Similar equation can be obtained if one starts from the conventional form of the Lagrange's equation to derive the equation of motion corresponding to ℓ

$$\frac{d}{dt}\left(\frac{\partial KE}{\partial\dot{\ell}}\right) - \frac{\partial KE}{\partial\ell} = Q_\ell \ , \tag{F.15}$$

where $KE = \frac{1}{2}(m + \rho\ell)\dot{\ell}^2$ and $Q_\ell = -T$. After some manipulation we can write

$$T = -(m + \rho\ell)\ddot{\ell} - \frac{1}{2}\rho\dot{\ell}^2 \ . \tag{F.16}$$

F.2 Concluding Remarks

In the study of dynamics and control of a two-body tethered satellite system, Kim [66] used the first assumption and obtained the equation of motion corresponding to ℓ with no extra term associated with the momentum transport at the attach point of the tether and the main-satellite. He then suggested using a pseudo generalized coordinate ℓ_0 in using the Lagrange's method to arrive at similar equations as those of the Newton's method. Instead of using this idea , which makes the derivation of motion difficult in a general case such as N-body tethered satellite system, one can start from Eq. (2.65) and integrate it for whole system.

For the formulation of an N-body system, developed in this thesis, it is equivalent to dropping $\mathbf{G}_{nj}$ in Eq. (2.71) and $\mathbf{L}_n$ in Eq. (2.84). If variation of the masses is to be ignored even in the kinematics, then all the $\dot{B}_j$ and $\ddot{B}_j$, $j = 1, 2, \ldots, N-1$ must be equated to zero. However as was mentioned earlier assuming similar velocity for the unreeled part and reeled part from one hand, and using the tension at one end of the reeled part of the tether as the applied tension by the reel mechanism from the other hand, are not consistent.

As the final words we would like to mention two points here: first, the difference between assuming similar velocity between the reeled part and unreeled part of the tethers and assuming smooth change in the velocity from zero to deployment/retrieval rate, appears only in the equation of motion corresponding to ℓ, i.e. none of the equations associated with librational as well as vibrational motion are affected, no matter which method is used. Secondly, the difference in reality even in the ℓ equation is so small in practical cases that it has been often ignored by the researchers.

To sense the difference let us consider a two-body tethered satellite system moving in a circular orbit, where the main satellite is coincident with the centre of mass. The system is assumed to have no librational motion. The tether is being deployed at a constant rate. With the three different assumptions of the previous Section, we would obtain the following equations:

$$-T_1 = (m + \rho\ell)\ddot{\ell} - 2(m + \frac{1}{2}\rho\ell)\ell\Omega_c^2 \ . \tag{F.17}$$

$$-T_2 = (m + \rho\ell)\ddot{\ell} - 2(m + \frac{1}{2}\rho\ell)\ell\Omega_c^2 + \rho\dot{\ell}^2 \ . \tag{F.18}$$

$$-T_3 = (m + \rho\ell)\ddot{\ell} - 2(m + \frac{1}{2}\rho\ell)\ell\Omega_c^2 + \frac{1}{2}\rho\dot{\ell}^2 \ . \tag{F.19}$$

For a system with the following parameters

$$m = 500\,\text{kg}, \ \rho = 4\,\text{kg/km}, \ \dot{\ell} = 5\,\text{m/s}, \Omega_c = 0.0012\,\text{rad/s}.$$

Table F.1 compares T_1, T_2, and T_3 for different lengths of the tether.

Table F.1: Comparison of tension in the tether

ℓ km	T_1 (N)	T_2 (N)	T_3 (N)
100	201.6	201.5	201.55
10	14.98	14.88	14.93
1	1.45	1.35	1.40
0.1	0.144	0.044	0.094

It can be seen that except for the tether with a small length, the difference is negligible. Taking into account the fact that $\dot{\ell}$ likely to be much smaller than 5 m/s in the early/final stage of deployment/retrieval , when the tether is short, one can realize that the tensions will be of the same order with either of the three assumptions. Note that including the librational as well as the vibrational dynamics of the tether as well as the dynamics of the mainsatellite will result in even smaller difference.